YEARBOOK '86/87

RESEARCH INSTITUTE FOR TECHNICAL PHYSICS
OF THE HUNGARIAN ACADEMY OF SCIENCES

yearbook '86/87

RESEARCH INSTITUTE FOR TECHNICAL PHYSICS
OF THE HUNGARIAN ACADEMY OF SCIENCES

MAGYAR TUDOMÁNYOS AKADÉMIA
Műszaki Fizikai Kutató Intézete

Budapest, 1987

PUBLISHED BY THE
Research Institute for Technical Physics
of the Hungarian Academy of Sciences

POSTAL ADDRESS:
H-1325, Budapest, Ujpest 1., P.O.B.76

RESPONSIBLE PUBLISHER:
Elemér NAGY, director

EDITOR:
Iván, C. SZÉP

ISSN-0139-4363
2015

Hozott anyagról sokszorosítva

8717718 MTA Sokszorosító, Budapest. F.v.: dr. Héczey Lászlóné

PREFACE

Dear Reader,

following the layout of the previous issue of our yearbook once again we offer first a collection of selected papers, this time of wider scope. It seemed to me appropriate to include results also from new fields of our activity which were introduced in past two years. Semiconductor superlattices, special ceramics, new methods of material testing as well as device modelling were added to the program. Due to demands on control of environment much work was devoted to development of new technological methods, especially in the field of hydro-metallurgy.

The interesting topic of fractals was pursued further with ambition by two of our staff-members who earned international recognition in this particular field.

Then surveys of the work carried out in the respective divisions of our institute are presented for general information.

Interest for our work may be characterised by the number of visitors to our institute coming from abroad; a short list of them included. Our participation in international scientific events is illustrated by names of speakers and list of conferences visited.

A comprehensive bibliography of papers published by members of our Institute during 1986-87, mostly in international journals, is given at the end. Finally, you can find a list of patent applications and patents issued to members of our institute.

If you need further information about details of our activity, please, send a card. We will gladly answer!

I.C. Szép
Ph.D., D.Eng.Sc.
Deputy Director

PREFACE

CONTENT

Selected papers

SEMICONDUCTOR RESEARCH DIVISION

METAL RESEARCH DIVISION

STRUCTURE RESEARCH DIVISION

DIVISION OF MICROWAVE DEVICES

DIVISION OF OPTICS AND ELECTRONICS

Reports on activities

Selected papers

Semiconductor Research Division

IDENTIFICATION OF THE CARBON ASSOCIATED RADIATION DAMAGE LEVELS IN SILICON

G.Ferenczi, C.A.Londos[x], T.Pavelka, M.Somogyi, A.Mertens[xx]

ABSTRACT

The dominant carbon related radiation damage centre in silicon was studied in detail. In contrast to previous studies the presence of two clearly distinguishable defects were established: one at $E_V+E_T = 0.370$ eV. $\sigma_p = 8\times10^{-18}cm^2$ and assigned as the C_S-Si_I-C_S complex, and another one at $E_V+E_T = 0.344$ eV, $\sigma_p = 1.1\times10^{-16}$ cm^2 and assigned as the COV_2 complex. It is suggested that the concentration of the C_S-Si_I-C_S centre is indicative to the overall carbon concentration, hence the peak separation technique presented in this paper can be used to measure low - with IR absorption non-detectable - carbon concentrations in silicon.

INTRODUCTION

The yield and properties of very large scale integration (VLSI) devices which are mainly fabricated on Czochralski (CZ) silicon wafers are significantly influenced by the behaviour of oxygen in the silicon substrates. It is well established[1,2] that the presence of carbon in the silicon lattice significantly influences the precipitation properties of oxygen acting as a nucleation site. It is argued[1] that low carbon concentration is favourable. The widely used IR absorption technique can not usually detect carbon concentrations below 1×10^{16} cm^{-3} on samples with standard wafer thickness. Alternative ways to detect low carbon concentrations would therefore be welcomed.

---

[x]Permanent address: University of Athens, Physics Department, Solid State Section, 104 Solonos Street, Athens, Greece

[xx] Humboldt Universität, Sektion Physik, Bereich 06, Berlin, GDR

Radiation damage levels are the best characterized defects in silicon, only a selection of the published results are referenced here[3-9]. It was shown that the most common defects introduced by irradiation are complexes involving carbon and oxygen beside the simple point defects. In the present work we intend to concentrate on a carbon related level usually reported with E_V+E_T = 0.36 eV, which forms around room temperature and anneals out around 400°C. This defect was first described more than 20 years ago[10] but its identity is still subject to controversy, the candidates being: COV_2 or C_i-C_s (recently corrected as C_s-Si_I-C_s by[11]). The intention of the present paper is to resolve this long standing controversy and suggest a calibration procedure for determining the concentration of carbon in silicon using the properties of this defect.

EXPERIMENTAL

10-15 ohmcm B doped p-type silicon materials were used. Three groups of samples were selected :

	Float Zone (FZ)	Czochralski low C	Czochralski high C
N_{O_I} [cm^{-3}]	$<10^{16}$	$5x10^{17}$	$5x10^{17}$
N_{C_S} [cm^{-3}]	$<10^{16}$	$<10^{16}$	$5x10^{16}$

Table I.

Schottky contacts were prepared by Ag^+ implantation (30 keV, $3x10^{16}$ dose/cm^2) as described in[12].

Subsequently the samples were implanted with H^+ at 300 keV and at room temperature, using varying dose levels between ($4x10^9$-$6x10^{10}$)dose/cm^2. DLTS measurements were performed with a high sensitivity lock-in spectrometer DLTS-82E, manufactured by SemiTrap,Hungary.

RESULTS, DISCUSSION

Six radiation damage levels were observed in the majority carrier spectra, in the present work we concentrate only on the level, labelled

as H_4 [13]. It was noted that the introduction rate of this defect is twice as high in $CZ_{high\ C}$ samples than that of the other levels. Detailed Isothermal Frequency-Scan[14] measurements were performed to determine the capture cross section of this level. Typical example is shown on Fig. 1.

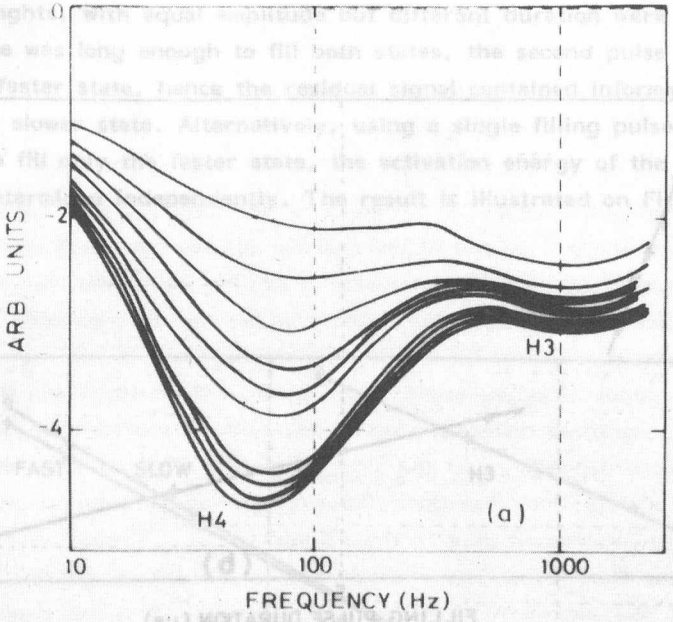

Fig.1/a. Series of capture cross section measurements in frequency scan mode at T = 200 K

H_4 is produced as a recoil cascade process by the A_g^+ implant, the maximum is centered at 180 nm, and by H^+ implant centered at 2.7 /um. Capture cross section measurement on the proton induced defect was performed selecting the amplitude of the reduced reverse bias pulse to reach a defect free part of the junction in order to eliminate the influence of the free carrier tail on the capture rate. Two clearly distinguishable capture rates were measured. The values of the capture cross sections averaged over 8 samples (the accuracy of the individual measurements are better than 5%):

$$\sigma_{pfast} = (1.1^{+}_{-}0.1)\times10^{-16}\ cm^2$$

$$\sigma_{pslow} = (8^{+}_{-}2)\times10^{-18}\ cm^2$$

The much lower value reported by [6] for the slow process is probably due to the influence of the edge layer effect.

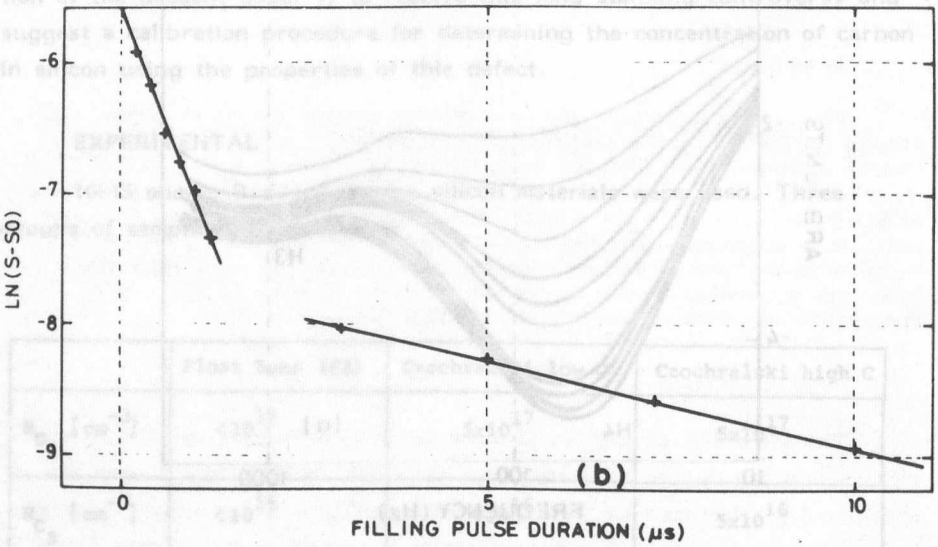

Fig.1/b. The corresponding evaluation of the two capture cross section

The H_4 level induced by Ag^+ implantation contains only the slow component, the H_4 level induced by high dose H^+ implantation in the CZ_{lowC} samples contains only the fast component within measurement accuracy. The peak labelled as H_3 on Fig.1/a was not reported previously. This is mainly due to the superior energy resolution of the frequency scan technique. (To achieve equivalent energy resolution with temperature scan significant data points should be recorded at every 0.04 K). We believe

that the large scatter - 0.33-0.38 eV - reported in the literature for the activation energy of H_4 [3-9] is partly due to the admixture of H_3. The capture cross section of H_3 is $\sigma_{pH3} = 2.7 \times 10^{-16}$ cm^2. It is important to decide whether the different capture rates observed for H_4 originate from the same defect or we are dealing with two different species. Using the Differential DLTS[15] variant of the Isothermal Frequency-Scan DLTS we succeeded to separate two levels. Two filling pulses, separated in time by half of the period lenghts, with equal amplitude but different duration were used. The first pulse was long enough to fill both states, the second pulse filled only the faster state, hence the residual signal contained information only about the slower state. Alternatively, using a single filling pulse, short enough to fill only the faster state, the activation energy of the fast state can be determined independently. The result is illustrated on Fig.2.

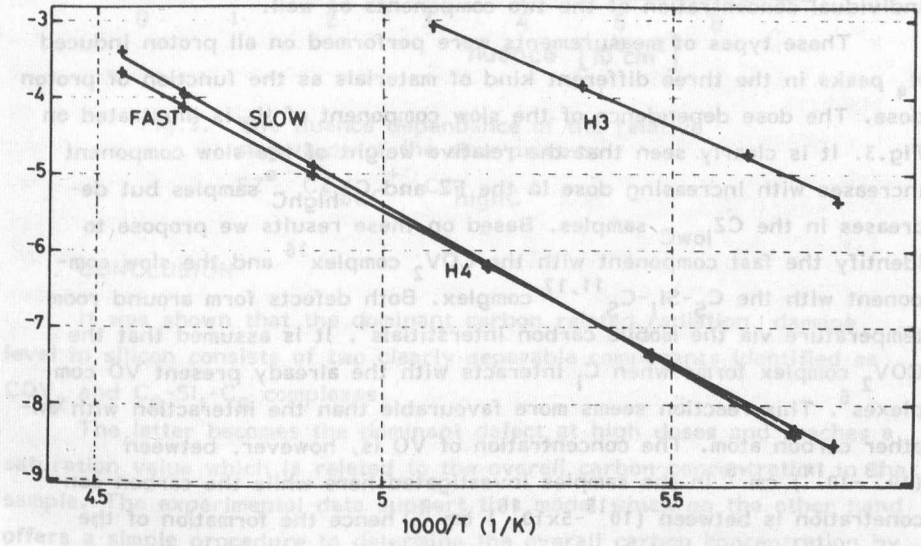

Fig.2. Arrhenius plots measured in frequency scan mode. The slow process was determined by the double pulse technique described in text

The measured activation energies (averaged over 8 samples, the accuracy of the measurement on a single sample is ± 1 meV):

$$(E_V+E_T)_{fast} = (0.344\pm0.005)eV$$

$$(E_V+E_T)_{slow} = (0.370\pm0.002)eV$$

For completness, the activation energy for H_3

$$(E_V+E_T)_{H_3} = 0.279\ eV$$

The unusual accuracy of the measurement data (capture cross section and activation energy) is due to the thermal equilibrium conditions achieved during frequency scan. As a conclusion it can be stated that the peak separation technique described previously allows the determination of the individual concentration of the two components as well.

These types of measurements were performed on all proton induced H_4 peaks in the three different kind of materials as the function of proton dose. The dose dependence of the slow component of H_4 is illustrated on Fig.3. It is clearly seen that the relative weight of the slow component increases with increasing dose in the FZ and CZ_{highC} samples but decreases in the CZ_{lowC} samples. Based on these results we propose to identify the fast component with the COV_2 complex[16] and the slow component with the C_S-Si_I-C_S[11,17] complex. Both defects form around room temperature via the mobile carbon interstitials[4]. It is assumed that the COV_2 complex forms when C_i interacts with the already present VO complexes[6]. This reaction seems more favourable than the interaction with another carbon atom. The concentration of VO is, however, between $(10^{13}-10^{14})$ cm^{-3} in the samples investigated here while the carbon conetration is between $(10^{15}-5x10^{16})$ cm^{-3}, hence the formation of the C_S-Si_I-C_S complex becomes more preferable at higher doses. The only notable exception is the CZ_{LowC} sample at $5x10^{10}$ proton/cm^2 where $N_O/N_C \sim 10^2$ as compared to other samples where $N_O/N_C \sim 10^1$, hence this data also supports our identification.

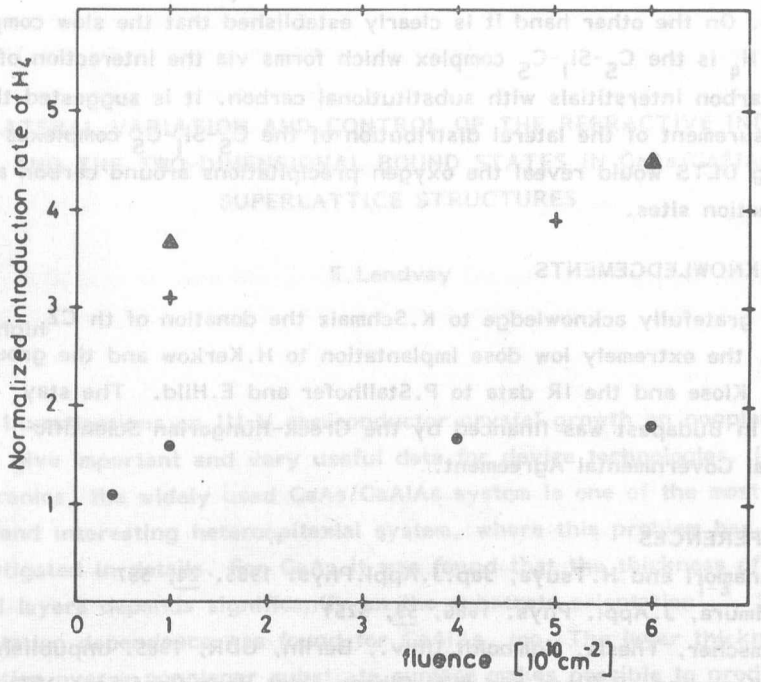

Fig.3. The fluence dependence of the relative magnitude of the slow process: $FZ^{\bullet}$, CZ_{lowC}^{+}, CZ_{highC} ▲

CONCLUSION

It was shown that the dominant carbon related radiation damage level in silicon consists of two clearly separable components identified as COV_2 and C_S-Si_I-C_S complexes.

The latter becomes the dominant defect at high doses and reaches a saturation value which is related to the overall carbon concentration in the sample. The experimental data support this model which on the other hand offers a simple procedure to determine the overall carbon concentration by measuring N_{H_4slow} at any given proton dose. To calibrate accurately the proposed carbon concentration measurement procedure large number of samples with different and known carbon and oxygen concentrations are needed.

The proposed carbon concentration measurement procedure of this paper should be viewed as a next step on the way to use H_4 for determining oxygen and carbon concentration in silicon as originally suggested by

Troxell[9]. On the other hand it is clearly established that the slow component of H_4 is the C_S-Si_I-C_S complex which forms via the interaction of mobile carbon interstitials with substitutional carbon. It is suggested that the measurement of the lateral distribution of the C_S-Si_I-C_S complexes by Scanning DLTS would reveal the oxygen precipitations around carbon atoms as nucleation sites.

ACKNOWLEDGEMENTS

We gratefully acknowledge to K.Schmalz the donation of th CZ_{highC} samples, the extremely low dose implantation to H.Kerkow and the group of Prof. Klose and the IR data to P.Stallhofer and E.Hild. The stay of C.A.L. in Budapest was financed by the Greek-Hungarian Scientific-Technical Governmental Agreement.

REFERENCES

1. M.Kanamori and H.Tsuya, Jap.J.Appl.Phys. 1985. 24, 557
2. F.Shimura, J.Appl. Phys. 1986, 59, 3251
3. K.Irmscher, Thesis, Humboldt Univ., Berlin, GDR, 1985. unpublished
4. L.C.Kimerling, P.Blood and W.M.Gibson, Inst.Phys.Conf.Ser. 1979. 46, 273
5. L.C.Kimerling, Inst.Phys.Conf.Ser. 1977. 31, 221
6. P.M.Mooney, L.J.Cheng, M.Süli, J.D.Gerson and J.W.Corbett Phys.Rev. 1977. B15, 3836
7. Y.H.Lee, L.J.Cheng, J.D.Gerson, P.M.Mooney and J.W.Corbett, Solid-State Com. 1977. 21, 109
8. J.W.Walker and C.T.Sah, Phys.Rev. 1973, B7, 4587
9. J.R.Troxell, Solid State Electron. 1983, 26, 539
10. E.Sonder and L.C.Templeton, J.Appl. Phys. 1965, 36, 1811
11. K.P.O'Donnell, K.M.Lee and G.D.Watkins, Physica, 116B, 258 (1983)
12. J.Bollmann, H.Klose and A.Mertens Proc.Physik der Halbleiteroberflache, 1984. 15, 247
13. G.Ferenczi, C.A.Londos, T.Pavelka, M.Somogyi and A.Mertens to be published in J.Appl. Phys., Dec. 1987.
14. G.Ferenczi, J.Boda and T.Pavelka, phys.stat.sol.(a), 1986.94, K119
15. G.Ferenczi, P.Krispin and M.Somogyi, J.Appl.Phys. 1983. 54, 3902
16. Y.H. Lee, J.W.Corbett and K.L.Brower phys.stat.sol.(a), 1987. 41, 637
17. K.L.Brower, Phys.Rev. 1974. B9, 2607

LATERAL VARIATION AND CONTROL OF THE REFRACTIVE INDEX AND THE TWO-DIMENSIONAL BOUND STATES IN GaAs/GaAlAs SUPERLATTICE STRUCTURES

E. Lendvay

Investigations on III-V semiconductor crystal growth on nonplanar surfaces give important and very useful data for device technologies. In optoelectronics, the widely used GaAs/GaAlAs system is one of the most important and interesting heteroepitaxial system, where this problem has been investigated in details. For GaAs it was found that the thickness of epitaxial layers depends significantly on the substrate orientation[1-3]. Similar orientation dependence was found for GaAlAs, too. The layer thickness variation over a nonplanar substrate surface makes possible to produce the so called buried heteroepitaxial laser structures necessary eg. for high power and long life-time LD devices, as well as the growth of different structures used for III-V sensors, detectors and planar devices. Previous studies of orientation dependent growth rate, however, were limited to relatively thick epitaxial layers, and only a few papers dealt with quantum-well structures[3,4]. On the other hand, in superlattice (SL) structures the physical properties in the semiconductor system very strongly depend on the L periodicity. It was expected, eg. that the variation of the SL period (layer thickness) with orientation gives rise to effects which are significantly different from those resulting from thickness variations of thicker ($L > 50$ nm) epitaxial layers. In particular, the change of L results in the change of the refractive index according to the equation (1)

$$n(\omega) = \left\{ \frac{\varepsilon_1(\omega)}{2} + \frac{1}{2} \left[\varepsilon_1(\omega)^2 + \varepsilon_2(\omega)^2 \right]^{1/2} \right\}^{1/2} \qquad (1)$$

where ε_1 is the real, ε_2 is the imaginary part of the dielectric constant. ε_1 is strongly dependent on L periodicity and. owing to this fact, the

refraction index is very sensitive to the superlattice parameters. The variation of n_{SL}/n_{GaAs} is seen in Fig.1. In the range of thin ($10a_o$-$50a_o$, eq. 5.6 nm - 28.0 nm) SL layers, where a local maximum in the n_{SL}/n_{GaAs}-L function can be found, the change of the refractive index is very strong, and at about 40 a_o ($\sim$20 nm) has a minimum value of $n_{SL}/n_{GaAs} \sim 0.95$ meaning a $\Delta n \sim 5$ % variation sufficient for optical guiding.

Similar effects in the bound state energies can also be expected. According to Fig.2. bound state formed in the quantum wells have energies of

$$E_n = \frac{\hbar^2 \pi^2}{2m_e^x} \left(\frac{n}{L}\right)^2 J\,(m_e^x,\ L,\ V_o) \qquad (2)$$

where n = 1,2,3 ...; V_o is the depth of the quantum well and function J takes account of finite depth value of V_o in the box.

To study the guiding and recombination properties, different non-planar SL structures were grown by an improved LPE technique[6-9]. A vertical rotating LPE system was applied to prepare patterned SL structures.

Growth temperatures ranging from 700°C to 960°C were used. The (100) GaAs substrates were chemically-mechanically polished prior to growth. Masking patterns were formed by chemical etching using conventional photolithography. Lines and spaces aligned in the <110> direction were investigated. The mesa and groove structures were etched using an etchant of $4H_2SO_4:H_2O_2:H_2O$ at room temperature. Superlattices consisting of 15-60 periods of alternate (20-50 nm thick) GaAs and GaAlAs layers were grown onto the patterned substrates. The growth was performed above the oxide desorption temperature (680°C). Figs. 3,4 and 5. show cleaved and etched cross sections of SL wafers, where the SL region was grown by LPE onto the patterned regions. In Fig.3 superlattice grown into an etched groove is seen. Similar picture for mesa-substrates is illustrated in Fig.4, where the mesa itself is a SL region. On surfaces defined by oxide stripe quantum-wire structures can also be grown: a characteristic sample is seen in Fig.5. As the figures show the superlattice period changes significantly by changing the tilt angle of the growth plane and increases with increasing angle. Generally, the transition between different faces in the SL region is smooth and occurs within a few nm period,

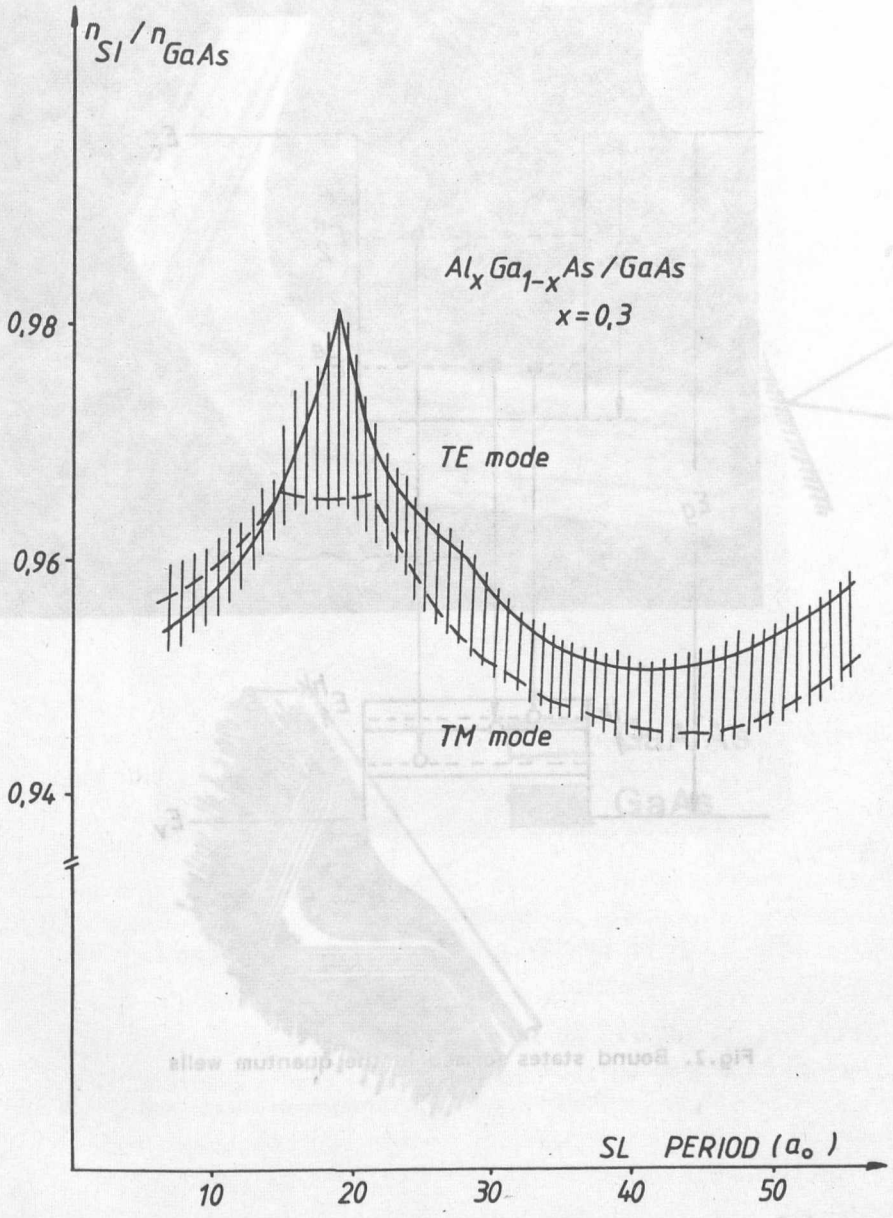

Fig.1. Variation of n_{SL}/n_{GAs}

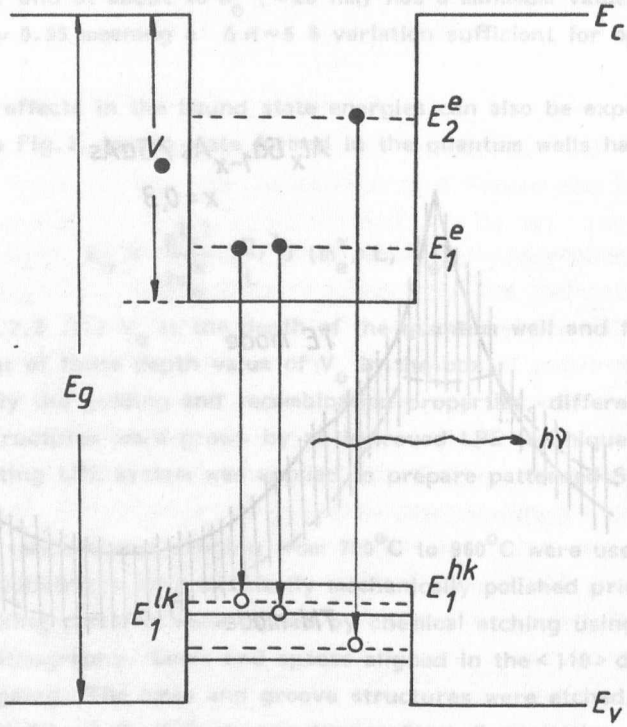

Fig.2. Bound states formed in the quantum wells

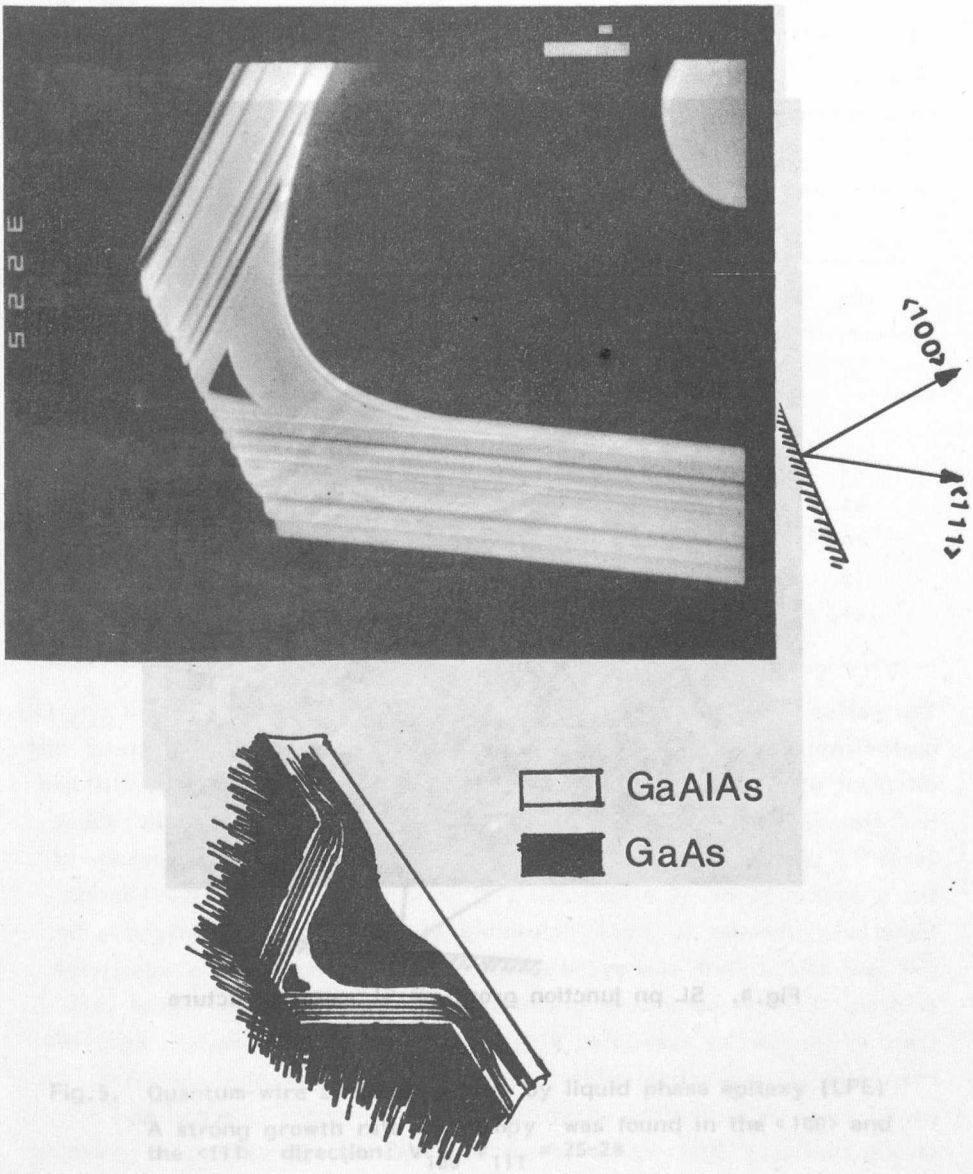

Fig.3. Superlattice confinement grown by LPE technique in a GaAs groove .

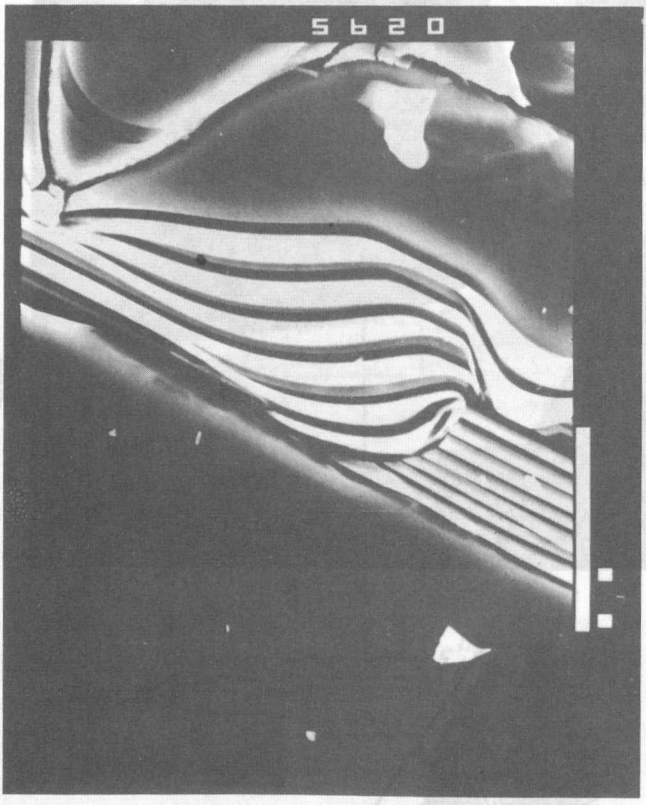

Fig.4. SL pn junction grown on SL mesa structure

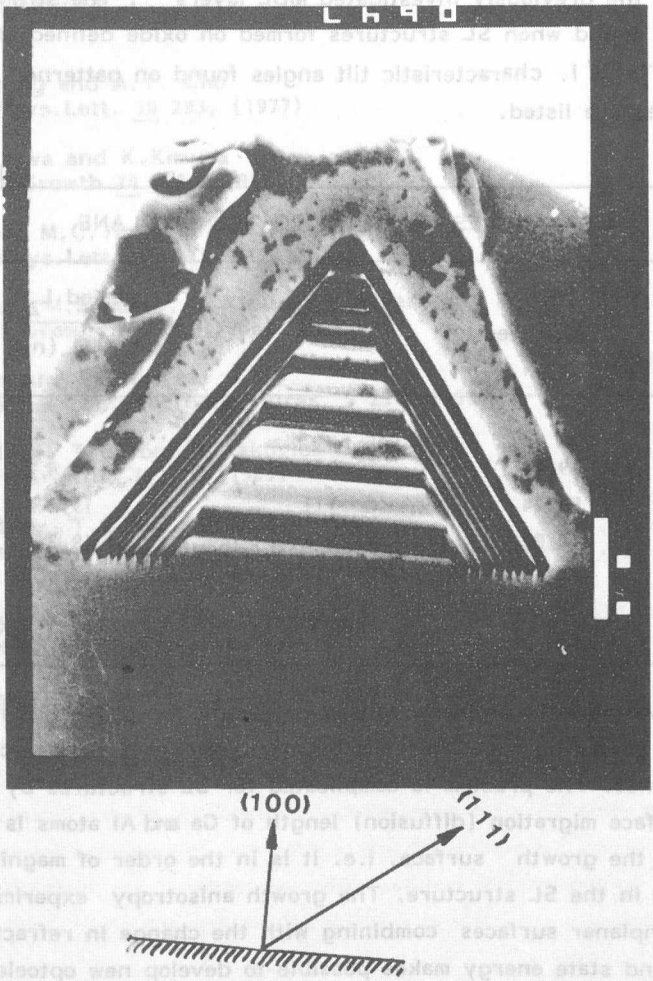

Fig.5. Quantum-wire structure grown by liquid phase epitaxy (LPE)
A strong growth rate anisotropy was found in the <100> and the <111> direction: $V_{100}/V_{111} = 25\text{-}28$

according to the previously investigated MBE layers[3,9]. The strongest anisotropy was found when SL structures formed on oxide defined stripes (Fig.5). In Table I. characteristic tilt angles found on patterned (100) GaAs surfaces are listed.

Table I.

TILT ANGLES RELATIVE TO THE 100 PLANE

Θ_m measured (deg)	Θ_c calculated (deg)	Crystal plane	period L_z / cos Θ (nm)
22	19,47	411	19,4
53	54,74	111	19,1
10	10,02	811	19,3
12	11,42	711	11,4
59	60,5	544	16,2

The period variation is probably caused partly by the difference in sticking coefficients, partly by the difference between component fluxes across the different planes. The problem is complicated for SL structures by the fact that the surface migration (diffusion) length of Ga and Al atoms is about 20-30 nm on the growth surface, i.e. it is in the order of magnitude of the L period in the SL structure. The growth anisotropy experimentally found on nonplanar surfaces combining with the change in refractive index and bound state energy makes possible to develop new optoelectronic devices. In these structures grown on nonplanar substrates lateral variations in properties associated with SL periods can be expected. Eg., the change in $n(\omega)$ makes possible to form optical wave guiding along the cavity axis. In structures shown in Fig. 5 e.g. modus selection and a strong confining effect can be expected. Similarly, SL structures grown into GaAs grooves can also be applied for modus selection giving, in principle, new directions for semiconductor laserdiode developments.

REFERENCES

1. W.T.Tsang and A.Y. Cho
   Appl. Phys.Lett. 30 293, (1977)

2. J.Nishizawa and K.Kimura
   J.Cryst.Growth 74 331, (1986)

3. E.Kapon, M.C.Tamargo and D.H.Hwang
   Appl. Phys.Lett. 50 341, (1987)

4. K.Kamon, M.Shimazu, K.Kimura, M.Mihara and M.Ishii
   J.Cryst.Growth 7 297, (1986)

5. I.Kahen and P.Leburton
   Superlattices and Microstructures, 3 251, (1987)

6. E.Lendvay, T.Görög, V.Rakovics
   J.Cryst.Growth, 72 616 (1985)

7. E.Lendvay, T.Görög and V.Rakovics
   Physics and Technology of Compensated Semiconductors
   Ed. V.S.Gopalam ICSU-COSTED, Madras, 1985.

8. T.Görög, E.Lendvay and V.Rakovics
   Acta Phys. Hungar. 61 149 (1987)

9. J.S.Smith, P.L.Derry, S.Margalit and A.Yariv
   Appl. Phys.Lett 47 712, (1985)

ELECTRON MICROSCOPE STUDY OF OXIDE ISOLATED STRIPE LASER

Judit Pfeifer, Árpád Barna, Attila L.Tóth

ABSTRACT

Ion milling was used for the thinning of metallized oxide isolated laser structures of GaAs-GaAlAs. The sequence of layers and the p-n junction were studied on the resulted bevelled section in the scanning electron microscope. Backside aligned ion milling produced thinned samples for transmission electron microscopy. Microcracks created in the vicinity of oxide window were identified.

INTRODUCTION

The performance of heterojunction devices is critically dependent on the regular lattice arrangement across the heterointerface. Little is known on initial steps of epitaxial growth process creating heterointerfaces. Transmission electron microscopy of samples taken from various parts of heteroepitaxial crystalline structures seems to be promising. For transmission electron microscopy sectioning of the active zone is needed. The use of chemical and electrochemical material thinning methods has difficulties because these methods are generally too sensitive for structural defects and compositional variations.

In this paper we describe the results of several investigations carried out on oxide covered GaAs-GaAlAs samples prepared by ion beam milling. The low angle ion beam etching provides a good quality sample surface and it can be stopped at the p-n junction of the metallized sample with the help of optical beam induced current (OBIC) effect.

SAMPLE PREPARATION

Oxide-isolated GaAs-GaAlAs stripe laser structures were fabricated[1] and covered with CrAu and AuGe metallization. The fully metallized wafers

were submitted to thinning procedure by Ar^+ ion milling on both sides. The equipment developed for Ar^+ ion beam etching[2] is provided with a special rotating holder having electric connections (Fig.1.) The angle of incidence of the ions can be controlled.

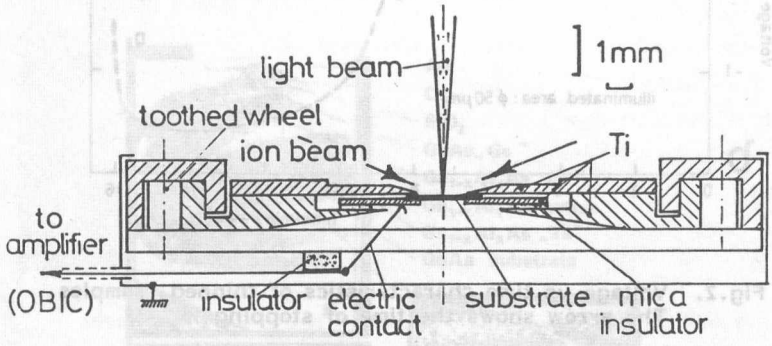

Fig.1. Cross sectional sketch of the rotating sample holder with the electric connections

The parameters of the ion beam preparation were as follows:

THINNING: Voltage: 10 kV
Source current: 1 mA for the p-side
Ion beam density: $\sim$2 mA/cm x cos 83°
3 mA for the n-side
Ion beam density: $\sim$5 mA/cm x cos 83°
Angle of incidence: 7° (from the sample surface)

FINAL POLISHING: Voltage: 4 kV Time 5 s

Thinning from the p-side was stopped at a depth close to the p-n junction, using the OBIC as indicator. Fig.2. is a plot of OBIC measured in the electric circuit of the thinned sample. SEM/EBIC (electron beam induced current) investigations were also carried out in a JSM-25S-III scanning electron microscope, showing that the etching broke the plane of the p-n junction through an area of $\emptyset \sim 120$ /um. Aligned ion milling was then performed on the backside until the appearance of optical transparency of the sample (Fig.3.)

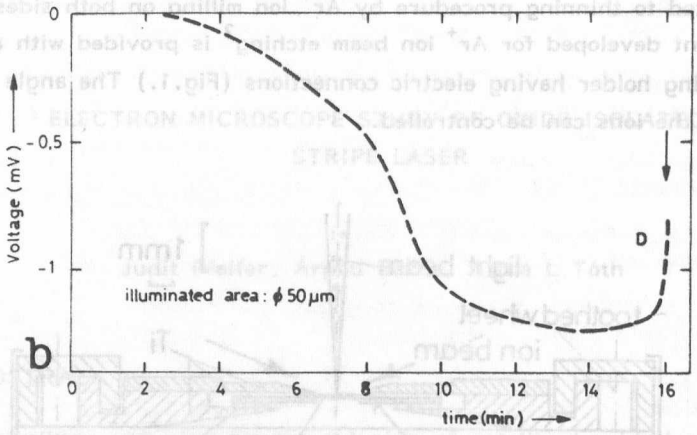

Fig.2. Voltage vs time characteristics of thinned samples. The arrow shows the time of stopping

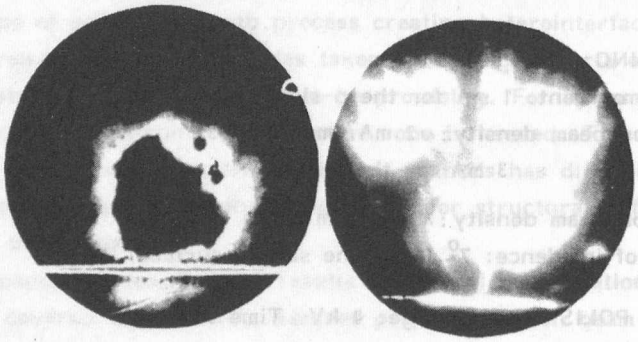

Fig.3. (a) EBIC image of the p-side after the ion etching. (b) TEM micrograph of the sample after backside aligned thinning at the same magnification.

EXPERIMENTAL RESULTS

Ion milling on the p-side produced a small angle bevelled section where the identification of the layers, the localization of the p-n junction and the observation of a transition layer between the inner confinement and the active layer were possible (Fig.4.a-c.).

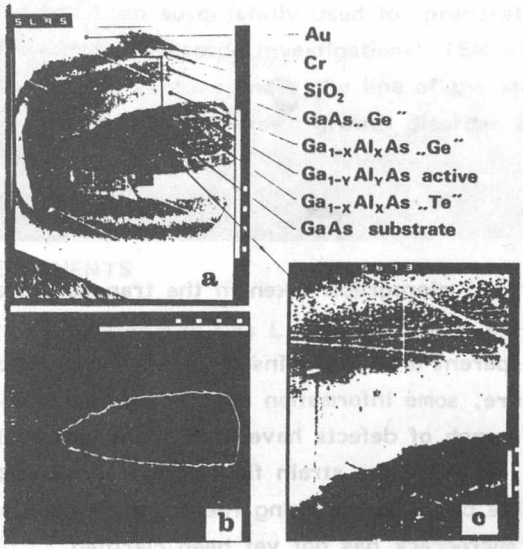

Fig.4. (a) SEI image on bevelled section of the fully metallized oxide-isolated GaAs-GaAlAs laser structure. Ion milling carried out on non-rotating substrate.

(b) EBIC contrast at the same magnification.

(c) SEI of the same sample at a higher magnification showing an intermediate layer between the n-type GaAlAs confinement and the n-type active layers.

After the backside aligned milling procedure transparent areas of $\emptyset \sim 200$ µm were obtained, without a visible hole. The transparent area contains layers of both sides of the p-n hetero-interface.

Micrographs of this transparent area taken in a JEOL 100D transmission electron microscope do not show any evidence of characteristic defects, lattice point misalignment or disorder (Fig.5.). The vicinity of the p-n heterojunction seems to be not different from the matrix material. Dislocations are observed but their density is smaller than it has been expected.

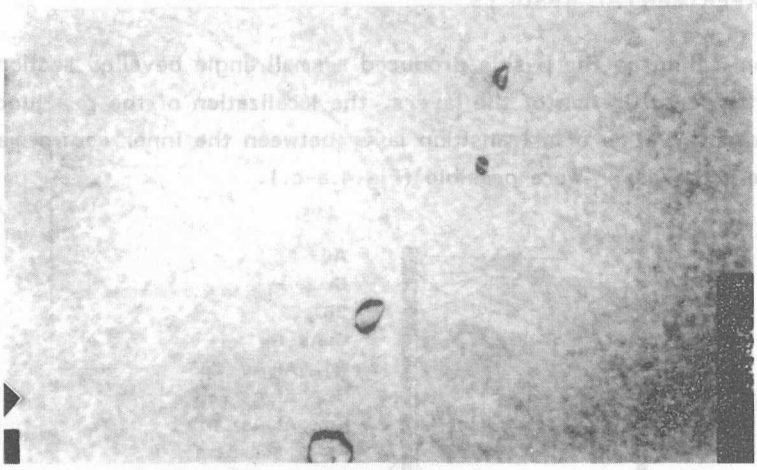

Fig.5. Typical micrograph taken in the transparent area

As the trasparent area contains a certain region under the stripe of the laser structure, some information on this area can also be obtained. Cracking and a bunch of defects have been found under the line of the stripe (Fig.6.). Probably the strain field at the edges of the window in the oxide can give cause for cracking.The origin of dislocations coming directly from the microcrack has not yet been clarified.

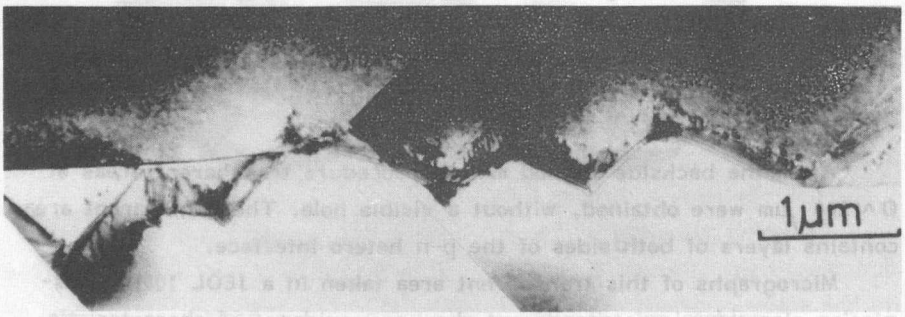

Fig.6. Cracking and dislocations shown in the TEM micrograph of the transparent area under the stripe of the laser

CONLCUSION

In this paper we have demonstrated that low incidence angle Ar^+ ion beam etching of rotating metallized GaAs-GaAlAs wafers produces suitable quality bevelling from the active side. Either EBIC or OBIC can be used to stop the thinning at the depth of the p-n heterojunction. Backside aligned ion milling has been successfully used for preparation of samples for transmission electron microscope investigations. TEM micrographs show cracking and dislocation structure under the line of the stripe. On the other hand, our samples have not shown growth disorder across the hetero-interface.

ACKNOWLEDGEMENTS

The authors are grateful to Drs L. Zsoldos and F.Koltay for valuable discussions.

REFERENCES

1. Andor L.et al.
Finommechanika-Mikrotechnika 24. (1985) pp.318-335

2. A.Barna
Proc. 8th European Congress on Electron Microscopy,
Budapest (1984) Vol.1. pp.107-108

THE GENERATION OF PICOSECOND OPTICAL PULSES BY MODE-LOCKING OF LASER DIODES

M. Serényi

The generation of coherent optical pulses by mode-locking of semiconductor lasers is important for applications e.g. in ultrafast optical communication. Bandwidth limited single pulses as short as 1.6 ps have been obtained from a passively mode-locked index guided laser diode[1] while the typical pulse durations reported for active mode-locking of GaAs/AlGaAs laser range between 5-30 ps[2-4]. The combination of active and passive mode-locking techniques provides an increase in stability and background suppression but has brought about almost no improvement with respect to the pulse durations[5].

It is well established that a fast and significant gain transient is important to initiate short pulse emission from an actively mode-locked laser. Thus it seems to be surprising that almost no attention has been drawn to the photon energy dependence of the pulse length.

We have performed a systematic investigation of the dependence of pulse duration on output wavelength for an actively mode-locked GaAs/AlGaAs laser diode. Our experiments reveal a continuous decrease of the pulse duration from 20 ps at the gain maximum (823 nm) to 7 ps at 802 nm. The remarkable pulse shortening with increasing photon energy can be qualitatively explained by the dynamics of the carrier distribution of the degenerate electron-hole plasma. The laser diode (Hitachi HLP 1400) is mounted in an external cavity formed by one crystal facet and a 100% mirror combined with a NA=0.45 microscope objective. The second surface of the diode facing the external resonator is covered with non-stoichiometric silicon nitride antireflection layer providing a residual reflectivity as low as 2×10^{-4}. Such an extremely low reflectivity has been achieved by "in situ" monitoring of the laser output during the deposition[6,7].

A narrow band interference filter ($\Delta\lambda$ = 5 nm, peak transmission 95%) within the external cavity serves for bandwidth control and tuning of the emission wavelength. The diode is electrically excited by the pulse train of a comb generator (HP 33002A) driven by the amplified output of a frequency synthesizer operating at about 80 MHz. The comb generator provides pulses with 150 ps duration and a peak amplitude of up to 20V on 50Ω. The laser diode is terminated by a matching resistor to a 50Ω transmission line and prebiased by a variable dc voltage connected via a 50 Ω bias-tee circuit.

The temporal and spectral distribution of the output are analysed by a synchroscan streak camera (10 ps resolution for the present experimental conditions) and a 1 m grating spectrometer equipped with an optical multichannel detector.

The cw threshold of the antireflection coated diode in the external cavity without interference filter is 54 mA. If the feedback from the external mirror is blocked no laser action up to a dc current of 100 mA is observed.

Fig.1. shows the variation of the measured pulse duration versus emission wavelength which could be continuously tuned across the gain curve by tilting of the interference filter. For this experiment the laser is pumped by a constant pulse current with a peak amplitude I_{pulse}=250mA while the dc bias current is optimized for each wavelength setting for generation of the shortest pulses which could be excited without any satellites.

Tuning of the laser from longer to shorter wavelength results in a decrease of the measured streak width from 26 ps at 835 nm to 12 ps at 802 nm. For the shortest pulses the finite time resolution of the streak camera has to be taken into account. Assuming a gaussian profile for the pulse shape and streak camera function a pulse duration as short as 7 ps follows from the deconvolution. Many details of the experiment and a new method to achieve bandwidth-limited pulses have already described in Refs. 8 and 9.

The strong dependence of the pulse width on emission wavelength can be explained by the dynamics of the injected electron-hole plasma. In the degenerated, inverted electron-hole plasma the gain transient is fastest at the very high energy side of the gain curve corresponding to about the energy separation of the electron and hole quasi-Fermi levels.

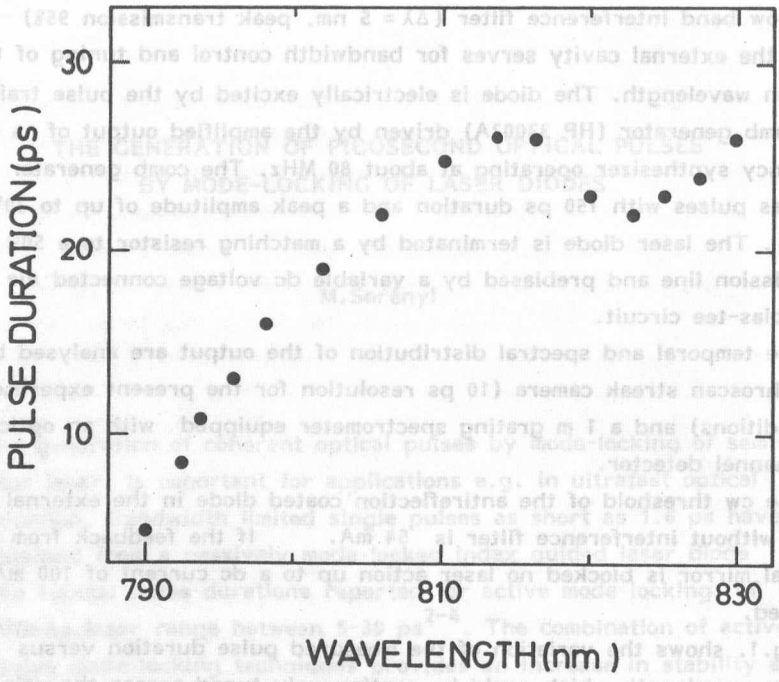

Fig.1. Variation of the measured pulse duration vs emission wavelength of the diode laser. Constant pulse current (I_{pulse} = 250 mA) is superimposed to the dc bias

The built up of the optical pulses results in a decrease of electron-hole density and hence a decrease of the spacing of the quasi-Fermi levels. Thus the high energy side of the gain profile is most strongly affected by the gain saturation and the gain can turn over into absorption very rapidly. The gain transient at the high energy side is therefore generally faster than at the low energy side.

In conclusion we have studied the wavelength dependence of the pulse width t_p for a broadly tunable actively mode-locked GaAs/AlGaAs laser diode. A continuous decrease of t_p with increasing photon energy from t_p = 22 ps at 823 nm (gain maximum) to 7 ps at 802 nm is found. This behaviour is qualitatively explained by the rapid shift of the Fermi level of the plasma during pulse formation, which results in faster gain transient at the high energy side of the gain profile than at lower energies.

ACKNOWLEDGEMENT

The experimental work has been peformed at the Max-Planck-Institute für Festkörperforschung in Stuttgart. The author acknowledges the hospitality and support.

REFERENCES

1. Y.Silberberg, P.W.Smith, D.J.Eilenberger, D.A.B.Miller, A.C.Gossard and W.Wiegmann,
Opt. Lett. 9, 507 (1984)

2. M.B.Holbrook, W.E. Sleat, and D.J.Bradley
Appl. Phys.Lett. 37, 59 (1980)

3. J.C.AuYeung and A.R.Johnston
Appl. Phys.Lett. 40, 112 (1982)

4. J.P. van der Ziel
J.Appl. Phys. 52, 4435 (1981)

5. W.A. Stallard and D.J.Bradley
Appl. Phys. Lett. 43, 626 (1983)

6. M.Serényi, W.Lauer, and H.-U. Habermeier
Nucl.Instruments and Methods in Phys.Res., B18, 659 (1987)

7. M.Serényi and H.-U. Habermeier
Appl. Opt. 26, 845 (1987)

8. M.Serényi, J.Kuhl and E.O.Göbel
Appl. Phys.Lett. 50, 1213 (1987)

9. J.Kuhl, M.Serényi and E.O.Göbel
Opt.Lett. 12, 334 (1987)

Metal Research Division

SINTERING STUDIES ON SIALON TYPE CERAMICS

Péter Arató, István Hangos, Ferenc Wéber

Sialon type ceramics represent a new, very interesting class of high performance ceramics. Their name is originated from the chemical composition silicon-aluminium-oxygen-nitrogen, other additives such as yttrium are also used. A special combination of properties - high strength, high temperature resistance, good toughness, excellent heat shock resistance - results in many different applications, for instance: structural material of engine and turbine components, cutting tools, bearings[1,2].

In our institute L.Bartha and L.Kozma began to investigate the sialon system in 1984. Part of the experiments was carried out in Stuttgart in the Max-Planck-Institute für Metallforschung.

A systematic study of the relationship among the structure, the mechanical properties and the manufacturing parameters began in 1986 with the financial help of the State Committee for Technical Developments (OMFB). In this paper we report our first results.

There are several methods for producing sialon type ceramics: reaction sintering, pressureless sintering, hot pressing, hot isostatic pressing, and combinations of them. In our study pressureless sintering in nitrogen atmosphere was used on ceramics formed by dry uniaxial pressing at 100-300 MPa, the firing temperature and time were 1650-1900^{o}C and 0.5-5 hours, respectively.

The structure of specimens was investigated by scanning electron microscopy, energy dispersive and wave length dispersive X-ray analysis, and by X-ray diffraction. The fracture strength was measured by a three-point bending apparatus. Machining test of our ceramics was done by continous turning of cast iron and GO3 steel.

The following phases were detected by X-ray diffraction: β-Si_3N_4, α-Si_3N_4, Si_2N_2O, $Si_{12}Al_{18}O_{39}N_8$, Y_2O_3, AlN. The main com-

ponent was β -Si_3N_4 in all samples having relatively good mechanical properties. α-Si_3N_4 phase was dominant if the sintering time was too short. In some cases we obtained Si_2N_2O as major component. These results are in agreement with published data. Si_2N_2O and $Si_{12}Al_{18}O_{39}N_8$ may develop when the sintering temperature and atmosphere are inproperly chosen for the given composition[3,4], while an insufficient degree of sintering results in the formation of the other observed phases.

The appropriate phase composition may not be sufficient to obtain ceramics with good quality. Low pressing pressure weakens the bonding of the grains and lowers the value of the strength. If the binder material is burned out too quickly bubbles can develop (Fig.1.a). Our best samples showed a dense structure, with only a few pores (Fig.1.b), similar pictures were reported in the case of appropriate sintering[5].

The microanalysis revealed the evaporation of silicon at the surface. The obtained weak layer played a decisive role in the fracture (Fig.1.d). The evaporation can be hindered by embedding the specimen into a powder bed.

We noticed in many cases, that cracks causing the fracture of samples nucleated at some structural inhomogenity (Fig.1.d), in other samples a homogeneous fracture was observed (Fig.1.c).

The machining test gave a good correlation between the life time and the rupture strength. The inserts manufactured by us were suitable for 100-200 m/min speed, and 0.2-0.25 mm/rev feed.

Our results clearly reflect the usefulness of structural examinations in optimizing the manufacturing process of ceramics. A considerable amount of further efforts are required to obtain a clear picture about the structure and properties of sialons.

The participation at J.Boncók, K.Horacsek, K.Kajdi, J.Lábár and J.Zsoldos in the examinations is gratefully acknowledged.

REFERENCES

1. Adv.Mat. and Proc. 1987/1, 131 p.8.

2. R.N.Katz. Mater,Sci.Eng., 1985. 71, p.227

3. S.Boskovic, L.J.Gauckler, G.Petzow, T.Y.Tien, Powder Met.Int. 1979. 11, p.169

4. P.Greil, J.Weiss. J.Mater.Sci., 1982, 17, p.1571

5. L.K.Falk, G.L.Dunlop, R.Pompe, Mater.Sci.Eng.,1985. 71, p. 123

Fig.1. SEM micrographs of fracture surfaces of sialon samples

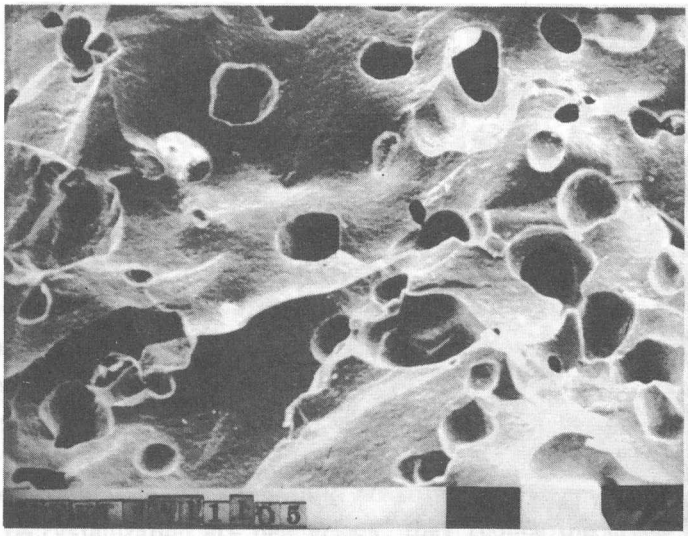

a) Bubbles in an incorrectly sintered sample
M = 130 X

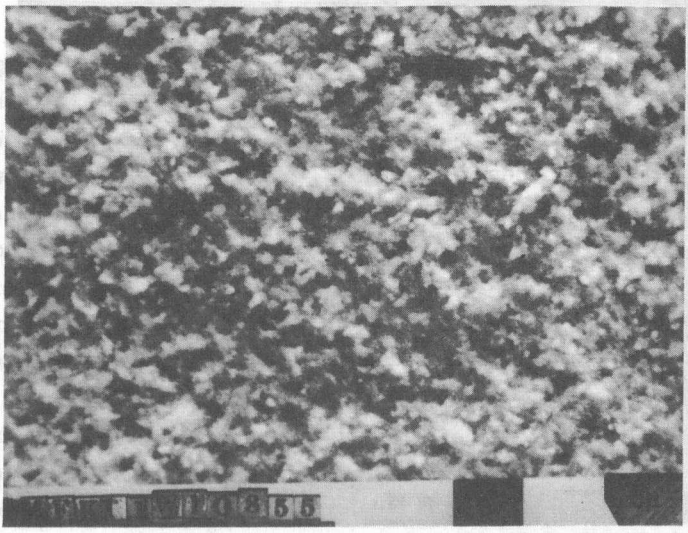

b) Symphathic structure M = 1300 X

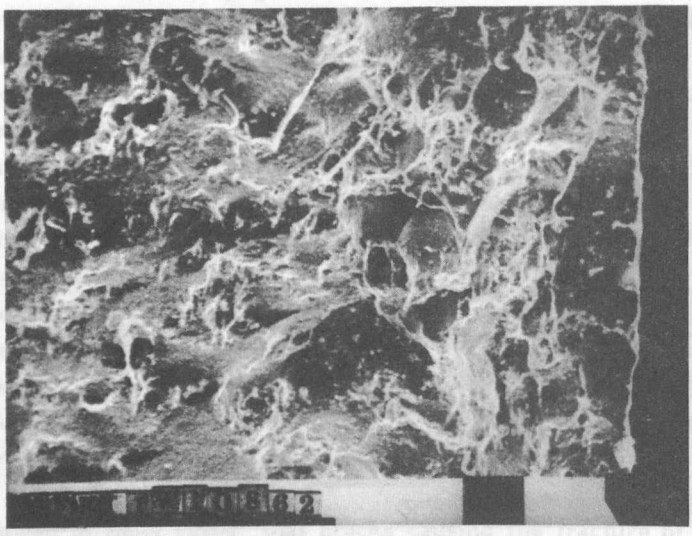

c) Homogeneous fracture M = 130 X

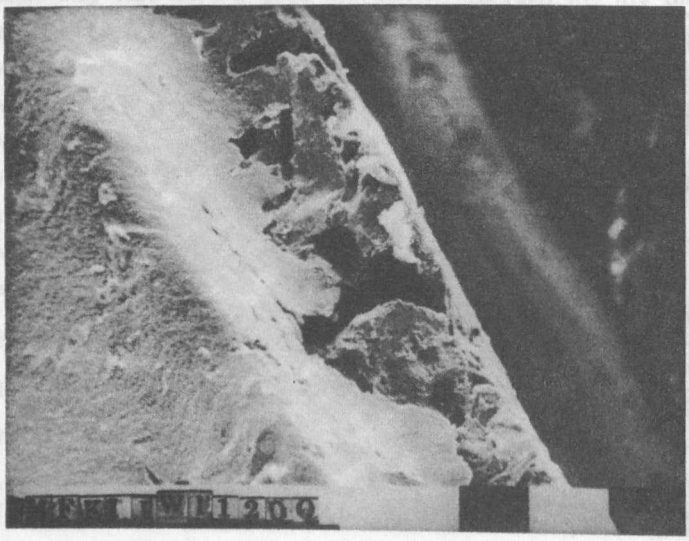

d) Fracture caused by surface faults M = 130 X

CHEMICALLY INDUCED GRAIN GROWTH

I. Gaal

It has long been known[1] that surface contamination of K-Al-Si doped tungsten with nickel and other metals (e.g. Pd, Al, Mn, Pt, Fe, Mo) induces recrystallization in heavily drawn wires at much lower temperatures then at which the interlocking coarse grain structure in uncontaminated wires develops. Also oxygen exerts a similar effect, if its partial pressure is high enough in an inert annealing atmosphere. Both kinds of chemically induced recrystallization are deleterious: they reduce the creep strength[2,3]. The latter effect has been attributed to the smaller size and lower aspect ratio of the grain structure formed during induced recrystallization.

There is ample evidence that rows of fine potassium filled bubbles restrict normal grain growth and stabilize the grain structure against abnormal grain growth in uncontaminated heavily drawn doped tungsten up to temperatures between 2000 and 2300 K[4]. The onset of abnormal grain growth in this temperature range and the subsequent development of the coarse interlocking grain structure seem to be connected with a sort of short range bodily migration of those bubbles which are dragged by the grain boundaries with extreme high forces[5]. In connection, it is important to realize that bubble migration is a necessary prerequisite of exaggerated grain growth in absence of Ostwald ripening, since an absolutely stable bubble structure should stabilize the grain structure up to the melting point of the matrix. (The Ostwald ripening of potassium filled bubbles is inhibited by the extremely low solubility ($c_{max} < 10^{-10}$) of potassium both in the tungstem matrix and in the grain boundaries.)

The substances inducing recrystallization are often called activators, because they should somehow "activate" the migration of grain boundaries by "neutralizing" the pinning effect of the bubbles[1]. The aim of the present

work is to direct attention to some mechanisms by which the activators can exert their influence, and marked grain growth can take place at as low temperatures as 1500 K.

Hitherto the interest in chemically induced recrystallization has been confined to the rationalization of the amazingly high diffusivity of some activators (Ni, Pd, Fe) along the grain boundaries during induced recrystallization as well as to the clarification of the mechanism by means of which substitutional solid solutions can be formed inside the recrystallized grains at temperatures where the bulk diffusion is frozen in[6-8]. It seems to us[9] that a segregated monolayer of the activator on the grain boundaries may account for the observed enhanced diffusivity, as it was suggested by Kaysser, Hofmann-Amtenbrink and Petzow[7]. Further on, the formation of a solid solution at frozen in bulk diffusion should be taken as a hint for diffusion induced grain boundary migration (DIGM)[10], and Kaysser, Puckert and Petzow[11] gave also direct evidences for DIGM during nickel uptake of high purity thin polycrystalline tungsten sheets at 1500 K.

Since the nature of the early annealing stages in uncontaminated heavily drawn tungsten has not been fully clarified[5,12], it seemed to be of advantage to compare at first the effect of the activators in two appropriately chosen annealing procedures. At the first kind of annealing, the activator is present in the full course of heat treatment, as usual[1, 6-8]. In this case, one may speak of chemically induced recrystallization. At the second kind of annealing, a bubble stabilized grain structure with low dislocation density is established in absence of any activator at 1800 K[5], and the effect of the activators is studied in subsequent annealings at temperatures between 1400 and 1600 K[9]. Since in this case merely grain growth takes place in the presence of the activator, we shall call this process chemically induced grain growth. It turned out[9] that the envolution of the microstructure was quite similar during both nickel (or silicon) induced recrystallization and grain growth. Thus, we may conclude that dislocations play only a secondary role in these processes. The most important common features of the two processes are: [9] (i) the change in the microstructure takes place along a relatively sharp circular reaction front, which moves from the surface to the centre of the wire; (ii) in the wake of the front, a tungsten-nickel (or a tunsten-silicon) solid solution is formed at temperatures where the lattice diffusion is frozen in; (iii) nickel (or silicon) is transported to the reaction front along the grain boundaries.

Let us realize that during chemically induced grain growth the bubble structure can cease to stabilize the grain structure against growth for two reasons:

(i) The activator uptake gives rise to an excess driving force for grain boundary migration, this abolishes the balance between Zener-drag and curvature connected driving force; consequently the grain boundaries can break away from the bubbles. Such an excess driving force can be e.g. the consequence of diffusion induced grain boundary migration[10]. (The excess driving force arises in this case from the transfer of the segregated activator atoms from the grain boundary to the lattice.)

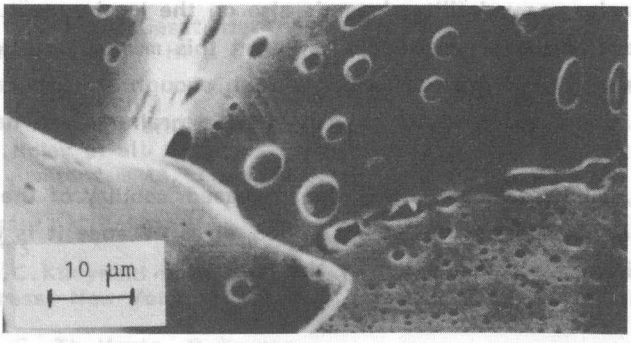

Fig.1.

(ii) The activator may enhance the mobility of the bubbles, consequently the grain boundaries can drag the "activated" bubbles along with them by the same material transport processes which occur in sintering[13]. Because Ni and Pd enhance surface selfdiffusion with many orders of magnitudes[14], also the faster bubble mobility may have its own influence at Ni and Pd activated grain growth.

Because substitutional solutes are potential agents for DIGM[10], mechanism (i) is a likely candidate for the explanation of induced grain growth in case of metallic activators. But also mechanism (ii) may play its own role, as the following two observations show. When a doped wire with a proper interlocking coarse grain structure is coated with nickel and annealed at 1500 K for few hours, no large scale grain boundary migration can be observed, but large pores are formed at the grain boundaries as shown in Fig.1 [9]. It seems to us that this is an evidence for the nickel

induced coarsening of the potassium filled bubbles, which requires marked bubble migration, as potassium is insoluble in the tungsten grain boundaries. Similarly many pores with a size of few microns were formed, when wires were heated after Ni or Si induced grain growth to temperatures above 2800 K after the removal of the Ni or Si coatings[9].

In case of oxygen induced grain growth, mechanism (ii) seems to play the dominant role, because interstitial solutes are not considered as likely agents for DIGM[10]. Oxygen may increase the bubble mobility by chemical transport reactions involving volatile tungsten oxides. The concentration difference of the tungsten oxide gas molecules inside the bubbles comes from an asymmetric shape distorsion of the bubbles attached to curved grain boundaries, as volatility depends also on the local curvature of the bubble surface. Thermochemical data support this mechanism, because the partial pressure of the volatile oxides is high enough at temperatures and oxygen partial pressures where oxygen induced grain growth have been observed.

Finally, let us emphasize that the increased mobility of the bubbles reduces also the creep strength of the doped wires because it is governed by the pinning of the dislocation by the bubbles[15].

REFERENCES

1. T.Montelbano, J.Brett, L.Castleman, L.Seigle
Trans.AIME, 242, 1973 (1968)

2. W.Schilling, H.Paschedag
Techn.-Wiss. Abh.d.Osram-Gesellschaft, Band 8,
Springer Verlag, Berlin, p.167, 1983.

3. R.Warren, C.H.Andersson
Fatique and Creep of Composite Materials (Eds. N.Lilholt and A.Taljera)
RisØ National Lab., Roskilde, p.336 1982.

4. D.B. Snow
Met.TRans. 7A, 783 (1976)

5. A.Barna, I.Gaal, O.Geszti-Herkner, G.Radnóczi, L.Uray
High Temperatures -- High Pressures 10, 197, (1978)

6. L.Kozma, E.-Th Henig
Sintering -- Theory and Practice
(Eds.: D.Kolar et al) Materials Science Monographs,
Elsevier, Amsterdam 14, 313 (1982)

7. W.A.Kaysser, M.Hofmann-Amtenbrink, G.Petzow
Sintering'85
(Eds.: G.C.Kucynski et al)
Plenun Press, New York, p.121 1987.

8. L.Kozma, E.-Th.Henig, R.Warren
Horizons of Powder Metallurgy
(Eds.: W.A.Keysser, W.J.Huppmann)
Verlag Schmid, Freiburg, p.1181, 1986

9. L.Lipták, G.Radnóczi, L.Uray, I.Gaal
Proc. 2nd Int.Conf. on Powder Metallurgy, Kiev, 1986.
(to be published)

10. R.W. Balluffi, J.W.Cahn
Acta Metall. 29, 493 (1981)

11. W.A.Kaysser, F.Puckert, G.Petzow
Powder Met. Int. 12, 188 (1980)

12. K.C. Thompson-Russel
Planseeberichte f. Pulvermetallurgie 22, 155 (1974)

13. M.A.Spears, A.G.Evans
Acta Metall. 30, 1281 (1982)

14. H.Roux, A.Piquet, G.Pralong, R.Uzan
Surface Science 71, 375 (1978)

15. P.Harmat, I.Gaal
Proc. 2nd Int.Conf. on Powder Metallurgy, Kiev, 1986
(to be published)

MICROSTRUCTURAL EVOLUTION IN THE FINAL STAGE OF SINTERING

I.Gaal and O.Horacsek

INTRODUCTION

There is ample evidence that the useful properties of sintered metallic and ceramic materials depend to a high degree on the pore and grain structure established at the end of commercial sintering. To predict technically advantageous schedules for solid state sintering and to realize the true merits of already exploited special sintering routes (e.g. rate controlled sintering), various models have been developed to explain the interplay of grain growth, pore shrinkage and pore coarsening[1].

Especially detailed models were put forward to describe normal grain growth during sintering[1]. It is assumed that the momentary grain size is determined by the momentary Zener-drag exerted by the pores attached to the grain boundaries, and consequently the rate of the normal grain growth is controlled by the annihilation and coarsening of pores. In this connection three competitive processes are of importance: annihilation of pores leading to densification, Ostwald ripening of pores without densification and bodily migration of the pores attached to the grain boundaries and their subsequent coalescence. (Moving pores will encounter other pores with quite a high probability).

When pores remain attached to moving grain boundaries, their migration is achieved by inducing flux of atoms from the leading to the trailing surface of the pores. The driving force for the atom flux is a gradient in curvature of the pore surface which is maintained by the drag of the attached grain boundary. Recent numerical simulations predict for this situation an appreciable deviation from the equilibrium shape. This shape distorsion has been also observed in ceramics with submicron sized pores in the final stage of sintering[2,3].

Since abnormal grain growth will usually inhibit any further densification, the clarification of the transition from normal to abnormal grain growth is of vital importance at the development of sintering schedules. It is well known that abnormal grain growth may be initiated by incomplete restriction of the normal grain growth or by a too broad grain size distribution, where some grains already have a size advantage required to unrestricted growth. In a sintered body the relatively large grains may have their origin either in a too broad size distribution of the primary powder particles, or in a too rapid local sintering and grain growth within some relatively large hard agglomerates which originally consisted of too fine primary particles[1].

The aim of the present work was to study the transition from normal to abnormal grain growth in sintered pure molybdenum bars.

EXPERIMENTAL

The starting material of the present work was a molybdenum bar produced on the standard route of commercial sintering with direct current heating in dry hydrogen atmosphere. The carbon and oxygen level of this material was low, i.e. no pores could be stabilized by carbon monoxid gas formed from oxygen and carbon dissolved in molybdenum[4]. The volume fraction of pores was about 5 per cent. The optical micrograph revealed the well known microstructure of sound sintered molybdenum[5]; i.e. the grain structure was homogeneous (as expected in case of normal grain growth), the average grain size amounted to 40 μms and the majority of pores was separated from the grain boundaries.

To simulate microstructural changes taking place during a prolonged sintering, samples were cut from the sintered bar and were annealed in dry hydrogen at 2100 C for 5 and 12 hours, respectively. The longer annealing time should simulate a twofold increase in sintering period at the peak temperature of sintering, if the sintering processes were governed by bulk diffusion alone. The corresponding effective increase in sintering time with respect to grain boundary and surface selfdiffusion was 15-fold and 20-fold, respectively.

It was of advantage in this study that the fracture of sintered molybden is intergranular, hence both the size and shape of pores attached to grain boundaries and the length of the grain edges could be determined

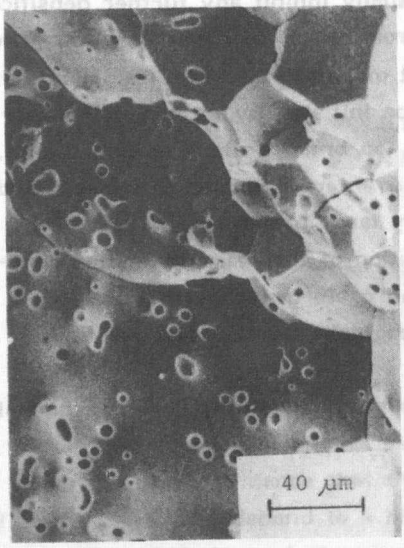

Fig.1.

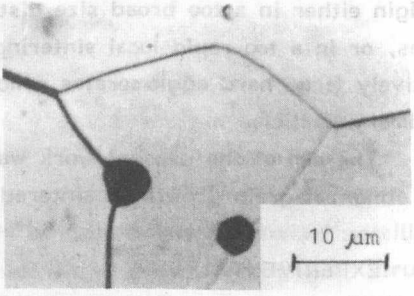

Fig.2.

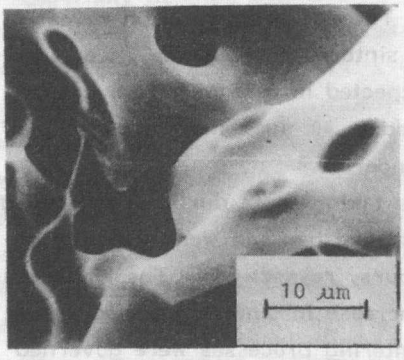

Fig.3.

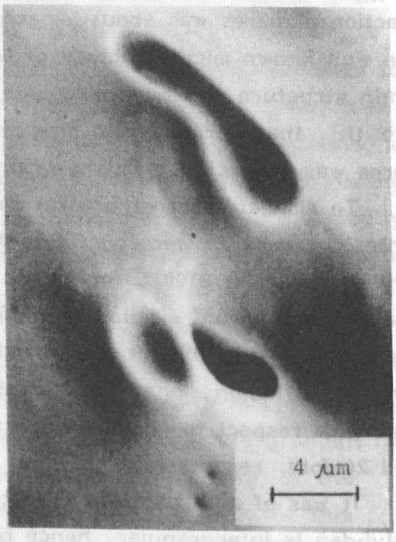

Fig.4.

by means of scanning electron micrographs (SEMs) taken on suitably tilted fracture surfaces.

RESULTS AND DISCUSSIONS

SEMs taken on the fracture surface of the "as sintered" bars revealed a homogeneous grain structure even when large areas amounting to 10 mm^2 were carefully examined at magnifications, where the edges of the individual grains could be clearly recognized. After an annealing for 12 hours at 2100°C few large grains were found on similarly large areas. These large grains were embedded into a homogeneous grain structure which was virtually identical with those of the "as sintered" material. (The boundary between a large grain and the homogeneous grain structure is shown in Fig.1.). Since these large grains were at least twice as large as the average size of the surrounding homogeneous grain structure, they should be considered as "nuclei" of the abnormal grain growth.

There are many evidences proving that the grain growth in the homogeneous grain structure is restricted by the Zener-drag of the pores. The most vivid evidence is shown in Fig.2., where a pore pulls back a grain boundary segment very effectively. This very effect appears also on the fracture surfaces as a local "hill" on the grain boundary with an opened up pore at the top of the "hill" (Fig.3.). The observed average grain size ($D \approx 40$ μm) is in the order of magnitude of the limiting grain size predicted by Zener's rule ($D_L = Cd_p/V_p$), since the average pore size, d_p, was about 4 μm and the porosity, V_p, amounted to 0.05. D and D_L will become equal, when C is considered as a fitting parameter, having a value of 0.5. This fitting seems to be acceptable according to the current estimates of this quantity[6].

The vanishingly small rate of the normal grain growth in the homogeneous part of the grain structure should be, therefore, a consequence of the stability of the pores attached to the grain boundaries. This conclusion is in accordance with the estimated rate of the shrinkage and Ostwald ripening of the pores attached to the grain boundaries[7], because even the smallest pores with appreciable frequencies were relatively large (their diameter was larger than 2 μm). Also the drag of the pores allows only a slow migration rate amounting to 0.1 μm/hour[3].

We believe that Fig.2. and Fig.4. show two independent evidences for pore migration:

(i) The optical micrograph in Fig.2 shows a pore on a grain boundary which seems to suffered that kind of shape distorsion which is predicted by the theory of dragged pores, i.e. the curvature of the pore surface in the direction of the supposed migration of the grain boundary (leading surface) is smaller than the curvature of the pore surface on the opposite part of the pore (trailing surface).

(ii) According to the SEM of Fig.4., the grain boundary curvatures change sign in the vicinity of pores which are close to each other with respect to their diameter. Therefore there is a driving force which will push the two pores together. On the same micrographs also an elliptical pore appears and the grain boundary curvatures in its vicinity suggest that this pore resulted from the coalescence of two pores.

At the present we are not able to make any quantitative estimates for the relative importance of the two routes by which the nuclei of the abnormal grain growth were formed.

REFERENCES

1. Exner, H.E., Arzt, H.
Physical Metallurgy (Eds.: R.W.Cahn, P.Haasen)
North Holland Physics Publishing Co. , 1983. Amsterdam, p. 1885

2. Hsueh, C.H., Evans, A.G., Coble, R.L.
Acta Metall. 30 (1982) 1269

3. Spears, M.A., Evans, A.G.
Acta Metall. 30 (1982) 1281

4. I.Gaal, O.Horacsek
Sintering'85
(Eds. G.C.Kuczynski et al), Plenum Press New York, 1987, p.317

5. Benesovksy, F.
Pulvermetallurgie und Sinterwerkstoffe,
Metallwerk Plansee, Reutte (Austria) 1986, p.46

6. Louat, N.
Acta Metall. 30 (1982) 1291

7. Swinkels, F.B., Ashby, M.F.
Acta Metall. 29 (1981) 259 .

DEVELOPMENT OF ELECTROMAGNETIC FLAW DETECTION SYSTEM

P.Ivanov, Z.Demendy, F.Tóbiás, H.Borody, I.Skopál

Continuing the research and development experiences on the field of nondestructive testing during the years 1984-1987 a family of electromagnetic flaw detection systems have been developed. The detecting apparatus is equally capable both for tubes and rods as well. By means of flaw detection systems an extensive study have been made on ferrous and nonferrous tubes and rods having various profiles and diameter. The welded area of several types of tubes have also been investigated.

During our experiences

the magnetic flux leakage
the magnetoinductive
and the eddy current

methods have been applied as a base of the flaw detection methodology. The test techniques were realized with various coil systems and electrical setups. The measurement techniques used are referred to as

encircling coil
and pick-up probe

techniques according to the sensor type.

MATHEMATICAL MODEL FOR THE EDDY CURRENT METHOD

To calibrate a measuring apparatus one has to know the impedance change of a coil due to the presence of a flaw in the conductor. In our measuring arrangements there is no eddy current flowing in the direction parallel to the axis of the receiver coil. Using appropriate cylindrical coordinates and introducing the complex stream function $\chi=\chi(r, \phi, z)$ defined via the relations

$$A_r = -\frac{1}{r}\frac{\partial \chi}{\partial \phi}, \quad A_\phi = \frac{\partial \chi}{\partial r}$$

the two coupled Helmholtz-type equations for the radial and the azimuthal components of the vector potential (A_r and A_ϕ, resp.) can be condensed

into a single Helmholtz-type equation. Moreover, the extra condition div A = 0 is automatically satisfied. The impedance change of the coil system can be obtained by an integration of the function X on the volume of the coils.

The Figs. 1. and 2. show complex impedance diagrams for a cylindrical and a pick-up coil, respectively. Here L_o is the inductivity of the empty coil, ΔR and ΔL are the real and imaginary part of the impedance change, respectively, f is the Wolman-frequency, moreover L_1 is the lift-off value.

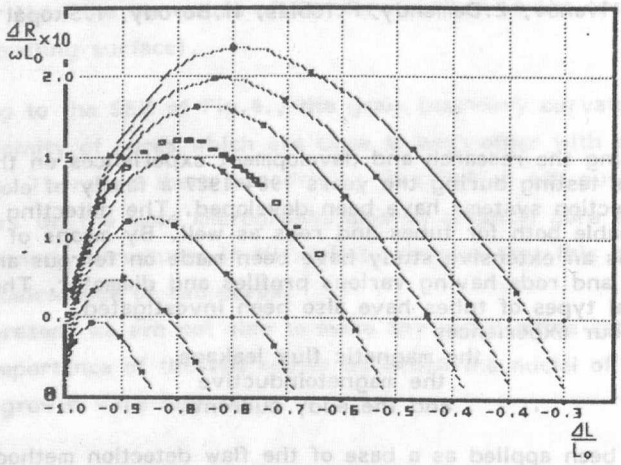

Fig.1. Impedance diagram for a cylindrical coil encircling a conducting cylinder. Each curve corresponds to a given coil geometry (length, inner and outer radii)

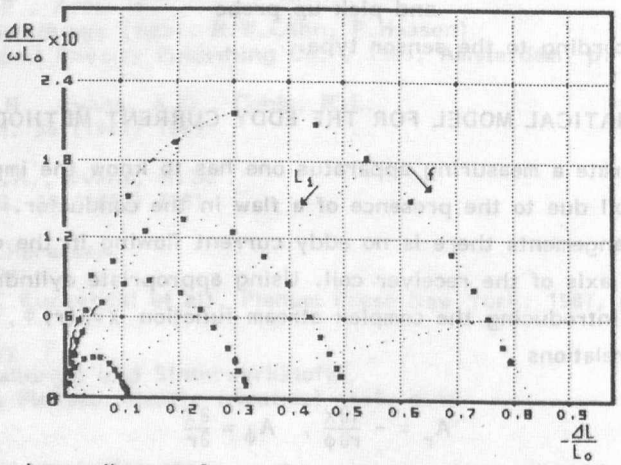

Fig.2. Impedance diagram for a pick-up coil with various lift-off values L_1

TEST METHODS AND THE INSTRUMENT

During magnetization the magnetic state of a material can most easily be characterised by means of the magnetic flux lines. Any material discontinuity (e.g. flaws, holes) causes considerable distortion in the flux-line structure of the defect-free material. In the case of a defect a part of the flux lines is by-passed into the air and so called leakage flux pattern sets up due to the local magnetic poles on the defect surface.

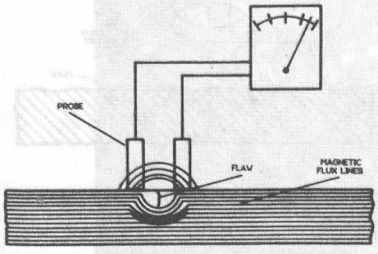

It is important to note that this method is only applicable to ferrous materials and to flaws perpendicular to the magnetization. The object under test must be magnetized near to the saturation.

We applied this method to testing ferrous rods both for surface and internal flaws. The orientation of the applied static magnetic field was parallel to the axis of the rod to be isspected. There were numerous pick-up probes[1] around the workpiece for detecting leakage flux. The probes were assembled in a supporting cassette. The distance of the probes from the surface of the specimen under test could continuously be adjusted.

Eddy currents will be induced in a metallic object placed into a time-dependent magnetic field. The spatial distribution of the eddy currents in rather sensitive to the geometry of the sample as well as to the frequency of the applied exciting field. The considerable redistribution of the eddy current stream lines in the vicinity of a flaw leads to a variation in the complex impedance of the detecting coils.

The magnetoinductive effect occurs together with eddy currents in ferrous materials, since a material discontinuity deforms the flux structure, too. It is important to note that the eddy current and the magnetoinductive methods are capable to detect near-surface defects.

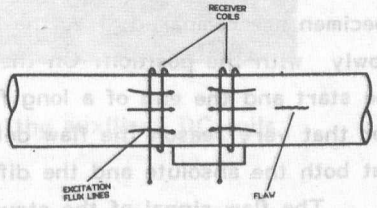

Our instrument contains both encircling -coil and pick-up probe techniques based on these methods[2]. The workpiece under test is almost magnetized to the saturation so as to decrease disturbing signals. Thus, the variation of the magnetic properties of the workpiece due to e.g. locked-in stress, hardness, etc. varying along the longitudinal axis of the specimen have no effect on the flaw detection. However, all the noise signals due to spatial variations of dimensions and shape of the workpiece, the inhomogeneous temperature distribution in the specimen, the deviation of the examined object from the coaxial position, etc. may cause crack-like response signals in sensing coil.

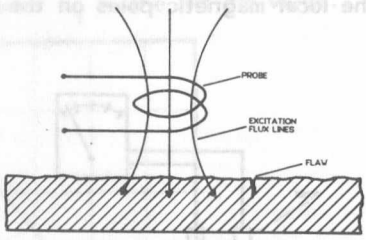

The concept of the design of our instrument was that all these measurements should be carried out on the same measurement site. The required measuring method can be selected by inserting the proper sensor-cassette in the magnetization head. A linear pass of the workpiece through the detection head along the inspection axis causes testing of the workpiece for cracks and flaws. The instrument utilizes DC coils arranged to generate an auxiliary magnetic field parallel to the longitudinal axis of the object under test. This static magnetic field is able magnetically to saturate the largest specimen of a given design.

MEASUREMENT AND SENSITIVITY

The absolute measurement method is very sensitive to the most kind of noises since the difference between a fixed sample free from defect and the moving workpiece under test is measured.

In the case of the differential method two near portion of the same specimen are compared, i.e. the noise signals are eliminated as they vary slowly with the position. On the other hand this method can only detect the start and the end of a long flaw with constant depth.
For that very reason the flaw detection system can simultaneously carry out both the absolute and the differential measurements.

The flaw signal of the structural NDT methods is generally not proportional to the depth of the flaw. The eddy current method gives signals depending not only on the depth but even on the direction and the shape of flaws. In the case of the magnetoinductive measurement the magnitude

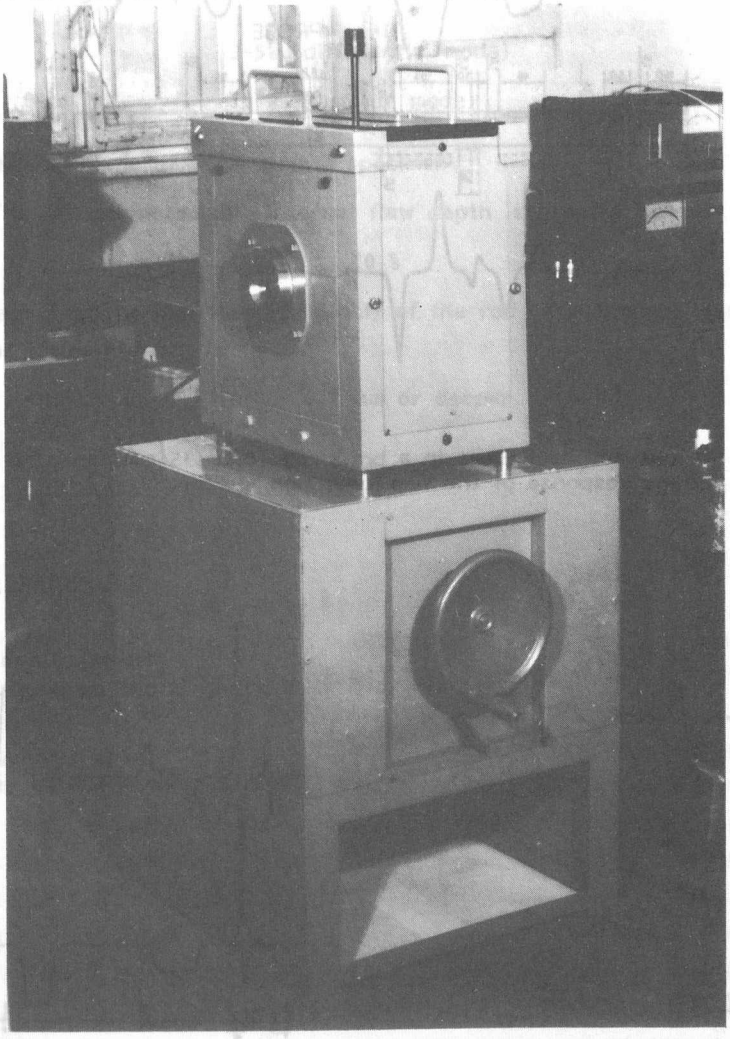

Fig.3. Detection head containing the auxiliary DC coils

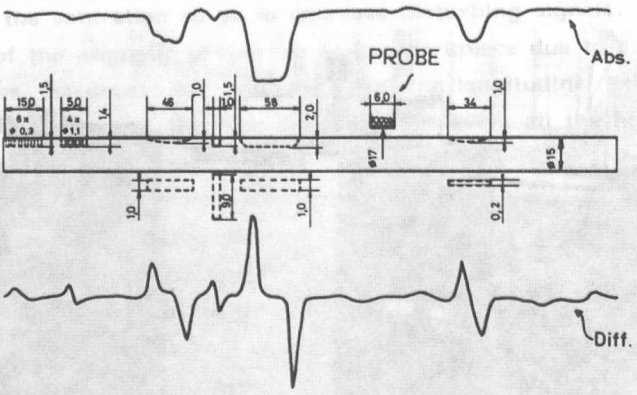

Fig.4. Various artificial flaws in a brass rod (diam.15 mm) and the output voltage response of the flaw detection system.

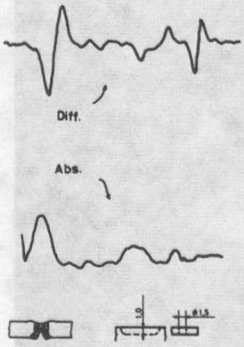

Fig.5. The recorded test result in the case of a welded rectangular tube with two artificial flaws and a seam defect on the internal surface

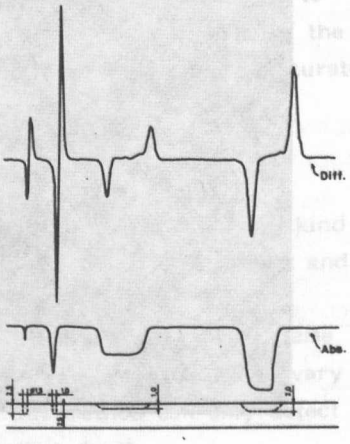

Fig.6. Signals due to various artificial flaws in a steel rod (diam. 8 mm)

of the flaw response can be influenced by the static auxiliary magnetization. Only flaws of the same type result in signals proportional to their depths.

We can generally state that the minimal depth of a detectable flaw is

3-5% (differential mode)

10 % (absolute mode)

with respect to the diameter of the specimen.

The minimal detectable internal flaw depth is greater than

10 %

with respect to the diameter (diagonal) of the rod. The surface flaws can be found if their depth is

0.1 - 0.2 mm or deeper.

REFERENCES

1. Tóbiás, F. et al:
J. Magnetism and Magnetic Materials, 41, (1984) 431

2. Ivanov, P. et al
Mérés és Automatika, 2, (1987) 60

SIMPLE ELECTRODIALYTIC METHOD FOR THE DECOMPOSITION OF HYDROLYZING SALTS

R.Oláh, K.Vadasdi

ABSTRACT

The recovery process of acid and base constituents of various salts composed of a strong base and a weak acid was investigated in a double cell electrodialytic system. A simple approximative relationship is presented to estimate the economically reasonable decomposition ratio of a certain salt solution if the dissociation constant of the weak acid component and the initial concentration of the salt solution are known.

INTRODUCTION

The effluent treatment applications of membrane separation technologies have won an increasing interest in the eighties. The recovery of waste salts from various effluents have become an essential question for the users of many technologies. However there is a wide range of industrial processes where not only the recovery of waste salt is needed, but the acid and base constituents should be regenerated from a waste salt solution. In these cases usually electrodialysis offers a unique method to decompose the salt contents of waste streams. Various electrodialytic methods are applied or suggested for this purpose. However, these methods apply three or more cells or bipolar membranes to reach appropriate decomposition ratio at high current efficiency[1-5].

The electrodialytic salt decomposition processes are based on the ion-transport through selective semipermeable membranes. The decomposition of various salts can be carried out by removing either the anionic or the cationic component of the salt through the appropriate membrane obtaining the corresponding acid on the one side and base on the other side of the membrane.

In this work the decomposition possibility of various salts was investigated in a simple double cell electrodialyzer.

RESULTS

When one of the ionic components of a salt is removed from its solution through a permselective membrane, H^+ ions replace the cations and OH^- ions replace the anions passed so the pH of the salt solution either decreases or increases during the process. Therefore the ion transport through the membrane is largely affected by the parallel transport of H^+ or OH^- ions. It is known that the parallel transport of H^+ or OH^- ions cannot only decrease the current efficiency of the cation or anion transport through a cation or anion selective membrane but can even prevent the full decomposition of the salt. Our aim was to study the correlation between the dissociation constant of the not transported component of the salt and the reasonable decomposition ratio that can be reached without considerable increase of the parallel ion transport.

Considering the case of the cation transport we found: when the dissociation constant of the constituent acid was high (e.g. $NaNO_3$) the pH of the anolyte dropped quickly as a small part of the cations left the anode cell. The formed strong acid acidified the anolyte immediately at the beginning of the process thus causing a rapid decrease of the current efficiency. The corresponding acid and base cannot be fully regenerated from salts of this type by a double cell method. Three or four compartments or possibly bipolar membrane process should be applied to make the regenerating process more effective.

Our investigations showed, when the acid component of the salt to be regenerated was a weak acid having a dissociation constant less than 10^{-2}, the decomposition process could be carried out under much better conditions even in a double cell system. As a demonstration, Fig.1. shows the transport parameters of sodium ions during the decomposition process of sodium acetate solution. In this case, a large part of the H^+ ions generated in the anode process were bound by the formed acetic acid because of its low dissociation constant. Therefore 87% of the sodium content of the sodium acetate can be recovered with a very high (practically 100%) current efficiency. The sodium acetate content of the regenerated acetic acid solution in this case is about 13%. As shown on Fig.1. the salt content of the acid can be decreased further but at a much lower current efficiency.

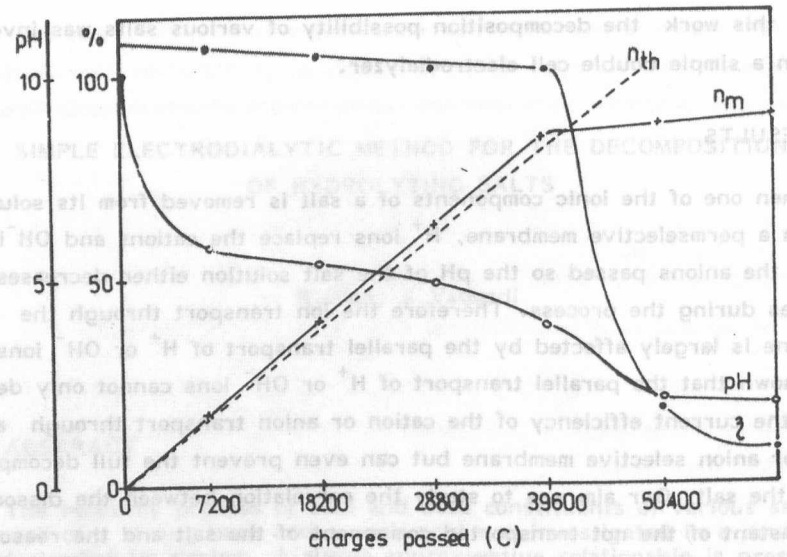

Fig.1. The pH, current efficiency - η (%), theoretical - n_{th}(%) and measured decomposition ratio - n_m(%) as a function of charges passed in the case of a 1 mol/dm^3 sodium acetate solution.

If the dissociation constant of the weak component of the salt was very low as in the case of boric acid ($K = 7.3 \times 10^{-10}$), a large decomposition ratio was obtained. During the decomposition process of a sodium tetraborate solution practically full sodium recovery can be reached, and the regenerated boric acid contains only a few per cents of sodium salt.

The second and third dissociation constants of the di- or tribasic acids are generally in the range of the dissociation constants of weak acids even if they are considered as strong acids. Consequently, the conversion of the salts of various polybasic acids into their acid salts (eg. $Na_2SO_4 \rightarrow NaHSO_4$, $Na_3PO_4 \rightarrow Na_2HPO_4$) can be carried out in a simple double cell system in most cases under good conditions.

DISCUSSION

During the regenerating process of salts composed of a strong base and a weak acid a mixed solution of a salt and a weak acid is formed in the anode cell of the electrodialytic equipment described above. This solu-

tion can essentially be regarded as a buffer solution having at least two sorts of cations: cation of the salt and H^+ ions. The parallel transport of H^+ ions, however, should be considered as an ineffective ion transport because it decreases the current efficiency of the decomposition process. The dominant factors from the point of view of the parallel ion transport are the concentration and the mobility ratio of the ionic components having similar charges. The ionic mobility of H^+ ions is about ten times greater than the mobilities of other cations, so the parallel H^+ ion transport can compete with the main cation transport even at a very low relative concentration.

If the applied cation selective membrane has no selectivity difference for the H^+ ion and the K^+ cation the parallel H^+ ion transport is presumably negligible if the $[K^+] / [H^+]$ concentration ratio is $\geq 10^2$ because of the large difference between the ionic mobilities. We can assume that the current efficiency of the cation transport starts to decrease at a concentration ratio of 10^2. The curves of the decomposition ratios (n_m) have break points at this concentration ratio, the slope of the curves begins to decrease. The decomposition ratio observed at this point may be called the critical (n_c) decomposition ratio.

The concentration of H^+ ions in a mixed solution of a weak acid and its salt can be calculated in a simple way if the dissociation constant of the acid is known.

Assuming that the amount of anion originating from the dissociation of the weak acid can be neglected we can derive the following simple relationship.

$$\frac{(100-n_c)^2}{10^4 n_c} = \frac{K}{C_s^o} \qquad (1)$$

where n_c is the critical decomposition ratio, C_s^o is the initial concentration of the salt solution to be decomposed and K is the dissociation constant of the weak acid component. This equation is also valid for the case of salts composed of a strong acid and weak base, but in this case the K corresponds to the dissociation constant of weak base.

Of course Eq.(1) gives only an approximate relationship and it seems to give an estimate of the reasonable decomposition ratio for a certain salt solution composed of a strong base and a weak acid or a weak base and

and/or strong acid if the dissociation constant of the weak component and the initial concentration of the salt solution are known.

The applicability of Eq.(1) is demonstrated in Table 1.

TABLE 1.

THE MEASURED AND CALCULATED CRITICAL DECOMPOSITION RATIOS IN CASE OF VARIOUS SALT SOLUTIONS

Salt to be decomposed	K	C_s^o mol/dm^3	$n_{th,c}$ %	$n^x_{th,c}$ %	$n_{m,c}$ %
Sodium acetate	1.8×10^{-5}	1.00	95,8	96,8	87.0
Sodium tetraborate	7.3×10^{-10}	0.488	99.99	100.0	100
Sodium dihidrogen phosphate	7.5×10^{-3}	2.25	38.2	42.0	44.0
Sodium format	1.8×10^{-4}	1.00	87.5	88.8	92.5

K Dissociation constant of the weak acid component of the salt

C_s^o Initial concentration of the salt solution investigated

$n_{m,c}$ Measured critical decomposition ratio

$n_{th,c}$ Calculated critical decomposition ratio

$n^x_{th,c}$ Calculated critical decomposition ratio corrected by the factor f

Calculated and measured critical decomposition ratios of different salt solutions are shown which can be reached without considerable decrease of the current efficiency by the parallel ion transport. It has to be mentioned that the anion concentration of the solution is continuously increasing during the decomposition process in the anode cell as a result of the O_2 gas formation and the water transport through the membrane. Consequently a better correlation can be obtained if the initial concentration in Eq.(1) is corrected by a factor (f) which takes into account the volumetric changes of the anolyte.

As shown in Table 1 the reliability of Eq.(1) is in some cases not better than 10%. Nevertheless, it may help to make a decision without experimental work whether the regeneration of a certain waste salt solution can be carried out presumably economically in a double cell system or other methods should be preferred. The above considerations suggest, the smaller the dissociation constant of the weak acid component of the salt is, the greater the decomposition ratio and the less the residual salt content in the regenerated acid will be. it should be mentioned that there are cases when the electrolytic decomposition of a salt is limited by the low conductivity of the formed acid solution and not by the parallel H^+ ion transport. Salts of this type have a weak component with a very low dissotiation constant. The degree of dissociation is very small in pure solutions of these weak acids or bases, therefore the conductivity of their solution drops quickly as the salt content of the acid solution formed decreases.

Furthermore it has to be added, that Eq.(1) can not be used even for rough estimates if association reactions can take place in the anolyte with decreasing pH. During association reactions both the concentrations and the character of the anionic species vary. In these cases further considerations are necessary to estimate the decomposition ratio that can be expected in a double cell system.

REFERENCES

1. N.M. Smirnova, b.N.Laskorin, J.S.Mishukova, A.V.Borisov
The application of electrodialysis with inoexchange membranes for treatment of sodium sulfate solutions,
Desalination, 46 pp.197-201 (1983)

2. M.Kato, S.Sato,
US .Pat. 3 704 218 (1972)

3. K.Nagasubramanian, F.P.Chlanda, K.J. Liu
Use of bipolar membranes for generation of acid and base - an engineering and economic analysis
J. of Membrane Sci., 2 pp.109-124 (1977)

4. I.C. Bassignana, H.Reiss
Ion Transport and water dissociation in bipolar ion exchange membranes
J. of Membrance Sci., 15 pp.27-41 (1983)

5. K.Mani, F.P. Chlanda,
US. Pat. 4 504 373 (1985)

SEPARATION OF Co-Ni WITH PC 88A AND CYANEX 272 IN SULPHATE AND CHLORIDE MEDIA

Ildikó Szilassy, Károly Vadasdi

INTRODUCTION

Sulphate and chloride solutions are conventional aqueous media for the separation of cobalt and nickel with solvent extraction processes. Recently developed organophosphorous acid reagents based on alkyl phosphonic and alkyl phosphinic acids (e.g. PC 88A, Cyanex 272) permit a more efficient separation of Co from Ni in sulphate solution than was possible with the established extractant di-2-ethylhexyl phosphoric acid (D2EHPA). In the last years a few papers[1,2,3] have been appeared on the solvent extraction separability of Co and Ni with 2-ethyl-hexyl phosphonic acid mono-2-ethyl-hexyl ester (PC 88A) and di-/2,4,4-trimethylpentyl/phosphinic acid (Cyanex 272) reagents. The author of reference[1] qualitatively shows that in media containing Cl^- and SO_4^{2-} ions the formation of Co and Ni chloro and sulphato complexes must be taken into account, however no significant change in the separation coefficients can be expected between the two metal ions since the stability constants of the corresponding chloro and sulphato complexes are very similar. As a result of metal-chloro and -sulphato complex formation the Extraction % - pH curves measured at different chloride and sulphate concentrations will be shifted as Figs. 1-4 show. The authors of papers[3] and [4] explain these shifts so that the measured pH values in such solutions are lower than their actual values. In this paper we show that the extraction of Co and Ni with PC 88A and Cyanex 272 reagents from media containing Cl^- and SO_4^{2-} ions can be quantitatively described considering only the chloro and sulphato complexes of these elements. On the basis of this model it can be shown that a significant change in the separation coefficient of the Co and Ni can be ex-

pected only at very high (> 3 mol/dm^2) Cl^- ion concentrations due to the formation of the $CoCl_4^{2-}$ species.

REAGENTS, EXPERIMENTS

Cyanex 272 sample was a gift of Cyanamid (Canada) Ltd, for which the authors are very grateful. PC 88A was the product of Daihachi Chemical Industry Co. (Japan). Shell MSB 210 solvent has been used and 2.5 vol% tributyl phosphate (TBP) as phase modifier. The effect of the latter material to the extraction of Co and Ni could be neglected in the frame of the model to be described, due to its relatively low concentration. All other reagents used were of analytical grade. The distribution of Co and Ni was measured with shaking funnel experiments at room temperature. Equal volumes of solvent and aqueous solution were contacted for 5 minutes. After separating the phases the metal content of the aqueous phase was analysed with AAS. In the course of our studies the distribution of Co and Ni has been investigated between the organic solvent and aqueous solution of nearly constant ionic strength (I=5.0) containing perchlorate - chloride or perchlorate-sulphate ions as a function of pH at different chloride and sulphate concentrations.[6]

Our experimental data are shown on Figs. 1-4. It can be seen that with increasing chloride or sulphate concentrations the Extraction % - pH curves shift parallel towards higher pH values. Plotting the log D values as a function of pH straight lines can be obtained in wide pH ranges. The slope of these curves was 1.00±0.05 in case of Ni - PC 88A and Ni - Cyanex 272 systems both in chloride and in sulphate solutions. The slope of different Co systems varied between 1.25 - 1.70 indicating a more complex process. According to reference[1] taking into account monomeric reagent concentrations integer numbers can be obtained in case of Co.

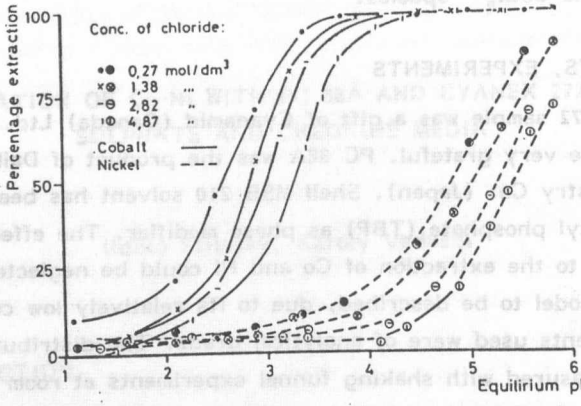

Figure 1. Extraction of cobalt and nickel by Cyanex 272 at different chloride concentrations

Organic phase: 20 vol% Cyanex 272, 2.5 vol% TBP in MSB 210

Aqueous phase: 0.051 mol/dm^3 Co, 0.086 mol/dm^3 Ni as chlorides, NaCl, $NaClO_4$; I = 5.0

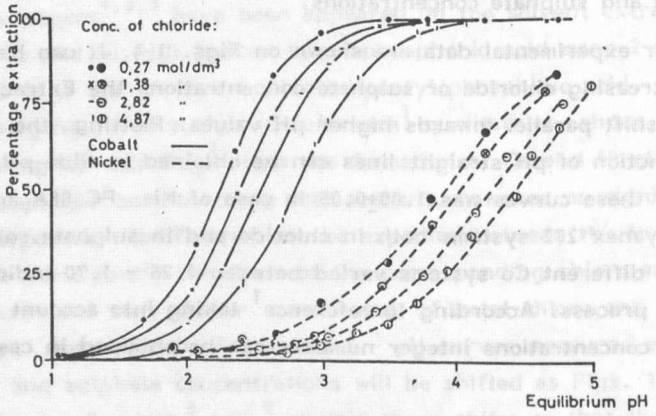

Figure 2. Extraction of cobalt and nickel by PC 88A at different chloride concentrations

Organic phase: 20 vol% PC 88A, 2.5 vol% TBP in MSB 210

Aqueous phase: 0.051 mol/dm^3 Co, 0.086 mol/dm^3 Ni as chlorides, NaCl, $NaClO_4$; I = 5.0

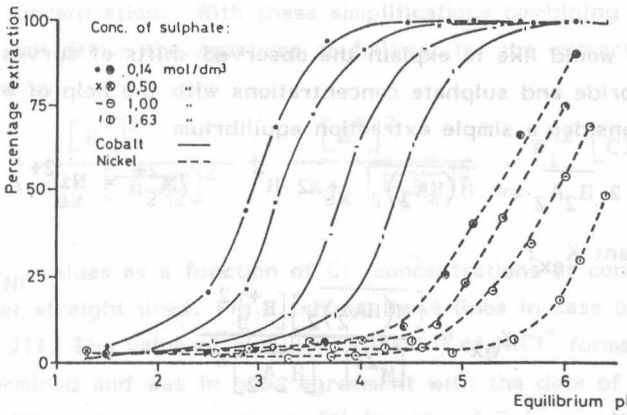

Figure 3. Extraction of cobalt and nickel by Cyanex 272 at different sulphate concentrations

Organic phase: 20 vol% Cyanex 272, 2.5 vol% TBP in MSB 210

Aqueous phase: 0.051 mol/dm^3 Co, 0.086 mol/dm^3 Ni as sulphates, Na_2SO_4, $NaClO_4$; I = 5.0

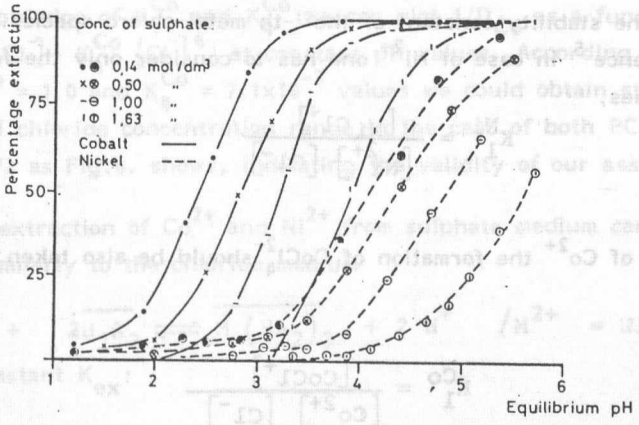

Figure 4. Extraction of cobalt and nickel by PC 88A at different sulphate concentrations.

Organic phase: 20 vol% PC 88A, 2.5 vol% TBP in MSB 210

Aqueous phase: 0.051 mol/dm^3 Co, 0.086 mol/dm^3 Ni as sulphates, Na_2SO_4, $NaClO_4$; I = 5.0

COMPUTATIONS, RESULTS AND DISCUSSIONS

Now we would like to explain the observed shifts of curves with increasing chloride and sulphate concentrations with the help of a simple model. We consider a simple extraction equilibrium

$$M^{2+} + 2\,\overline{H_2A_2} \rightleftharpoons \overline{M(HA_2)_2} + 2\,H^+ \qquad /M^{2+} = Ni^{2+},\ Co^{2+}\ /$$

with a constant K_{ex}:

$$K_{ex} = \frac{\left[\overline{M(HA_2)_2}\right]\left[H^+\right]^2}{\left[M^{2+}\right]\left[\overline{H_2A_2}\right]^2} \tag{1}$$

The distribution constant D in chloride medium is as follows:

$$D = \frac{\left[\overline{M(HA_2)_2}\right]}{\left[M^{2+}\right]\left(1 + \sum_i K_i^M \left[Cl^-\right]^i\right)} \tag{2}$$

here K_i^M is the stability constant of the i-th metal-chloro species. According to reference [5] in case of Ni^{2+} one has to consider only the formation of $NiCl^+$ species,

$$K_1^{Ni} = \frac{\left[NiCl^+\right]}{\left[Ni^{2+}\right]\left[Cl^-\right]} \tag{3a}$$

while in case of Co^{2+} the formation of $CoCl_4^{2-}$ should be also taken into account:

$$K_1^{Co} = \frac{\left[CoCl^+\right]}{\left[Co^{2+}\right]\left[Cl^-\right]} \tag{3b}$$

$$K_4^{Co} = \frac{\left[CoCl_4^{2-}\right]}{\left[Co^{2+}\right]\left[Cl^-\right]^4} \tag{3c}$$

In our experimental range the total analytical concentration of Cl^- ion and of reagent H_2A_2 is much higher than the concentration of Co^{2+} or Ni^{2+}

therefore their equilibrium concentrations are nearly equal to their total (analytical) concentrations. With these simplifications combining eqs. (1), (2), (3) we can derive the equations as follows: for the extraction of Ni^{2+} from Cl^- medium

$$\frac{1}{D_{Ni}} = \frac{[H^+]^2}{K_{ex}\,[\overline{H_2A_2}]^2} + \frac{[H^+]^2}{K_{ex}\,[\overline{H_2A_2}]^2} \cdot K_1^{Ni}\,[Cl^-] \qquad (4)$$

Plotting $1/D_{Ni}$ values as a function of Cl^- concentrations at constant pH values we get straight lines. Fig.5. shows these lines in case of PC 88A and Cyanex 272. The value of stability constant of $NiCl^+$ formation can also be determined and was in good agreement with the data of the literature [5]. A plot corresponding to eq. (4) in case of Co^{2+} resulted straight lines only at lower Cl^- concentrations indicating the significance of $CoCl_4^{2-}$ species too. Taking into account this species we can derive an equation as follows:

$$\frac{1}{D_{Co}} = \frac{[H^+]^2}{K_{ex}\,[\overline{H_2A_2}]^2}\left(1 + K_1^{Co}\,[Cl^-] + K_4^{Co}\,[Cl^-]^4\right) \qquad (5)$$

In the knowledge of K_1^{Co} and K_4^{Co} we can plot $1/D_{Co}$ as a function of $1 + K_1^{Co}\,[Cl^-] + K_4^{Co}\,[Cl^-]^4$ at constant pH values. According to ref.[5] using $K_1^{Co} = 1.0$ and $K_4^{Co} = 7.1\times10^{-3}$ values we could obtain straight lines in the full chloride concentration range in the case of both PC 88A and Cyanex 272 as Fig.6. shows, indicating the validity of our assumptions.

The extraction of Co^{2+} and Ni^{2+} from sulphate medium can be described similarly to the chloride medium

$$M^{2+} + 2\overline{H_2A_2} \rightleftharpoons \overline{M(HA_2)_2} + 2\,H^+ \qquad /M^{2+} = Ni^{2+},\ Co^{2+}/$$

with a constant K_{ex}:

$$K_{ex} = \frac{[\overline{M(HA_2)_2}]\,[H^+]^2}{[M^{2+}]\,[\overline{H_2A_2}]^2} \qquad (6)$$

However the formation of an adduct species between the MSO_4 and the reagent must be also taken into account.

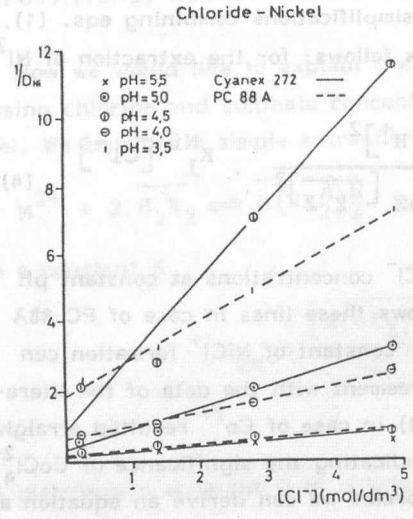

Fig.5. Plot of Ni^{2+}-Cl^- system according to eq.(4)

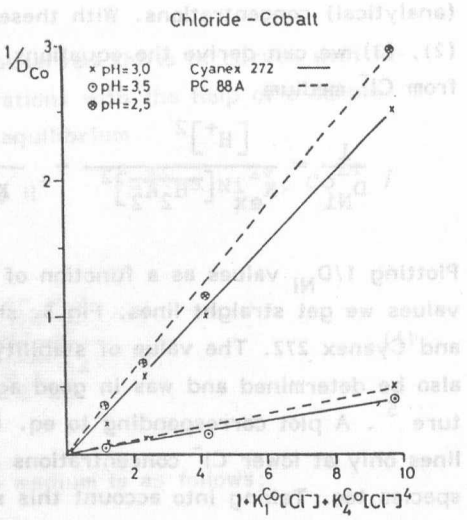

Fig.6. Plot of Co^{2+}-Cl^- system according to eq.(5)

$$MSO_4 + \overline{H_2A_2} \rightleftharpoons \overline{MSO_4 \cdot H_2A_2}$$

$$K_a = \frac{\left[\overline{MSO_4 \cdot H_2A_2}\right]}{\left[MSO_4\right]\left[\overline{H_2A_2}\right]} \qquad (7)$$

Therefore the distribution constant D in sulphate medium is as follows:

$$D = \frac{\left[\overline{M(HA_2)_2}\right] + \left[\overline{MSO_4 \cdot H_2A_2}\right]}{\left[M^{2+}\right]\left(1 + K_s \cdot \left[SO_4{}^{2-}\right]\right)} \qquad (8)$$

K_s is the stability constant of the metal-sulphato species.

$$K_s = \frac{\left[MSO_4\right]}{\left[M^{2+}\right]\left[SO_4{}^{2-}\right]} \qquad (9)$$

Combining eqs. (6), (7), (8) and (9) we get

$$D = \alpha \frac{1}{1+U} + \beta \frac{U}{1+U} \qquad (10)$$

where

$$\alpha = \frac{K_{ex} \cdot \left[\overline{H_2A_2}\right]^2}{\left[H^+\right]^2} \qquad \beta = K_a \cdot \left[\overline{H_2A_2}\right] \qquad U = K_s \cdot \left[SO_4^{2-}\right]$$

Rearrangeing (10) we get

$$D\,(1+u) = \alpha + \beta\, U \qquad (11)$$

Plotting D(1+U) values as a function of U at constant pH values we get straight lines (Fig.7.,8). For the calculation of U the following stability constants of Co^{2+} and Ni^{2+} sulphato species have been used: $K_s^{Co} = 794$ $K_s^{Ni} = 2.7$

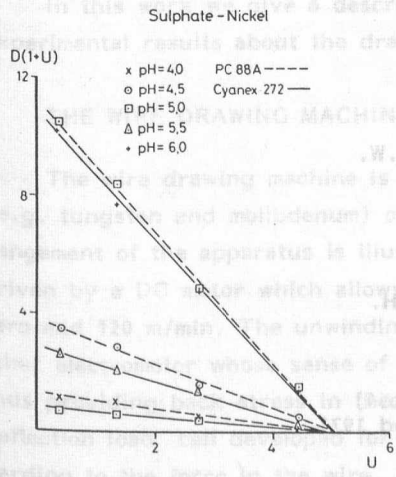

Fig.7. Plot of Ni^{2+}-sulphate system according to eq.(11)

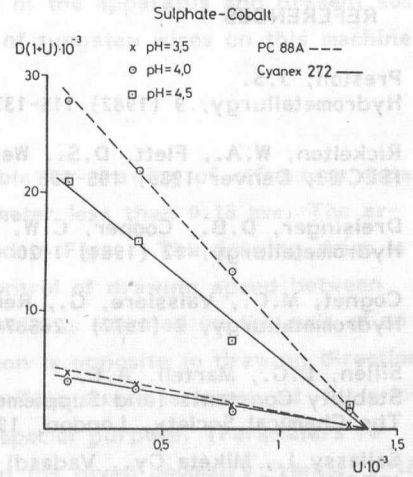

Fig.8. Plot of Co^{2+}-sulphate system according to eq.(11)

CONCLUSION

Investigating the extraction of Co^{2+} and Ni^{2+} by PC 88A and Cyanex 272 extractants the extraction %-pH curves shift parallel towards higher pH values with increasing chloride or sulphate concentrations at constant ionic strength.

With the help of a simple model these shifts have been described quantitatively for chloride solutions by the formation of $NiCl^{+}$, $CoCl^{+}$, and $CoCl_4^{2-}$ complexes.

In sulphate solutions the formation of an adduct species between the metal sulphato complex and the reagent must be also taken into account besides the formation of cobalt and nickel sulphato complexes.

On the basis of our models a significant change in the separation coefficient of Co^{2+} and Ni^{2+} can be expected only in the cloride solutions at very high Cl^{-} ion concentrations due to the formation of the $CoCl_4^{2-}$ species.

REFERENCES

1. Preston, J.S.
   Hydrometallurgy, 9 (1982) 115-133

2. Rickelton, W.A., Flett, D.S., West, D.W.
   ISEC'83, Denver 1983, 195-196

3. Dreisinger, D.B., Cooper, C.W.
   Hydrometallurgy, 12 (1984) 1-20

4. Cognet, M.C., Vaissiere, G., Renon, H.
   Hydrometallurgy, 2 (1977) 265-74

5. Sillén, L.G., Martell, A.E.
   Stability Constants (and Supplement No.1)
   The Chemical Society, London, 1964 and 1971.

6. Szilassy I., Mikéta Gy., Vadasdi K.
   ISEC'86, München, p.519-525

A NEW EQUIPMENT FOR PROCESS CONTROL OF DRAWING OF REFRACTORY METALS

László Varga, Attila T.Nagy

INTRODUCTION

The improvement of quality of tungsten wires, the main component of incandescent lamps, is an important task of lamp industry. Based on the traditional relationships between the TUNGSRAM corporation and our institute, we built a wire drawing machine for investigating the drawing process. The equipment provides a lot of measuring possibility of technological parameters. The perspective aim of this investigation is the realization of a computer-controlled drawing process.

In this work we give a description of the apparatus and present some experimental results about the drawing of tungsten wires on this machine.

THE WIRE DRAWING MACHINE

The wire drawing machine is suitable for drawing of refractory metals (e.g. tungsten and molibdenum) of diameter less than 0.18 mm. The arrangement of the apparatus is illustrated in Fig.1. The drawing drum is driven by a DC motor which allows a control of drawing speed between zero and 120 m/min. The unwinding spindle is mounted on the axis of an other electromotor whose sense of rotation is opposite to drawing direction thus providing back stress in the wire. This stress is measured by a low deflection load cell developed for this special purpose. (Parameters regarding to the force in the wire, i.e. in the given geometry: range: 0-18N, sensitivity: 1.60 mV/N, stiffness: 95N/mm.

The lubrication system is a simple gravitational one completed with a peristaltic pump.

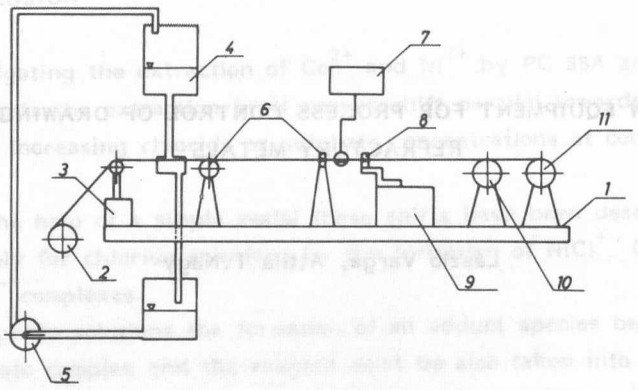

Fig.1. A schematic representation of the drawing machine
1-base, 2-unwinding spindle, 3-load cell, 4-lubrication system, 5-peristaltic pump, 6-current inlets, 7-IR thermometer, 8-drawing die, 9-load cell, 10-drawing drum, 11-winding spindle.

For the heating of wires we applied a method, the direct heating by electric current, which is not usual in tungsten technology. This was done because the current intensity can be controlled easier than the conventional gas-flame heating. The current feed is realized through a carbon roller and a drawing die. (The latter is made of tungsten carbide, which has a high conductivity.)

The temperature of the wires was measured by an IR thermometer also developed for this purpose. The instrument can measure the temperature of moving wires between 300 and 800^{o}C.

Having left the thermometer the wire enters the preheated diamond drawing die whose temperature is measured by a thermocouple. This die is mounted on a water cooled load cell (range: 0-50N, sensitivity: 0.22mV/N, stiffness: 1500N/mm/, so the load cell measures the support force of drawing die. The tensile force in the drawn wire is the sum of the two forces measured by the load cells.

All the above mentioned data were collected by a multichannel data processing system controlled by a Commodore computer.

DRAWING OF TUNGSTEN WIRE ON THE NEW EQUIPMENT

An experimental multi-step drawing was performed on the equipment described above. A tungsten wire of 176 /um in diameter was drawn to 60 /um in 15 steps. The drawing speed was 15 m/min and colloid graphite dispersed in water was used as a lubricant. At certain drawing steps the effect of different heating temperatures on the properties of the drawn wire and on the drawing parameters were investigated. The following parameters were measured or calculated:

a) Wire thickness, d. This actually involves the weighing of the wire of a given length.

b) Tensile strength, σ_B. This measurement was performed on an INSTRON tensile testing machine at room temperature.

c) Drawing temperature, T, directly measured by the IR thermometer.

d) Drawing stress σ_D at zero back stress $\sigma_B=0$. As in practice the back stress never can be zero, this quantity is determined by extrapolating the plot σ_D versus σ_B to zero back stress.

e) Coefficient of friction between the wire and the die, determined from the slope of the above mentioned plot.

f) Flow stress of material under drawing circumstances, σ_o. This is the quantity entering the yield criterion of Mises and can be also calculated from the $\sigma_D - \sigma_B$ plot. The results are displayed in Figs.2 and 3. Here the above mentioned parameters are plotted against the heating current at the 3. (Fig.2.) and at the 15. (Fig.3.) drawing step.

The scatter and reproducibility of the experimental data was about the same as observed during mass-production. We are making efforts to decrease the former and improve the latter, for which there is a good chance because of the abilities of the equipment. However, we think that only the fact that the multi-step drawing could be accomplished shows that direct heating deserves attention in tungsten technology and needs further investigations. Figs. 2. and 3. already shows that there is an optimum current (and so an optimum temperature) where the drawing stress has a minimum, mainly because of the minimum of the friction coefficient.

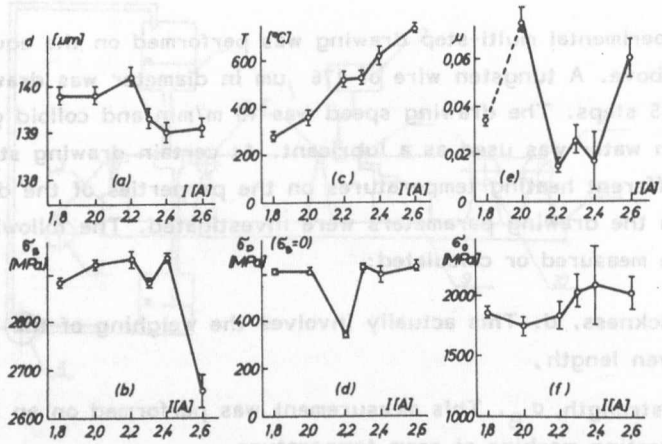

Fig.2. Mechanical and technological parameters after the 3. drawing step versus heating current
a-wire diameter, b-tensile strength at room temperature, c-temperature of the wire, d-drawing stress at zero back stress, e-coefficient of friction between the wire and the die, f-flow stress of the wire in the die

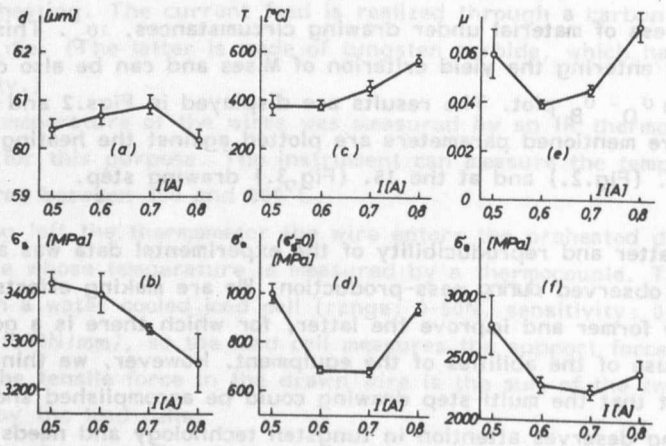

Fig.3. Same as Fig.2. but after the 15. drawing step.

SUMMARY

A wire drawing machine was built in our institute for measuring the technological parameters during drawing. The equipment turned out to be useful in studying the effects of changes in the technology.

LAPLACIAN PATTERN FORMATION

Tamás Vicsek and János Kertész

ABSTRACT

The formation of snowflakes, viscous fingers and electrodeposits is governed by analogous equations: these structures are all Laplacian patterns. In this paper we review model experiments and computer simulations which are widely used to study diverse morphologies resulting from the motion of unstable interfaces.

Far from equilibrium processes resulting in the growth of complex interfacial structures are common phenomena in many fields of science and technology. Examples for the formation of such patterns, among many others, include dendritic solidification when the crystalline phase is growing in an undercooled melt, viscous fingering which can be observed if a less viscous fluid is injected into a more viscous one and electrodeposition of ions onto an electrode. Figure 1. demonstrates the richness of complex interfaces which are formed under a wide variety of experimental conditions.

The explanation for the apparently analogous behaviour of these different growth processes lies in the equations which describe the motion of the interface. The basic equation is

$$\nabla^2 u = 0, \qquad (1)$$

where u may denote the distribution of pressure (viscous fingering), temperature (crystallization) or electric potential (electrodeposition). Equation (1) usually corresponds to some approximations, but it captures the essential physics.

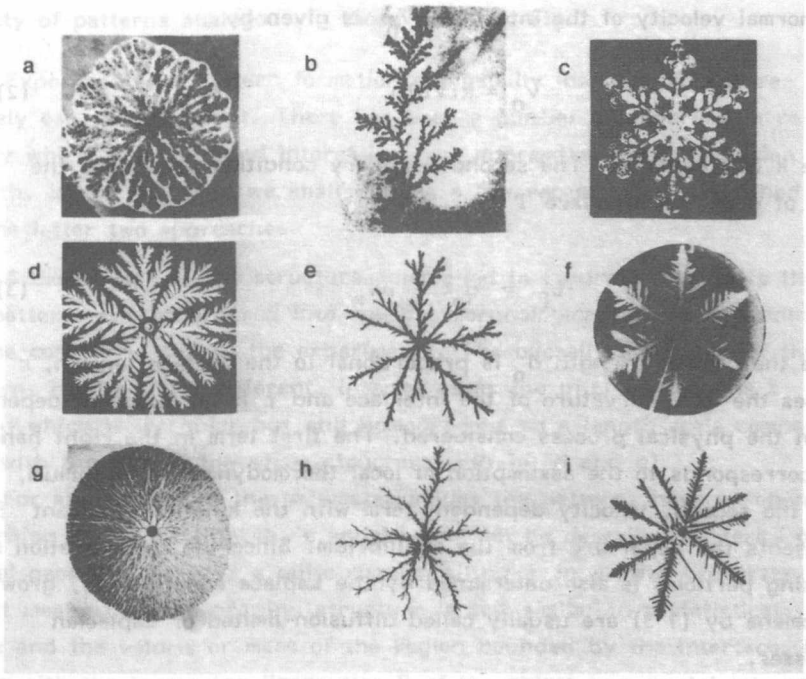

Fig.1. Laplacian patterns obtained under various experimental conditions

The three major types of structures observed in the experiments on crystallization (1a,b and c), viscous fingering (1d,e and f) and electrodeposition of zinc (1g, h and i) are grouped into separate columns. (sources: (1a) Ben-Jacob E., Deutscher G., Garik P.Goldenfeld N.D. and Y. Lareah Phys.REv.Lett 57 (1986) 1903, (1b) Radnóczy G., Vicsek T., Sander L.M. and Grier D., Phys.Rev. A35 (1987) 4012, (1c) Bentley W.A. and Humpreys W.J. Snow Crystals, (Dover Publications, 1962), (1d) Buka A., Kertész J. and Vicsek T., Nature 323 (1986) 424, (1e) Daccord G., Nittmann J. and H.E.Stanley, Phys.Rev.Lett. 56 (1986) 336, (1f) Ben-Jacob E., Godbey Y., Goldenfeld N., Koplik J., Levine H., Mueller T. and Sander L.M., Phys.Rev.Lett 55 (1985) 1315, (1g,i) Sawada Y., Dougherty A. and Gollub J.P. Phys.Rev.Lett. 56 (1986) 1260, (1h) Matsushita M., Sano M., Hayakawa Y., Honjo H. and Sawada Y., Phys. Rev.Lett. 53 (1984) 286.

When solving (1) one has to satisfy the appropriate boundary conditions. The normal velocity of the interface, v_n, is given by

$$v_n = k(\nabla u)n, \tag{2}$$

where k is a constant. The second boundary condition prescribes the value of u on the interface Γ

$$u_\Gamma = -d_o\kappa - \beta v_n^\gamma \tag{3}$$

where the capillary length d_o is proportional to the surface tension, κ denotes the local curvature of the interface and γ is an exponent depending on the physical process considered. The first term in the right hand side corresponds to the assumption of local thermodynamic equilibrium, while the second, velocity dependent term with the kinetic coefficient β represents the departure from the equilibrium. Since the concentration of diffusing particles is also determined by the Laplace equation (1), growth phenomena by (1-3) are usually called diffusion-limited or Laplacian processes.

Three main approaches have been developed to treat the problem posed by equations (1-3):

i) Analitic methods including stability analysis and search for solutions of significantly simplified versions of the original equations have been used by many authors. Groups at University of California, Schlumberger-Doll Research and Ecole Normale Superieure in Paris have demonstrated the crucial role of anisotropy of the surface tension in pattern formation and the existence of a solvability condition which determines the discrete set of interfacial velocities from which the largest one is selected.

ii) To study the geometrical properties of very complex patterns it is more effective to use various simulation techniques. The diffusion-limited aggregation (DLA) model introduced by Witten and Sander in 1981 has been shown to capture the most important features of Laplacian pattern formation with noise. In this model randomly walking particles launched from distant points stick to the surface of the growing aggregate whenever they hit it. DLA and its generalizations have contributed to the

understanding of diffusion-limited pattern formation by leading to a large variety of patterns analogous to those shown in Fig.1.

iii) Experiments on pattern formation are usually inexpensive and relatively easy to carry out. There has been a number of experiments recently which have revealed interesting new information about Laplacian growth. In the following we shall discuss a few recent results obtained by the latter two approaches.

A closer look at the structures displayed in Figure 1. suggests that the patterns can be ordered into specific morphological phases depending on the conditions during the experiments. The overall appearence of the patterns can be quite different: in some cases the interface bounds a region which is irregular but still homogeneous on a length scale comparable with the size of the whole structure (Fig.1a, d and g).

For another set of the parameter values the patterns have an open branching structure (Fig.1b, e and h) and can be described in terms of fractal geometry. This is a quite common situation in growth processes and it means that the growing structure is self similar in a statistical sense and the volume or mass of the region bounded by the interface, M, scales with the increasing linear size R of the object in a nontrivial way

$$M \sim R^D \qquad (4)$$

Here D is called fractal dimension and is smaller than the Euclidian dimension d of the space the fractal is embedded in. Of course, the above scaling in a physical system holds only for length scales between a lower and an upper cutoff.

What are the most important parameters and under what conditions do they determine the morphological phase to which a given growth process leads? These are the main questions to be answered by the studies of pattern formation. In the last few years much progress has been made in this field and it has turned out that the formation of patterns is determined by a number of important parameters such as anisotropy, noise and driving force.

The complex behavior leading to the development of structures has its origin in the instability due to the moving boundary condition (2).For Example, in a radial Hele-Shaw cell when air (or a less viscous fluid)

is injected into a quasi two-dimensional viscous fluid held between glass plates, the growth is driven by the pressure gradient. The so called Saffmann-Taylor or Mullins-Sekerka instability takes place in this system for bubble sizes exceeding a characteristic length depending on the surface tension and the growth velocity. In this case, whenever one part of the interface advances locally faster than the surrounding region the pressure gradient at this protrusion becomes larger in analogy with the increased electric field at the tip of a charged needle. The increased pressure gradient leads to a faster growth of the interface which, in turn, results in a further increment of the gradient. Therefore, the interface becomes unstable against perturbations (noise) and elongated "fingers" grow out of it. The fingers are getting longer and thicker until their tips become too flat to be stable: they split. Under specific conditions (viscous fingering in a random medium or in a non-Newtonian fluid with vanishing surface tension) tip splitting is followed by a competition between the new-born branches. During this process the more advanced, longer fingers screen the shorter ones. Since this process is triggered by noise, a random pattern can result from a sequence of such instabilities (Fig.1e). Similar mechanisms are responsible for the complex geometries developing in other Laplacian processes as well, leading to open, random fractal patterns with $D < d$.

DLA-clusters can be considered as a result of the above described sequence of instabilities: tip splitting resulting in branching and competition between the branches due to screening. The growth process leads to an open ramified structure with a well defined fractal dimensionality ($D = 1.71$ in two dimensions).

If the noise is small the screening between the branches does not prevail. In this case the fingers emerging from tip splitting keep growing and the space becomes almost filled with the patterns. This phase has a stable envelope and is called dense branching morphology. Its dimensionality is equal to the Eucledian embedding dimension.

Another stable morphological phase develops if there is large enough anisotropy either in the surface tension or in the factor β of equation (3) preventing the tips from splitting. Due to the anisotropy directions of easy growth are present in which the interface proceeds faster which stabilizes the tips. This is the mechanism how regular dendritic crystals like snowflakes grow.

If diffusion-limited aggregation is simulated on a lattice (e.g. on a square mesh) the anisotropy - which was shown to be relevant for Laplacian growth - is expected to influence the shape of the clusters significantly. In this case the lattice axes represent directions of easy growth. According to the simulations of Paul Meakin from du Pont, Wilmington, however, only extremely large clusters (containing about 10^6 particles) show a tendency towards an overall cross shaped form. The actual shape of lattice DLA-clusters emerges from an interplay between fluctuation and anisotropy.

The fluctuations in DLA can be controlled by the so called noise reduction method: instead of adding the randomly walking particle to the cluster after it hits a growth site, one keeps counting the trajectories terminating at a given site. Only those sites are added to the cluster at which the counter reaches a prescribed value m. Large m corresponds to low level of noise: the m = 1 case is usual DLA.

For a fixed number of particles in the cluster an interesting morphological transition can be observed as a function of the noise reduction parameter m (Fig.2). "Noisy" DLA-clusters grown on the square lattice are open branced structures like off lattice aggregates. If the noise is reduced, the anisotropy due to the grid breaks through and the clusters become cross-shaped with stable tips reminiscent to dendritic crystals. For large values of m even the side branches vanish and one recovers needles growing out of a centre, reflecting the geometry of the lattice. Furthermore, noise reduction is a suitable tool to study the asymptotics of DLA-clusters since the relative weight of fluctuations decreases not only with increasing the parameter m but also with the increasing size.

The almost perfect symmetry and enormous number of different snowflakes represents a long standing puzzle. It is quite natural to assume that this problem should be treated by a technique with no spatial fluctuations. Indeed, a deterministic growth model designed to provide a good approximation to the equations (1-3) on a triangular lattice is capable of reproducing the basic types of snowflakes. The process starts with a seed particle. Then the Laplace equation is solved on the triangular grid (providing the sixfold symmetry). The decision whether a particular surface site is filled at a given stage of the growth is made on the basis of comparing the value of the calculated temperature gradient at that site with a time dependent parameter.

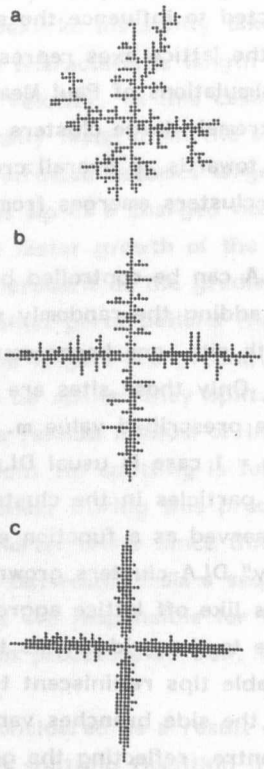

Fig.2. The effect of noise reduction on the structure of DLA clusters grown on the square lattice. With the decreasing amount of fluctuations (with growing m) the clusters consisting of 400 particles go through a sequence of morphological changes (from Kertész J. and Vicsek T., J.Phys. A-19, (1986) L257)

A typical pattern obtained by varying a parameter of the deterministic model during the growth is shown in Fig.3. According to the simulations the great variety of dendritic patterns (like snowflakes) produced by the same solidification process is likely to be due to the temporal changes in such environmental conditions as undercooling or vapour pressure.

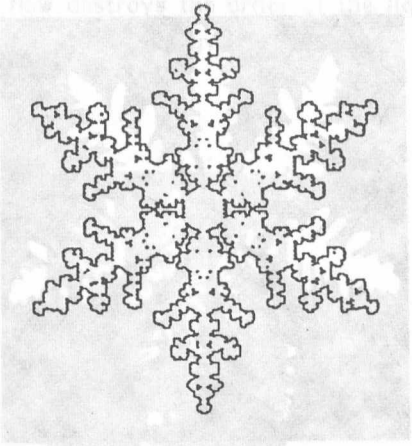

Fig.3. This pattern was grown in the computer using the deterministic aggregation model (from F.Family, D. Platt and T.Vicsek, preprint) described in the text. Many different snowflake-like clusters are produced by this method and the one shown here resembles the real snowflake displayed in Fig. 1c.

Perhaps the most versatile experimental realization of Laplacian pattern formation is viscous fingering. Virtually all the above mentioned important influencing factors can be investigated with relatively small effort. The effect of the driving force is studied by changing the pressure of the less viscous fluid. Noise or anisotropy can be introduced by appropriate preparation of the cell: randomly positioned hindrances are put into the cell or a mash is grooved onto one of the plates.

What happens if in a Hele-Shaw cell the viscous fluid is inherently anisotropic? Injecting air into a liquid crystal is a realization of this situation. In the case of nematics where the elongated molecules of the liquid have a long range order characterized by a vector called director, an interesting reentrant morphological transition can be observed as a function of the increasing driving force. In this medium radial anisotropy is built up by the flow. For low pressure the shape of the interface is very similar to the usual viscous fingering patterns obtained with isotropic liquids. If higher pressure is applied the tips of the fingers are stable and the bubble becomes dendritic, snowflake-like (Fig.4).

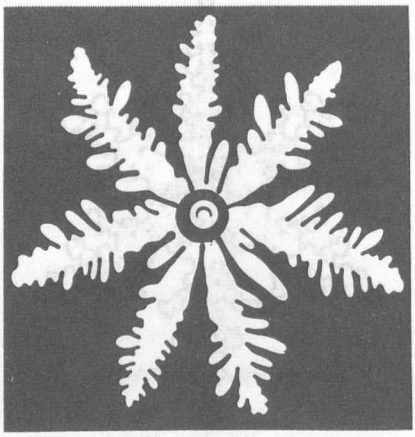

Fig.4. Dendritic viscous fingers obtained in a radial Hele-Shaw cell with a nematic liquid crystal between the plates for intermediate pressures of the injected air. For lower pressures the pattern is similar to those obtained in usual isotropic liquids. For larger pressures of the injected air the dense branching morphology shown in Fig. 1d is obtained (source: the same as Fig.1d)

By further increase of the pressure tip splitting sets in again, probably because the stronger flow results in a disordered, chaotic motion of the director, therefore the effective anisotropy is decreasing and the pattern has a dense branching morphology (DBM) illustrated in Fig.1a, d and g.

We have seen that tip splitting with large fluctuations leads to the fractal DLA-structure while without strong noise the nonfractal (DBM) develops. Viscous fingering patterns in a smectic A liquid crystal undergo a morphological phase transition from the DLA to the DMB structure as a function of the pressure of the injected air. The structure of smectics is more ordered than that of nematics: the alligned molecules are arranged into layers which can slip on each other determining this way directions of easy growth of the bubble. The domain structure of the liquid crystal introduces an orientational disorder into the system which leads for low pressures to DLA-type structures. The effective fractal dimension D_{eff} of

the pattern on Fig.5a is 1.6, very close to the two-dimensional DLA value. For high pressure the flow destroys the order of the liquid crystal and we recover the dense branching morphology with $D_{eff} \approx 2$.

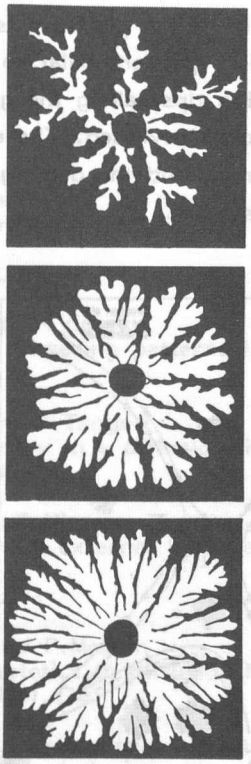

Fig.5. On increasing the pressure of injected air in the experiments on viscous fingering in smectics a crossover from a DLA-type fractal interface (a) to a nonfractal, dense branching morphology (c) can be observed (from Horváth V., Kertész J. and Vicsek T. to appear in Europhys. Lett).

In order to study the effects of anisotropy on the shape of viscous fingers one can use an alternative approach by engraving a mesh on the surface of the plates. This trick was first used by Ben-Jacob and his

collaborators to obtain a sequence of morphological changes as a function of the increasing pressure of injected air. Perhaps the simplest kind of anisotropy can be introduced by etching a set of parallel grooves on one of the plates.

The results are quite interesting: the morphological phase diagram (Fig.6) of this system shows a variety of patterns unexpected for such type of anisotropy. For example, if the pressure is low, the growth can be stable in the "hard" direction (perpendicular to the grooves) and simultaneously unstable (splitting tips) along the grooves. On increasing the pressure the situation becomes reversed. The effects induced by the competition between the anisotropy and the driving force result in a truly complicated behaviour in this system.

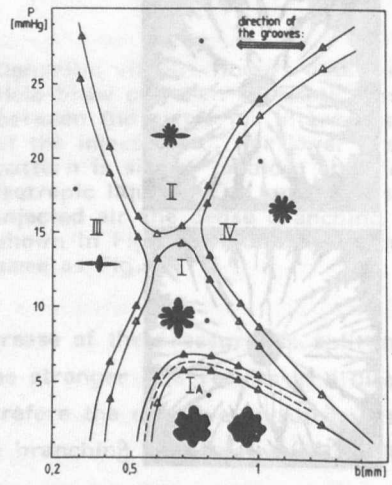

Fig.6. Morphological phase diagram of the interfacial patterns observed in a uniaxially engraved radial Hele-Shaw cell (from V.Horváth, T.Vicsek and J.Kertész, Phys.Rev. A35 (1987) 2353). The transitions between the different phases indicated by characteristic patterns is relatively sharp as a function of the pressure (p) and the distance of the plates (b) .

The above simulations and experiments elucidate the crucial role of anisotropy, noise and driving force in the formation of unstable interfaces. The interplay of these factors determines the actual shape of the patterns.

Although much progress have been made in the last few years towards understanding the major features of Laplacian growth phenomena we are far from being able to explain complex morphological phase diagrams. The open fundamental problems include the existence of critical parameters, the effect of fluctuations on side branching or the role of temporal fluctuations. Important future work, both experimental and theoretical, is expected in this field.

REFERENCES

1. J.Kertész and T.Vicsek
Diffusion-Limited Aggregation and Regular Patterns: Fluctuations versus Anisotropy
J.Phys. A19, (1986) L257

2. A.Buka, J.Kertész and T.Vicsek
Transitions of viscous fingering patterns in nematic liquid crystals
Nature 323 (1986) 424

3. F.Family, T.Vicsek and B.Taggett
Lattice-induced anisotropy in a diffusion-limited growth model
J.Phys. A19 (1986) L727

4. F.Family, Y.C.Zhang, T.Vicsek
Invasion percolation in an external field: electric breakdown in random medea
J. Phys. A19 (1986) L733

5. J.Kertész, T.Vicsek and P.Meakin
Singularities and asymptotics in diffusion limited aggregation,
Phys.Rev.Lett. 57 (1986) 3303

6. T.Vicsek, F.Family, J.Kertész and D.Platt
Distribution and entropy of clusters in growth models
Europhysics Lett. 2, 823, 1986.

7. V.Horváth, T.Vicsek and J.Kertész
Viscous fingering with uniaxial anisotropy
Phys.Rev. A35 (1987) 2353

8. P.Meakin, F.Family and T.Vicsek
Viscous fingering simulated by off-lattice aggregation
J.Interface Sci. 117 (1987) 394

9. P.Meakin and T.Vicsek
Diffusion-limited aggregation with radial bias
J.Phys. A20 (1987) 171

10. Gy.Randóczy, T.Vicsek, L.M.Sander and D.Grier
Growth of fractal crystals in amorphous $GeSe_2$ films
Phys.Rev. A35 (1987) 4012

11. T.Vicsek
Formation of solidification patterns in aggregation models
in Fractals in Physics, edited by L. Pietronero and E. Tosatti
(North Holland, Amsterdam, 1986) p.247

12. P.Meakin and T.Vicsek
Internal anisotropy of diffusion-limited aggregates
in Fractals in Physics, edited by L.Pietronero and E.Tosatti
(North Holland, Amsterdam, 1986) p.213

13. J.Kertész, J.Szép and J.Cserti
Dendritic growth by Monte Carlo
in Growth and Form: Fractal and Nonfractal Patterns in Physics
edited by H.E.Stanley and N.Ostrowsky, (Nijhoff, Dordrecth, 1986)
p.219

14. Vicsek T.
Mintázatképződés aggregációs folyamatokban
Magyar Tudomány, 5 (1986) 356 (in Hungarian)

15. V.Horváth, J.Kertész and T.Vicsek
Viscous fingering in a smectic liquid crystal
Europhys. Lett., in press

16. C.Amitrano, L. de Arcangelis, A.Coniglio and J.Kertész
Regular versus irregular Laplacian growth: multifractal spectroscopy
J.Phys. A., in press

17. J.Kertész
Fluctuations, anisotropy and scaling in growth processes
Phil.Mag., in press

18. T.Vicsek
Formation of interfacial patterns in aggregation and viscous flows
Physica Scr. in press

19. T.Vicsek and J.Kertész
Laplacian pattern formation
Europhys. News, in press

Structure Research Division

THE POSSIBILITY OF SURFACE POLISHING BY ION BEAM THINNING

Á. Barna

INTRODUCTION

Ion beam machining is widely used for preparation of electron microscopic samples both for TEM and SEM[1,2]. The surfaces of samples must be as smooth as possible. That means we have to choose such parameters for ion beam thinning or cutting which leads to a polishing effect. Almost all special features of ion beam etching (sputter speed, topographical changes, radiation damage, etc.) depend directly or indirectly on the ion beam incidence angle θ: where θ is measured from the average surface normal. From our experience a pronounced polishing effect can happen if $\theta > 80\text{-}85^{o}$. But the sputter speed goes down to 0 if θ approaches 90^{o}. However the "high speed" ion milling equipment working with "Teletwin" ion guns, developed in our laboratory[3], makes possible to carry out ion beam machining also at high incidence angles up to $\theta = 89^{o}$, near to the exact grazing incidence. On the basis of experimental results a kinetic model was developed to follow the surface topographical changes during ion beam thinning.

THE MODEL

The basic surface elements of the model are inclined macrosteps (steps with dimensions larger than the cascade area of ion impact). Their angle of inclination α is measured from the average surface (Fig.1.a).

In case of structureless[x] and homogeneous samples the original topography is modified through the modification and displacement of these macro steps.

---

[x] The sputter speed does not depend on crystallographic orientation e.g. amorphous materials, Si, Ge, GaAs..., $LiNbO_3$, MgO, Al_2O_3 etc.

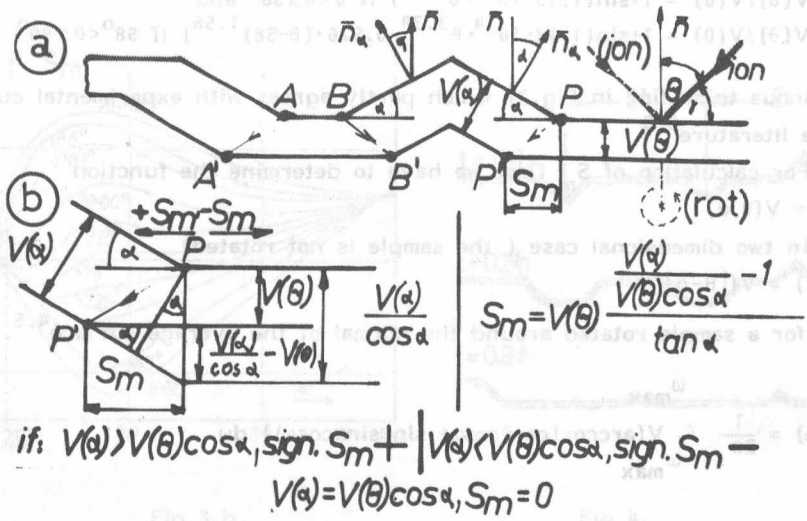

Fig.1.a, 1.b

In case of a single step the ion erosion can change only the position and the shape of the step. The latter happens when the angle of inclination is not constant. Height changes of step e.g. increase, decrease or annihilation can happen only by concurrence of steps.

The height of a new step resulted from concurrence of steps can not be higher than the maximum height amplitude of the original surface roughness[xx].

The speed of a step movement is given in (Fig.1.b), where $V(\alpha)$ and $V(\theta)$ are erosion speeds measured in the direction of the surface normal of the average surface and of the inclined step respectively. (This movement can be observed immediately during the experiment).

For experiments and for calculations we have choosen Si as model material. The dependence of $V(\theta)/V(0)$ on θ is given in (Fig.2). From our measurements we have determined for Si an analytically defined function of $V(\theta)/V(0)$

---

xx If the sample can not be regarded as structureless material (e.g. polycrystalline metals etc.) the effect of new topographical elements developed during ion beam thinning must be taken into consideration[6] and in this case, of course, a new step height can be higher than the original height amplitude.

$$V(\theta)/V(0) = 1+\sin(1.13\cdot10^{-4}\cdot\theta^{3.39}) \text{ if } 0<\theta\leq 58^{o} \text{ and}$$
$$V(\theta)/V(0) = 1+\sin(1.13\cdot10^{-4}\cdot\theta^{3.39}-0.926\cdot(\theta-58)^{1.56}) \text{ if } 58^{o}<\theta\leq 90^{o}$$

(continous thick line in Fig.3) which partly agrees with experimental curves in the literature[4,5].

For calculation of S_m first we have to determine the function $V(\alpha) = V(\theta,\alpha)$.

In two dimensional case (the sample is not rotated)

$V(\theta,\alpha) = V(|\theta-\alpha|)$

and for a sample rotated around the normal of the average surface[4,5].

$$V(\theta,\alpha) = \frac{1}{2\pi}\int_{-\omega_{max}}^{\omega_{max}} V(\arccos(\cos\theta\cos\alpha+\sin\theta\sin\alpha\cos\omega))\,d\omega$$

and

$$\omega_{max} = \arccos\left\{-\frac{\cos\theta\cos\alpha}{\sin\theta\sin\alpha}\right. \quad , \text{ or } \pi \text{ , whichever is maller}$$

where ω is the angle of the rotation, and $V(\theta)$ is determined experimentally.

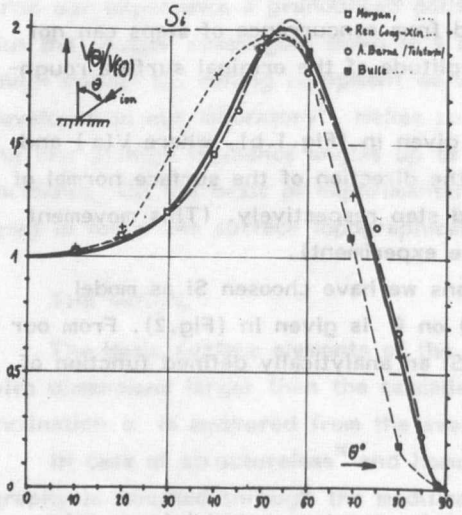

Fig.2.

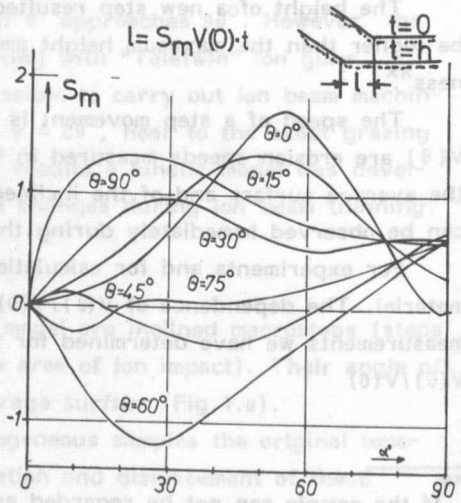

Fig.3.a.

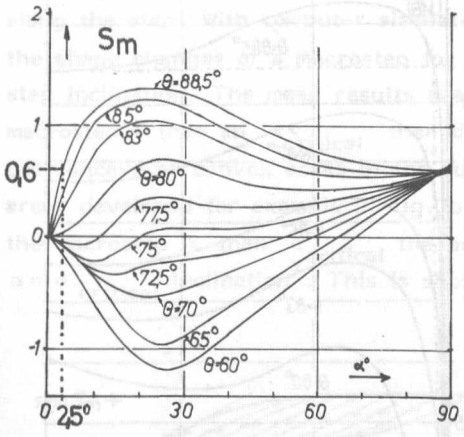

Fig.3.b.

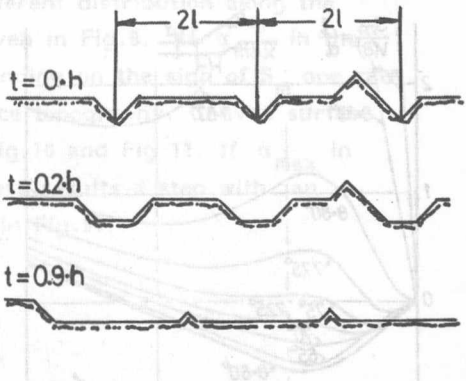

Fig.4.

RESULTS OF EXPERIMENTS AND MODEL CALCULATIONS

The Figs. 3a and b show the dependence of $S_m/V(\theta)$ on α. Here "l" is the step displacement and "t" is the sputtering time. If the period length of some topographical elements (steps) is 2·l, all steps will be annihilated (Fig.4.).

The Figs.5a, and 5b show the dependence of $S_m/V(\theta)$ on α. This is ratio between t and d where "d" is the erosion depth in the average surface normal direction.

The Fig.6. shows the backside of a Si wafer and its cross section (normal and interference optical micrographs). This rough Si surface was etched in the ion milling equipment at different θ. During ion beam thinning the sample was rotated.

According to the model calculation for rotated Si sample and for Ar as sputter gas the $S_m(\theta,\alpha)$ has a negativ maximum at $\theta = 60^o$ and $\alpha = 30^o$. (Fig.3a and Fig.5a). Because of negativ step movements the bottom surface of a crater will be smaller during the sputtering (Fig.7b) Substituting Ar by Kr both $V(\theta)$ and $S_m(\theta,\alpha)$ will change. Therefore in the case of Kr but otherwise under the same experimental conditions one gets quite different results seen Fig.7.a, compared to Fig.7 b. In this case the structure of the surface topography was near preserved during the thinning time.

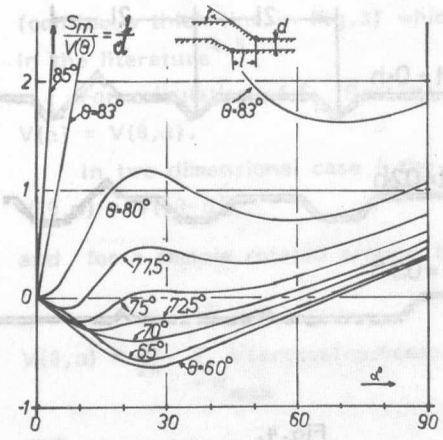

Fig.5a.

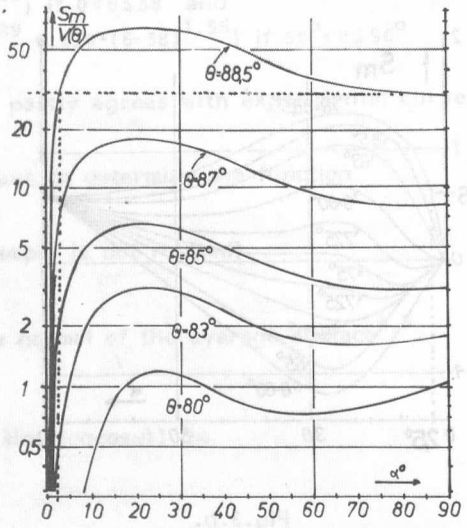

Fig.5b

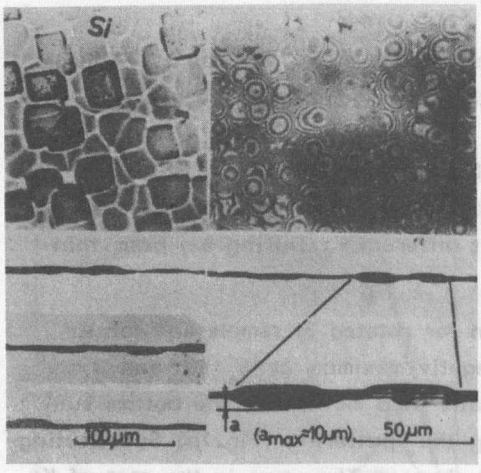

Fig.6.

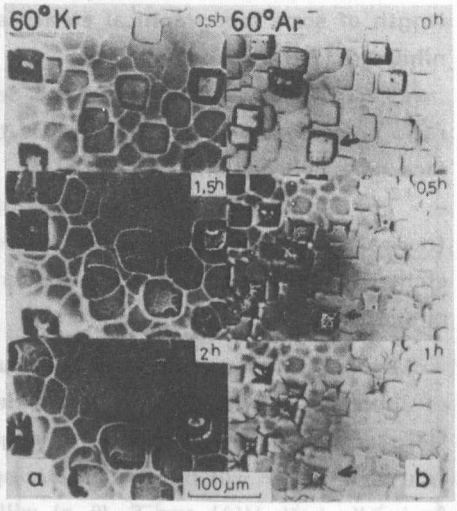

Fig.7a,7b.

In reality the step angle is not constant but it has a distribution along the step. With computer simulation using $S_m(\theta,\alpha)$ one can follow the shape changes of a macrostep for different distribution along the step inclination. The mean results are given in Fig.8. If α_{max} in the macrostep < than an $\alpha_{critical}$ then depending on the sign of S_m one can get concave or convex areas in the surface topography. Convex surface areas developed for example in Fig.7b, Fig.10 and Fig 11. If α_{max} in the macrostep > than $\alpha_{critical}$ the process results a step with an $\alpha = \alpha_{critical}$ inclination[7]. This is shown in Fig.9.

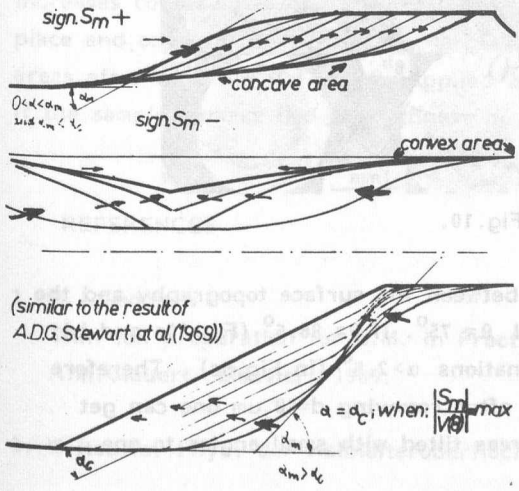

Fig.8.

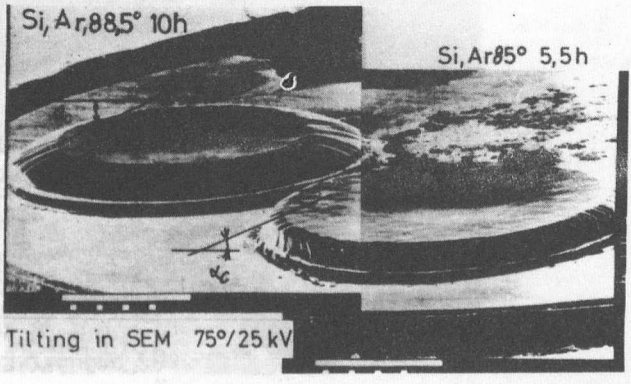

Fig.9.

If $\theta > 80^{o}$ then $S_m/V(\theta)$ considerably increases. Fig.10. shows the surface polishing effect for $\theta = 88.5^{o}$ followed by in situ optical observation during ion beam machining. In the sputtering time larger and larger smooth convex surface areas are developing.

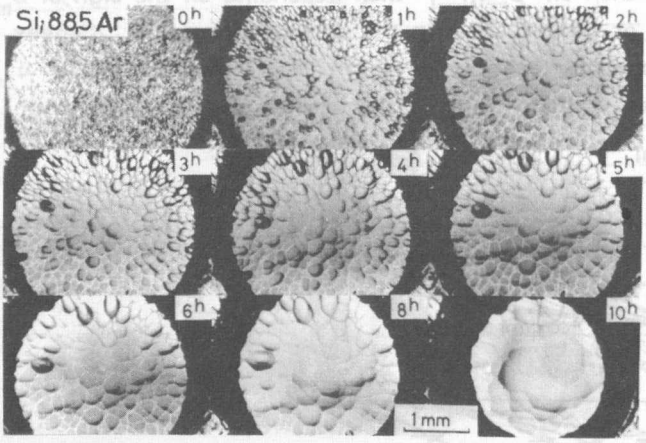

Fig.10.

The Fig.11 shows the relation between the surface topography and the sputter depth (d) for $\theta = 88.5^{o}$ and $\theta = 75^{o}$. If $\theta = 88.5^{o}$ (Fig.11a and b) then $S_m/V(\theta) > 30$ for all step inclinations $\alpha > 2.5^{o}$ (in Fig.5c) . Therefore effective polishing takes place and after removing d=40 µm one can get sufficiently large smooth surface areas tilted with small angles to one another at their boundaries.

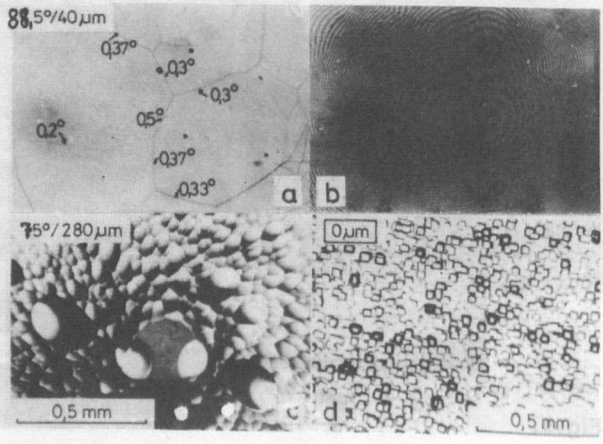

Fig.11.

According to the model calculation the $S_m/V(\theta)$ value is low in the whole $\alpha=0-90^o$ range for $\theta=65-80^o$, generally used in the thinning techniques, and it has a minimum at $\theta = 75^o$. Therefore the original surface topography - or the topography developed at the beginning of the thinning in consequence of latent faults of mechanical grinding and polishing - remains unchanged more or less. This effect is seen in Fig.11c where θ was 75^o and in spite of removing d=280 /um the original surface topography (Fig.11d) has modified only in a small degree.

The model considering the behaviour of macrosteps (displacement and concurrence) can give a good idea on the evolution of surface topography and its changes during ion beam thinning. The relative step displacement increases considerably for $\theta > 85^o$, therefore an effective polishing takes place and one can get sufficiently large (200-300 /um) smooth surface areas after reaching the usually applied 20-25 /um sputter depth, even if the sample surface had a roughness of some /um-s at the beginning.

REFERENCES

1. P.J.Goodhew
   Thin foil preparation for E.M. in Pract.Methods in E.M., Ed.: A.M.Glauert, Elsevier, 1985.

2. W.Hauffe, Phys. der Halbleiteroberfläche 13, 177, (1982)

3. A.Barna, Proc. 8th European Congress on E.M., Budapest 1984, Vol.1. p.107

4. C.W.T. Bulle-Lieuvma et al,
   Proc. XIth Int.Congr. on E.M., Kyoto, 1986, Vol.1. p.353

5. R.Cong-Xin et al, Radiation Effects, 77, 177 (1983)

6. A.Barna, P.B.Barna, A.Zalar, to be published in Proc. in ECASIA, 1987, Stuttgart

7. O. Auciello, J.Vac.Sci.Technol., 19, 841, (1981).

INTRINSIC OPTICAL CONSTANTS OF ALUMINIUM

Z. Bodó and G.Gergely

Ellipsometry is a practical method for determining the optical constants $n/\lambda/$ refractive index and $k/\lambda/$ extinction coefficient for λ wavelength. For an atomically clean and perfectly flat surface the ellipsometric parameters ψ and Δ define unambigously $n/\lambda/$ and $k/\lambda/$ and vice versa. For determining the optical constants of any solid a nomogram has been elaborated (Fig.1. in[1]), displaying ψ and Δ versus n and k material parameters, covering the ranges n=0.2 - 1.6 and k=3-8.

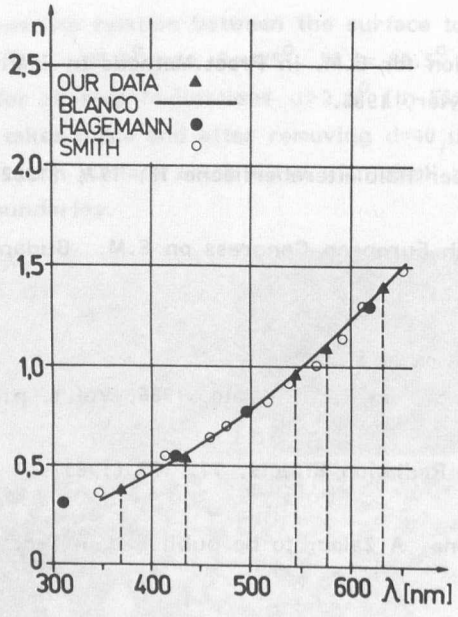

Fig.1.

It can be applied for any clean and optically flat surface. In practice however apart from noble metals and oxides or wide band gap insulators the surface is covered by a thin oxide (or hydrated oxide) overlayer stabilizing it and in many cases preventing further oxidation. In most cases it is very difficult to fulfill the second requirement: optically flat surface with roughness $\bar{r}$ on atomic scale.

Real metal and semiconductor surfaces are characterized by a thin oxide film[2] (d thickness) and $\bar{r}$ [3]. Ellipsometric ψ and Δ parameters are strongly affected by them. Ellipsometry only is not able to determine $n/\lambda/$ and $k/\lambda/$ but they can be measured by completing ellipsometry with some auxiliary method supplying d and $\bar{r}$.

d and $\bar{r}$ have been determined on Al by x-ray specular reflection[2] in the Institut d'Optique, Orsay/France. It turned out, that $\bar{r}$ varied between 0.8 - 1.5 nm on samples prepared in our Institute by vacuum deposition on perfectly flat glass substrates supplied by Institut d'Optique. Making use of d and $\bar{r}$ values and evaluating our ellipsometric measurements in the λ = 365-633 nm range with a new computer optimization procedure, $n/\lambda/$ and $k/\lambda/$ have been determined.[1,2,4]. They are presented in Figs.1 and 2.

The same procedure has been applied for evaluating experimental ψ and Δ data of Blanco et al[3] and assuming d=4.8 nm hydrated oxide (neglected in[3]), for their most perfect sample ($\bar{r}$=1.49 nm). These optical constants are also indicated in Figs.1 and 2. They exhibit a perfect agreement with our results. The optical constants of Al determined by synchrotron spectroscopy[5,6] are also presented on Figs.1 and 2. The agreement with our results is striking. The good agreement of optical constants of Al determined in 4 laboratories with different samples and methods let consider them as intrinsic optical constants of Al.

The computer analysis of the relationship between ψ , Δ and n-k on Al samples characterized by d oxide overlayer and $\bar{r}$ roughness revealed their effects on the apparent optical constants, resulting in[7]:

$$\frac{dn}{d\bar{r}} \sim \frac{dn}{n} = 10^{-2}, \qquad \frac{dk}{d\bar{r}} \sim \frac{dk}{k} = 7\times10^{-3}$$

for $d\bar{r}$ = 1 nm change in $\bar{r}$ roughness and

$$\frac{dn}{n} = 9\times10^{-2} \qquad \frac{dk}{k} = 4.8\times10^{-2} \text{ at } \lambda = 400 \text{ nm}$$

for d = 1 nm change in thickness of oxide overlayer.

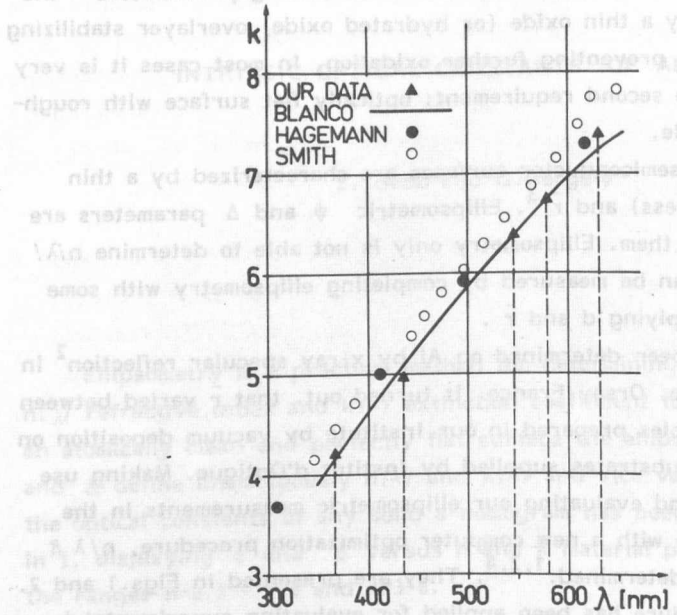

Fig.2.

Considering the real parameters of an Al sample covered by a natural oxide overlayer of d=2-4 nm, the same optical constants have been deduced on samples studied in various laboratories[1,4]. Below $\bar{r} < 2$ nm, the surface can be considered as optically flat. On the other hand the oxide overlayer is of crucial importance and its neglection can produce 20-40% uncertainty in $n/\lambda/$ and 10-20% in $k/\lambda/$.

ACKNOWLEDGEMENTS

Results described in this paper have been achieved in cooperation with our colleques Dr.P.B.Barna, J.Ádám (Tungsram) and prof. P.Croce (Institut d'Optique, Orsay). Authors appreciate their cooperation. We are indepted to Deutsches Elektronen-Synchrotron DESY, Hamburg and to prof. D.Y. Smith, Vermont University (USA) for kindly sending their reports cited in 5,6.

REFERENCES

1. Bodó Z. and Gergely G.
Intrinsic optical constants of aluminium
Appl. Opt. 26 2065 (1987)

2. Barna P.B., Bodó Z.,Gergely G., Croce P., Adam J. and Jakab P.
Ellipsometric and x-ray specular reflection studies on naturally grown overlayers on aluminium thin films
Thin Solid Films 120 249 (1981)

3. Blanco J.R., McMarr P.J. and Vedam K.
Roughness measurements by spectroscopic ellipsometry.
Appl. Opt. 24 3773 (1985)

4. Barna P.B., Bodó Z., Gergely G. and Adam J.
Spectral ellipsometric TEM and electron spectroscopic investigations on oxidized aluminium thin films
Vacuum 36 465 (1986)

5. Hagemann H.-J., Gudat W. and Kunz C.
Optical constants from the far infrared to the X-ray region: Mg,Al, Cu, Ag, Au, Bi C and Al O DESY SR-74/7 Report (1974)

6. Smith D.Y., Shiles E. and Inokuti M.
The optical properties and complex dielectric function of metallic aluminium from 0.04 to 10^4 eV.
Argonne National Laboratory Report. ANL-83-24 (1983)

7. Gergely G., Bodó Z. and Croce P.
Determination of the optical constants of metals and semiconductors by combining ellipsometry with electron spectroscopy, microscopy and x-ray specular reflection analysis.
11th Internat. Seminar on Surface Physics, Piechowice May 1987.
Abstracts p30 Ed: University of Wroclaw.
Seminar Proc. Ed: Surface Sci. (in preparation)

THIN FILM AND SURFACE ANALYSIS BY ELECTRON SPECTROSCOPY, ELECTRON MICROSCOPY AND ELLIPSOMETRY

G.Gergely and P.B.Barna

This report is presenting a brief review on research and developments achieved in surface and thin film analysis. Thin film research was carried out with interdisciplinary studies incorporating:

- Auger electron spectroscopy (AES) with Ar^+ ion depth profiling
- Electron energy loss spectroscopy (EELS), non destructive depth profiling
- Elastic peak electron spectroscopy (EPES)
- Transmission electron microscopy (TEM) with cross-sectionally thinned samples (XTEM) and replica

This paper is confined to new results omitting the great number of routine AES, TEM and XTEM studies, associated with materials research and semiconductor device development.

IMPROVEMENT OF THE DEPTH RESOLUTION IN AES DEPTH PROFILING

The depth resolution of Ar^+ ion milling profiling is gradually decreased with the thickness of the layer removed by sputtering. Beside several factors, the roughening is playing a dominant role among artifacts. As shown[1] considerable imporovement in depth resolution was achieved by using grazing incidence of the ion beam impinging on a rotating sample. In the analysis of semiconductor devices, failure shooting of the Si-contact interface is of primary interest. The main difficulty lies in the thick contact layer system deposited on the Si crystal. A multilayer system consisting of a 500 nm Ni -50 nm Au -30 nm Cr- oxidized Si substrate was analysed by removing the thick overlayer with our new method[2], in our

ion beam thinning device. After presputtering the sample was subjected to conventional AES depth profiling in our Riber OPC 103 CMA analyser, using Ar^+ ion sputtering with a PHI 04-191 scanning ion in gun operated at 2 keV, 30 ^{o} angle of incidence. A marked improvement of depth resolution was observed, reducing the width of the apparent interface by a factor of 3-4[2].

NON DESTRUCTIVE DEPTH PROFILING BY ELECTRON ENERGY LOSS SPECTROSCOPY

A well known problem of AES and XPS is their constant sampling depth determined by the inelastic mean free path (IMFP) λ /E/ of the corresponding Auger or XPS peak. It is different for each element and compound, its range is determined by its characteristic energy E. In most cases only 1-2 XPS peaks are available for the majority of elements and confined to E < 1.2 keV. The sampling depth can be varied continuously by scanning the primary energy E_p in EELS (Ito cited in[3]). Working in the E_p = 1-3 keV range with a CMA λ /E_p/ is covering the 1-6 nm. Two new methods have been developed in our Laboratory and applied for determining the thickness d of a natural oxide overlayer on Al and Si substrates. They are based on EELS combined with EPES.

Electrons producing the ionization loss (ILS) peak N/E_L/ of oxygen are used for this purpose. N/E_L/ contains electrons backscattered elastically before or after the ionization loss event. $E_L = E_p - E_i$, E_i = ionization energy of the oxygen K shell. N/E_L/ is proportional to the elastic peak N/E_p/ and affected by d^4. The calculations were based on a single elastic scattering approach.

N/E_L/ was calculated for the E_p = 1-3 keV energy range and for d = 0.6 - 6 nm. Fitting the theoretical N/E_L/ curves to experimental results, a resonable agreement was found with ellipsometric results on Al_2O_3(natural)-Al.

The N/E_L/ ILS signal is very low, it was determined by data acquisition and processing of 50 scans with the CMA spectrometer-cumputer system. Much larger EELS signals are produced by the plasmon loss peaks, but they are broad and some times overlapping with other peaks and not very adequate for surface analysis. Their attenuation was used for determining the thickness d of the natural oxide overlayer on Al and Si[4].

Primary electrons producing the first $N/E_{pl1}/$ and subsequents plasmon loss peaks of the substrate are attenuated by the natural Al_2O_3 or SiO_2 thin overlayer. The loss spectrum of a thick Al_2O_3 layer exhibits a very broad loss peak with a maximum at E_L = 24 eV, partly overlapping with E_{pl1} = 15 eV for Al, but decreasing continuously above E > 24 eV and producing a slowly varying background[4]. The plasmon loss spectrum of Al was determined by Ar^+ ion bombardment removal of the thin natural oxide overlayer. Experimental loss spectra of Al (atomically clean) and of the sample Al_2O_3 (natural) on Al are presented in Figs. 1 and 2 for E=1 and 3 keV.

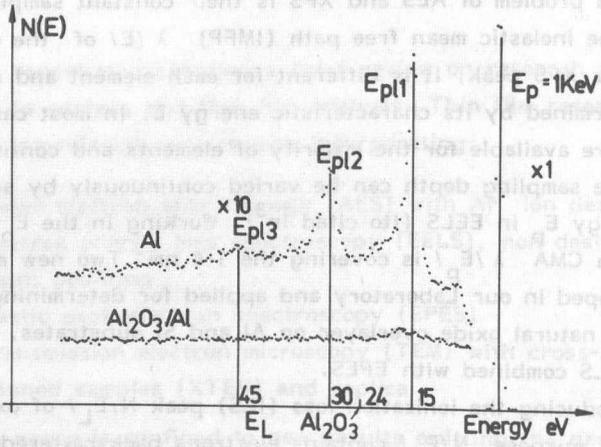

Fig.1.

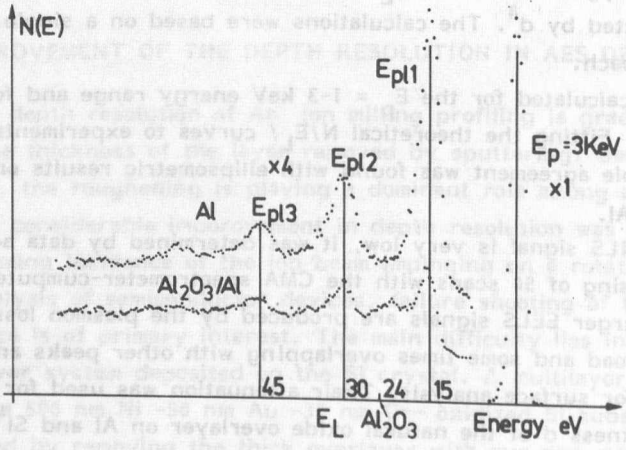

Fig.2.

On Fig.1 the plasmon loss peaks of the substrate Al are fully suppressed by the thin oxide overlayer, whereas at 3 keV they appear attenuated. The determination of a d was based on the $N/E_{pl2}/$ and $N/E_{pl3}/$ second and third plasmon peaks. These measurements were made on the KRATOS ES 300 high resolution electron spectrometer in the Isotope Inst. Budapest.

ELASTIC PEAK ELECTRON SPECTROSCOPY

Further development was achieved in EPES, suitable for surface analysis, non destructive depth profiling and an auxiliary method for AES, EELS and SEM. The present status of EPES and its possible applications are summarized in a recent review paper[3]. New results have been achieved in the angular distribution of elastic electron scattering [5,6,7], and in the determination of λ IMFP. The angular distribution I/θ / of elastically backscattered electrons was analysed with our single elastic scattering approach using differential scattering cross sections of Fink and Reimer[3]. Some results are presented in Fig.3 for Al, Cu, Ag and Au at E=1 keV and 75° angle of electron incidence. /I/θ / in arbitrary units, different for each element/.

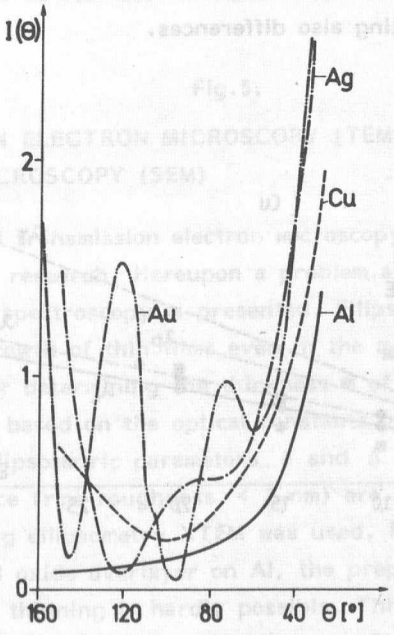

Fig.3.

These theoretical I/θ / curves are quite similar to experimental results of Bronshtein (cited in[7]).

The effective elastic backscattering cross sections have been extended to the 5-40 keV kinetic energy range in the Z=3-40 atomic number domain. Calculations were based on the Thomas-Fermi-Dirac atomic potential model and first Born approximation, useful, for this energy range[5,6].

The IMFP of electrons was determined by CMA elastic peak measurements evaluated with angular corrections, using differential elastic scattering cross sections of Fink, Reimer (cited in[3]) and new data calculated by Jablonski with the partial wave expansion method for a number of elements and energies. Results of cooperation with the Inst. Phys.Chemistry (Warsaw) have been published in[8].

The IMFP of electrons is now in the focus of interest of international research. Theoretical results[8] of Ashely (λ_A), Liljequist (λ_L), Powell (λ_P), and Tokutaka (λ_T) are presented in Fig.4 for Cu, containing our CMA experimental results and RFA results of Seiler evaluated with angular corrections[7]. Fig.4. shows also some XPS literature data. MS denotes our experimental point at E=2.2 keV evaluated by Jablonski with multiple scattering Monte Carlo analysis. The CMA and RFA data are scattered among the theoretical curves, exhibiting also differences.

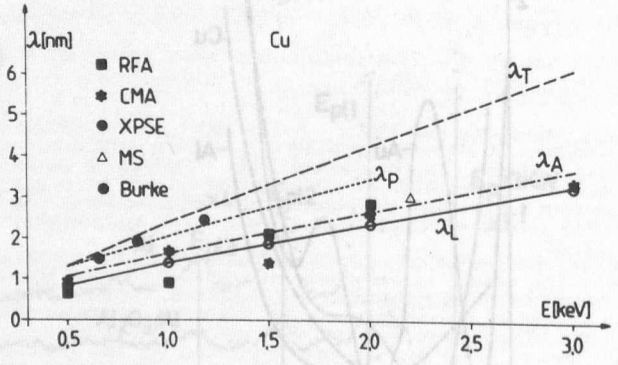

Fig.4.

103

In a more refined analysis, double and multiple elastic scattering of electrons should be taken into consideration. This is obvious by comparing λ_e elastic mean free path with λ IMFP[3], as shown in Fig.5. λ_e was based on Jablonski's new results and in some cases on those of Reimer (cited in[3]).

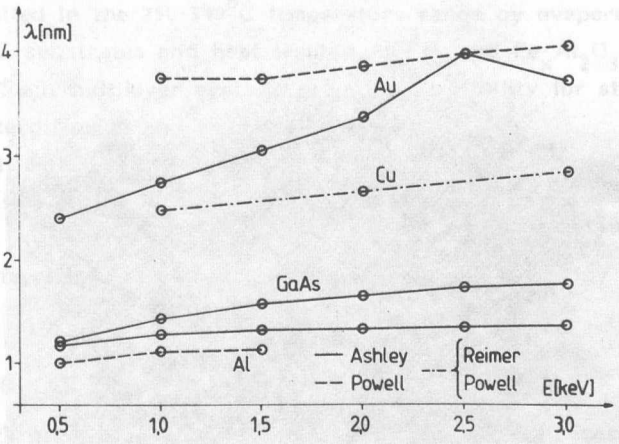

Fig.5.

TRANSMISSION ELECTRON MICROSCOPY (TEM) AND SCANNING ELECTRON MICROSCOPY (SEM)

Cross sectional transmission electron microscopy (XTEM) became a powerful tool in thin film research. Hereupon a problem associated with ellipsometry and electron spectroscopy is presented. Ellipsometry is very sensitive to measuring the growth of thin films even in the monolayer range. However ellipsometry only for determining the thickness d of a transparent overlayer (e.g. Al_2O_3 on Al) based on the optical constants of the substrate is rather problematic. The ellipsometric parameters ψ and Δ characteristic of a perfectly smooth surface (rms roughness < 2 nm) are affected by the roughness. For calibrating ellipsometry XTEM was used. Regarding a very thin (d 2-4 nm) natural oxide overlayer on Al, the preparation of the XTEM sample by ion beam thinning is hardly possible. This problem was solved by developing a special multilayer structure on a Si (111) substrate[9].

It consists of a 1000 nm Al-thin Al_2O_3 film prepared by oxidation in dry O_2 10^{-1} Pa, 300°C, 1 h and 500 nm Al vacuum deposited. The HRTEM image of this layer structure embedding the thin oxide film was made in the Internat. Center of electron Microscopy, Halle GDR. It is shown in Fig.6 [10].

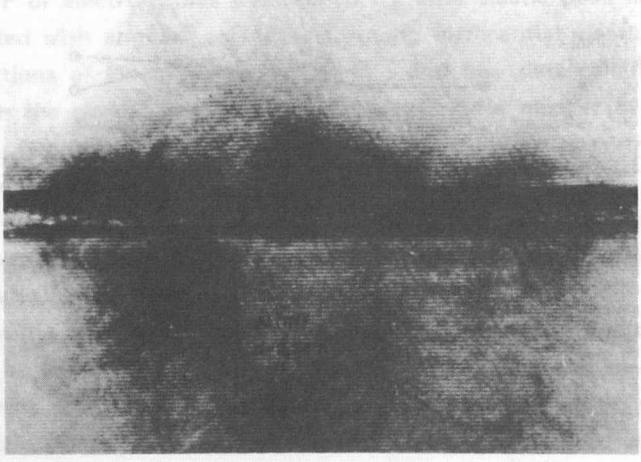

Fig.6.

The XTEM image reveals lattice fringes of Al (111) missing in the embedded Al-oxide region. This means a simple geometrical determination of the oxide layer thickness. Regular distance of the lattice fringes corresponding to Al (111) planes (0.234 nm) was used for calibration, resulting in d=2 nm in the oxide layer.

The morphology and structure of thin film-substrate systems were studied by TEM replica techniques and by SEM as well. TEM and SEM studies on the effect of oxygen on the structural development of evaporated Cu films revealed a correlation between the surface growth morphology and grain size distribution with the partial pressure of oxygen and film thickness. The development of growth hillocks was interpreted by surface microchemistry of the crystal face[11]. The very early stages of SiO_x film formation on NaCl (100) surfaces revealed the selective nucleation of SiO_x on the surface defects resulting in decoration patterns produced by three dimensional SiO_x grains. The experiments have been extended to their morphology and to activated condensation of Au on NaCl covered by a thin

SiO_x film[12]. The surface roughening produced by ion milling on SiO_x/Si surface was studied by TEM in cooperation with Dr.A. Zalar (IEVT, Ljubljana) and prof. Rasigni (Université d'Aix Marseille). The sputtered surface was shadowed by Pt for TEM studies, displaying the surface roughness[1].

Intermetallic phase formation by reaction of Al and transition metals (Mn, Fe, Cr) has been studied in thin films by TEM and x-ray diffraction in cooperation with ALUTERV-FKI. Bilayer and multilayer thin films have been deposited in the 250-530°C temperature range by evaporation in 10^{-6} Pa onto a-C substrates and heat treated Al_xFe_y and $Fe_xAl_2O_3$ phases were observed. Such multilayer systems provide a possibility for studying phenomena of interdiffusion and solid state reactions[13].

Interdisciplinary investigation of air pollutants have been carried out in cooperation with ATOMKI (Debrecen). Air pollutants collected by Cu and Pt samples in a cascade impactor have been analysed by SEM and EPMA in our Institute, determining particle size (1-4 μm) morphology and composition[14].

ACKNOWLEDGEMENTS

Results presented in this report have been achieved in cooperation with our collegues: Dr.Á.Barna, L.Gosztola, Dr.M.Menyhárd, Dr.I.Pozsgai, G.Sáfrán and A.Sulyok, with research institutes in Hungary: J.Ádám, TUNGSRAM Research (Budapest), Dr.Á.Csanády, ALUTERV-FKI (Budapest) Dr.L.Kövér and coworkers, ATOMKI (Debrecen), Dr. Z.Schay, Isotope Research Inst., (Budapest) and with international cooperation:

- Prof. Liljequist, University of Stockholm, for kindly sending his results
- Prof. G.Guenter, University of Zürich
- Prof. K.Urban, Metal Research Institute, Stuttgart, (BRD)
- Dr. A.Jablonski and Dr.P.Mrozek, Inst. Phys. Chemistry, Polish Acad.Sci., Warsaw, Poland
- Prof. M.Rasigni, Centre d'etude des Couches Minces, (Université d'Aix Marseille III (France)
- Dr. F.M.Reicha and Dr.M.El Hiti, guest scientists, Monsoura University, Faculty of Sciences, Monsoura (Egypt)
- Dr.G.Scholz, Inst.Solid State Phys. Electron.Microscopy, Halle (GDR)
- Dr. A.Zalar, Inst.Electronics and Vacuum Technics, Ljubljana (Yugoslavia).

Authors appreciate their cooperation.

REFERENCES

1. Barna P.B., Gosztola L, Zalar A., and Rasigni M.
Direct TEM study of the roughening of Si/SiO_2 interface induced during AES depth profiling
Surf. Interface Anal. 9 328 (1986)

2. Sulyok A. and Sáfrán G.
Improvement of depth resolution in Auger electron spectroscopy depth profiling by presputtering.
4th Internat.Conf. Quantitative Surface Analysis, Teddington, Nov.1986. Abstracts P3.

3. Gergely G.
Elastic peak electron spectroscopy. Scanning 8 203 (1986)

4. Gergely G., Menyhárd M. and Sulyok A.
Some new possibilities in non-destructive depth profiling using secondary emission spectroscopy: REELS and EPES
Vacuum 36 471 (1986)

5. Gergely G., Jablonski A., Menyhárd M., Mrozek P. and Sulyok A.
Angular effects of the differential elastic scattering in elastic peak electron spectroscopy.
Acta Univ. Wratislawiensis No.937. Matematyka, Fizyka 48 41 (1986)

6. Gergely G., Menyhárd M., Sulyok A., Jablonski A. and Mrozek P.
Determination of the mean free path of electrons in solids from the elastic peak. III.
Acta Phys.Hung. 60 289 (1986)

7. Gergely G. Angular corrections for determining the electron inelastic mean free path (IMFP) by elastic peak electron spectroscopy.
Vacuum 37 149 (1987)

8. Яаблоньски А., Гергели.
О стандардизации процедуры определения средней длины неупругого пробега электрона
Поверхность, No.10 (1987), 74

9. Barna P.B., Bodó Z., Gergely G. and Ádám J.
Spectral ellipsometric,TEM and electron spectroscopic investigations on oxidized aluminium thin films.
Vacuum 36 465 (1986)

10. Sáfrán G. and Scholz G.
Cover photograph. Fizikai Szemle (Journal of the Hungarian Physical Society Eötvös Loránd). No.8-9 (1986)

11. Reicha F.M., El Hiti M., Barna P.B.
Effect of oxygen on the structure and growth morphology of vapour deposited Cu films,
Vacuum 37 93 (1987)

12. El Hiti M., Barna P.B. and Reicha F.M.
Structure and growth morphology of SiO_x films deposited on NaCl (001) faces.
Vacuum 37 97 (1987)

13. Csanády Á., Guenter J.R., Marks O. and Barna P.B.
Intermetallic phase formation by reaction of thin films of aluminium and iron. Proc. 11th Int.Congr. Electron Microscopy, Kyoto (Japan) 1987 1409

14. Kövér L., Tóth J., Schág J.B., Borbély-Kiss I., Barna P.B., Pozsgai I., and Medve F.
Surface analysis of air pollutants collected in populated areas
Vacuum 37 175 (1987)

A COMPUTER CONTROLLED DOUBLE CRYSTAL X-RAY GONIOMETER

J.Marinka-Tóth, L.Zsoldos

The double crystal x-ray topographic goniometer RT-3, built in the institute just ten years ago, has been modified and completed for high resolution diffractometry in order to determine the strain distribution in near surface layers of otherwise perfect crystals. The characteristic features and most important parameters of the system is described in the paper below.

GONIOMETER

The following modifications were necessary

i) Exhange of the DC motor of the crystal (sample) rotation (ω-axis) to a stepping motor (Gamma ML 330/220/k, 200 steps/turn[x]), which drives direct the spindel of a worm gear with a differential screw. A single step of the motor corresponds to 10^{-5} degree on the axis. The smallest step during the measurements is 10^{-4} degree. A similar motor can be applied for sample translation ($\pm$25 mm), but the original DC drive was kept temporary.

ii) A special sample holder was built with stepping motor driven rotation around the azimutal (ϕ) axis, which is normal to the sample plane (Fig.1). Here a single motor step corresponds to 10^{-2} degree sample rotation. (Motor: 11MS154 Moore Reed Ltd, 24 steps/ turn.)

iii) A motor driven filter disc was placed in front of the entrance slit, in order to keep the conuting rate below a level of appr. 4.10^3 counts/s. The disc contains 8 openings which are covered by Ni foils of appropriate thicknesses, for giving attenuation factors of appr. 6, 50 and 300 or 4, 20 and 100 respectively.

---

[x]Gamma Works, Budapest, Hungary

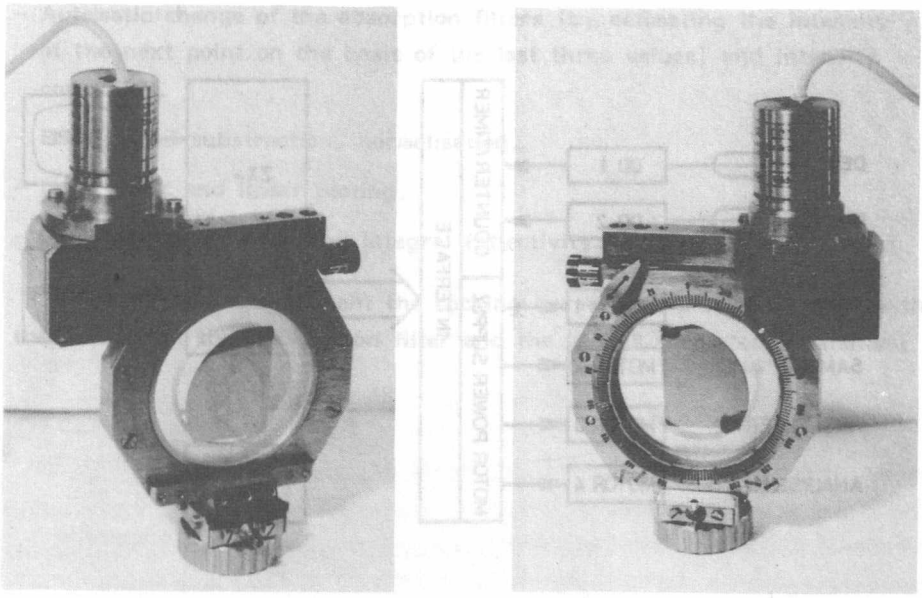

Fig.1. Sample holder with stepping motor for azimuthal rotation

The monochromator is made of Si, in asymmetric cut for the 422 reflection of CuKα_1 radiation (b = 0.02, ϑ_B = 44.05° thus the reflected beam is practically polarised perpendicular to the plane of incidence). The beam size at the sample site is ≤ 10x50 mm with a divergency of 0.6" and with intensity of 3.10^4 counts/smm^2 (using 1.2 kW sealed off fine focus tubes).

CONTROL SYSTEM

The control system (Fig.2) is based on a ZX-Spectrum 48 K microcomputer and a special interface (with built in monitor Tungsram TUV 211[x]) which allows the control of the power supply of four stepping motors and two timer-counter circuits for two independent detectors. (Two detectors are necessary e.g. for the simultaneous measurement of the O and H beams in Laue-case). One of the four motor connections is free in the present configuration. It can be used either for the sample translation or for the rotation of an eventual third (analyser) crystal. Simultaneous operation of two or more motors is not possible. The actual status of operation is indicated by a set of LED-s.

[x] TUNGSRAM Co.Ltd., Budapest, Hungary

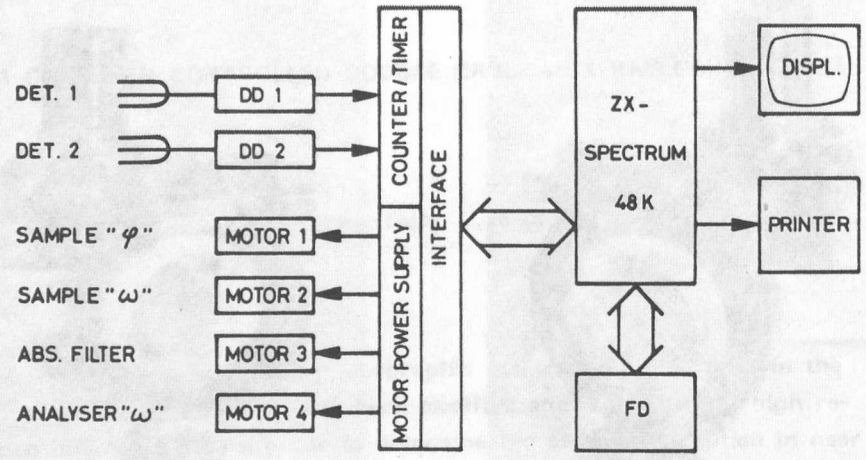

Fig.2. The block diagram of the system

As mass storage a floppy drive (1.2 MB) is applied which is compatible with that of the IBM PC-s thus experimental data are accessible for further operations using more powerful computers.

The detectors are Gamma ND131, Ø 60 scintillation counters connected to Gamma NK350 lin-log ratemeters (DD1, DD2).

SOFTWARE

The main programme which is written in BASIC, but includes machine-code routins for controlling the stepping motors and counter/timer circuits, consists of the following parts:

- Direct commands for the motors and counters,
- Measurement of the intensity of the primary beam (I_O, without sample) and background,
- Automatic fine adjustment of the sample with respect of the azimuthal angle ℓ (the position corresponding the highest intensity is searched, using a narrow but high slit),
- Scanning across the Bragg-peak (with pre-selected step size and range),

- Automatic change of the absorption filters (by estimating the intensity at the next point on the basis of the last three values) and intenstiy correction,
- Background substraction, normalisation,
- Logarithmic and linear ploting,
- Determination of peak and integral reflectivity.

During the measurement the rocking curve is displayed together with the position of the absorption filter and the last 20 corrected intensities.

HIGH LATERAL RESOLUTION X-RAY FLUORESCENCE ANALYSIS IN THE SCANNING ELECTRON MICROSCOPE

I. Pozsgai

The excitation of specimens by X-rays for analytical purposes can be easily carried out in an electron microscope by putting a thin foil into the electron beam which plays the role of a transmission X-ray source. The scheme of the experimental set-up of this technique of energy dispersive X-ray fluorescence analysis (EDXRF) can be seen in Fig.1.[1]

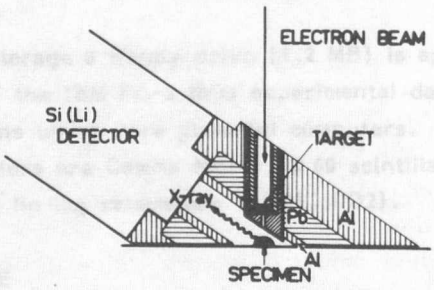

Fig.1. The scheme of the X-ray fluorescence attachment

By the help of an X-ray fluorescence attachment to an energy dispersive X-ray spectrometer detection limits down to 1 ppm can be achieved in an electron microscope[2]. Unfortunately the excellent detection limits could be obtained only at the cost of sacrificing the good lateral resolution of the electron beam microanalysis. An X-ray spot size of 6 mm was used in the above cited paper[2].

The aim of this short note is to show that the lateral resolution of the EDXRF can be considerably improved while retaining the possibility of trace element analysis in the electron microscope. Bauxite has been chosen as specimen to demonstrate the capabilities of the technique.

EXPERIMENTAL

Here we describe a preliminary study of bauxite by EDXRF in a JSM 35 scanning electron microscope. An improvement of the lateral resolution of our technique from 6 mm to 0.3 mm is an important factor of this study, which aimed at revealing the local trace element content of bauxite and a possible correlation of main components and trace elements. The chances of finding the above correlation depend largely on the size of the X-ray beam because the broader the beam the higher may be the inhomogeneity of the irradiated area. Commercial fluorescence analysiers produce a spot size of 30 mm, while specialized ones do that of 2 mm. The electron microscope itself plays an important role in the selection and observation of the specimen area of interest and in the precise aiming.

For the analysis we have used a Mo target 10 /um in thickness. The accelerating voltage of the microscope was 39 kV while 25 /uA electron current could be produced. A characteristic feature of this technique is that it allows both electron beam microanalysis (when the retractable detector is at "out-position") and X-ray fluorescence analysis (when the detector is "in").

The lateral resolution of EDXRF was determined by moving a 30 /um thick Ni wire along a line across the X-ray beam and by measuring the Ni intensity distribution during the movement of the microscope stage with the Ni wire on it. Fig.2. shows the Ni intensity profile in question and the full width at half maximum of this curve (0.3 mm) is taken for the lateral resolution of the technique.

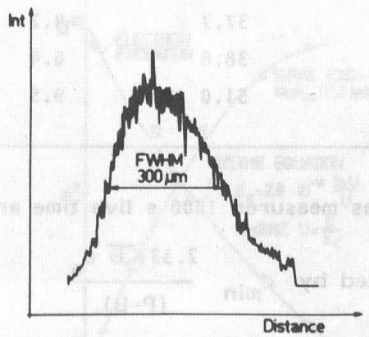

Fig.2. Ni intensity distribution taken while moving a 30 /um thick Ni wire across the X-ray beam. Its FWHM is considered to be the lateral resolution.

The detection limits were checked on a NBS 612 glass standard (Fig.3) and they were found to be only by factors 2 or 3 worse (Table 1) than in the case of applying a 100 /um Mo target (cf. ref 2).

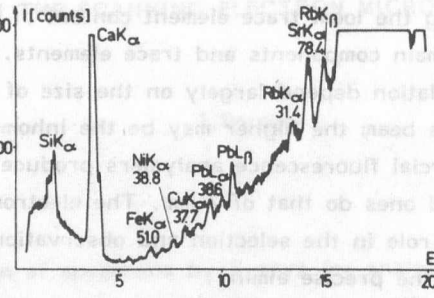

Fig.3. EDXRF spectrum of a NBS 612 glass standard (39kV, 10 /um thick Mo target, 1000 s live time)

TABLE 1.

Detection limits measured on NBS 612 glass standard (Mo target 10 /um thick)

	c_o(ppm)	c_{min}(ppm)
Rb	31.4	3.3
Sr	78.4	3.7
Pb	38.5	3.1
Cu	37.7	4.2
Ni	38.8	6.4
Fe	51.0	9.9

Remark: c_{min} was measured 1000 s live time and calculated by $c_{min} \frac{2.33\sqrt{B}\, c_o}{(P-B)}$

where P- peak intensity, B- background

The application of a thin Mo target (10 µm) is a must if we want to maintain high enough intensity in spite of the high collimation of X-rays. Another consequence of the high locality of analysis is a deterioration of spectral cleanliness of the blind spectrum (Fig.4). Iron and lead can occur in the blind spectrum measured on a Si wafer but the extent of contamination is so small that it can not be confused with trace elements in the specimen to be analysed.

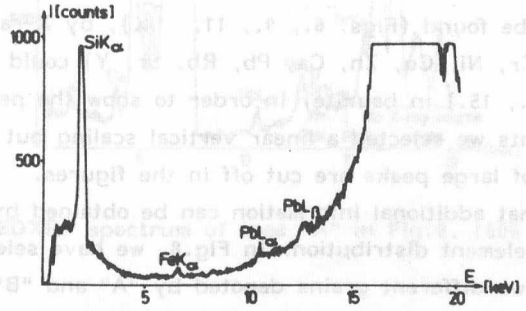

Fig.4. Blind spectrum measured on a Si wafer

Another point to be made is the difference in the atomic number dependence of cross sections of excitation for electrons and X-rays respectively (Fig.5).

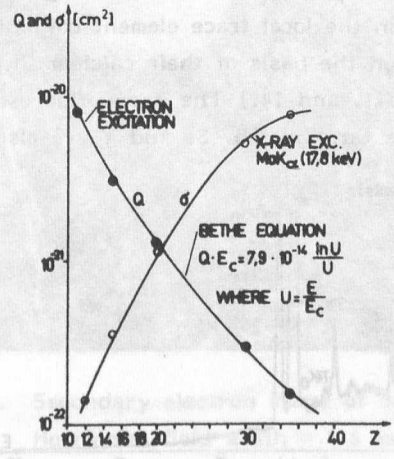

Fig.5. Comparison of ionisation cross sections for electron and X-ray excitation of X-rays. The latter is taken from ref.3.

This causes a higher sensitivity of EDXRF at medium and higher atomic numbers and a sensitivity loss at light elements. This should be taken into account when interpreting the spectra to follow. The excitation cross sections for low Z elements can be improved by using appropriate transmission X-ray foil sources instead of Mo[2].

RESULTS

While by electron excitation elements with atomic number higher than 26 (Fe) could not be found (Figs. 6., 9., 11., 14.), by X-ray excitation 9 more elements (Cr, Ni, Cu, Zn, Ga, Pb, Rb, Sr, Y) could be detected (Figs. 7., 10., 12., 15.) in bauxite. In order to show the peaks belonging to trace elements we selected a linear vertical scaling but as a consequence the top of large peaks are cut off in the figures.

Let us see what additional information can be obtained by EDXRF regarding the trace element distribution. In Fig.8. we have selected an area in bauxite where two different grains denoted by "A" and "B" can be seen. As the electron probe microanalysis (EPMA) shows (Figs.6. and 9.) the grain "A" and "B" can be contrasted based on their calcium and iron content. (In the righ upper corner of the spectra a capital letter indicates the analysed area). According to the EDXRF spectra (Figs.7. and 10.) on area "A" trace elements like Pb, Rb and Sr could be found while area "B" contained Ni, Cu, Zn, Pb, Sr and Y in trace quantitites.

The fluorescence analysis of another area (Fig.13) provides similar additional information on the local trace element content. The grains "C" and "D" differ mainly on the basis of their calcium and iron content as the EMPA shows (Figs.11. and 14.) The X-ray fluorescence spectra reveal that trace elements like Cu, Zn, Pb, Sr and Y are also present.

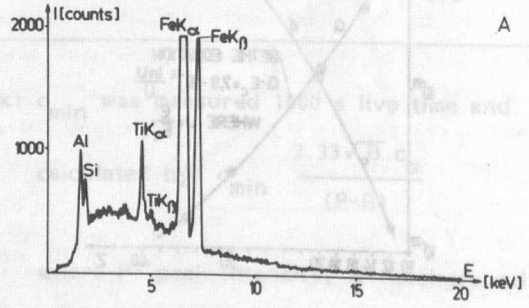

Fig.6. Electron probe microanalysis (EPMA) of area "A" in Fig.8 (25 kV, 200 s live time)

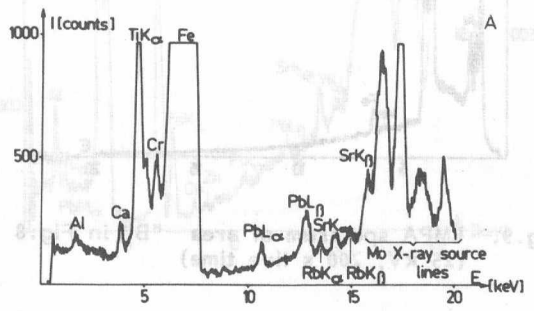

Fig.7. EDXRF spectrum of area "A" in Fig.8. (600 s live time)

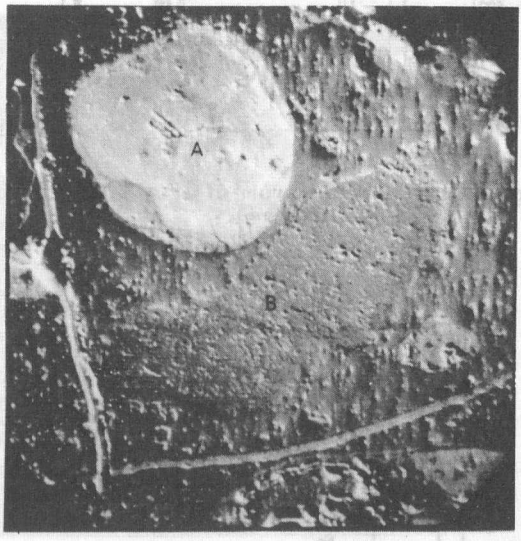

Fig.8. Secondary electron image of bauxite
Horizontal field width = 4.5 mm

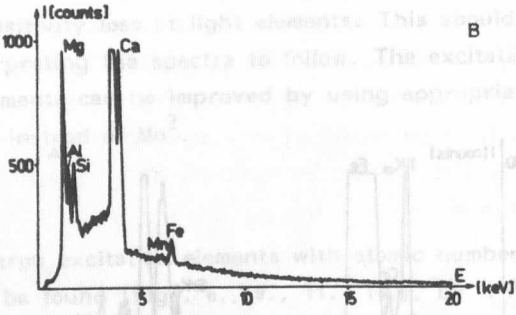

Fig.9. EMPA spectrum of area "B" in Fig.8 (25 kV, 200 s live time)

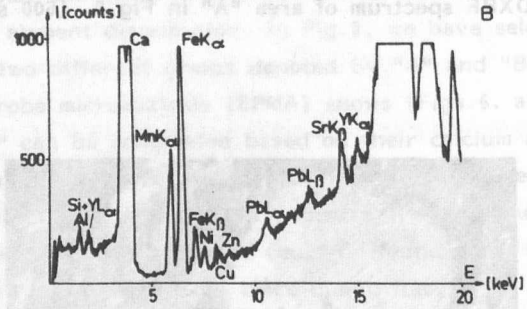

Fig.10. EDXRF spectrum of area "B" in Fig.8. (600 s Live time)

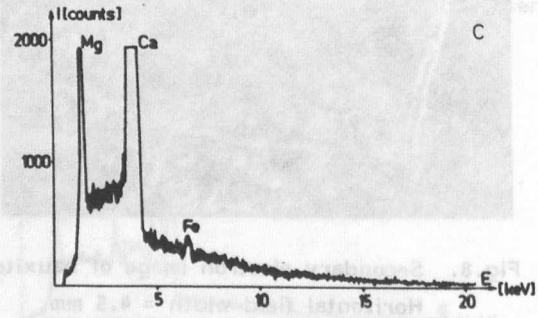

Fig.11. EPMA spectrum of area "C" in Fig.13. (25 kV, 200 s live time)

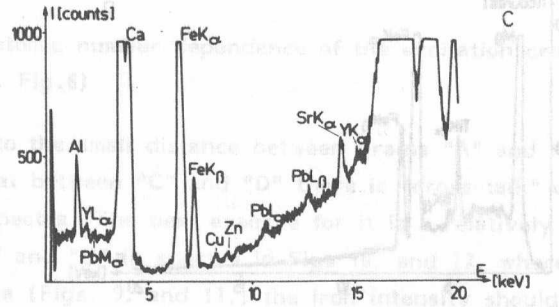

Fig.12. EDXRF spectrum of area "C" in Fig.13. (600 s live time)

Fig.13. Secondary electron image of a second area in bauxite. Horizontal field width=4.5 mm

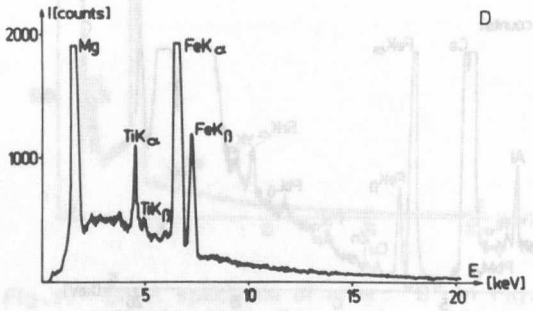

Fig.14. EPMA spectrum of area "D" in Fig.13. (25 kV 200 s live time

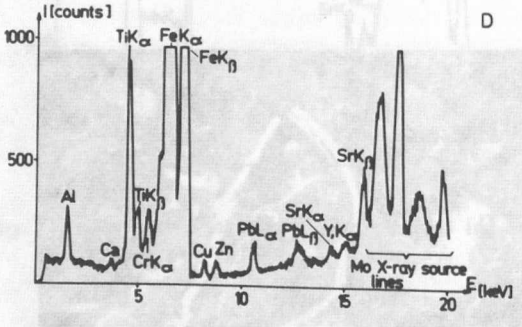

Fig.15. EDXRF spectrum of area "D" in Fig.13. (600 s live time)

DISCUSSION

If the EDXRF spectra are compared with the blind spectrum (Fig.5) then it becomes quite clear that the small peaks of trace elements can not be ascribed to spectral contamination of the equipment. On the other hand a perfect one-to-one correspondence of the peak intensities of main components in electron and X-ray excited spectra can not be expected for more than one reasons:

a) the depth of generation of X-rays in the specimen is at least by one order of magnitude higher for X-ray excitation than for electron excitation.

b) the atomic number dependence of the excitation cross sections is different (cf. Fig.6)

c) due to the small distance between grains "A" and "B" (0.1 mm) as well as that between "C" and "D" there is "cross-talk" of elements in the EDXRF spectra. The best example for it is a relatively high iron peak in grains "B" and "C" in spectra in Figs 10. and 12. where according to the EPMA data (Figs. 9. and 11.) the iron intensity should be low.

In order to be able to draw conclusions regarding the correlation between main components and trace elements in minerals a more systematic study is needed.

CONCLUSIONS

Summarizing the results it is concluded that the lateral resolution of EDXRF could be considerably improved while retaining the trace element analysing capability of the method. The electron microscope as environment plays an important role in the selection of area for EDXRF. Among others secondary and backscattered electron imaging as well as EPMA can aid the area selection. The prospects for the further improvement of locality of the EDXRF analysis are good.

REFERENCES

1. I.Pozsgai
Patent pending

2. I.Pozsgai
Electron Microscopy and X-ray analysis
1985, Inst.Phys.Ser. No.78. pp. 201-202

3. Watson R.L. et al.
Advances in X-ray Analysis
Plenum Press, 1978. Vol.21. pp.105-118

P/N JUNCTION LOCALIZATION IN SEMICONDUCTOR LASER STRUCTURES

Attila L. Tóth

INTRODUCTION

Semiconductor lasers as well as LEDs are multilayer heterojunction devices where the composition changes across the layers due to the working principle and the epitaxy method of the production. The knowledge of their parameters as e.g. p/n junction position is very important in physical and technological relation. This paper shows a quantitative SEM line profiling method developed and used to solve this problem in the practice of laser device R+D.

The layer structure of the laser device simplifies the measurement to one dimensional case (unlike the localization of curved junctions of IC structures requiring etching or EBIC mapping), but the need of simultaneous localization of the GaAs active layer and the junction excludes the use of etching method and of voltage contrast for their localization respectively. Both of these methods are based on secondary electron imaging, which could provide the required overall resolution in the 20-50 nm range.

To solve the problem the use of backscattered electron (BE) and electron beam induced current (EBIC) signals seems to be appropriate. The difference in mean atomic number between the GaAs and GaAlAs is enough to show the active layer on the compositional BE image as white stripe due to enhanced backscattering. The measurement can be carried out on smooth cleaved cross-sectional surface, not disturbing the EBIC measurement.

MEASUREMENT AND DATA PROCESSING

Optimalization of the parameters of the measurement is far from simple. To simplify the EBIC profiling relative deep excitation, i.e. high beam

energy of 15-25 keV is needed. In this way the contribution of surface recombination is less, and the energy of backscattered electrons is high enough to be detected by semiconductor detectors. On the other hand the beam diameter had to be kept minimal, limiting the beam current less than 1 nA.

The resolution limit of both the BE and EBIC signals is in the range of 0.1 /um, due to the electron scattering and carrier diffusion process, respectively. To overcome this, the line profiles have to be differentiated (resulting the DBE and DEBIC curves). This was done either numerically by the computer, or by modulating the beam position and detecting the derivative signal using a lock-in amplifier (EG+G 5208).

The measurement were carried out in a JSM25 SIII type scanning electron microscope. The specimen stage has been modified to handle the small laser chips without difficulty, and to provide large solid angle for the appropriate BE detection in the subnanoampere probe current range (Tóth 1987). Both signals were amplified by a Keithley 427 fast current amplifier, digitized and collected by an Apple II computer, which performed the data manipulation, store and representation as well.

RESULTS AND DISCUSSION

Typical results can be seen in Figs.1a-1d. In the derivative mode the heterointerfaces (inflection points of BE profile) show well localized sharp extrema, while the smeared maximum of EBIC profile (generally interpreted as the junction position) corresponds to the zero crossing of the DEBIC curve. The whole measurement was carried out at 100.000x magnification of the SEM, reaching the 0.02 /um precision of the junction location in a 0.2 /um thick active layer.

The p/n junction location coincides with the EBIC maximum only in the case of symmetric EBIC profile, where the diffusion lengths and the resistivities are equal on both sides of the junction. To estimate the inaccuracy of our measurements, Monte Carlo simulations were performed. The basic MC program is one of Joy and Pimentel (1985), modified to calculate the EBIC profile across of a surface perpendicular p/n junction with different diffusion lengths on its sides. Simplifications had to be made to speed up the program (run in compiled BASIC on an Apple II computer with Accelerator), but despite of these the simulated line profiles show acceptable agreement with the measured ones.

Typical curves are shown in Fig.2a. with L1=L2=1 /um and L1=1 /um, L2=5 /um values. The beam energies and the depletion layer widths were 15 keV and 0.1 /um for both cases. Analyzing a set of such curves, a simple semilogarithmic relationship has been found between the ratio of diffusion lengths and the EBIC peak position shift in the 0.1 - 10 /um diffusion length range, as shown in Fig.2b., providing an estimation of the systematic error of the line scan measurement.

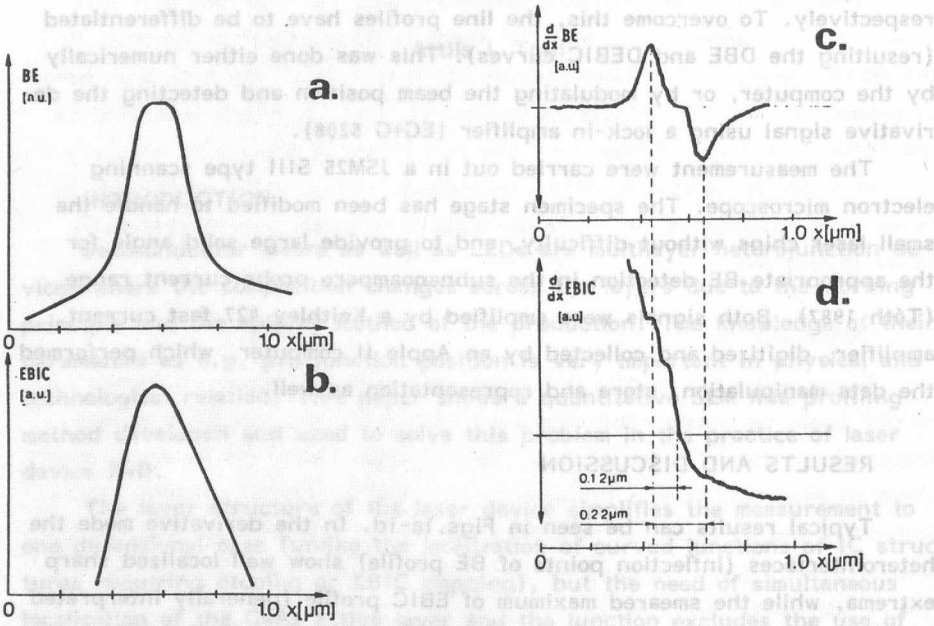

Fig.1. BE and EBIC line profiles across a laser structure
1a: BE, 1b: EBIC, 1c: DBE, 1d: DEBIC

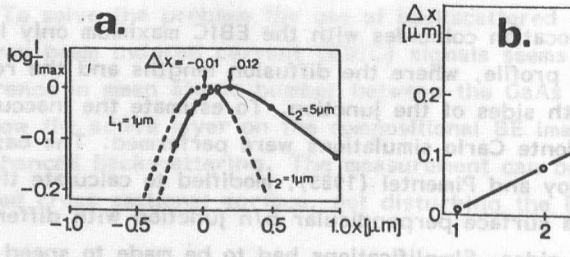

Fig.2. MC simulation results
2a: EBIC line profiles with different L values
2b: the EBIC peak shift v/s L ratio dependence

ACKNOWLEDGEMENT

I am grateful to Dr. D.C. Joy for the MC program and A. Konkol for his help in measurement. I also thank to Dr. J. Pfeifer for supplying the specimens.

REFERENCES

Joy D.C. and Pimental C.A. 1985. Inst. Phys.Conf. Ser. No.76 355

Tóth A.L. 1987. to be published

Division of Microwave Devices

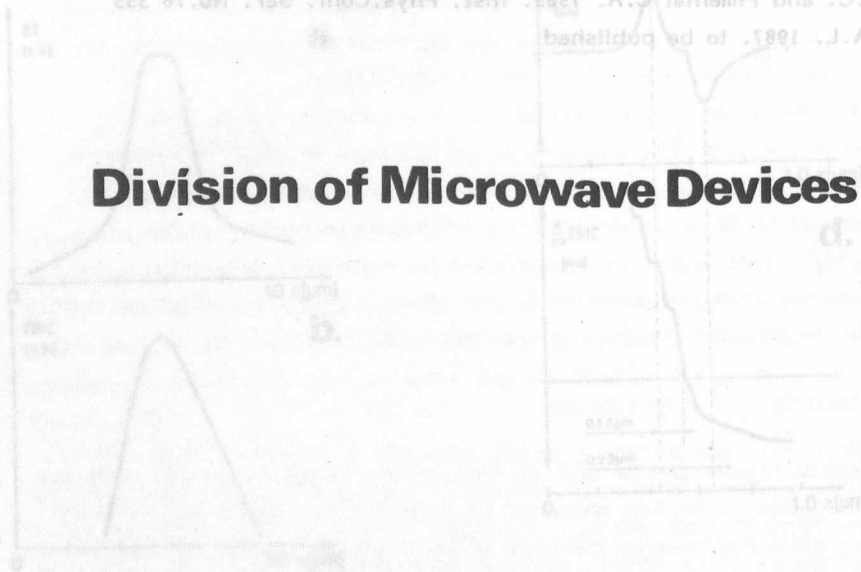

TEST PATTERN - A POWERFUL TOOL FOR OPTIMIZATION AND PROCESS CONTROL OF GaAs MESFET TECHNOLOGY

B.Kovács, S.Biró, I.Mojzes, B.Szentpáli,
M.Németh-Sallay, P.Gottwald[+]

ABSTRACT

To study and control both the epitaxial layer parameters and the electrical parameters of actual devices a set of test patterns were constructed for GaAs MESFET technology.

Five different gold-based ohmic contact structures were investigated to optimize the MESFET technology. The best results were obtained using the AuGe/Ni/Au ohmic contacts with 10% Ni amount in it.

INTRODUCTION

Recently compound semiconductor devices have become increasingly important in the group of microwave active devices.

To investigate and control the GaAs MESFET technology a set of test patterns was constructed. Applying these test patterns it is easy to measure both the epitaxial layer and the device parameters.

This work deals with the designed test patterns and demonstrates how to use it to optimize the device technology then the influence of material and technological parameters on the MESFET characteristics are shortly discussed.

TEST PATTERNS

To monitor device technology we have to apply the test patterns in the same technological process as applied for the real MESFET structures. This means that the processing of the test patterns should not introduce extra

[+]Department of Electronic Devices of the Technical University of Budapest
1111 Budapest, Goldman Gy. tér 3. , Hungary

steps into the technology. Moreover the test patterns do not require submicron lithography.

The test pattern set was designed for use in a computer controlled wafer tester system. To minimize the number of the measuring probes the different test patterns have identical pad arrangement.

When investigating new technological steps or new materials the test patterns can be placed on a separate mask set. When controlling MESFET processing the layout of the test chip can be integrated into MESFET's mask set.

The test chip containing all of the test patterns is shown in Fig.1.

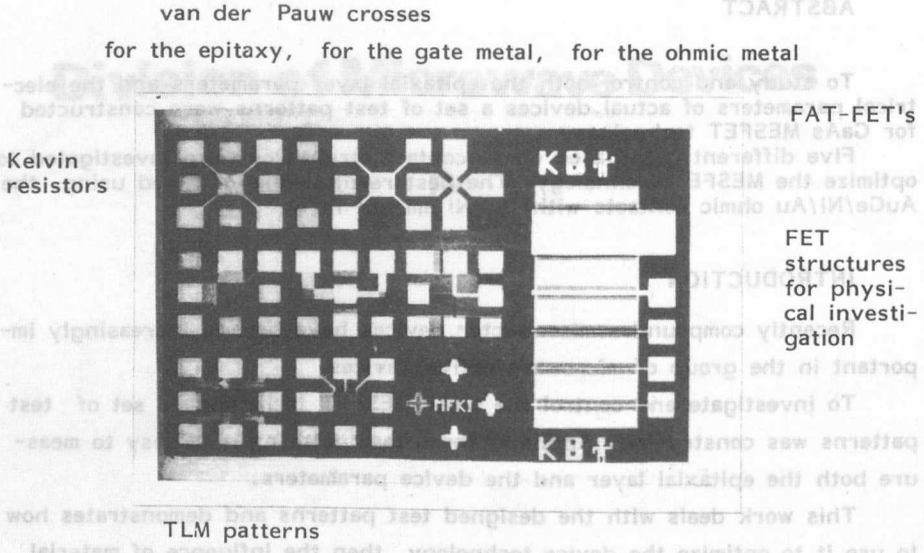

Fig.1.

The test patterns used for the sheet resistances, the specific contact resistance[1], and Hall-mobility measurements were placed on the left part of the chip. Since the sheet resistance of the ohmic metallization has great importance[2], increased attention was devoted to measure this parameter.

The so-called FAT-FET's are in the right top corner. There are two FAT-FET's on the chip with different gate lengths. Applying these struc-

ture the influence of series resistance on the capacitance - voltage measurements was investigated. Comparing the results obtained by these structures the smaller FAT-FET was chosen for the final measurements due to its smaller series resistances. The FAT-FET's were used for the determination of carrier concentration and drift mobility profile[3] as well as for Schottky junction qualification by the measurement of its current - voltage characteristics. There are three MESFET structures on the bottom of the FET column. They have identical gate lengths but different source - drain distances. Comparing the parameters of these structures the effect of the parasitic channel resistances could be determined.

THE MEASUREMENT SYSTEM

As we have mentioned above the test patterns as well as the MESFET's were measured by a computer controlled measurement system. The controller is a Commodore VC 64 microcomputer which communicates with the measuring instruments through IEEE-488 bus. To increase the quality - accuracy and reliability - of measurements the system is based on Keithley instruments. The versatile software of this system makes us capable of investigating different test layouts, too[1].

SAMPLE PREPARATION

The applied epitaxial layers were made by Effer-method, and the carrier concentration and layer thickness were checked by electrolytic profiling. A typical result is shown in Fig.2.

To minimize the parasitic series resistance of source and drain contacts of MESFET's and to minimize the heat stress of the Schottky gate metallization, five ohmic metallizations with different amounts of Ni were investigated. The ohmic metallizations consisted of AuGe/Ni/Au layer structures and the Schottky metallization consisted of a Cr/Ag/Cr/Au structure. The composition of ohmic metal structures was varied from the 0% of Ni to the amount of AuGe eutectic up to 13% of Ni to the AuGe eutectic.

The heat treatment of the samples were carried out in an open tube furnace applying a relatively slow heat pulse with 3 minute rise time. Three typical heating profiles are shown in Fig.3. The alloying atmosphere was forming gas with 30% H_2: 70% N_2 composition. The studied temperature range was from 300°C to 500°C.

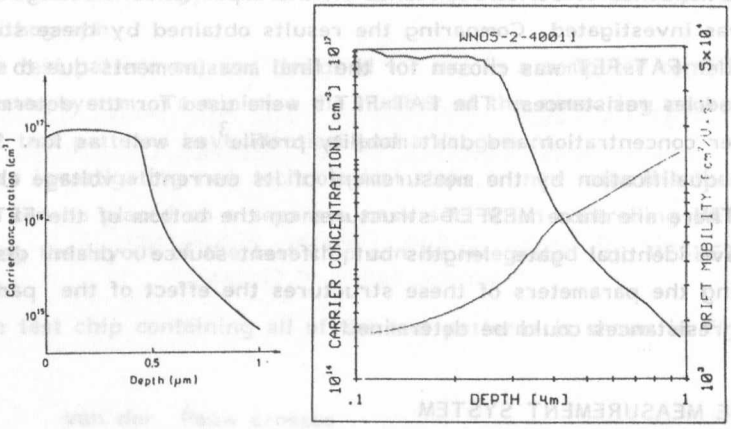

Free carrier concentration of the epitaxial layer measured by electrolytic C-V profiling

Carrier concentration and drift mobility measured by FAT-FET

2. ábra

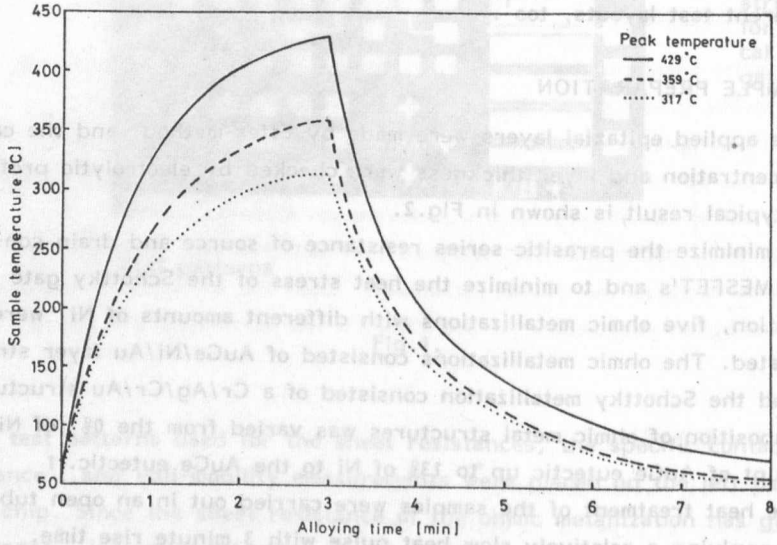

The alloying of ohmic metallization was carried out in an open tube furnace.
The applied atmosphere was 30% H_2 and 70% N_2.

3. ábra

RESULTS

Comparing the carrier concentration profiles obtained by electrolytic profiling and the profiles obtained by C-V measurements on the FAT-FET's, the profiles show a good agreement. (See Fig.2) The difference of measured layer thickness is due to the etching before the Schottky-gate evaporation. The reason of increasing drift-mobility is probably the damages under the metallization caused by the evaporation and the heat treatment.

The test patterns were used to study the effects of the heat treatment temperature on the device parameters. Comparing the different metallizations the results showed that the optimal heat treatment temperature didn't decrease with increasing the amount of Ni in the ohmic metallization.

Fig.4 shows the parasitic series resistances versus the heat treatment temperature.

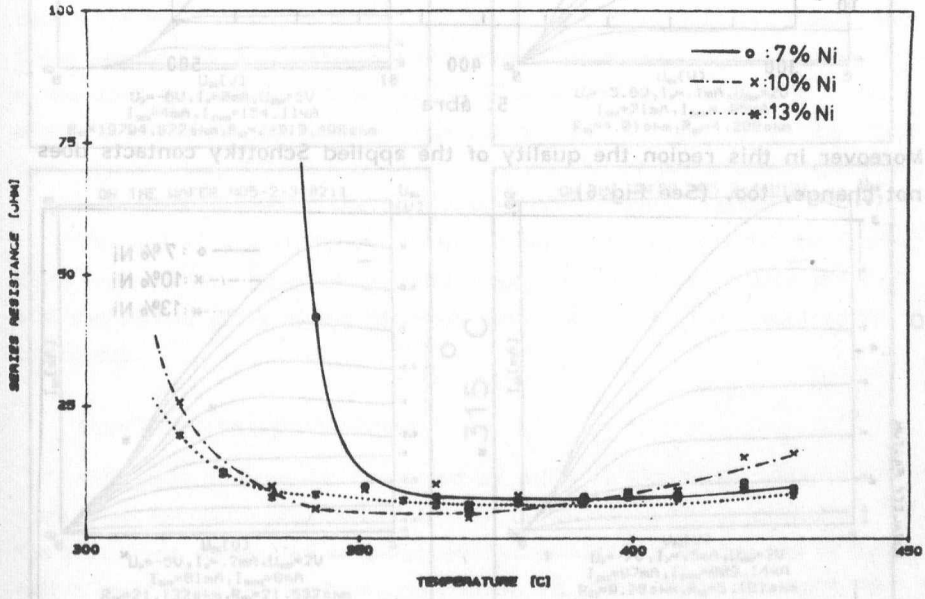

4. ábra

As we see, reaching a critical temperature - e.g. 340°C in the case of 10% Ni composition - the series resistance decreases and does not change above this temperature. Comparing this result to the obtained specific contact resistances the agreement is very good. (Fig.5)

Mesured by Kelvin resistor pattern (2-6)

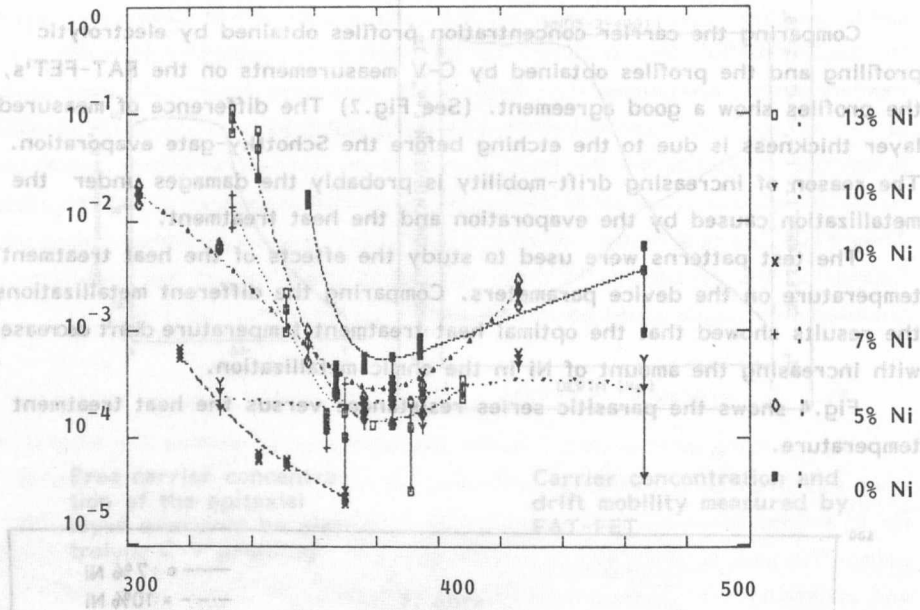

5. ábra

Moreover in this region the quality of the applied Schottky contacts does not change, too. (See Fig.6)

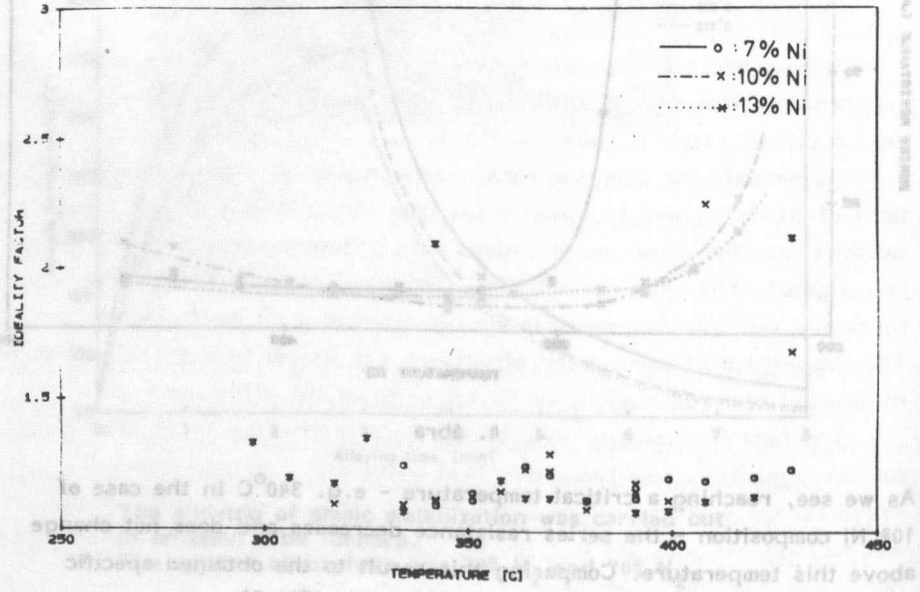

Fig.6.

Studying the surface morphology, the metallization with 10% Ni proved to be the best choice.

Fig.7. shows the output characteristics of MESFET's depending on the heat treatment process. As we see, the output characteristics did not change significantly as the heat treatment was carried out at a higher temperature then the critical one.

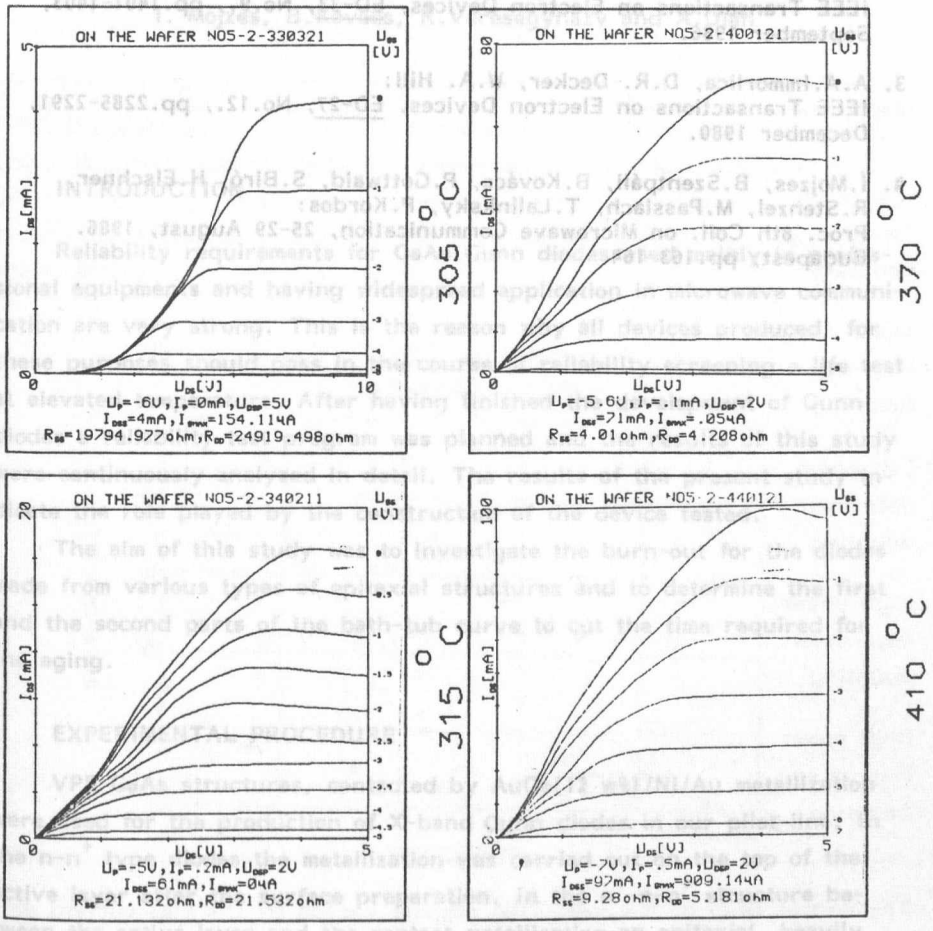

GaAs MESFET characteristics
The ohmic contact metallization consists of 10% Ni in it
The annealing was carried out at different temperatures

Fig.7.

REFERENCES

1. B.Kovács, I.Mojzes, R.Veresegyházy, B.Pécz:
'Improved Determination of Specific Contact Parameters and their Correlation with Arsenic Loss of AuGeNi/GaAs Contacts',
16th European Solid State Device Research Conference,
University of Cambridge, 8-11 September 1986.

2. B.Kovács, I.Mojzes:
IEEE Transactions on Electron Devices, ED-33, No.9., pp.1401-1403,
September 1986.

3. A.A.Immorlica, D.R. Decker, W.A. Hill:
IEEE Transactions on Electron Devices, ED-27, No.12., pp.2285-2291,
December 1980.

4. I.Mojzes, B.Szentpáli, B.Kovács, P.Gottwald, S.Biró, H.Elschner,
R.Stenzel, M.Passlach, T.Lalinksky, P.Kordos:
Proc. 8th Coll. on Microwave Communication, 25-29 August, 1986.
Budapest, pp.163-164

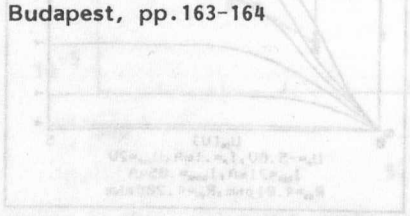

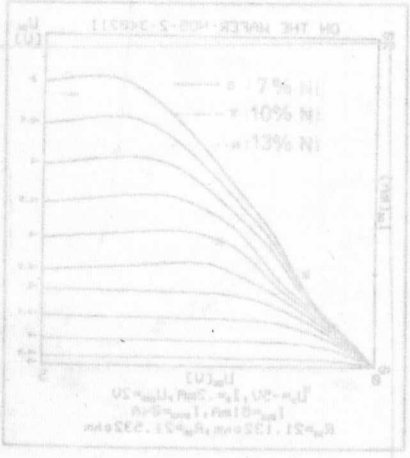

RELIABILITY OF GUNN DIODES: AN ELEVEN YEAR STUDY

I. Mojzes, B.Kovács, R.Veresegyházy and A.Oláh

INTRODUCTION

Reliability requirements for GaAs Gunn diodes used mainly in professional equipments and having widespread application in microwave communication are very strong. This is the reason why all devices produced for these purposes should pass in the course of reliability screening a life test at elevated temperature. After having finished the development of Gunn diodes a reliability test program was planned and the results of this study were continuously analyzed in detail. The results of the present study indicate the role played by the construction of the device tested.

The aim of this study was to investigate the burn-out for the diodes made from various types of epitaxial structures and to determine the first and the second parts of the bath-tub curve to cut the time required for the aging.

EXPERIMENTAL PROCEDURE

VPE GaAs structures, contacted by AuGe(12 w%)/Ni/Au metallization were used for the production of X-band Gunn diodes in our pilot-line. In the n-n^+ type diodes the metallization was carried out on the top of the active layer after the surface preparation. In the n^+-n-n^+ structure between the active layer and the contact metallization an epitaxial, heavily doped n^+ layer was applied. From these structure face-up (low power, $P_{max} < 40$ mW) and face-down (high power, 40 mW $< P_{max} <$ 300 mW) diodes were produced by means of rapid annealing [1]. The diodes were encapsulated into standard metalloceramic package. The structure of the tested devices is demonstrated in Table 1. For the aging experiment a home

made tester was use[2,3,4,5]. In this equipment each device under test (DUT) is protected by a series electronic circuit, limiting the current flowing through the device. The DUT, the measuring resistor and the electronic protection circuit are connected in series with the bias supply.

Table 1.

THE INVESTIGATED SAMPLES AND THEIR AVERAGE BURN OUT PERCENTAGE

Diode type	Construction	Symbol	Mean burn-out percentage %
Low power Face-up mounting	M-n-n^+-M	O, A	42
Low power Face-up mounting	M-n^+-n-n^+-M	▲, B	13
Low power Face-down mounting	M-n-n^+-M	●, C	15
High power Face-down mounting	M-n-n^+-M	+, E	42
High power Face-down mounting	M-n^+-n-n^+-M	Δ, F	11

The voltage drop on the measuring resistor caused by the bias current of the given diode, flowing through the diode at the applied bias voltage will be compensated in the protection circuit at the beginning of the test. In this way the voltage signal proportional to the deviation of the bias current during the aging will be measured and registered. If this deviation will be higher than 20% the DUT will be immediately disconnected by the protection

circuit. Using this approach the deterioration of the device can be "frozen in" and the results of processes taking place in the first part of the degradation can be analyzed by SEM and electrical measurements. During aging only DC parameters were tested and registered, RF measurements were carried out before and after the life test. In some cases thermal resistance measurements were also carried out before and after the aging.

RESULTS AND DISCUSSION

The results presented in this work are based on our 850.000 device-hour experience. In Table 1. the average burn-out percentage for various types of diodes is presented. The lowest value was obtained for metal (M)-n^+-n-n^+-M types and the highest one for the M-n-n^+-M type face-down mounted devices. For comparison the burn-out percentage for all tests is shown in Fig.1.

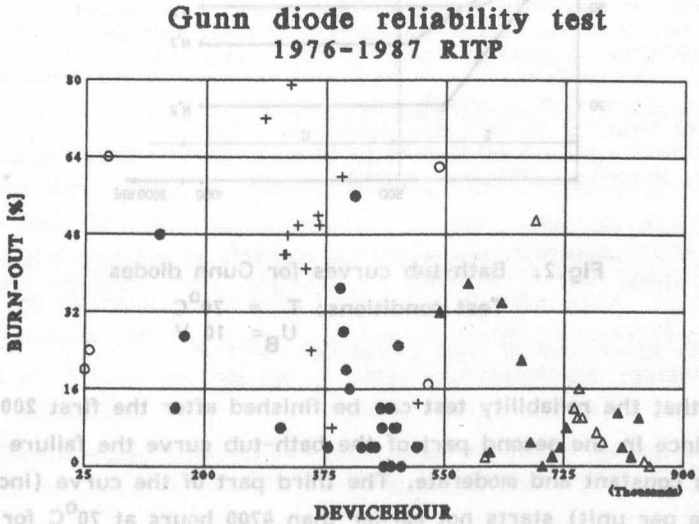

Fig.1. Burn-out percentage for various types of Gunn diodes

O, A - low power, face-up mounted dioes without contacting layer
▲, B - low power, face-up mounted diodes with contacting layer
●, C - low power, face down mounted diodes without contacting layer
+, E - high power, face-down mounted diodes without contacting layer
▲, F - high power, face-down mounted diodes with contacting layer

As it follows from this figure not only the average burn-out percentage but the scattering is higher for diodes without n^+ epitaxial contacting layer. Inhomogeneity of metal-high purity semiconductor contact, and possible formation of an intermediate surface layer after the etching prior to metallization are the main reasons for these results. In the case of devices with a low-resistivity contact layer the ohmic contact preparation is easier when the layer to be contacted is highly doped. To determine the bath-tub curve life tests with various duration were carried out. From these experiments we concluded that the first part of the bath-tub curve (decreasing failure rate per unit) finished before 200 .... 500 hour aging at 70°C at a bias of 10V. (See. Fig.2.)

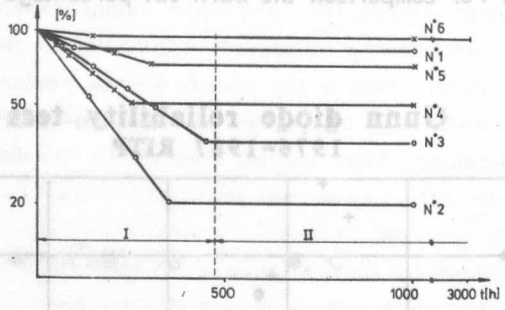

Fig.2. Bath-tub curves for Gunn diodes
Test conditions: T = 70°C
U_B = 10 V

It means, that the reliability test can be finished after the first 200 hours of aging since in the second part of the bath-tub curve the failure rate per unit is constant and moderate. The third part of the curve (increasing failure rate per unit) starts not earlier than 4700 hours at 70°C for diodes without n^+ contact layer mounted face-down. For diodes with n^+ layer this duration should be longer. From these results using Eyring-Arrhenius plot the failure rate per component at room temperature was found to be in the range of $(10...50)\times10^{-3}$%. An apparent activation energy for the processes taking place and causing the degradation was calculated from the results. This value was found to be E_a = 0.22 eV. It should be considered that this

value is close to the value obtained for the aging process in n-InP-AuGeNi system. The activation energy in this case was calculated to be E_a = 0.37 eV [6]. These values obtained for both GaAs and InP based systems are characteristic for the processes in thin films and it is close to the value obtained for the diffusion of some contact materials such as gold. There are no published data for AuGe based metallization systems, but Oliver and Bower[7] obtained a value of 1.0 eV for Au, and Behmann a value of 1.5 eV from realiability assessment of small signal GaAs FET's with gold based metallization of the gate[8]. These values are much lower than that of for silver based metallization, where for the Sn(10%)+Ag(90%) contacts the activation energy was found to be in the range of 2.3 ... 2.6 eV [9].

Thermal resistance measurements carried out for Gunn diodes (Type C) showed a significant increase in the thermal resistance during the aging. This increase was found to be about 10 %. It is assumed that this phenomena can be attributed to the deterioration of the metallization at elevated temperatures.

REFERENCES

1. Mojzes, I., Barna, A., Barna, B.P.
"Technological optimization of GaAs Gunn diodes"
Proc. of the Sixth Coll. on Microwave Communication, MICROCOLL'78
Budapest, Hungary, 1978, II. pp. V-2/10.1-10.4

2. Mojzes, I., Lánc, J., Németh, K., Oláh, A.
"Life test equipment for Gunn diodes", (in Hungarian),
Proc. of the CONSTRONIC'76, Budapest, Hungary, 1976, pp. 245-351

3. Mojzes, I.
"Investigation of reliability Gunn diodes", (in Russian)
4th Symp. on Reliability in Electronics, RELECTRONIC'77, Budapest,
Hungary, 1977, Proc. 1, pp. 459-468

4. Mojzes, I.,
"Reliability studies of medium power Gunn diodes".
Proc. 6th Coll. on Microwave Communication, MICROCOLL'78, Budapest,
Hungary, 1978, Proc. II. pp. IV-3/19.1-19.4

5. Bakk, L., Kazi, K., Kovács, B., Mojzes, I., Oláh, A., Veresegyházy,R,
and Zsebe, L.
"Equipment for reliability testing of high power Gunn diodes".
Proc. of 4th Conf. on Mechanical Aspects of Electronic Design,
CONSTRONIC'84, Budapest, Hungary, 1984, pp.231-223

6. Mojzes, I., Kovács, B., Németh-Sallay, M.
"Reliability study of contact metallization to n-InP"
Proc. of 5th Symposium on Reliability in Electronics RELECTRONIC'82,
Budapest, Hungary, 1982, pp.395-404

7. Oliver, C., Bower, D.
"Theory of the failure of semiconductor contacts by electromigration"
Proc. 8th Ann. Ref. Phys. Symp., Las Vegas, USA, 1970, pp.136-138

8. Behmann, F.
"Reliability assessment of small signal GaAs FET's"
Microelectronics and Reliability, 1979, 19, pp.107-115

9. Kuru, I.
"Performance degradation of Gunn diodes at elevated temperature"
Jap.J.Appl.Physics, Supplement, 1979, 40, pp.137-142

ANALYSIS OF VARACTOR TUNED GUNN OSCILLATORS

B. Pődör

ABSTRACT

A simple lumped element circuit model of varactor tuned microwave Gunn oscillators is presented and discussed. The proposed model accounts for the effect of series resistance on the tuning characteristics of the oscillator. The model has been successfully applied for the interpretation the frequency versus tuning voltage characteristics of microwave Gunn oscillators.

INTRODUCTION

The technique of varactor tuning of solid-state negative resistance oscillators such as Gunn and avalanche diode oscillators is well known. Varactor diodes are the only tuning devices which can be used for fast tuning and high frequency modulation of microwave oscillators. Tuning by varactor diode is widely used in the X-, J-, Ka-, and Ku-bands, or even in the range of mm-waves [1-3]. Various medium- and wide-band varactor tuned Gunn oscillators have been reported in the literature[2-16]. A survey of the literature data has shown that typical tuning bandwidths of a few per cent or 20 to 30 percent can be achieved in a parallel or series coupled circuit, respectively[1,3]. For Gunn oscillators mounted in a standard-height waveguide cavity, typical reported electronic tuning ranges are of the order of a few hundred MHz[1,3,8,9]. Greater tuning ranges may be achieved using inherently low-Q cavities in the form of either reduced-height waveguide or coaxial line strucutres but only at the expense of worse noise properties and temperature stability[8]. E.g. Lee and Hodgart[4] reported 1 GHz tuning range in the J-band, while Smith and Crane[5] obtained 1.1 GHz tuning range in the X-band. Downing and Myers[7] achieved 1.95 GHz electronic tuning in the X-band with a reduced height cavity. As a comparison Joshi[8] achieved a tuning range of nearly 700 MHz in a full height X-band cavity.

In our laboratory an X-band varactor tuned Gunn oscillator has been developed[17,18]. The design of this oscillator is based on in-house fabricated GaAs Gunn diodes and GaAs hyperabrupt varactors. The full electronic tuning bandwidth of the oscillator in the 10 to 11 GHz range is 250 to 350 MHz. The output microwave power reaches 50 to 70 mW with variations less than about 1 to 2 dB in the useful tuning range.

It is known that the varactor parasitic elements strongly influence or even control the tuning range of oscillators as well as the nonlinearity of the tuning characteristics in the cm- and mm-wave bands (e.g.[2,19,20]). In varactor tuned oscillators the primary factor limiting the tuning range is the resistive loading effect of the varactor diode itself. This effect is already present in the cm-wave band because of the low varactor Q-factor at this frequencies. The varactor Q-factor is inversely proportional to the frequency, therefore at higher microwave frequencies the application of higher Q-factor GaAs varactors are preferred to Si varactors. At mm-wave frequencies the parasitics of the varactor package play an important role in determining the frequency of operation as well as the tuning range of the varactor tuned oscillator.

The solid-state negative-resistance power source (e.g. the Gunn diode) and the varactor diode are generally mounted in a microwave cavity, and the resulting oscillator circuit consists of a complex circuit containing lumped elements and distributed elements as well. For this reason, as well for the fact that only very approximate equivalent circuits for the Gunn diode itself exist, these circuits are not well suited for rigorous analysis.

In this paper I propose a simple method of analysis which accounts for the effect of the varactor series loss resistance on the tuning characteristics of the oscillator. This analysis is based on a lumped element equivalent circuit model of the varactor tuned oscillator. It will be demonstrated below that this model reproduces satisfactorily the frequency versus varactor voltage characteristics of the oscillator, moreover the values of the elements of the equivalent circuit can be deduced from the measured characteristics using this model.

LUMPED ELEMENT EQUIVALENT CIRCUIT OF THE VARACTOR TUNED OSCILLATOR

The lumped element equivalent circuit of a parallel coupled negative-resistance oscillator with varactor tuning in the region of the operating

frequency is shown in Fig.1.a. The negative-resistance element (i.e. the Gunn diode) is represented by a negative conductance, $-G_d$, the load by the conductance G_l. The resonant cavity in the region of its resonant frequency is represented by a lumped element shunt resonant circuit using suitable values of L_c, C_c and G_c so as to provide the correct resonance frequency, the correct rate of change of susceptance with frequency, and the correct Q-factor, i.e.

$$L_C = \frac{2}{\omega_o^2 \left.\frac{dB}{d\omega}\right|_{\omega=\omega_o}} \tag{1}$$

$$C_C = \frac{1}{2} \left.\frac{dB}{d\omega}\right|_{\omega=\omega_o} \tag{2}$$

$$G_C = \frac{\omega_o \left.\frac{dB}{d\omega}\right|_{\omega_o}}{2 Q_o} \tag{3}$$

where ω_0 is the resonant (circular) frequency of the cavity, Q_0 is the (unloaded) Q-factor of the cavity and $dB/d\omega|_{\omega_o}$ is the derivative of the susceptance with respect to the circular frequency at the resonant frequency.

Following the usual practice the varactor diode is represented by a series resistor-capacitor circuit, where C_v is the active (layer) capacitance of the varactor chip and R_v is the series loss resistance of the varactor. All parasitic elements (of the varactor and Gunn packages) are assumed to be included into the equivalent circuit of the resonator itself. This equivalent circuit is valid at frequencies near the resonance if the varactor impedance, including the package parasitics is a smooth function of the frequency and of the tuning/bias voltage and the impedance plot does not exhibit loops.

Since the main part of the oscillator circuit is represented by a shunt resonant circuit it is convenient to transform the varactor into its parallel equivalent circuit as shown in Fig.1.b.

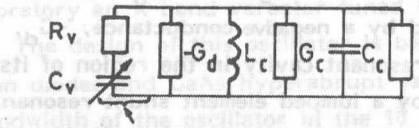

Fig.1.a.

VARACTOR

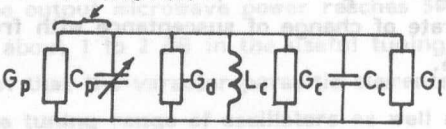

Fig.1.b.

Fig.1.a. Equivalent circuit of a varactor tuned negative resistance oscillator with the varactor represented by a series RC circuit

b. Equivalent circuit with the varactor represented by a shunt RC circuit.

The elements of the parallel equivalent circuit of the varactor, C_p and G_p are given in terms of its series elements as

$$C_p = \frac{C_v}{1 + \frac{1}{Q_v^2}} \tag{4}$$

$$G_p = \frac{1}{R_v} \frac{1}{1 + Q_v^2} \tag{5}$$

with

$$Q_v = \frac{1}{\omega C_v R_v} = \frac{\omega_v}{\omega} \tag{6}$$

here Q_v is the Q-factor of the varactor and $\omega_v = 1/C_v R_v$ is the cutoff frequency.

It is customary to suppose that in the operating frequency range $Q_v^2 >> 1$ and to put

$$C_p \approx C_v \tag{7}$$

$$G_p \approx \frac{1}{R_v Q_v^2} = \omega^2 C_v^2 R_v \tag{8}$$

But already in the range of cm-waves, at low varactor bias voltages the above condition is not fulfilled. This means that the equivalent tuning capacitance will depend on the frequency and also on the series resistance of the varactor. Therefore in the analysis what follows the full expression for C_p will be used.

From the condition of oscillations (e.g.[2,21,22]) we get

$$\frac{1}{\omega^2} = L_C\left(C_C + \frac{C_V}{1+\omega^2 C_V^2 R_V^2}\right) \tag{9}$$

which yields a quadratic equation for ω^2 or for $1/\omega^2$

$$\frac{1}{\omega^4} - \frac{1}{\omega^2}\left[L_C(C_C+C_V) - R_V^2 C_V^2\right] - R_V^2 C_V^2 L_C C_C = 0 \tag{10}$$

The solution of this equation is

$$\frac{1}{\omega^2} = \frac{1}{2}\left\{\left[L_C(C_C+C_V) - R_V^2 C_V^2\right]^2 + \right.$$
$$\left. + \sqrt{\left[L_C(C_C+C_V) - R_V^2 C_V^2\right]^2 + 4R_V^2 C_V^2 L_C C_C}\right\} \tag{11}$$

Eqs.(9) through (11) show that the frequency of oscillation depends not only on the varactor capacitance C_V, but also on the series loss resistance of the varactor R_V, through the $R_V C_V = 1/\omega_V$ product. Only in the limiting case of $R_V = 0$ is the simple formula for the frequency

$$\frac{1}{\omega^2} = L_C(C_C + C_V) \tag{12}$$

applicable.

One of the important consequences of Eq. (9) is that it gives the dependence of the maximum available electronic tuning range on the series loss resistance. For a varactor the capacitance is at maximum when the bias voltage $V = 0$, then $C_V = C_{V0}$ is the maximum capacitance. Let $\omega = \omega_0$ when $C_V = C_{V0}$ and $\omega = \omega_C = 1/L_C C_C$ when $C_V = 0$. Then from Eq.(12) the maximum available electronic tuning range $\Delta\omega$ referenced to ω_0 is obtained as

$$\frac{\Delta\omega}{\omega_o} = \frac{\omega_c - \omega_o}{\omega_o} =$$

$$\sqrt{\frac{1}{2}\left\{\left(1+\frac{C_{V_o}}{C_C}\right) - \frac{\omega_C{}^2}{\omega_{V_o}^2} + \sqrt{\left[\left(1+\frac{C_{V_o}}{C_C}\right) - \frac{\omega_C{}^2}{\omega_{V_o}}\right]^2 + 4\frac{\omega_C{}^2}{\omega_{V_o}}}\right\} - 1} \qquad (13)$$

here $\omega_{v0} = 1/R_v C_{v0}$ is the cutoff frequency of the varactor at zero bias.

In Fig.2. the relative tuning range $\Delta\omega/\omega_0$ is plotted versus ω_c/ω_{v0} the ratio of the unperturbed frequency of the oscillator to the cutoff frequency of the varactor at zero bias, with C_{v0}/C_c as the parameter. It can be seen as R_v i.e. ω_c/ω_{v0} is increased the relative tuning range decreases.

Typical calulated tuning characteristics of X-band oscillators with flat-profile varactors using realistic varactor and cavity parameters are presented in Fig.3. with varactor series loss resistance as parameter. Maximal available tuning range and "useful" tuning range, i.e. for 0 to 10 V bias excursion for the same oscillator are shown in Fig.4.

APPLICATION OF THE MODEL

The model described above is now applied to the analysis of measured tuning characteristics of waveguide mounted X-band varactor tuned Gunn oscillators, i.e. for the interpretation of frequency and output power versus varactor voltage characteristics[23,24].

The construction and performance of the varactor tuned Gunn oscillators considered here have already been described in [17,24]. The Gunn device and the varactor diode were mounted on conical post structures near the short circuit wall of an X-band waveguide type resonator. Between the symmetrically placed diodes a metal post was placed to couple the semiconductor devices to the cavity. The centre frequency is mechanically tunable by two dielectric posts in a range greater than 400 MHz. The load matching network consisted of a resonant iris with a tuning screw. The Gunn device which has an output power greater than 100 mW, measured in a standard waveguide test cavity, and the GaAs hyperabrupt Schottky varactor diode[25, 26, 27] were in-house fabricated devices.

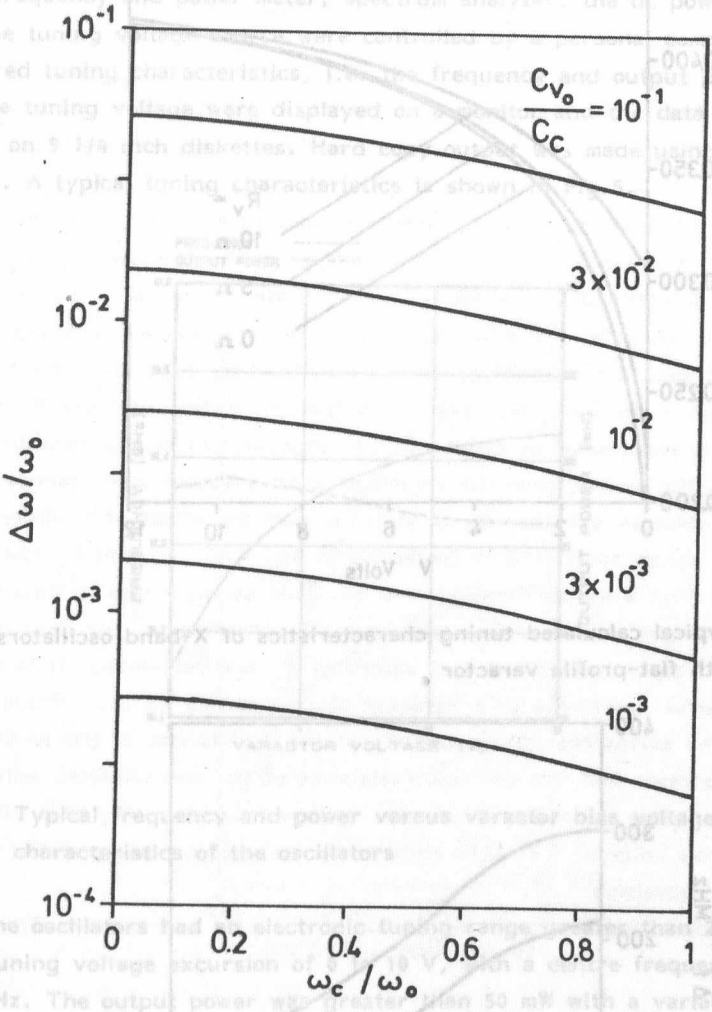

Fig.2. Plots of the relative tuning range $\Delta\omega/\omega_0$ versus ω_c/ω_0, the ratio of the unperturbed frequency of the oscillator to the cutoff frequency of the varactor at zero bias. The parameters of the curves are the capacitance ratios C_{v0}/C_c.

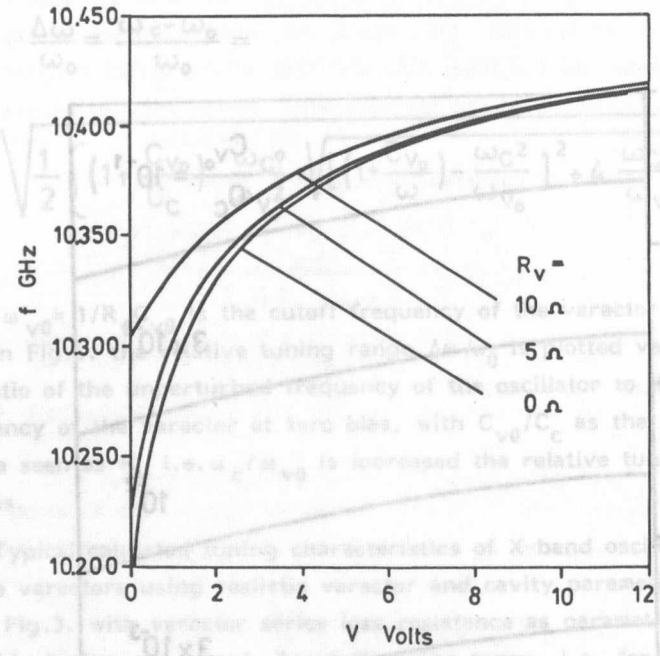

Fig.3. Typical calculated tuning characteristics of X-band oscillators with flat-profile varactor

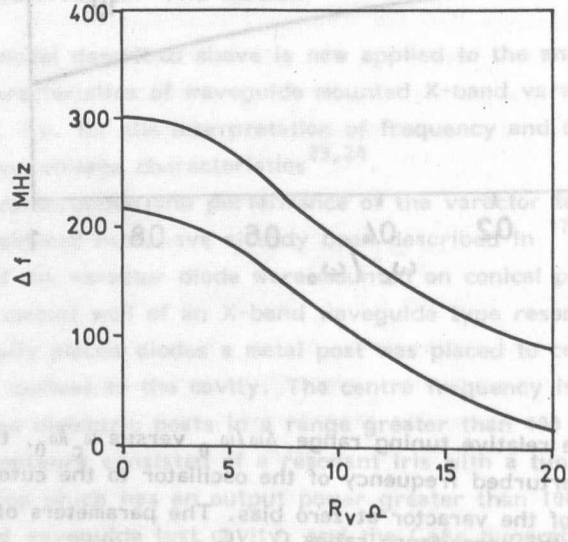

Fig.4. Typical values of maximal and "useful" tuning ranges versus the series resistance of the varactor

For the characterization of the varactor diodes and microwave oscillators a computer controlled measuring system has been used[28]. The microwave frequency and power meter, spectrum analyzer, the dc power supply and the tuning voltage source were controlled by a personal computer. The measured tuning characteristics, i.e. the frequency and output power versus the tuning voltage were displayed on a monitor and the data were stored on 5 1/4 inch diskettes. Hard copy output was made using a digital plotter. A typical tuning characteristics is shown in Fig.5.

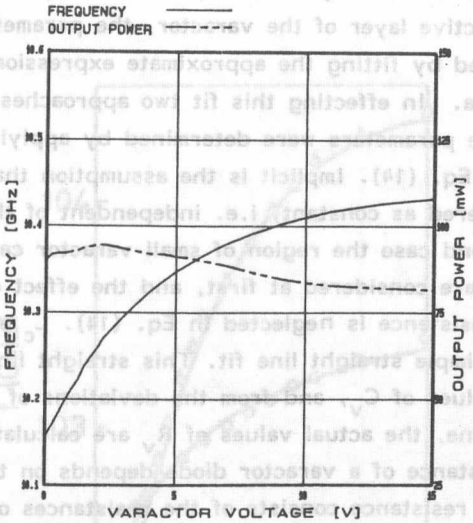

Fig.5. Typical frequency and power versus varactor bias voltage characteristics of the oscillators

The oscillators had an electronic tuning range greater than 250 MHz for a tuning voltage excursion of 0 to 10 V, with a centre frequency of 10.3 GHz. The output power was greater than 50 mW with a variation of less than 1 to 2 dB in the full tuning range. The oscillators were capable of modulation with frequencies up to 150 MHz and beyond. The oscillators showed a satisfactory performance in the temperature range from $-40^{o}C$ to $+55^{o}C$ [17,18].

Notwithstanding that the exact solution of Eq.(9) can easily be given, for the purposes of the analysis of the measured tuning characteristics it is convenient to use a series expansion, which results in the approximative

cubic equation

$$\frac{1}{\omega^2} = L_c(C_c + C_v) - \frac{R_v^2 C_v^3}{C_c} \qquad (14)$$

The parameter of series expansion in Eq.(14) is C_v/C_c which means that for the case of $C_v/C_c \ll 1$, which is usually fulfilled, the above expansion is of sufficient accuracy.

If the reciprocals of the squared frequencies are plotted against the capacitance of the active layer of the varactor, the parameter L_c, C_c and R_v can be determined by fitting the approximate expression, Eq. (14), to the measured data. In effecting this fit two approaches have been used. In the first case the parameters were determined by applying a least squares method for Eq. (14). Implicit is the assumption that the R_v series resistance is considered as constant, i.e. independent of the varactor voltage. In the second case the region of small varactor capacitances, i.e. large bias voltages are considered at first, and the effect of nonlinearity due to the series resistance is neglected in Eq. (14). L_c and C_c are then determined from a simple straight line fit. This straight line is then extrapolated to larger values of C_v, and from the deviations of the data points from this straight line, the actual values of R_v are calculated, It is known that the series resistance of a varactor diode depends on the voltage applied. The series resistance consists of the resistances of the leads, contacts, substrate, and the variable resistance of the non-depleted epitaxial layer. This latter depends on the bias voltage in such a way that with increasing bias voltage, i.e. with decreasing varactor capacitance the series resistance decreases[2, 29].

The total capacitance of the packaged varactor was approximated by the expression

$$C = C_s + C_v = C_s + \frac{C_{v_o}}{\left(1 + \frac{V}{\phi}\right)^{\gamma}} \qquad (15)$$

where C_s is the package stray (parasitic) capacitance (its value for our varactor diodes is 0.25 - 0.35 pF), and C_{v0} is the depletion layer capacitance at zero bias, ϕ is a parameter having the dimensions of voltage, and the exponent γ is equal to 1/2 for varactors with flat doping profile, and is equal to 1-1.4 for hyperabrupt varactors with special doping

profils[25, 26, 27]. For varactors with flat doping profile ϕ is the built-in potential, its value for the AuCr-GaAs Schottky varactors used in this work is equal to 0.8 ± 0.1 eV[27]. The actual values of C_s, C_{v0}, γ and ϕ for each varactor were determined by analysing the measured capacitance versus bias voltage curves of packaged varactors and also of unpackaged varactor chips.

Some typical results of the model fit to the measured frequency versus bias voltage curves are shown in Fig.6.

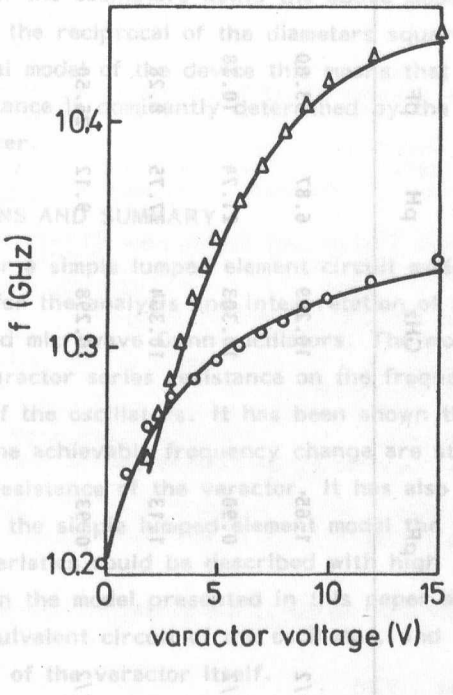

Fig.6. Fit of the lumped element circuit model to the observed tuning characteristics. Circles and triangles - measured data, full lines - model fit

The parameters of the varactors and of the equivalent circuit of the oscillator cavity deduced from the fits are collected in Table 1. In the last but one column of Table 1 the values of R_v determined under the assumptions that it is constant are also shown.

TABLE 1.

Parameters of the oscillators and of the varactors

Varactor type	C_v(3.5 V)	f (3.5 V)	L_c	C_c	f_c	R_v	R_v^x
	pF	GHz	pH	pF	GHz	ohm	ohm
GaAs γ = 1/2	1.65	10.269	6.87	33.80	10.444	3.82	2.0-3.6
GaAs γ = 1/2	0.90	10.303	21.74	10.38	10.595	6.94	5.2-8.5
GaAs γ = 1	1.13	10.304	27.75	8.28	10.501	13.88	7.5-15.5
Si(pn) γ = 1/2	0.93	10.298	9.12	25.50	10.439	5.57	2.6-7.2

Using this values in conjunction with the values of L_c and C_c also listed there, the tuning characteristics of the oscillators could be described in a range of 150-200 MHz with an average deviation of $\pm$ (2-4) MHz, as demonstrated in Fig.6. The last column of Table 1. lists values of R_v determined assuming it as a variable quantity. It can be seen, that the values of R_v determined in this way decrease with increasing bias voltages, as could be expected from the physical model of the device.

In a series of experiments GaAs Schottky varactor were used coming from the same slice but having different diameters i.e. different capacitances. The corresponding series resistances deduced from the tuning characteristics of the oscillators using the above model turned out to be proportional to the reciprocal of the diameters squared. In accordance with the physical model of the device this means that in the given case the series resistance is dominantly determined by the resistance of the non-depleted layer.

CONCLUSIONS AND SUMMARY

In this paper a simple lumped element circuit model has been presented and applied for the analysis and interpretation of the tuning behaviour of varactor tuned microwave Gunn oscillators. The model accounts for the effects of the varactor series resistance on the frequency versus voltage characteristics of the oscillators. It has been shown that the relative tuning range and the achievable frequency change are strongly affected by the series loss resistance of the varactor. It has also been shown that with the help of the simple lumped element model the measured frequency--voltage characteristics could be described with high accuracy. The analysis based on the model presented in this paper also yields the actual values of the equivalent circuit of the oscillator, and the values of the series resistance of the varactor itself.

ACKNOWLEDGEMENTS

Grateful acknowledgements are due to the coworkers of the Microwave Devices Division of the Institute especially to Mr. Zs.Horváth, Dr.K.Kazi and Mr. L.Tajti for performing most of the measurements referred to in this work and making available the raw data. Thanks are due to Mr. Zs. Horváth also for the comparative analysis of varactor models and for discussions and detailed informations concerning the properties of varactors.

REFERENCES

1. V.P.Taranenko, B.A. Kotserzhinski, L.A. Tkachenko, Izv. VUZ-ov SSSR, Radioelektronika 19 (10) 5 (1976)

2. M.J. Howes, D.V.Morgan Variable Impedance Devices, Wiley, New York, 1978

3. V.P. Taranenko, B.A. Kotserzhinski, E.A. Machusski Izv. VUZ-ov SSSR, Radioelektronika 21 (10) 4 (1978)

4. B.K. Lee, M.S. Hodgart Electron.Lett. 4 240 (1968)

5. R.B. Smith, P.W.Crane Electron.Lett 6, 139 (1970)

6. P.G. Wilson, B.Minakovic IEEE Trans. Electron Devices ED-18 450 (1971)

7. B.J. Downing, F.A. Myers Electron.Lett 7 407 (1971)

8. J.S. Joshi IEEE Trans. Microwave Theory and Techniques MTT-21 137 (1973)

9. M.Dean, M.J.Howes IEEE Trans. Electron Devices ED-20 597 (1973)

10. C.S. Aitchison, R.Davies Int. J.Electronics 35 105 (1973)

11. R.A. Gough, B.H.Newton IEEE Trans. Electron Devices ED-20 863 (1973)

12. B.J.Downing, F.A. Myers Electron.Lett. 9 244 (1973)

13. M.Dean, M.J.Howes IEEE Trans. Electron Devices ED-21 563 (1974)

14. C.Aitchison Electron.Lett. 10 488 (1974)

15. A.Schlegel, L.Szabó Archiv elektrischer Übertragung 35 342 (1980)

16. J.J.Sowers, B.A.Janis, J.D. Crowley, F.B.Fank, Electron.Lett 17 708 (1981)

17. F.Csányi, L.Dobos, I.Jászberényi, K.Kazi, I.Mojzes, A.Oláh, A.Tichy-Rács Finommechanika-Mikrotechnika 25 78 (1986)

18. Zs.J.Horváth, I.Gyúró, M.Németh-Sallay, B.Szentpáli, K.Kazi, L.Dobos, Á.Fogt, T.Kolumbán
Proc. 8th Colloquium on Microwave Communication, Budapest, Aug.25-29 1986. Publishing House of the Hungarian Academy of Sciences, p.379

19. S.F.Paik
IEEE Trans. Microwave Theory and Techniques MTT-22 578 (1974)

20. M.C.Martin, B.J.Downing
Electron.Lett. 22 306 (1986)

21. T.Berceli
Hiradástechnika 27 321 (1976)

22. T.Berceli
Nonlinear Active Microwave Circuits
Akadémiai Kiadó, Budapest, 1987

23. B.Pődör, Zs.Horváth, L.Tajti
Finommechanika-Mikrotechnika 26 186 (1987)

24. K.Kazi, B.Pődör, Zs.Horváth, L.Tajti
Proc. Int.Symp. on Electronics Technology, Budapest, Sept. 15-18 1987, p. 163

25. Zs. Horváth, M.Németh-Sallay, I.Gyúró, B.Szentpáli, K.Kazi, I.C.Szép
Finommechanika-Mikrotechnika 25 52 (1986)

26. Zs. J.Horváth, I.Gyúró, M.Sallay-Németh, B.Szentpáli, K.Kazi
phys.stat.sol.(a) 94 719 (1986)

27. Zs.Horváth, I.Gyúró, M.Sallay-Németh, B.Szentpáli, K.Kazi, Á.Fogt, L.Dobos, T.Kolumbán, P.Tüttő
Hiradástechnika, to be published

28. R.Veresegyházy, K.Kazi, I.Mojzes, S.Biró, P.Harmat, Gy. Füle
Finommechanika-Mikrotechnika 25 80 (1986)

29. S.M.Sze
Physics of Semiconductor Devices, Wiley, New York, 1981

ALLOYED AuGeNi OHMIC CONTACTS ON GaAs

R.Veresegyházy, I. Mojzes, R.E.Miles[+], M.O'Keefe[+]

ABSTRACT

The metallurgy of AuGeNi/GaAs contacts is briefly reviewed. Contact resistivity measurements were performed on samples alloyed in forming gas. The resistivity of the epitaxial layer between the contacts was also determined.

INTRODUCTION

The AuGeNi system is the most widely used ohmic metallization for n-type GaAs. The as deposited contact is usually rectifying, so heat treatment is used to make it ohmic. The mechanism responsible for the formation of good ohmic contacts was thought to be the melting of the metallization, which dissolves a thin layer of GaAs. Upon cooling and solidification, regrowth of this layer takes place incorporating the Ge as a dopant leading to the formation of an n^+ or n^{++} layer. The role of Ni was merely to improve the wetting of the melt. However, most experiments do not support the existence of a molten phase and indeed formation of good ohmic contacts was observed below $300^{o}C$, where the formation of a molten phase can be excluded[1].

THE METALLURGY OF AuGeNi/GaAs CONTACTS

In order to understand the complicated processes taking place in this system it is necessary to review the possible reactions among the constituents. In evaporated layers of Au, Ge and Ni on an inert substrate Ge quickly diffuses to the Ni forming Ni-Ge compounds independent of the order of evaporation [2]. In the Au/GaAs system, Au forms compounds with Ga, while the volatile component (As) evaporates[3]. Ni forms compounds both with Ga and As[4], but does not mix with Au.

[+]Department of Electrical and Electronic Engineering
University of Leeds, Leeds LS2 9JT, UK

During alloying of the usual Au/Ni/AuGe/GaAs system the first important process is the diffusion of a portion of Ni to the semiconductor interface and the formation of NiAs. Germanium diffuses to the Ni to form Ni-Ge compounds in the metallization. At a temperature of about 350°C Ni-Ge-As compounds form at the interface[5]. Upon further annealing the Ge begins to diffuse into the underlaying semiconductor, forming the desired n^+ layer. The Ga, liberated during these reactions accumulates in the Au while the As tends to evaporate. It should be emphasized that the structure of the metallization is not layered because Au-Ga and Ni-Ge-As phases coexist at the interface. At even higher temperatures the interaction of Au with the GaAs will dominate. As a consequence, large amounts of arsenic evaporate, and the Au-Ga grain size increases until eventually at a high Ga content the metallization melts.

ELECTRICAL PARAMETERS

There is a close connection between the electrical parameters and the metallurgical changes taking place during alloying. In the initial stages the Schottky barrier increases, because of the diffusion of Ni to the interface[6]. The incorporation of Ge into the GaAs lattice has the effect of narrowing the barrier. When electrons can pass through by quantum mechanical tunneling the contact is ohmic. The specific contact resistivity has minimum value at a certain alloying temperature. It is therefore an important step in the development of ohmic contacts to optimize this minimum with respect to the other parameters, such as the thickness of different metallic layers. What are the processes leading to a minimum specific contact resistivity? It is well known that Ge is an amphoteric dopant[7]. The presence of gold enhances the outdiffusion of Ga leaving the vacant sites to be occupied by the Ge atoms, where they act as donors. At higher temperatures, as a consequence of strong evaporation of As, Ge will occupy more and more arsenic sites (where it acts as an acceptor). Further deterioration of the contact takes place as the ratio of Ni-Ge-As to Au-Ga grains decreases[5] and finally melting (i.e. balling up) of the metallization occurs.

EXPERIMENTAL RESULTS

The samples were (100) oriented, epitaxial layers (vapour phase grown on semiinsulating substrates), $\approx 2.5\ \mu m$ thick, sulphur doped to a

density of $10^{17}/cm^3$. The evaporated layers were deposited in the order Ni(5nm) AuGe(75nm) Ni(30nm) and Au(200nm). Alloying was carried out in flowing forming gas ($10\%H_2+90\%N_2$). The samples were heated to the desired temperature in 1 minute and were held there for a further minute.

Two series of samples were alloyed. The first set (three samples for control purposes) were alloyed at 300°C, then subsequently at 25°C intervals up to 500°C. After each alloying, contact resistivity measurements were carried out by the Transmission Line Method. The results are shown in Fig.1. and are as expected. However an unexpected feature is that the resistivity of the epitaxial layer between the contacts has a maximum value at about 450°C. Several explanations for this are possible, e.g. the diffusion of Cr into the epitaxial layer from the substrate, the redistribution of dopants or the formation of vacancies and vacancy-complexes. Simple calculations have shown that the lateral diffusion of Ge does not modify the value of the resistivity of the epitaxial layer.

In the second series of experiments several samples were alloyed, each at a temperature between 350°C and 525°C. The minimum of specific contact resistivity was again at 470-500°C. The resistivity of the metallization was also measured by direct probing of large metallised squares. It was very low below 300°C, and increased substantially at higher temperatures. The reason for the very low value is that the resistivity of the Au layer is low. At higher temperatures the Au incorporates more and more Ga and the layered structure changes to a columnar structure. The effect is to increase the measured resistivity.

The specific contact resistivity values at the optimum alloying temperature are slightly lower than in the case of samples heat treated several times. This is in accordance with the fact that the best contacts can be obtained with short alloying circles[8].

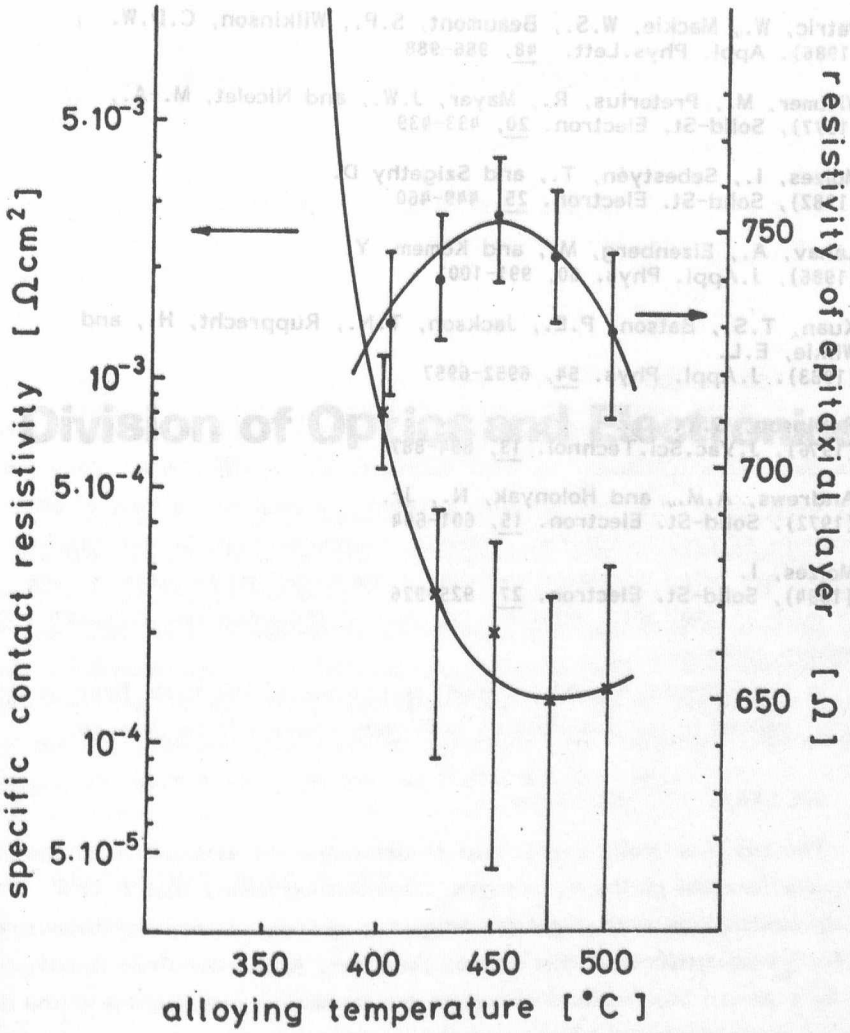

Fig.1. The specific contact resistivity and the resistivity of epitaxial layers between the contacts vs alloying temperature curve of a sample annealed several times. The actual sample temperatures were estimated to be about 30°C lower than measured by the thermocouple

REFERENCES

1. Patric, W., Mackie, W.S., Beaumont, S.P., Wilkinson, C.D.W. (1986). Appl. Phys.Lett. 48, 986-988

2. Wittmer, M., Pretorius, R., Mayer, J.W., and Nicolet, M.-A., (1977), Solid-St. Electron. 20, 433-439

3. Mojzes, I., Sebestyén, T., and Szigethy D. (1982), Solid-St. Electron. 25, 449-460

4. Lahav, A., Eizenberg, M., and Komem, Y. (1986), J.Appl. Phys. 60, 991-1001

5. Kuan, T.S., Batson, P.E., Jackson, T.N., Rupprecht, H., and Wilkie, E.L. (1983). J.Appl. Phys. 54, 6952-6957

6. Robinson, G.Y. (1976). J.Vac.Sci.Technol. 13, 884-887

7. Andrews, A.M., and Holonyak, N., Jr. (1972). Solid-St. Electron. 15, 601-604

8. Mojzes, I. (1984), Solid-St. Electron. 27, 925-926

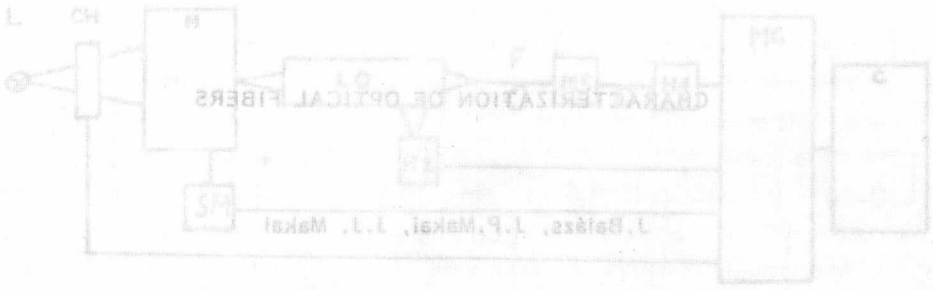

Division of Optics and Electronics

CHARACTERIZATION OF OPTICAL FIBERS

J.Balázs, J.P.Makai, J.J. Makai

INTRODUCTION

Optical communication using glass fibers is a rapidly growing branch of the data communication. In many countries among them in Hungary too it has been installed in the telephon network. In addition, a host of other applications as process control, computer interconnection, sensor applications etc. are being developed because of the beneficial features of the fibers such as small size, light weight, lack of induction and crosstalk and broadband operation.

In the following the measurement techniques of the basic fiber parameters, realized in our Institute on multimode fibers will be detailed.

SPECTRAL ATTENUATION

The cut-back method was used to determine the attenuation of the fiber as a function of the wavelength. This method means that first a fiber of length L is excited by the help of a monochromator and the output power (P_L) is measured at the end of the fiber. Next, the fiber is cut-back to a length of l without changing the launching conditions and the power is again measured. The ratio of these two values at every position of the wavelength gives the spectral attenuation of the fiber piece of length $L-l$

$$a = \frac{10 \log_{10} \frac{P_l}{P_L}}{L-l} \quad dB/km$$

Fig.1. shows the simplified block diagram of the system.

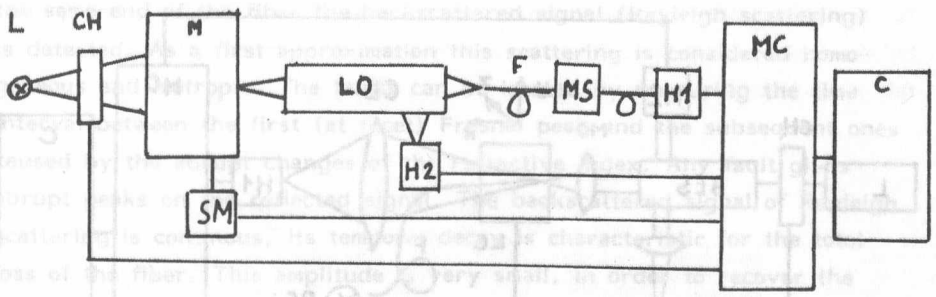

Fig.1. Measuring set-up to determine the spectral attenuation (L-halogen lamp, CH-Chopper, M-monochromator, SM-stepper motor, LO-Launching optic, F-fiber, MS-mode scrambler and stripper, H 1,2-measuring heads, MC-measuring and control unit, C-computer)

It causes the double channel method to eliminate the fluctuation effect of the light source. The two channel measuring unit (patent pending) operates according to the boxcar principle but it carries out both the measurement and the zero correction in the same channel. This unit combined with the control unit is based on a microcomputer and it is connected to a computer. The setting of the wavelength by the help of the stepper motor and the measurement takes place automatically. The computer displays the spectral attenuation curve in the range of 0.8 - 1.6 μm.

REFRACTIVE INDEX PROFILE

In order to measure the refractive index profile across a fiber diameter, the end of the fibre is inserted into a nearly index matching liquid cell which is capable of moving so as to scan the fiber end across a stationary focused laserbeam. The numerical aperture of this light beam is much greater then that of the fiber. Some of the beam will be guided in the conventional way whilst the remainder will escape and appear as a hollow cone around the fiber. The light escaping closest to the fiber axis is of uncertain composition and is therefore removed by a concentric blocking disc but the rest is collected and focused onto a detector. The collected power is inversely proportional to the refractive index of the fiber at the entry point of the beam. Fig.2. shows the block diagram of the equipment.

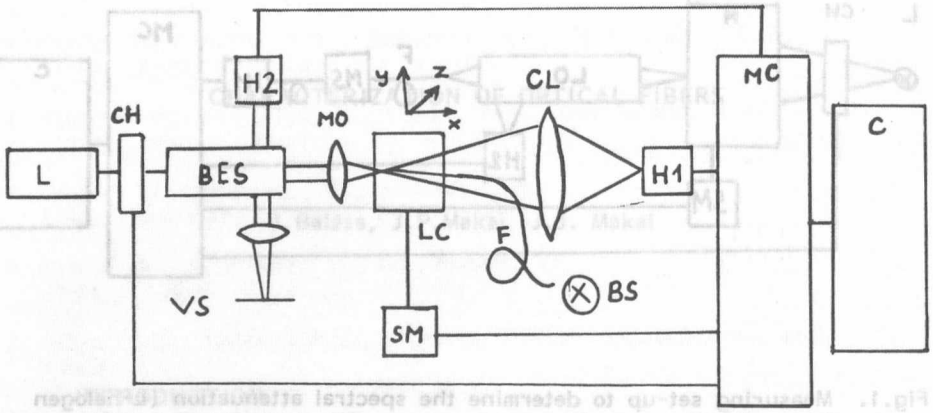

Fig.2. Optical fiber refractive index profiler
(L He-Ne laser, Ch-chopper, BES-beamexpander splitter, VS-viewing screen, MO-microscope objective, LC-liquid cell on 3 directional state, F-fiber, CL-collecting lens, SM-stepper motor, H 1,2 -measuring heads, MC-measuring and control unit, C-computer, BS-back illumination system)

The optical system projects an image of the back illuminated fiber end face under test onto a viewing screen, which aids both focusing and alignment of the fiber. The liquid cell containing the fiber end is positioned and scanned by the help of linear, high resolution stage. The blocking disc is mounted on the back of the cell. The same measuring electronic system is used as under point 2, the results of the automatic measurement and the calculated values of the refractive index as a function of the radius are shown on a display.

A calibration method has been elaborated which from the refractive index value of the liquid and from a single fiber measurement calculates the refractive index as a function of the position.

OTDR (OPTICAL TIME DOMAIN REFLECTOMETRY)

The OTDR method based on the light backscattering can be applied to determine the loss of fibers, splices and the fault location (detection of faults). This method is non-destructive and the access to only one fiber end is needed. Due to the fault location ability the OTDR equipment is one of the most important field instruments of optical communication.

A short optical pulse is launched periodically into the fiber and at the same end of the fiber the backscattered signal (Rayleigh scattering) is detected. As a first approximation this scattering is considered homogeneous and isotropic. The faults can be located by measuring the time interval between the first (at facet) Fresnel peak and the subsequent ones caused by the abrupt changes of the refractive index. Any fault gives abrupt peaks on the reflected signal. The backscattered signal of Rayleigh scattering is continous, its temporal decay is characteristic for the total loss of the fiber. This amplitude is very small, in order to recover the useful signal from the large noise special electronics e.g. boxcar-integrator or sampling unit is needed.

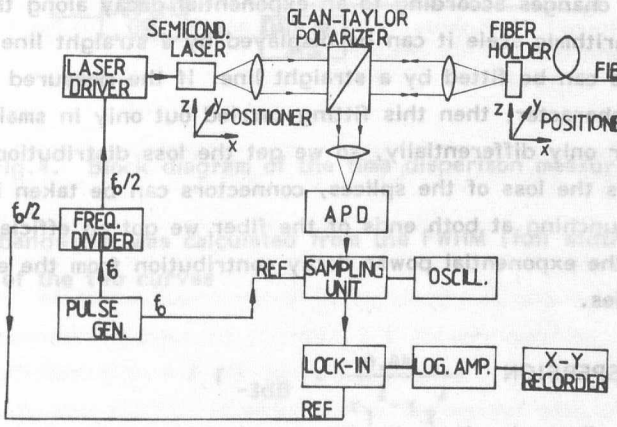

Fig.3. Block diagram of the OTDR measurement

Semiconductor injection pulse lasers of different power are used in the 0.8 - 0.9 /um wavelength region, the pulse width is 100 ns. The direction coupler of the system is a Glan-Taylor polarising prism. It has a double role in decreasing non-linearity: first to assure that only signals from the fiber reach the detector, second to suppress the undesirable (facet) Fresnel reflections. The backscattered signal falls on an avalanche photodiode (APD). The signal of the APD is measured by the sampling unit. As the zero level of the sampling unit is not stable, it was useful to choose the pulse frequency of the laser as half of the trigger frequency

of the sampling unit. This also improved the signal-to-noise ratio. The useful signal and the zero level are measured alternately and then processed by the lock-in amplifier. The average loss can be determined from the following formula

$$\bar{\alpha} = - \frac{10 \log \frac{P_1}{P_2}}{2 (X_2 - X_1)} \text{ dB/km}$$

where P_1 and P_2 are the backscattered power values from X_1 and X_2 points ($X_1 < X_2$). The distances X_1 and X_2 are measured from the facet of the fiber. This evaluation can be applied if the power of the backscattered light changes according to an exponential decay along the fiber. Then on a logarithmic scale it can be displayed by a straight line or the measured curve can be fitted by a straight line. If the measured curve is not of this character, then this fitting carried out only in smaller parts of the curve or only differentially, so we get the loss distribution along the fiber. Thus the loss of the splices, connectors can be taken into account. By launching at both ends of the fiber we got an efficient method of separating the exponential power decay contribution from the effects of the irregularities.

TIME DISPERSION

The time dispersion is an important optical parameter of the optical fibers. It gives account on the information density of a given fiber. At the so called time-domain technique a very narrow light pulse is launched periodically into the fibre and at the other end of the fiber its widening is measured. The wavelength of the semiconductor laser is 820 nm, the halfwidth of the quasi-Gaussian light pulse approximately 150 ps. The signal was detected by a Si APD or pin diode of fast (300-500 ps) response time. The signal processing was made by a sampling oscilloscope (Fig.4)

In the measurement we first detect the shape of the transmitted signal at the end of the test fibre after that we cut back the fiber to approximately 2m, and we again measure the transmitted signal under unchanged launching conditions. The latter is considered as input signal and the former as the output signal. The bandwidth was determined in two

different ways. First it was assumed, that the input and the output curves were quasi-Gaussian.

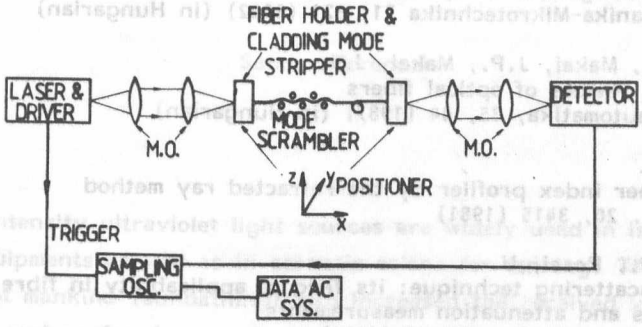

Fig.4. Block diagram of the time disperison measurement

Then the bandwidth was calculated from the FWHM (full width of half maximum) of the two curves

$$f_{-3dB} = \frac{0.44}{\tau_1^2 - \tau_2^2}$$

where τ_1 and τ_2 are the FWHM-s of the output and input curves, respectively. In the second case the input and output signals were Fourier transformed, and the transfer function of the system was estimated. A calculated curve was fitted to the transfer function. The bandwidth was obtained from the - 3 dB point of this curve. The agreement between the two estimations was satisfactory. To improve the reproducibility of measurements a temperature stabiliser and a digital delay line wer built. To control our system some measurements were carried out by frequency domain technique. The agreement was reasonable.

REFERENCES

1. Marcuse, D.,
Principles of optical fiber measurements
Academic Press, 1981

2. Andor, L., Balázs, J., Gál, M., Hoffmann, G.
Optical investigations of optical fibers
Finommechanika-Mikrotechnika 21, 321 (1982) (in Hungarian)

3. Balázs, J., Makai, J.P., Makai, J.J.
Measuring devices of optical fibers
Mérés és automatika, 35, 44 (1987) (in Hungarian)

4. Young, M.
Optical fiber index profiler by the refracted ray method
Appl. Opt. 20, 3415 (1981)

5. Di Vita, P., Rossi, U.
The backscattering technique: its field of applicability in fibre diagnostics and attenuation measurements
Opt. and Quantum E1. 11, 17 (1980)

6. Stone, f.T.
Problems in bandwidth measurement and a suggested solution
J. of Lightwave Technology, LT1, 207 (1983)

MEASUREMENT OF ULTRAVIOLET IRRADIANCE

Sándor Ferenczi

High intensity ultraviolet light sources are widely used in industry, medical equipments as well as in cosmetic salons for tanning. The changing habit of mankind (sunbathing) also increased the received yearly ultraviolet dose and surfaced a growing concern on the evaluation of UV hazard of the natural and artificial illumination.

In this way there is a need for portable and inexpensive instruments for the measurement of ultraviolet irradiance. The Mod. 211 UV-meter and the Mod. 212 UV-A meter have been developed in our institute. The instruments consist of a pocket-size electronic unit and a small optical head with diameter of 30 mm connected with the electronic unit by a signal cable.

The instrument is powered with one 9 V battery and the measured values are displayed on a 3 1/2-digit LCD display (Fig.1).

The instrument has the following measuring ranges with manual range change:

0 - 19.99 $\mu W/cm^2$
0 - 199.9 $\mu W/cm^2$
0 - 1.999 mW/cm^2
0 - 19.99 mW/cm^2

The Mod.211 UV meter measures the ultraviolet irradiance in the 250-400 nm spectral region. The Mod. 212 UV-A meter measures the ultraviolet irradiance in the UV-A region (320 nm ... 400 nm). The typical spectral responses of the UV meters can be seen in Fig.2. The spectral response of both instruments has a maximum close to 365 nm. In this way the absolute sensitivity of the instruments is measured and calibrated on

the wavelength of the 365 nm monochromatic emission line of mercury lamps.

The absolute calibration is performed with the following method: The light of a stabilized mercury lamp is filtered with a 365 nm interference filter to produce monochromatic irradiation and the UV radiation is projected onto the surface of the optical head. The UV irradiance is measured with an electrically calibrated pyroelectric radiometer and the measured value is adjusted by the sensitivity setting potentiometer of the UV meter.

The accuracy of absolute calibration is $\pm$ 5%. An other important parameter which characterizes the quality of UV meters is their sensitivity in the visible and near-infrared (VIS-NIR) spectral regions. As it is well known, ultraviolet sources generally emit only 5-20% of their total optical power in the UV region and the majority of the power is radiated in the VIS-NIR region. In this way a relatively low VIS-NIR response of the UV detector can cause a significant error in the UV irradiance measurement. Unfortunately there is no internationally agreed recommendation for the measurement of this parameter and therefore the quality of UV meters of different producers cannot be compared quantitatively. To overcome this difficulty we worked out a simple method for the measurement of the VIS-NIR response:

The ultraviolet detector is homogeneously illuminated with the light of standard source A. To filter out the ultraviolet portion of the radiation a GG400 type glass filter is placed in the light beam (3 mm thickness, Schott product). The minimal illuminance level in the plane of the UV detector must be 1000 lux. The measured value on the display of the UV meter is regarded to the VIS-NIR response.

The VIS-NIR response can be expressed in Wm^{-2} lux^{-1} units. An other way for presentation of the VIS-NIR response is based on the calculation with the luminous efficacy of the standard source A. In the 400 nm ... 2500 nm spectral region a blackbody source with the colour temperature 2856 K (standard source A) has a luminous efficacy of about 20 lumen W^{-1}. This means when the detector is illuminated with the standard source A producing 20 lux illumination, the total irradiance on the detector surface is 1 Wm^{-2}. In this way the error caused by the VIS-NIR sensitivity of an UV-meter ($f_{VIS-NIR}$) can be calculated from the following equation:

$$f_{VIS-NIR} = \frac{20 \times [\text{measured irradiance } /Wm^{-2}/]}{[\text{illuminance } /lux/]} \times 100\%$$

when the UV meter is irradiated with standard source A filtered with GG400/3 mm and the illuminance level is at least 1000 lux. The Mod.211 UV meter and the Mod. 212 UV-A meter have a VIS-NIR sensitivity of 10^{-4} Wm^{-2} lux^{-1} and

$$f_{VIS-NIR} = 0.2\%$$

This error is a very small one, but in the case of light sources with very low UV content the VIS-NIR response can cause erraneous results.

For the further improvement of our UV meters we make experimental work in two fields:

- application of new photodetectors
- better optical filtering.

REFERENCES

Ferenczi S.:

Actinic effects of ultraviolet radiation
Mérés és Automatika 35(2), 39-43 (1987)

Ferenczi S.

The effects of ultraviolet radiation on man
Symposium on Nonionizing Radiation in Outdoor Applications
Stockholm 12-16. 08. 1987.

Ferenczi S.

Biological effects and measurement of ultraviolet radiation.
Oszvescsenyie'87, Várna, 8-10.10. 1987.

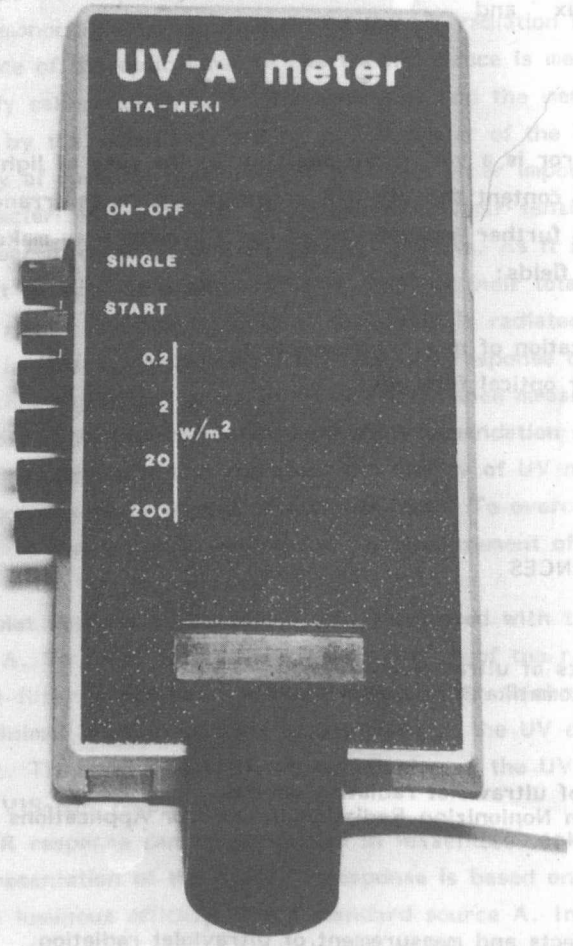

Fig.1. Mod. 212. UV-A meter

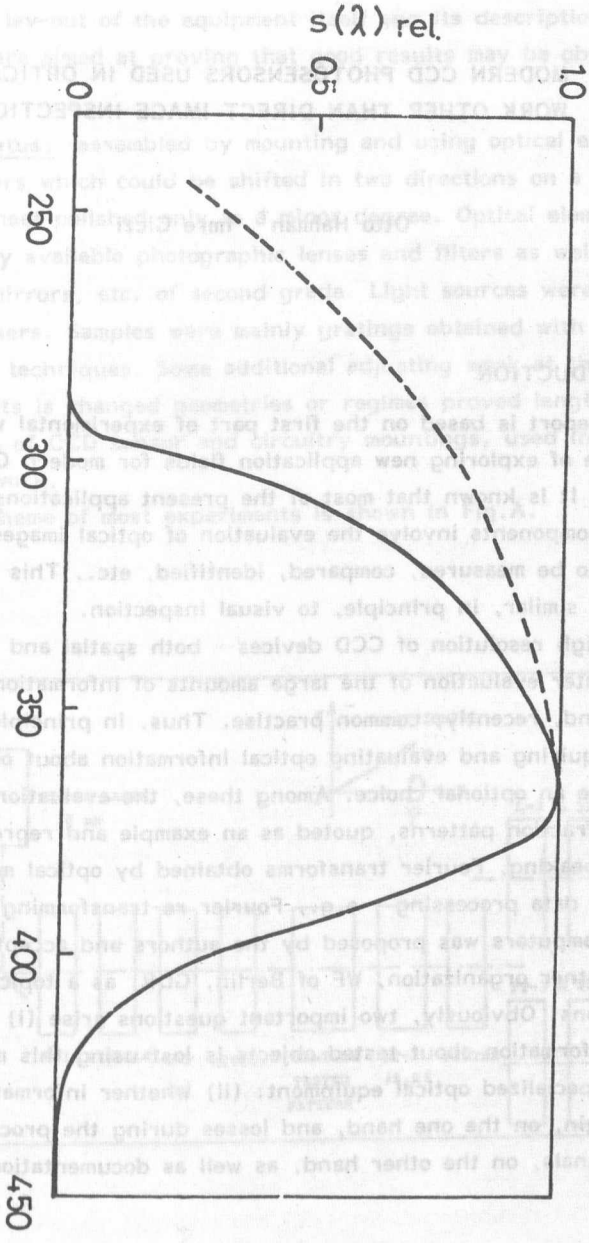

Fig.2. Typical spectral response of the Mod.211 UV meter (----) and the Mod.212 UV-A meter (————)

MODERN CCD PHOTOSENSORS USED IN OPTICAL WORK OTHER THAN DIRECT IMAGE INSPECTION

Otto Haiman[+], Imre Giczi

INTRODUCTION

This report is based on the first part of experimental work done with the purpose of exploring new application fields for modern CCD photodetector arrays. It is known that most of the present applications of these optoelectronic components involve the evaluation of optical images of the objects which are to be measured, compared, identified, etc.. This is usually done by methods similar, in principle, to visual inspection.

The high resolution of CCD devices - both spatial and temporal - has made computer evaluation of the large amounts of information obtained a necessity and, recently, common practise. Thus, in principle, different ways of acquiring and evaluating optical information about object parameters have become an optional choice. Among these, the evaluation with CCD sensors of diffraction patterns, quoted as an example and representing, mathematically speaking, Fourier transforms obtained by optical means, and the subsequent data processing - e.g., Fourier re-transforming or filtering - by micro-computers was proposed by the authors and accepted by MFKI and its partner organization, WF of Berlin, GDR, as a topic for preliminary investigations. Obviously, two important questions arise (i) whether much relevant information about tested objects is lost using this method any rather unspecialized optical equipment: (ii) whether information losses of optical origin, on the one hand, and losses during the processing of the electric signals, on the other hand, as well as documentation and display

---

[+]Eötvös Loránd University, Budapest, Hungary

deficiencies to be expected with work on the microcomputer hardware and software level are reasonably in proportion to each other.

Both the lay-out of the equipment itself and its description given in the following are aimed at proving that good results may be obtained using the following.

Optical Apparatus: assembled by mounting and using optical elements on magnetic holders which could be shifted in two directions on a table coated with a steel sheet polished only to a minor degree. Optical elements included commerically available photographic lenses and filters as well as positioning devices, mirrors, etc. of second grade. Light sources were plain miniwatt He-Ne lasers. Samples were mainly gratings obtained with IC mask manufacturing techniques. Some additional adjusting work at the beginning of measurements is changed geometries or regimes proved lengthy due to the clumsiness of CCD sensor and circuitry mountings, used in this first phase of the work.

The optical scheme of most experiments is shown in Fig.A.

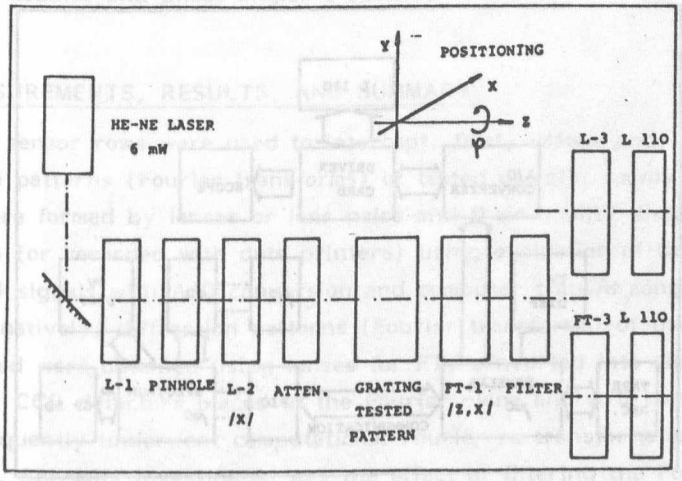

FIG. A

Electronic Hardware, whose units worth mentioning consisted of:

- a CCD light sensor row type L 110 (256 pixels)
  (WF, Berlin, GDR/ and its auxiliary circuitry

- a home-made A/D converter, 8 bit, successive approximation in EPROM:
  minimal conversion time 20 /us: data output parallel

- a HOMELAB 3 micro-computer, assembled by students.
  Micro-processor Z/80, 16 kB ROM, (16 + 2x32) kB RAM: Z/80 PIO

- A Sinclair SPECTRUM micro-computer + 2 micro-drives.
  Micro-processor Z/80A. 16 kB ROM, (16 + 2x32) kB RAM:

- PIO Interface Card Z/80A

The electronic set-up is shown in Fig.B.

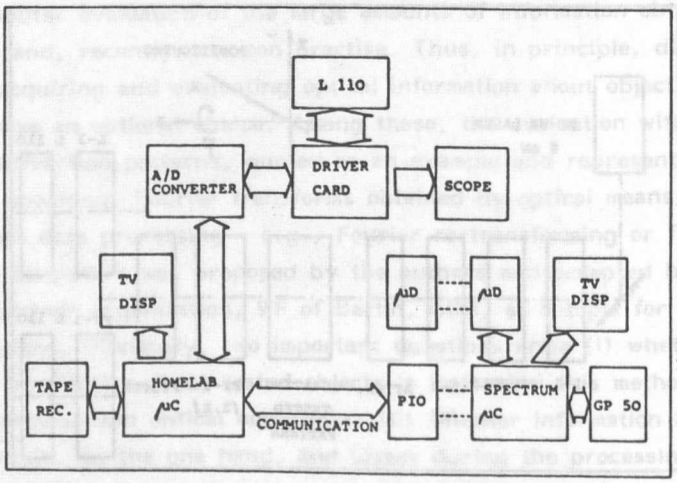

FIG. B

Software:

- A/D converter data feeding into the HOMELAB
- Fast Fourier Transformation program for the HOMELAB requiring 2 seconds for 256 measuring points with 3 Byte data
- HOMELAB = SPECTRUM data exchange accomplished by communication routine in machine code of 230 Byte length: exchange rate 4 kB/s
- Sinclair SPECTRUM functions:

  a) general: documentation TV screen
  printer
  micro-drive
  list

  b) subsequent data processing and documentation
  spectrum analysis in PASCAL
  8 sectors of 256 points each
  4 function generators: sin, triangle,
  Walsh, noise simulation and Constant
  operations on sections resp. between
  sections: multiplication, addition
  window, SQRT
  FFT and Inverse FFT
  complex amplitudes 6 seconds
  modules and phase angles 8 seconds

MEASUREMENTS, RESULTS, AND SUMMARY

CCD sensor rows were used to intercept, first, images and, second, diffraction patterns (Fourier transforms) of tested objects, mainly gratings. Images were formed by lenses or lens pairs and their quality displayed on TV screen (or recorded with data printers) using evaluation of the image plane CCD signals with A/D conversion and computer transforming.

Alternatively, diffraction patterns (Fourier transforms) of the objects to be tested were obtained using lenses for FT, converted into electrical signals by CCD detectors placed in the Fourier plane and A/D converters and subsequently underwent computational Fourier re-transformation and evaluation. Specially investigated was the effect of filtering the Fourier transforms by optical and computational methods, with the aim of selective detection and parameter determination. The results obtained (illustrated by Figs.1-6) show that in cases, when Fourier transform processing and

evaluation is preferable to image evaluation - as when periodic structures, interference patterns, spectra or microscopic objects are investigated - CCD-s may well be used, e.g. for the determination of diffraction maxima or spectral line positions to a fraction of a pixel.

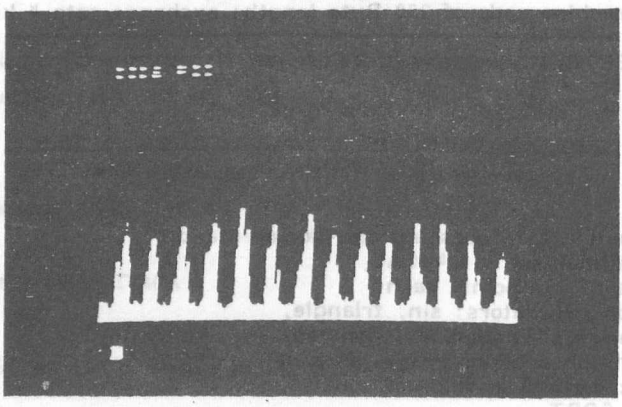

Fig.1. Picture of a grating on CCD L110 grating constant is 100 /um (d)

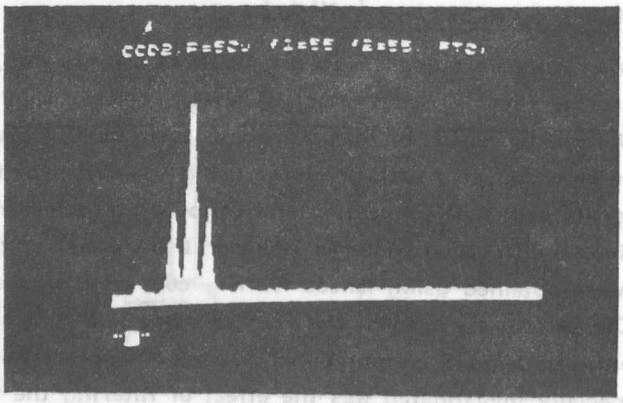

Fig.2. Optical Fourier Transform (OFT) of the grating (see above) with orders 0, $\pm$1, $\pm$3

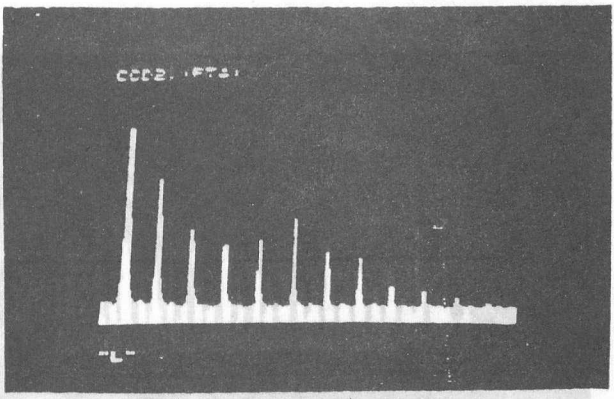

Fig.3. OFT of the grating from the order No. 5th

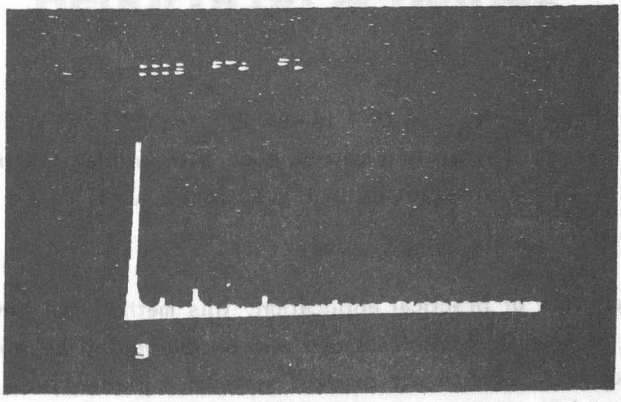

Fig.4. Filtered OFT from the order No. 5th

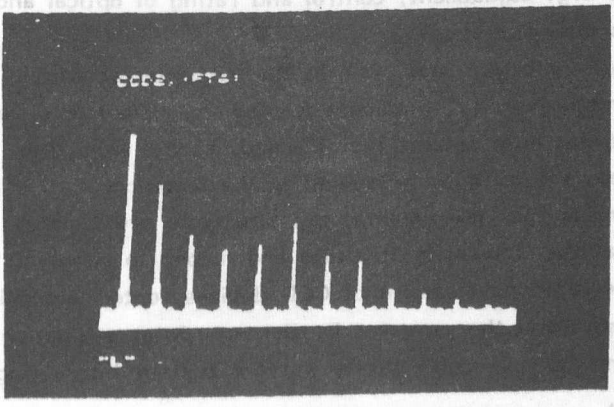

Fig.5. The same as Fig.3. It can be compared with Fig.4.

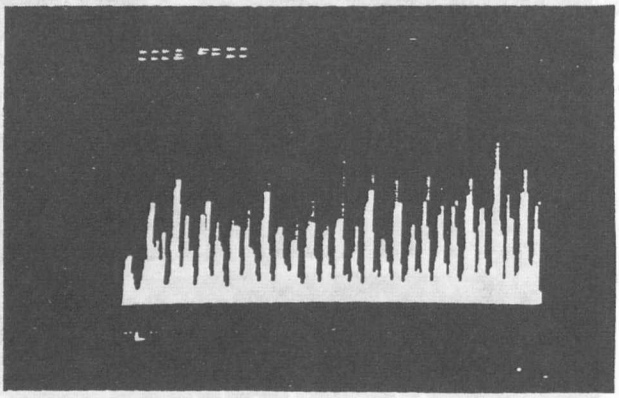

Fig.6. Inverse OFT of the Filtered OFT. (Fig.3) A grating can be seen with smaller grating constant as in Fig.1. (d=50 /um)

For each case of practical application, this method will have to be implemented in specific optical set-ups and supplemented by appropriate software. However, even in its present state of implementation, it can be used in advanced students' laboratories and in R/D work to solve everyday problems, as e.g. adjustment, control and rating of optical and opto-electronic components and apparatus.

The work reported was done in the Institute for Atomic Physics of Eötvös Loránd University, Budapest for the Opto-Electronic Department of the MFKI. It was only not the result - and, at the same time, the source - of new ideas and methods presented to the technical staff of WF, Berlin, manufacturers of CCD components, but also gave new impetus to the educational work at the University Institute and helped to supply it with modern sensors. The rapid development of CCD devices, opto-electronic measurement techniques and the progress in micro-computer evaluation methods at WF, MFKI and EL University surely warrant further interesting results to be expected.

Reports on activities

PERSONAL DATA

Scientific staff 119
Technical Assistants 88
Administration 63
Services 52

Scientific divisions	Scientific members	Technical members
Semiconductor Research	30	21
Metal Research	33	17
Structure Research	20	15
Microwave Devices	19	17
Optics and Electronics	17	18

MEMBERS WITH ACADEMIC DEGREES

Members of HAS 2
Academic Doctors of Science 3
Candidates of Science 25
University doctors 20

Semiconductor Research Division

E. Lendvay

Research at the Semiconductor Division deals mainly with the investigation of new III-V semiconductors, structures and optoelectronic devices, as well as with studies on deep levels not only in III-V materials but also in Si. The broad range of this research required the application of various disciplines; solid state physics and chemistry, material science, electronic device characterization and applied research developing equipments supporting the experimental activity.

The division consists of 3 different groups. One of them conducts research on GaAs based laserdiode structures, and their application in optical telecommunication. The main emphasis lies on the development of high power LD-s with low threshold current and high reliability. This group maintains liquid phase epitaxy (LPE) facilities and a variety of equipments available and used in heteroepitaxial wafer production, low temperature luminescence investigations and LD production and characterization. The center of activities in the group is the development of GaAs/GaAlAs double heterojunction laserdiodes for transmitter modules applied in optical telecommunication systems. The group investigates the influence of impurity-, dopant- and defect densities in epitaxial layers of GaAs and GaAlAs grown by LPE on the laser parameters mainly concerned with the formation and the movement of dark lines in the active region of the LD. A special experimental technique has been developed for the observation of the mentioned effects through a stripe-window made on the lateral contact area at the substrate--side. Near and far-field patterns of the LD are also studied. In the device technologies thin film technologies including the usual vacuum evaporation techniques together with microlithography are applied. Both broad-area and stripe laserdiodes have been produced and built-in into optical transmitter modules.

The work in the second group is concentrating on problems of new semiconductors, mainly on antimonides and on new structures. This work involves the preparation of pseudo-ternary antimonides (AlGaInSb or GaPAsSb) as well as the growth of double heterojunctions consisting of these materials. A prime example of the mentioned is the GaAs/GaPAsSb DH system, which is a candidate for substituting the usual GaAs-GaAlAs DH laserdiode structures. This system has been grown by LPE and it was proved that an intensive injection and recombination in the GaAs active region can be achieved using lattice matched quaternary antimonide cladding layers.

The group is also concerned with the LPE growth of superlattice structures. The experimental technique and the vertical rotating LPE reactor were developed in the group and multilayer GaAs/GaAlAs heterosystems up to a layer number of 100 and with a layer thickness (periodicity) of 20 nm were grown. Detailed investigations of doping effects on growth rate and on nucleation were done using these model materials, and the results were applied directly for the growth of superlattice (SL) laser structures. Examples are GaAlAs confined SL active region laserdiodes and DH structures consisting of the usual GaAs/GaAlAs DH region and a SL dislocation barrier inserted between the GaAs substrate and the DH structure.

For InP based laserdiode structures a new LPE furnace system using semitransparent Au shield instead of ceramics have been developed. This system decreases drastically the number of experiments necessary for the determination of solidus and liquidus points because the dissolution or the formation of solid phase on the melt surface can be directly observed. Using this system efforts in producing buried InP/GaInAsP laserdiode structures (e.g. in growing double channelled LD structures) have been extended considerably.

During these works a number of interesting results have been obtained. On the pseudo-ternary antimonide side not only GaAs/GaPAsSb laserdiode structures but an AlGaInSb/GaSb photodiode with a very wide spectral response covering both the Si and Ga detector field was developed.

The fabrication of a real device is a subject of further study. There has been a continuing activity on SL laserdiodes, too. Using very short growth times the insufficiency of the existing diffusion limited growth theories was demonstrated. Also a very strange enhancement of growth rate depending on dopants was observed.

Applying the very strong growth rate anisotropy in the GaAs/GaAlAs system quantum wire structures, as well as index guided optical SL elements were grown on patterned GaAs substrates using the strong change of refractive index with SL periodicity. Such non-planar growth is essential in LD structures with current confining blocking layers and lateral index-guiding, and it is very useful in optoelectronic integration.

In the reported period a series of research and industrial equipments applied in optoelectronics was also realized. First a Bridgman type horizontal GaAs growth system has been perfected. There are no moving parts in the system, the thermal gradient at the melt/solid interface moves along the direction of freeezing as a result of computer driven change of the temperature in the multizone furnace elements. GaSb boules were also grown using the system. The required soft-ware has also been developed to perform all the measurements needed for an improved growth method. Answering the increasing need for automatic selection and ageing, as well as the measurements of the most important parameters and characteristics of laserdiodes, desk-top computer driven systems for GaAs and InP LD-s were constructed and exported to GDR and the Sovietunion. In these systems data of LD-s up to a chip (or diode) number of 64 can be registered and stored in the first 1000 hours of LD lifetime.

In the third group the DLTS technique is one of the most powerful methods to provide information on deep levels in Si and III-V semiconductors. During the past years a dedicated DLS system named as Semitrap DLS-82 has been developed and distributed by the Materials Development Corp. (MDC) all over the world.

The equipment has an excellent signal-to-noise ratio and consequently, a very high sensitivity on the one hand, and the possibility of constant frequency scan, on the other. At this moment this technique is being applied to Si structures as well as to III-V Schottky barriers and p/n junctions to determine depth profile of energy levels, capture cross sections etc. Similarly, implantation damage, annealing and recovery process in semiconductors can also be studied. In order to implement its research programs as fully as possible, this group made intensive development in both hard-ware and soft-ware concerned with the DLS system. In Si, eg. the carbon contamination related radiation defects caused by ion implantation were separated into two levels identified as COV_2 and C_s-Si_i-C_s

complexes. To overcome the difficulties of capacitive methods a novel method for semiconductor characterization, the microwave absorption spectroscopy (MAS) has also been developed. The MAS method is a novel technique for the characterization of free carriers in semiconductors produced by induced emission from deep levels within the space charge region of a pn-junction or Schottky barrier using a microwave cavity perturbation. This method has significantly broader range of emission and capture rate measurement than the usually applied space charge spectroscopy (SCC) has and its capability higher, sensitivity against leakage currents lower than the SCS methods. Experimental verification of previous expectations was done on Au ($10^{11}cm^{-3}$) doped Si, where the free carrier concentration was 8.10^{12} cm^{-3}.

Metal Research Division

K.Vadasdi

The scope of our activity was broad, it covered the following topics: pattern formation with special emphasis on the fractal aspects, structural changes during sintering, as well as R+D work in chemical and mechanical technology, processing of ceramics and development of on-line equipments for process and quality control.

The studies of pattern formation were primarily concerned with the effects of fluctuations, driving force and the anisotropy on the growth of two-dimensional unstable interfaces. To reach a deeper understanding of these far from equilibrium phenomena we used computer simulations and carried out experiments on viscous fingering. Our results demonstrate that the various aggregation models capture many of the most important features of fractal pattern formation. In the viscous fingering experiments with nematic and smectic liquid crystals we found a number of unexpected morphological phase transitions including crossovers from tip splitting to dendritic growth and from fractal to homogeneous structures. The investigations reported in this volume (see T.Vicsek and J.Kertész: "Laplacian pattern formation" and in the publications referenced therein) suggest that the role of noise, driving force and anisotropy is crucial in the formation of patterns and it is the complex interplay of these factors which produces the great variety of morphologies found in nature.

The activity in the field of sintering was motivated by the fact that the useful properties of sintered metallic and ceramic products depend to a high degree on the grain and pore structure established at the end of commercial sintering. There is ample evidence that the interplay of grain growth, pore shrinkage and pore coarsening explains the sensitivity of the final microstructure to sintering routes, dopants and trace impurities.

In the past two years, investigations have been carried out from these aspects along three lines: grain growth in pure porous systems, mechanisms for the enhancement of the grain growth rate by some solutes present in trace amounts and effect of grain growth on fine pores filled with an insoluble gas.

On the first two subject separate reports are given in this yearbook. The motivation of the last subject was that it is generally believed that grain growth during sintering leads to a redistribution of the insoluble gases trapped in fine pores. In this connection, the behaviour of potassium in K-Al-Si doped tungsten has been studied. We put forward arguments evidencing that at the beginning of the final stage of sintering there are two sorts of pores. The first sort of pores is formed by the closure of the open porosity. These pores are nearly empty and their sizes range between 1 and 10 μm. The second sort of pores is formed in the place of potassiumaluminosilicate particles upon internal reduction in the course of sintering. In the final stage of sintering these are filled with potassium gas and since their most frequent size is below 0.5 μm, they are dragged by the grain boundaries during grain growth. Consequently also some of the originally empty pores will be filled with potassium, when the sintering is performed for a too long period of time. This model is supported both by metallographic evidences and by Auger electron spectroscopy.

The R+D work in mechanical technology was directed on processing of fine doped tungsten wires used as incandescent lamp filaments. There is ample evidence that the useful properties of the fine wires depend beside the overall processing parameters (i.e. total wire drawing strain, working temperature and process annealings) also on the fine details of the drawing (lubrication, reduction schedule, drawing angle etc.). To determine the parameters of a well controlled drawing, a drawing machine has been developed. It is equipped with a number of different fast sensors, in order to get great variety of data for process control. The analysis of the first set of data is now under publication.

Diamond dies are of basic importance in the production of fine tungsten wires. Polycrystalline diamond can be advantageously used as material of wire drawing dies, because its structure related mechanical properties, such as wear resistance, are superior with respect to natural diamond. Since on the thermal stability of polycrystalline diamond only few experimental data have been published, the structural evaluation of

various sorts of polycrystalline diamond has been followed up between 500 and 900°C, because polycrystalline diamond blanks are likely to be heated into this temperature range in two periods of their life; during the production of the tool and later, when the tool is in use.

The R+D activity on ceramics - after an introductory period - has been intensified in 1986. The main target of the work is the laboratory scale production of Si_3N_4 based ceramics to clarify some relations between structure and certain physical properties.

We have constructed a high temperature sintering furnace with graphite heating tube and prepared samples under different, well-defined conditions in N_2 atmosphere. Phase and grain structure, density and banding fracture strength were measured. The high performance mechanical properties could have been reached only if the volatility of the material was suppressed and if both α -Si_3N_4 and also β -Si_3N_4 phases were present. The phase properties had a great influence on the strength and on the density values. In the future we tend to clarify optimal composition and the role of the surface quality.

In the field of chemistry, most of the work was carried out in the research of separation methods. Following the national efforts for utilising secondary raw-material sources, processes were investigated which can help to reprocess and to separate valuable metallic components from scrap in both an economical and environmentally acceptable way. Beside the necessary chemical investigations, equipment was constructed for the realization of processes both on laboratory and also on production scale, developing complete technologies.

In order to study ion separation through ion-exchange membranes, several single- and multicell electrodialysis units were built in the 100 - 25000 cm^2 membrane area range. Properties of construction materials, efficiency and economy of steps and several chemical side-effects, like precipitation, change in permeability, etc. were investigated. The method of electrodialysis proved to be very advantageous for the recovery of alkaline ions from solutions of ores leached by alkaline hydroxides, the metallic component of the ore being further processed. The recovery of the alkaline hydroxide is not only of economic advantage but also decreases the salt-contamination of the environment. This method was developed to industrial scale in case of the Na_2WO_4 solution, when a stable, dissolved isopolyacid was formed with excellent properties, it was easily transformed

to ammonium paratungstate (APT) - a usual intermediate product in tungsten metallurgy.

One of the most up-to-date separation methods is the liquid ion-exchange extraction technique based on specific formation of metallorganic compounds which can be extracted by organic solvents. It has several advantages:

- the active organic reagent and the organic solvent can be recycled. In this way small amounts of transporting agents are able to carry great amounts of metal to be processed;
- the great choice of active organic reagents with different functional groups provides high selectivity in case of "hard to separate" metals;
- reactor vessels can be switched in cascade and a number of metallic components can be separated at the same time;
- because of the intimate contact of the material, relatively small reactor vessels are needed;
- the possibilities of continuous operation mode and of process control.

We have constructed mixer-settler type reactor vessel units of 200 ml and of 20 l and of 100 l (the latter having a separation capacity of 10-15 kg W/hour/ for laboratory tests, pilot and industrial purposes.

In the course of chemical investigation a solvent mixture was found for the extraction of the above mentioned tungstic-isopolyacid, prepared by electrodialysis, which helped us to transform it to a high-purity APT.

The electrodialysis and solvent extraction, coupled together, form the fundament of a new, efficient method for APT production with low effluent emission. We have built a production line of a capacity of 70 t APT/year using this process. The extraction method was successfully used for the separation of the components of mixed metals like Co-Ni, Ta-Nb, Ni-Cd, Ga-Al, Cu-Ag-Au.

Based on this research new processes have been developed for the recovery of valuable components of Ni-Cd batteries, mixed metal scraps, etc.

The separation of valuable metal components requires dissolution as the first step. Very often, by applying nitric acid as an oxidation agent

toxic nitrous oxides evolve. In case of several metal-mixtures H_2O_2 was successfully used instead of nitric acid. The oxidation potential of H_2O_2 can be influenced by homogeneous catalysts. In this way selective dissolution of certain metals, such as Mo beside W, can be carried out. Another example is the dissolution of the binder phase of sintered, polycrystalline diamond tools in order to recover diamond grains. For this purpose an automatic, dissolving unit of industrial size was constructed. The costs of recovery are a small fraction of the value of the diamond grains.

An electrochemical process was invented for the specific dissolution of a galvanically bound abrasive diamond layer recovering also the high-value tool bodies for repeated use.

Both diamond recovery processes have been in use for 2 1/2 years by the home industry.

Our patented electrochemical method for the desintegration and dissolution of hard metal scraps was developed further in respect of the machinery and of the recovery of the valuable W component.

The chemical activity described above has a necessary analytical background based mainly on AAS, ASP, NAA but also on some further classical methods

Development work has been carried out in the last decade on equipments for on line process and quality control. In recent years a series of magnetic and magneto-inductive devices for non-destructive testing has been developed for on line flaw detection of ferromagnetic and non-ferromagnetic metallic parts. This work is still going on, although some units work already in production plants.

The cooperation with various universities, research institutions and companies had a lively influence on our activity also in past two years.

Structure Research Division

L. Zsoldos

Within the rather broad field of structure research we are dealing on the whole with the structure and behaviour of solids with structural and/or chemical inhomogeneities, including surface effects. Some results of this work are reported in separate articles of this wolume, therefore only a summary of other results will be outlined here.

The study of the growth morphology of thin films was continued also on other materials. TEM and SEM studies of the effect of oxygen on the structure of evaporated Cu films revealed a correlation of surface growth morphology and the grain size distribution to the partial pressure of oxygen and the film thickness. The development of growth hillocks was interpreted in terms of crystal face dependence of surface microchemistry. (M.L.Hiti, et.al).

At the very early stage of SiO_x formation on NaCl (100) the selective nucleation of SiO_x on surface defects resulted in decoration patterns by developing three-dimensional SiO_x grains. The activated condensation of Au on NaCl covered by a thin SiO_x was also studied.

Experiments on the growth of Al based (Al+transition metal) quasi-crystals showed that quasicrystalline phases can be produced both by heat treatment of film couples or multilayers and by high temperature successive deposition. In this latter case orientational relationships between the host Al crystal and the quasicrystals were verified (A.Csanády, K.Urban et.al, Csanády Á., Guenter J.R. et al., Csanády, Á., P.B.Barna et al., Barna P.B., G.Radnóczi et al)[x]

[x] See "Bibliography" of this volume

In evaporated Ni-Cr thin films characteristic quasi-periodic density fluctuations were found, whose parameters can be correlated to the deposition conditions. The geometrical effect of substrate surface roughness has been simulated by a simple model which explains qualitatively the virtually thickness dependent resistivity of the films deposited on ceramic substrates. (L. Tóth, A.Barna; Á.Barna, G.Sáfrán; L.Tóth).

TEM investigations of layer structures in cross section were successfully applied to many systems, using the ion-beam thinning unit developed earlier (Á.Barna, Proc. 8th Congr. on Electron Micr., Budapest, 1984. p.107).

As an example Fig.1. shows the growth structure of a diamond thin film.

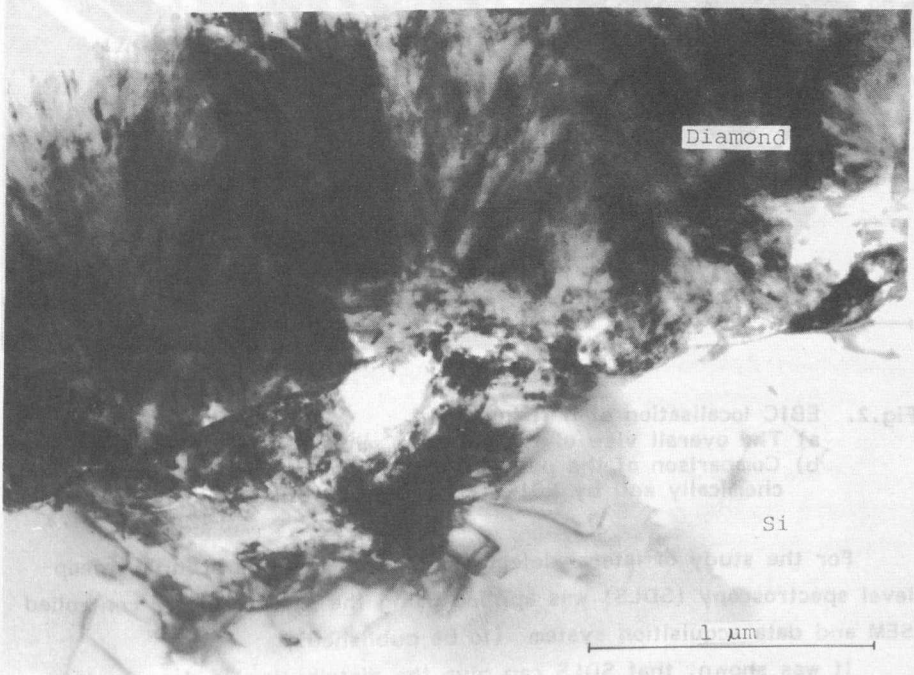

Fig.1. Cross section TEM micrograph of a diamond thin film. The film was prepared at the Pennsylvania State University.

As a new application of ion beam milling a method was developed for cutting a groove into the sample making possible the SEM investigations of the cross section e.g. in semiconductor layer structures. It was shown namely that the quality of the EBIC images depends on surface treatment. Freshly cleaved surfaces tend to form an inversion layer which makes the p/n junction localisation impossible. Although the surface inversion can be reduced by slight chemical etching or by ion (electron) bombardment, the best EBIC imaging was obtained on surfaces prepared by ion beam milling (to be published). Fig.2. illustrates the junction localisation by this method.

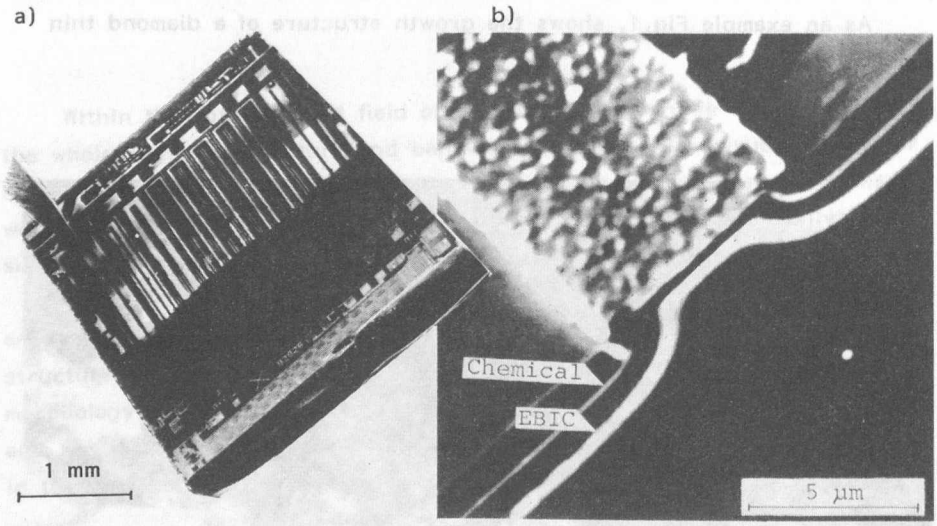

Fig.2. EBIC localisation of n^+/p junction
a) The overall view of the ion beam milled NMOS test device,
b) Comparison of the position of the junction as delineated chemically and by EBIC (superimposed SEI and EBIC images).

For the study of lateral defect distribution in GaAs scanning deep-level spectroscopy (SDLS) was applied using the microcomputer controlled SEM and data acquisition system (to be published).

It was shown, that SDLS can give the distribution of deep centers only if the SDLS signal saturates as a function of EBIC current and the filling factor of the pulse length. It was also proved that the concentration distribution can be determined by choosing appropriate measuring system (to be published).

A considerable progress was attained in quantitative X-ray microanalysis by improving the evaluation routines in two aspects. On one hand the backscatter loss calculations were revised (J.L.Lábár), and on the other hand the L-line intensity ratios were evaluated taking also the radiation free transitions into consideration. (J.L.Lábár).

A comparative X-ray topographic investigation of GaSb samples grown by Bridgman method in space and in terrestrial environment revealed not only the larger average crystallite size of the space sample, but the decrease of liability of the GaSb to twinning in microgravity circumstances. (L.Petrás, I.Gyuró et al).

Defect annealing studies of implanted Si - by double crystal diffractometry - proved that in case of high dose implantation, after a regrowth at 630°C, the structure is metastable; further processes are taking place if annealing is repeated at higher temperatures (L.Zsoldos, G.Pető et al.)

The anisotropic and reversible lattice deformation - similar to that observed earlier during heat treatment of GaOOH and ammonium-paratungstates - was studied in ZrO_2 and HfO_2. By increasing the temperature up to 1000°C the monoclinic angle β approaches 90° whereas $\underline{b}$ remains nearly constant. This high degree of anisotropy can be responsible for stresses resulting often in cracks in ceramics (M.Farkas-Jahnke, L.Petrás).

Division of Microwave Devices

I. Mojzes

The main tasks of the Division of Microwave Devices are the research and development of the technology of microwave devices, the investigation of processes taking place during the technological processes of compound semiconductor structures. In this broad field our efforts are devoted to the following major fields:

1. The research and development of microwave active semiconductor devices including design, technology, measurement and testing;

2. The investigation of metal-compound semiconductor junctions and especially the interaction between the metal and the semiconductor during heat treatment;

3. The application of microwave semiconductor devices and the microwave techniques for measurement, material testing, remote sensing, and controlling purposes.

As the basis for semiconductor microwave devices GaAs VPE epitaxial structures are obtained in a $AsCl_3/H_2/Ga$ system. Though the main part of epitaxial structures are grown for device purposes this VPE system and the properties of the layers are investigated and also methods for their qualification were developed.

The main purpose is to improve the layer quality, purity, homogeneity and the reproducibility.

The main activity in device development was focused on the development of X-band MESFET's. For these purposes VPE GaAs layers were used.

Classical and self aligned technologies were used and investigated. Processes taking place during the etching, phenomena arising during the heat treatment, the lift-off process are the most important steps in device technology. For the broad investigation of these mainly thin film processes a wide and very fruitful collaboration with a number of other institutions was arranged.

Using the results achieved in the compound semiconductor device technology we made a start of the monolithic microwave integrated circuits. First wave propagation experiments are the basis for the design of GaAs IC's. Gunn and Schottky diodes, varactors have been produced in our pilot-line production. Technological experience accumulated in last 10 years made it possible to use these devices for the most rigorous application fields both in this country and by foreign companies. These in-house semiconductor devices formed a very good basis for the activity of their application in the field of measurement and control.

Microwave distance measuring (ranging) head, vehicle sensing and identification, motion detection modules, are our latest results put into production. Licences were granted to three industrial enterprises.

One of the most important achievements in the last period is the introduction of computer controlled measuring systems. Computer controlled systems for microwave device testing, for microwave module characterization, for DC-parameter test of MESFET's, for evolved gas analysis of compound semiconductor structures covered with thin metallic layers, for the Hall, Van der Pauw and angle dependent magnetoresistance measurements are very effective tools in our work. PC's facilitated our administration including the preparation of our papers. (Ideas are yet generated in a traditional way....)

Division of Optics and Electronics

J. Schanda

Optoelectronics has developed by now to the Number I. area of microelectronics. It became the most important element of computer input and output devices, it penetrated the home-electronics market by the use of laser light in compact disc players, the communication electronics by short-, medium and long range optical data transmission, the most diversed industrial areas by using photochemical reactions, modern medical technologies by using optical irradiation treatment, optical methods of analysis, etc. The Optoelectronic Division of our Institute realized several years ago the importance, what measurement technologies play in all these areas and started systematic investigations in a number of directions to help better usage of optical radiation in the different fields of applications.

Some results of our endeavours to achieve an independent measurement scale of optical radiation and light intensity has been covered in our previous report. Since then major progress has been achieved both in Si-photovoltaic cell and operational amplifier technology that enabled the development of a self-sustained absolute radiometer system lending the possibility to realize absolute optical power measuring scales without external standards.

International comparison of our optical radiation scale based on the unit quantum efficiency of Si showed residual uncertainties well below 1%. A major achievement of the past 2 years was the tieing in into this scale also the photometric scale, by using the high-precision $V(\lambda)$-correction technique developed in our Institute. These measurement techniques have been used extensively in a number of applications. Thus e.g. the measurement of biologically active radiation has attained special interest. In report written for the CIE, the literature data have been summarized. On

this basis a number of methodological statements could be developed (a summary of which is the basis of a thesis written by one of the staff-members of the Division) together with new instruments, a short description of which is found in a subsequent paper.

For light measurement the V(λ)-correction technique has been further developed and utilized in a number of photometric instruments. One of the newest members of the family of photometers is an experimental model of a luminance-meter, using a Si-cell as detector, but competing in a number of applications with instruments using photoelectric multipliers.

An other member of this series of instruments is a computerized colorimeter that can be used not only to determine the chromaticity of light sources, but also to calculate higher order correlates of brightness, a very up-to-date question to evaluate visibility of displays and similar devices.

The visibility and readibility of computer color monitors attracted our attention several years ago, and a model has been elaborated to quantify these findings. With the new instrument, and with the help of an other new development, the LED-Anomaloscope, an instrument to investigate the color-aptitude of observers, it becomes now possible to perform also the necessary objective - subjective comparisons, which will, eventually, lead to a computer program for direct visibility evaluation.

Besides display visibility a new project has been started to develop methods and instrumentation (questions that are principally tackled always in parallel) for working place illumination evaluation. On the theoretical side these works lean on the CIE publications on contrast rendition, on the instrumental side studies have been started to use CCD cameras for task and surround luminance evaluation.

Important steps in this project were the characterisation of CCD matrices, the development of the CCD-computer interface and of the V(λ)-correction filter for our CCD-matrices.

An other waste field of radiometry has been opened up by optical communication techniques. Here instruments for power measurement in the first three windows (0,85: 1,3: 1,55 /um) have been developed together with a number of other instruments used in optical communication techniques (see special paper in this book).

It is hoped that with this very short summary of the fields of activities of the Division for Optoelectronics we could show that this Division

is developing as dinamically as the technology and it has to serve with some fundamental and some applied investigations. During the past two years a number of new projects have been started (e.g. in fibreoptic instrumentation, application of CCD-matrices) which promote further basic investigations and practical applications.

International relations

As introduced in Table 1, relations with scientific institutions of other countries have been fostered and in case of mutual interest new contacts have been established during 1986-87.

Common project work was preferred and a number of institutions has agreed to this more advanced form of cooperation. As seen from the bibliography quite a lot of common papers was published as a result.

Running a race with rising expenditures we have tried to maintain the previous level of our representation on international scientific events, sometimes recurring to an expedient of organizing conferences in this country, what eventually turned out to be a great success.

A list of conferences where our staff members acted as invited speakers during 1986-87, is presented in Table 2. The names and affiliation of foreign visitors coming from different countries are also given, indicating growing interest in our activity (Table 3).

A limited number of foreign scholarship was awarded to our members, others have performed long-term scientific work abroad being on leave of absence.

is developing as dinamically as the technology and it has to serve with some fundamental and some applied investigations. During the past two years a number of new projects have been started (e.g. in fibreoptic instrumentation, ...) which will lead to a number of new topics for investigations and practical applications.

International relations

As introduced in Table 1, relations with scientific institutions of other countries have been fostered and in case of mutual interest new contacts have been established during 1986-87.

Common project work was preferred and a number of institutions has agreed to this more advanced form of cooperation. As seen from the bibliography quite a lot of common papers was published as a result.

Running a race with rising expenditures we have tried to maintain the previous level of our representation on international scientific events, sometimes recurring to an expedient of organizing conferences in this country, what eventually turned out to be a great success.

A list of conferences where our staff members acted as invited speakers during 1986-87, is presented in Table 2. The names and affiliation of foreign visitors coming from different countries are also given, indicating growing interest in our activity (Table 3).

A limited number of foreign scholarship was awarded to our members, others have performed long-term scientific work abroad being on leave of absence.

TABLE 1.

AUSTRIA

J.Kepler Universität, Linz
Institut für Experimental Physik

Technische Universität, Wien
Institut für Angew. u.Techn.Physik

Technische Universität, Wien
Institut für Chem.Techn.anorg.Stoffe

BULGARIA

Institute of Electronics,
Bulgarian Academy of Sciences,
Sofia

CZECHOSLOVAKIA

Institute of Radioelectronics,
Czechoslovak Academy of Sciences
Prague

Electrotechnical Institute of the
Slovak Academy of Sciences
Bratislava

GREECE

University of Athens
Solid State Section

cont.TABLE 1.

FEDERAL REPUBLIC OF GERMANY

Physikalish-Technische Bundesantalt
Braunschweig

Max Planck Institut
Institut für Werkstoffwissenschaft
Stuttgart

FINNLAND

University of Turku (U.T.)

FRANCE

Institute of Optics,
University of Orsay,

Institute for Electrondiffraction and
Microscopy,
University of Marseille

GERMAN DEMOCRATIC REPUBLIC

Zentral Institut für Elektronenphysik der AdW,
Berlin

Institut für Festkörperphysik und Elektronen-
mikroskopie, Halle

Institut für Halbleiterphysik,
Frankfurt/O

Zentralinstitut für Isotopen- und
Strahlenforschung, Leipzig

Werk für Fernsehelektronik,
Berlin

ITALY

MASPEC Laboratories of CNR,
Parma

cont. TABLE 1.

POLAND

Institute for Electron Technology,
Warsaw

Institute for the Technology of Electronic
Materials,
Warsaw

Institute of Physics,
Polish Academy of Sciences,
Warsaw

SOVIET UNION

Institute for Superhard Materials,
Ukrainian Academy of Sciences, Kiev

Baikov Institute for Metallurgy,
Moscow

Institute for Technical Physics,
Academy of USSR, Leningrad

Institute for Semiconductor Physics
of the Academy of USSR, Siberian
Branch, Novosibirsk

Institute of Crystallography,
Academy of Sciences of USSR, Moscow

Institute for Semiconductors,
Ukrainian Academy of Sciences, Kiev

Institute for Solid State Physics
Academy of USSR, Chernogolovka

SWEDEN

Linköping Institute for Technology
Department of Physics and Measurements
Technology

cont. TABLE 1.

UNITED STATES OF AMERICA

National Bureau of Standards,
Washington

YUGOSLAVIA

Institute for Electronics and Vacuum Physics,
Ljubljana

TABLE 2.

P.Barna	10th Int.Vacuum Congress Baltimore, USA	October, 1986
F.Beleznay	7th Conf.on the Condesed Matter Division Pisa, Italy	June, 1986
L.Dózsa	Structure and Properties of Dislocations in Semiconductors Zvernigorod, Soviet Union	March, 1986
S.Ferenczi	Int.Sci.Conf: Work with Display Units Stockholm, Sweden	May, 1986.
G.Ferenczi	18th Int.Conf.on the Physics of Semiconductors Stockholm, Sweden	August, 1986.
I.Gaál	Int.Conf. on Powder Metallurgy Düsseldorf, FRG	July, 1986.
B.Kovács	16th European Solid State Device Research Conference Cambridge, UK	September,1986
E.Lendvay	Int.Conf on Crystal Growth York, UK	July, 1986
I.Mojzes	Microwave Technology and Optoelectronics Wiesbaden, FRG	June, 1986.
T.Pavelka	14th Int.Conf. on Defects in Semiconductors Paris, France	August, 1986.
L.Petrás	XIIth Conference on Applied Crystallography Cieszyn, Poland	August, 1986
I.Pozsgai	11th Int.Congr.on Electron Microscopy Kyoto, Japan	September,1986.
B.Szentpáli	Microelectronics'86 Plovdiv, Bulgaria	October, 1986.

cont. TABLE 2.

P. Barna	National Symposium of the Vacuum Society Anaheim, USA	November, 1987.
G. Ferenczi	Conf. on Deep-Level Impurities in Semiconductors Cagliary, Italy	September, 1987.
M. Farkas (Mrs.)	Advanced Methods in X-ray and Neutron Structure Analysis of Materials Karlovy Vary, Czechoslovakia	October, 1987
I. Gaál	VIIth Int. Conf. on Powder Metallurgy, Pardubice, Czechoslovakia	September, 1987.
J. Kertész	14th Seminar of the Middle-European Cooperation in Statistical Physics Puidoux-Chexbres, Switzerland	September, 1987.
E. Lendvay	Int. Conf. on Semiconductor Injection Lasers Holzhau, GDR	October, 1987.
J. Makai	Photonic-Measurements'87 Braunschweig, FRG	September, 1987
I. Mojzes	5th International School on Microwave Physics and Engineering, Sofia, Bulgaria	October, 1987.
R. Oláh	3rd World Congress on Desalination and Water Reuse Cannes, France	September, 1987.
A. Tóth	Microscopy of Semiconducting Materials, Oxford, England	April, 1987.
T. Vicsek	General Conf. of the Condensed Matter Division of the EPS Pisa, Italy	April, 1987.
L. Zsoldos	XIVth Congress and General Assembly of Int. Union of Crystallography Perth, Australia	August, 1987.

TABLE 3.

1986

M.L.Amadori	University of Urbino	Italy
H.Bangert	Technical University of Vienna	Austria
T.Frank	Institute of Physics Jena	GDR
B.Gruzza	Univ.Clermant Ferrand	France
J.J.Hasia	National Bureau of Standards, Washington	USA
H.Heinrich	University of Linz	Austria
P.P.Hossuntasvili	Gruzian Academy of Sciences	Soviet Union
S.Janusz	POLAM, Warsaw	Poland
Kim Zon Mun	Korean Academy of Sciences	Korea
J.Kristofik	Institute of Physics, Prague	Czechoslovakia
Liu Xun Lang	Institute of Semiconductor Physics, Beijing	China
C.A.Londos	University of Athen	Greece
V.Malina	Institute for Radioelectronics	Czechoslovakia
A.Malog	UNITRA-ITE, Warsaw	Poland
K.Murata	Osaka University	Japan
S.Nettel	Rensselaer Polytechnik Institute New York	USA
B.Olescsinszkaja	UNITRA-ITME, Warsaw	Poland
P.Pauli	Institute for Vacuum Physics Ljubljana	Yugoslvaia
I.Rechenberg	Central Institute for Optics and Spectroscopy	GDR
L.Ronchi	National Institute for Optics, Firenze	Italy

cont. TABLE 3.

K.Schmalz	Institute for Semiconductor Physics, Frankfurt/O	GDR
V.Smid	Institute of Physics, Prague	Czechoslovakia
B.N. Szverdlov	Lebedev Physical Institute, Moscow	Soviet Union

1987

J.Bekish	UNITRA-ITME, Warsaw	Poland
J.Betko	Institute of Electrical Engineering, Bratislava	Czechoslovakia
W.Buckel	University of Karlsruhe	FRG
E.Bugiel	Institute for Semiconductor Physics, Frankfurt/O	GDR
I.Cerveny	TESLA-VUST, Prague	Czechoslovakia
Ju.A.Gelman	Institute of Crystallography Moscow	Soviet Union
A.Gombia	CNR-MASPEC, Parma	Italy
B.S.V.Gopalam	Indian Institute of Technology, Madras	India
B.Gruza	Univ. Clermont Ferrand	France
Ju.P.Jakovlev	Ioffe Institute for Technical Physics, Leningrad	Soviet Union
W.Jantsch	University of Linz	Austria
J.Jarominski	UNITRA-ITE, Warsaw	Poland
V.I.Judaev	Institute for Semiconductor Physics, Novosibirsk	Soviet Union
H.Köster	Universität Rostock	GDR
P.Krispin	Zentralinstitut für Elektronenphysik, Berlin	GDR
C.A.Londos	University of Athen	Greece

cont. TABLE 3.

V. Malina	Institute of Radioelectronics Prague	Czechoslovakia
R. Messier	Pennsylvania State University	USA
M. J. Milnes	University of Leeds	England
I. Netkow	Institute of Electronics	Bulgaria
J. Nielsen	Aarhus University Institute of Physics	Denmark
E. Omeljanovszkij	Institute of Rare Metals, Moscow	Sovjet Union
L. Papadimitriou	University of Thessaloniki	Greece
Peng Rui Wu	Institute of Metallurgy, Shanghai	China
K. B. Povarova	Bajkov Institute, Moscow	Soviet Union
F. M. Reicha	Mansoura University	Egypt
A. A. Sulzsenko	Institute for Superhard Materials, Kiev	Soviet Union
Tran Quoc Tuy	University of Hanoi	Viet-Nam
K. Yada	Tohoku University, Tokyo	Japan

List of publications

List of publications

1986

ARATÓ,P., Sulzshenko, A.A.:
On the thermal stability of polycrystalline diamonds. Horizons of powder metallurgy.
Proc. Int.PM Conference, Düsseldorf (Eds. W.A.Kaysser, W.J.Huppmann) Verlag Schmid, Freiburg, 1986., pp.255-257

ARATÓ, P., Bochenchka, A.A., Kozéky, L., Venk, J., Varga, L.:
Damage and failure of polycrystalline diamonds
Proc. 9th Congress on Material Testing (Ed. Czoboly), GTE (Scientific Society of Mechanical Engineers), Budapest, 1986. pp.252-253

BARNA, A., Geszti, O., Gosztola, L., Seyfried, É.:
Cross-sectional TEM study of obliquely evaporated Si-O thin films in Materials Research Society Symposia Proceedings Vol. 61."Defect in Glasses" pp.367-374, eds. F.L.Galeener, D.L.Griscom, M.J.Weber, (1986)

Tracz, E., BARNA, A.:
Preparation of support grains for transmission electron microscopic studies
J.Chromatography 355, (1986) pp.421-426

Bangert, H., Kaminitschek, R., Wagendristel, R., BARNA, A., Barna,P.B., Radnóczi, G.:
Ultramicrohardness measurement on Al films evaporated under various conditions
Thin Solid Films 137, (1986) pp.193-198

BARNA,P.B., Barna, A., Radnóczi, G.:
Some aspects of tayloring thin films
10th Jugoslovenski Vakuumski Kongres, 1986, Proceedings pp.35-41

BARNA,P.B., Gosztola, L., Zalar, A.:
Direct TEM study of the roughening of SiO_2/Si interface induced during AES depth profiling
Proc.ECASIA 85 - Surface and Interface Anal., 9, (1986) p.328

BARNA,P.B., Bodó, Z., Gergely, G., Ádám, J.:
Spectral ellipsometric TEM and electron spectroscopic investigations on oxidized aluminium thin films
Vacuum 36, No.7-9, (1986) pp.465-469

Kótai, E., Pászti, F., Manuaba, R., Mezey, G., Gyulai, J., BARNA,Á., Barna, P.B., Radnóczi, G.:
Damage structure induced by high-dose helium implantation into single crystal silicon
5th Int.Conf.on Ion Beam Modification of Materials, Catania, Italy, 1986.

Csanády, A., Guenter, J.R., Marles, O., BARNA, P.B.:
Intermetallic phase formation by reaction of thin films of aluminium and iron.
9th Int.Congress on Electron Microscopy, 1986 Kyoto, Japan
Proceedings, Vol.2., p.1409

Kövér, L., B.Schág, J., Tóth, J., Borbély-Kiss, I., BARNA, B.P.,
Pozsgai, I., Medve, F.:
Examination of air-pollutant materials by micro- and surface analytical methods, gathered in Debrecen area.
Egészségtudomány, 30, (1986) pp.219-229. (in Hungarian)

BELEZNAY, F.:
Remarks on high field collision rates in polar semiconductors
J.Phys.C.: Solid State Phys. 19 (1986) p.L447

BELEZNAY, F.:
Estimations for asymptotic series using modified Romberg Algorithm. I.
J.Phys.A.: Math.Gen. 19 (1986) p.551

BELEZNAY, F.:
Metamorphosis of a routin semiconductor experiment: The quantum Hall-effect I-II.
Fizikai Szemle, (1986) p.94, 121 (in Hungarian)

CSÁNYI, F., Dobos, L., Jászberényi, I., Kazi, K., Mojzes, I., Oláh, A.,
Tichy-Rács, Á.:
Microwave tranceiver for X-band
Finommechanika-Mikrotechnika 25, (1986), pp.78-79 (in Hungarian)

DÓZSA, L.:
On the Reliability of Minority Carrier Injection Spectra
phys.stat.sol.(a) 94, (1986) p.735

DÓZSA,L.:
Selective detection of deep recombination centers
Solid State Electronics, 29 (1986) p.861

Sztaniszláv, A., Balla, M., Sári, K., FARKAS-JAHNKE, M.:
Garnet forming solid state reaction in Y_2O_3, Fe_2O_3, $CaCO_3$ and ZrO system
Proc. of 7th Conf. Soft Magnetic Materials, 1986, pp.276-278

Sztaniszláv, A., Balla, M., Sári, K., FARKAS-JAHNKE,M.:
Solid state reactions in the Fe_2O_3, $CaCO_3$ and Y_2O_3 system.
Proc. of 7th Conf.Soft Magnetic Materials, 1986, pp.279-281

FARKAS-JAHNKE, M.:
Relation between different types of stacking faults and the occurence of certain polytype stackings.
Bulletin Mineral. 109 (1986) pp.69-80.

FERENCZI, G., Boda, J., Pavelka, T.:
Isothermal frequency-scan DLTS
phys.stat.sol.(a) 94, (1986) p.K119

FERENCZI, G., Huber, D., Jantsch, W., Brunthaler, G.:
Characterization of deep levels by microwave absorption spectroscopy
Materials Science Forum 10-12, (1986) p.521

FERENCZI,G., Londos, C.A., Pavelka, T., Somogyi, M., Mertens, A.:
Identification of the carbon associated radiation damage levels in silicon
Materials Science Forum 10-12 (1986) p.947.

FERENCZI,G.:
Scientists view on innovation
Magyar Tudomány 10, (1986) p.162 (in Hungarian)

FERENCZI,G., Huber, D., Pavelka, T., Somogyi, M.:
Isothermal DLTS: Examples and application
15th School on Phys. of Semiconductor Compounds
Jaszowiecz-Ustron, Poland,
Acta Phys.Polonica, Vol.A-71, No.2. (1986) p.319

FOGT,Á., Kazi, K., Tóth, A., Mojzes, I., Szentpáli, B.:
Investigation of packages for microwave devices
Finommechanika-Mikrotechnika, 25, (1986) pp.59-63 (in Hungarian)

GAÁL, I., Makarov, P.V., Povarova, K.B., Ungar, T.:
Characterization of tungsten powders. Horizons of powder metallurgy.
Proc. PM Conference, Düsseldorf, (Eds. W.A.Kaysser, W.J. Huppmann)
Verlag Schmid, Freiburg, 1986, pp.151-154.

GAÁL,I., Makarov, P.V., Povarova, K.B.:
Some characteristics of technically pure tungsten powders
Proc. of the 11th Plansee Seminar, Vol.3. (Eds. H.Bildstein and H.M.
Ortner) Metallwerk Plansee, Reutte, 1986, pp.99-114

GEREY,G., Neugebauer, J., Gróh, R.:
Über Zwischen stufen in der Reduction von Ammoniummolybdaten zu MoO_2
Proc. of the 11th Plansee Seminar, (Eds: H.Bildstein, H.M.Ortner)
Metallwerk Plansee, Reutte, Vol.3., (1986) pp.37-41

GERGELY, G.:
Elastic peak electron spectroscopy
Scanning 8, (1986) p.203

GERGELY, G., Menyhárd, M., Sulyok, A.:
Some new possibilities in non-destructive depth profiling using secondary
emission spectroscopy: REELS and EPES
Vacuum 36, (1986) p.471

GERGELY,G., Jablonski, A., Menyhárd, M., Mrozek, P., and Sulyok,A.:
Angular effects of the differential elastic scattering in elastic peak electron
spectroscopy
Acta Univ. Wratislawiensis, No.937, Matematyka, Fizyka 48 (1986) p.41

GERGELY, G., Menyhárd, M., Sulyok, A., Jablonksi, A., and Mrozek,P.:
Determination of the mean free path of electrons in solids from the elastic
peak. III.
Acata Phys.Hung. 60 (1986) p.289

GESZTI, O., Gosztola, L., Seyfried, É.:
Cross-sectional TEM study of obliquely evaporated Si-O thin films
Thin Solid Films 136, (1986) pp.L35-38

GYURÓ, I., Somogyi, K., , Nemcsics, Á.:
Vapour phase epitaxial growth of GaAs and the factors influencing the layer inhomogeneity
Finommechanika-Mikrotechnika 25, (1986) pp.36-39 (in Hungarian)

GYURÓ, I., Somogyi, K., Nemcsics, Á., Mészáros, I.:
The present activity of the Institute for Technical Physics of HAS in the field of VPE growth of GaAs structures for microwave device purposes
Proc. 8th Coll. on Microwave Communication, August 25-29, 1986. Budapest, pp.159-160

GYURÓ, I., Mészáros, I., Somogyi, K.:
Growth of GaAs epitaxial layers at low temperatures
Proc. 2nd Conf. on Phys. and Technol. of GaAs and Other III-V Semiconductors, Sept. 8-11, 1986, Budapest
Cryst.Properties and Preparation, Vol.12, (1987) pp.23-27

HORACSEK, O.:
Creep fracture of dispersion strengthened tungsten
9th Congress on Material Testing (ed: E. Czoboly)
Scientific Society of Mechanical Engineers, Budapest, GTE (1986) pp.277-278

HORVÁTH, Zs., Stubnya, G., Németh, T., Tüttő, P., Ponomarenko, Ju.:
Breakdown investigations of dielectric films deposited at low temperatures
Hiradástechnika XXXVII, (1986) pp.371-374 (in Hungarian)

HORVÁTH, Zs.J., Gyuró, I., Németh-Sallay, M., Szentpáli, B., Kazi, K.:
GaAs Schottky varactors for linear frequency tuning in X-ban
phys.stat.sol.(a) (1986) pp.719-726

HORVÁTH, Zs., J., Gyuró, I., Németh-Sallay, M., Szentpáli,B., Kazi,K., Dobos, L., Fogt, Á., Kolumbán, T.:
GaAs Schottky varactors for microwave frequency tuning.
Proc. 8th Coll.on Microwave Communication, August 25-29, 1986, Budapest pp.379-380

HORVÁTH, Zs.J., Németh-Sallay, M., Gyuró, I., Kazi, K., Szentpáli,B., Fogt, Á., Dobos, L., Tüttő, P., Kolumbán, T.:
GaAs-CrAu Schottky tuning varactors
Proc. 5th Int.Scientific-Technical Conf. MICROELECTRONICS'86
Oct. 23-25, 1986, Plovdiv, Bulgaria, V3, pp.328-333

HORVÁTH, Zs., Németh-Sallay, M., Gyuró, I., Szentpáli, B., Kazi,K., Szép,I.:
Development of GaAs microwave tuning varactors
Finommechanika-Mikrotechnika 25, (1986) pp.52-55 (in Hungarian)

Berceli, T., Juhász, K., KAZI,K., Mojzes, I., Szendrényi, B.:
Application of Gunn diodes in J-Band
Finommechanika-Mikrotechnika 25 (1986) pp.44-46 (in Hungarian)

KERTÉSZ, J., Szép, J., Cserti, J.:
Dendritic Growth by Monte Carlo
in: "On Growth and Form: Fractal and Nonfractal Patterns in Physics"
ed: H.E.Stanley and N.Ostrowsky, (Martinus Nijjhoff, 1986), p.249

KERTÉSZ, J.:
Extrapolation of transfer matrix data for percolation and lattice animals by the Romberg-Beleznay algorithm
J.Phys. A19 (1986) p.599

Szabó, Gy., KERTÉSZ, J.:
Lattice gas model on tetrahedral sites of bcc lattice: anisotropic diffusion in the intermediate phase
J.Phys. C19 (1986) p.L273

KERTÉSZ, J., Vicsek, T.:
Diffusion-limited aggregation and regular patterns: fluctuations versus anisotropy.
J.Phys. A19 (1986) p.L257

KERTÉSZ, J., Vicsek, T., Meakin, P.:
Singularities and asymptotics in diffusion limited aggregation
Phys.Rev.Lett. 57, (1986) 3303

Buka, A., KERTÉSZ, J., Vicsek T.:
Transitions of viscous fingering patterns in nematic liquid crystals.
Nature 323 (1986) p.424

KOVÁCS, B., Mojzes, I.:
Influence of finite metal overlayer resistance on the evaluation of contact resistivity
IEEE Trans., ED-33 (1986) pp.1113-1114

Jároli, E., Khanh, N.Q., Mezey, G., Zsoldos, É., KOVÁCS, B., Mojzes,I., Lohner, T., Kotai, E., Manaube, A., Fried, M., Gyulai, J.:
Intermetallic compound formation of Ge-Ni and Ge-Al-Ni systems by furnace annealing and ion beam intermixing
Nuclear Instruments and Methods in Phys. Res. B15 (1986) pp.703-706

KOZMA, L., Henig, E-Th., Warren, R.:
Is the grain boundary phase the key to activated processes: Horizons of powder metallurgy.
Int.Conference on PM Düsseldorf, 1986. pp. 11 1181 1184

KOZMA, L., Warren, R., Henig E-Th.:
Diffusion Aspects of Activated Recrystallization- Recovery, Recrystallization and Grain Growth Proc. VII. Int.RisØ Symp. on Metallurgy and Materials Sciences (Eds. N.Haansen et al)
Roshilde, 1986. pp.397 397-402

LÁBÁR, J.L.:
Comparison of backscatter loss calculations in electron probe microanalysis
Scanning Vol.8 (1986) pp.188-191

Beregi, E., Hartmann, E., LÁBÁR, J.L.:
Dissolution forms of rare-earth gallium-iron garnets
J.of Crystal Growth 79 (1986) pp.825-828

LENDVAY, E., Görög, T.:
A novel DH structure: the GaAs/GaPAsSb system
J.Cryst.Growth 79 (1986) p.928

LENDVAY, E.:
New semiconductors: pseudo-ternary III-V antimonides
Chemtronic 1 (1986) p.112

LENDVAY, E., Görög, T., Petrás, L.:
LPE growth of lattice matched GaPAsSb/GaAs heterojunction
Fourth Hungarian Conference on Crystal Growth, Budapest, 1986.
Collected Abstracts. p.1

LENDVAY, E., Görög, T., Andor, L., Petrás, L., Tóth, A.:
A novel double heterostructure: the GaAs/GaPAsSb system
Journal of Crystal Growth 79 (1986) pp.928-934

LENDVAY, E.,
Semiconductor lasers
"Lasers" CRIP publications, 1986. (in Hungarian)

Fürderer, K., Döring, K-P., Gladisch, M., Hass, N., Herlach, D.,
MAJOR, J., Mundinger, H-J., Rosenkranz, J., Schafer, W., Schimmele, L.,
Schmolz, M., Schwarz, W., Seeger, A.:
u^+ SR study of vacancies in thermal equilibrium in ferromagnets.
Hyperfine Interact. 31 (1986) pp.81-86

MAJOR, J., Mundy, J., Schmolz, M., Seeger, A., Döring, K-P., Fürderer,
K., Gladisch, M., Herlach, D., Majer, G.:
Zero-field muon spin rotation in monocrystalline chromium
Hyperfine Interact. 31 (1986) pp.259-264

Abela, R., Arnold, K-P., Fürderer, K., Gladisch, M., Herlach, D.,
Krenke, M., MAJOR, J., Mundinger, H-J., Mundy, J., Rosenkranz, R.,
Schafer, W., Schimmele, L., Schwolz, M., Schwarz, W., Seeger, A.:
Positive muons in antiferromagnetic chromium crystal: diffusion and inter-
action with spin density waves
SIN Newsletter 19 (1986) 85-89

MOJZES, I.:
Development and pilot line production of microwave devices in 1980-1984
Finommechanika-Mikrotechnika 25 (1986) pp.33-35 (in Hungarian)

MOJZES, I., Kazi, K., Oláh, A., Reisinger, G., Körmendi, J.,
Gyuraszevics, J.:
Microwave remote sensing and identifying of vehicles in mines (in Hungarian)
Proc. XXIII. Ipari Elektronikus Mérés és Szabályozás Szimp.,
1986. szept. 4-6, Balatonszéplak, pp.223-234

MOJZES, I., Kazi, K.,Szen pál.,B., Tichy-Rács,Á.,Reisinger,G., Oláh,A.,
Jászberényi,I.:
Microwave techniques for measuring and control
Finommechanika-Mikrotechnika 25 (1986) pp.85-87 (in Hungarian)

MOJZES, I., Szentpáli, B., Kovács, B., Gottwald, P., Biró, S., Elschner, H., Stenzel, R., Passlach, M., Lalinsky, T., Kordos, P.:
Measuring and modeling of DC characteristics of ionimplanted MESFET's.
Proc. 8th Coll. on Microwave Communication, August 25-29, 1986, Budapest, pp.163-164

MOJZES, I., Veresegyházy, R., Malina, V.:
Thermal dissociation of InP covered with metallic contact layers
Thin Solid Films, 144 (1986) pp.29-40

Kafediiska, E.I., MOJZES, I., Veresegyházy, R., Pécz, B.:
Mass-spectrometric study of the dissociation of GaSb covered with contact layers
phys.stat.sol.(a) 93 (1986) pp.K125-K128

PÁL,E., Tóth, K., Pungor, E., Farkas-Jahnke, M., Ebel, H., Ebel,M.F.:
Crystallographic study on metal sulphide - active material for cadmium ion-selective electrodes
Analytica Chimica Acta, 180 (1986) pp.313-321

PETRÁS, L., Pécz, B., Farkas-Jahnke, M., Zsoldos, E., Jároli, E., Mojzes, I.:
Investigation of reaction between gold and $A^{III}B^{V}$ semiconductors by X-ray diffraction.
Proc. XIIth Conf. on Appl. Crystallography, Aug. 10-14, 1986, Cieszyn, Poland, ed. Z.Bojarski, T.Bold, V2, pp.295-299

PÉCZ, B., Jároli E., Radnóczi, G., Veresegyházi, R., Mojzes I.:
Pyramidal pit formation at the Au/GaAs interface during heat treatments
15th School on the Physics of Semiconducting Compounds
Jaszowiec-Ustrom, Poland
phys.stat.sol. (a) 94 (1986) p.507

PÉCZ, B., Jároli, E., Veresegyházy, R., Mojzes, I., Petrás, L.:
On the reaction of Au with GaP
Second Conf. on Physics and Technology of GaAs and other III-V Semiconductors, Budapest, 1986, Collected Abstracts

Jároli, E., PÉCZ, B., Gyulai, J., Fried, M., Petrás, L., Zsoldos, É., Lohner, T., Mojzes, I.:
Effect of ion beam treatment on thermal annealing of GaAs-Au layer sturctures
Nuclear Instruments and Methods in Phys.Res., B15 (1986) pp.767-772

Biró, K.T., POZSGAI, I., Vladár, A.:
Electron beam microanalysis of Obsidian samples from geological and archeological sites
Acta Archeologia Academiae Scientarium Hungaricae, 38 (1986) pp.257-278

POZSGAI, I., Vladár, A., Tóth, A.:
Trace element analysis of bauxite in the scanning electron microscope.
Proc. XI. Int.Congr. on Electron Microscopy, Kyotó, Japan, 1986.
pp.547-548

PŐDÖR, B.:
Transport coefficients for neutral impurity scattering
phys.stat.sol.(b) 134 (1986) pp.K145-K148

PŐDÖR, B.:
On three-phonon processes in gallium phosphide
phys.stat.sol.(b) 136, (1986) pp.K9-K12

PŐDÖR, B.:
On the temperature dependence of the 1/f noise Hooge parameter α_H in n-channel silicon JFET's.
IEEE Electron Dev.Lett., EDL-7 (1986) pp.610-611

Ajayi, O.B., Akanni, M.S., Lambi, J.N., Burrows, H.D., Osasona, O., PŐDÖR,B.:
Preparation and optical characterization of pyrolytically deposited thin films of some metal oxides
Thin Solid Films, 138 (1986) pp.91-95

RADNÓCZI, G., Barna, P.B.:
Grain boundaries in thin metallic films
Acta Universitatis Wratislawienesis NZ.937, p.106-112 (1986)
Proc. 9th Seminar on Surface Physics

RADNÓCZI, G., Skakov, Yu.A.:
The structure of grain boundaries in tungsten wires annealed at temperatures above 1800 K
Poverkhnost Fizika, Chemia, Mechanika, 1 (1985) p.120-122 (in Russian)

Makarov, P., Povarova, K., Zawarzina, E., RADNÓCZI, G., Gaál, I., Uray, L., Nagy, A.:
Fine structure and properties of carbide strengthened drawn tungsten wires
Fizika i himija obrabotki Materialov N6 (1986) pp.119-124 (in Russian)

RAKOVICS, V., Görög, T., Lendvay, E.:
Semitransparent LPE reactor and its application for InP/GaInAsP DH junction growth
phys.stat.sol. 94 (1986) p.658

SCHANDA, J.:
The influence of changes in the reflectance spectra of the test samples on the colour rendering index
Mérés az Automatika 34/5 (1986) pp.167-75 (in Hungarian)

SCHANDA, J.:
Proposal for a new formulation of the colour rendering index
Kolorisztikai Értesitő, 5-6, (1986) pp.185-202 (in Hungarian)

SOMOGYI, K.:
On the qualification of the n-GaAs epitaxial structures
Finommechanika-Mikrotechnika 25 (1986) pp.41-43 (in Hungarian)

SOMOGYI, K., Gyuró, I.:
A method for studying parameter variations in VPE technology
phys.stat.sol.(a) 98 (1986) pp.K1-K4

SOMOGYI, M.:
Dopant concentration determination at frequencies above 10 kHz on GaP-electrolyte system
phys.stat.sol.(a) 94, (1986) p.731

SULYOK, A., Sáfrán, G.:
Improvement of depth resolution in Auger electron spectroscopy depth profiling by presputtering
4th Internat.Conf. Quantitative Surface Analysis, Teddington, Nov. 1986. Abstracts P3.

SZABÓ, J.:
Technological tendencies in the preparation of GaAs submicron structures by photolitography
Finommechanika-Mikrotechnika 25 (1986) pp.65-77 (in Hungarian)

Kuhn, T., SZENTPÁLI, B.:
Noise figure measuring instrument for qualifying receiver diodes
Proc. 8th Coll. on Microwave Communication, August 25-29, 1986. Budapest, pp.161-162

SZENTPÁLI, B., Kuhn, T.:
Monolithic microwave integrated circuit investigations
Proc. 8th Coll. on Microwave Communication, August 25-29, 1986. Budapest, p.435

SZENTPÁLI, B., Mojzes, I., Reisinger, G., Kazi, K., Tichy-Rács, A., Ivanics, L., Bodolai, P., Szücs, B.:
Development of microwave transmitter and receiver modules
Finommechanika-Mikrotechnika 25 (1986) pp.83-84 (in Hungarian)

SZENTPÁLI, B., Németh-Sallay, M., Tichy-Rács, Á.:
Development and small series production of Schottky diodes
Finommechanika-Mikrotechnika 25 (1986) pp.47-51 (in Hungarian)

TÓTH, L., Barna, A., Sáfrán, G.:
In-situ TEM annealing of NiCr thin films with simultaneous Hall-voltage measurements
10th Int.Vacuum Congr., Baltimore, USA 1986.

URAY, L., Tekula-Buxbaum, P.:
Resistivity contribution of solutes in tungsten
J.Less-Common Metals, 123 (1986) pp.95-100

VARGA, L., Wéber, F.:
Metallurgical processes leading to arcing on incandescent lamp filaments
9th Congress on Material Testing (ed: E.Czoboly)
Scientific Society of Mechanical Engineers, Budapest, GTE 1986, pp.150-154

VERESEGYHÁZY, R., Kazi, K., Mojzes, I., Biró, S., Harmat, P., Füle,G.:
Intelligent measuring system for the characterisation of varactor tuned microwave oscillators
Finommechanika-Mikrotechnika 25 (1986) pp.80-82 (in Hungarian)

VERESEGYHÁZY, R., Kovács, B., Mojzes,I.:
Au-Ge-Ni ohmic contacts on $A^{III}B^{V}$ compounds
Finommechanika-Mikrotechnika 25, (1986) pp.56-58 (in Hungarian)

VERESEGYHÁZY, R., Mojzes, I., Lendvay, E.:
Mass-spectrometric study of contact sintering in the GaSb/Au system
Thin Solid Films 138 (1986) pp.L55-L57

VERESEGYHÁZY, R., Mojzes, I., Pécz, B.:
Comparative mass spectrometric study of $A^{III}B^{V}$ compounds covered with gold layer.
Vacuum TAIP 36 (1986) pp.547-549

VERESEGYHÁZY, R., Pécz, B., Mojzes, I.:
The influence of gold layer on the thermal decomposition of InAs
phys.stat.sol. (a) 93, (1986) pp.K11-K12

VICSEK, T., Family, F., Kertész, J., Platt, D.:
Distribution and entropy of clusters in growth models
Europhys.Lett. 2, (1986) p.823

Family, F., VICSEK, T., Taggett, B.:
Lattice-induced anisotropy in a diffusion limited growth model
J.Phys. A19 (1986) p.L727

Family, F., Zhang, Y.C., VICSEK, T.:
Invasion percolation in an external field: Dielectric breakdown in random medea
J.Phys. A19 (1986) p.L733

VICSEK, T.:
Formation of solidification patterns in aggregation models
in: Fractals in Physics, edited by L. Pietronero and E.Tosatti
(North Holland, Amsterdam, 1986) p.247

Meakin, P., VICSEK, T.:
Internal anisotropy of diffusion-limited aggregates
in: Fractals in Physics, edited by L.Pietronero and E.Tosatti:
(North Holland, Amsterdam, 1986) p.213

VICSEK, T.:
Pattern formations in aggregation processes
Magyar Tudomány, 5 (1986) p.356 (in Hungarian)

1987

ÁDÁMNÉ-FARKAS, Zs., Németh, T.(Mrs):
Etching profiles of silicon-dioxid layers
Finommechanika-Mikrotechnika, 26 (1987) pp.173-179 (in Hungarian)

BALÁZS, J., Makai, J.J., Makai, J.P.:
Instruments for measurement of optical fibers
Mérés- és Automatika 35 (1987) p.44 (in Hungarian)

BALÁZS, J.:
Detectors for the time domain techniques of multimode fibers at the first window
13th International Symposium of the IMEKO Technical Committee TC2, Photonic Measurements, Braunschweig, 1987.

BALÁZS, J., Makai, J.J., Makai, J.P.:
Measuring instruments of fibers
Mérés és Automatika 2 (1987) pp.44-49 (in Hungarian)

BARNA, A., Sáfrán, G., Tóth, L.:
Structural and electrical studies of the effect of preparation conditions of NiCr thin films
Proceedings of the Symposium on Electronics Technology, 1987, pp.13-18

BARNA,P.B., Radnóczi, G., Csanády, A., Urban, K.:
Nucleation and growth of oriented quasicrystals with icosahedral phase on (111) and (001) faces of Al crystals at high temperature vapour deposition of thin films
(to be published in Script Met.)

Csanády, A., BARNA, P.B., Mayer, J., Urban, K.:
Icosahedral phase formation in vacuum deposited thin films of Al
2.International workshop on quasicrystals, held in Beijing (China) 30, 8-5, 9.1987.

Csanády, A., BARNA, P.B., Mayer, J., Urban, K.:
Preparation of aluminium based icosahedral thin films by high-temperature vapour deposition
(in print: Script.Met.)

Kövér, L., Tóth, J., Schág, J.B., Borbély-Kiss, J., BARNA, P.B., Pozsgai, I., Medve, F.:
Surface analysis of air pollutants collected in populated areas
Vacuum TAIP 37, 1-2, (1987) pp.175-177

Hiti, M.L., BARNA, P.B., Reicha, F.M.:
Structure and growth morphology of SiO_x films deposited on NaCl (001) faces
Vacuum TAIP 37 1-2, (1987) pp.97-99

Reicha, F.M., Hiti, M.L., BARNA, P.B.:
The effect of oxigen on the structure and growth morphology
Vacuum TAIP 37 1-2 (1987) pp.93-96

Csanády, A., Guenter, J.R., Marks, O., BARNA, P.B.:
Intermetallic phase formation by reaction of thin films of aluminium and iron.
Proc. 11th Internat. Congr. Electron Microscopy, Kyoto (Japan), 1987, p.1409.

Manaila, R., Dévényi, A., BARNA, P.B., Randóczi, G., Grigorovichi, R.:
Growth mechanism in amorphous films: A computer simulation
J.Non Crystalline Solids 90, (1987) pp.307-313

Csanády, A., Urban, K., Mayer, J., BARNA, P.B.:
Crystalline and quasicrystalline phases formed by interdiffusion in evaporated Al-Mn thin films
10th Int. Vacuum Congr., Baltimore, USA, 1986.
Vacuum Science and Technology, 5, 4 (1987) p.1733

BODÓ, Z., Gergely, G.:
Intrinsic optical constants of aluminium
Appl. Opt. 26 (1987) p.2065

CSONTOS, L. (Mrs), Hoffmann, G.:
Contact resistance profiling - An effective tool for failure analysis of GaAs/GaAlAs layer structures
2nd Conf. on Physics and Technology of GaAs and Ohter III-V Semiconductors, Budapest, 1986.
Proceedings, (Trans-Tech Publications, Switzerland), 1987.

DÓZSA, L.,
Investigation of deep levels in semiconductors by measurement of tranzients in space charge layer
Ph.D. Thesis, Budapest, 1987. (in Hungarian)

DÓZSA, L., Tóth, A.L.:
Determination of the lateral defect distribution by SDLTS
Poster, New Developments in Semiconductor Physics, Szeged, (Hungary) 31.Aug. - 4.Sept. 1987., Abstracts, p.43

DÓZSA, L., Smid, V., Mares, J., Hubik, P., Kristofik, J.:
Effect of N substrate on epitaxy interface on junction capacitance spectroscopy
(to be published in phys.stat.sol., 1987)

Serfőző, G., Naujokaitisz, R., Krafcsik, I., DÓZSA, L., Battistig, G., Riedl, P., Klopfer, E., Gerasimenko, N.N., Gyulai, J.:
Pulsed ion implantation of silicon with Se
Paper given Int.Conf.on Energy Pulse and Particle Beam Modification of Materials, Drezden, GDR, 1987. (to be published in the Proceedings)

Serfőző, B.G., Naujokaitisz, R., Krafcsik, I., Horváth, P., DÓZSA, L., Gyulai, J.:
Radiation damage due to pulsed Se implantation into silicon studied by DLTS
Paper given GADEST 1987, Garzau, GDR
(to be published in the Proceedings)

ERDÉLYI, K., Knapp, G.
A new SCR parameter extraction method to help design for reliability in CMOS circuits
ESSDERC'87, Bologna, 1987, pp.787-790

ERDÉLYI, K., Ferenczi, G., Somogyi, M.:
Layer thickness determination in multilayer structures by impedance analysis of the semiconductor/electrolyte interface
NDSP-2, Szeged, 1987, pp.45-46

FARKAS-JAHNKE, M., Petrás, L., Somogyi, M.:
Pre-transformation lattice processes
Phase Transition A, 8 (1987) pp. 324-325

FERENCZI, G.:
The application of deep level spectroscopy for studying defects in semiconductors
Thesis for the degree of Doctor of Sciences, Budapest, 1987.
(in Hungarian)

FERENCZI, G., Jantsch, W., Brunthaler, G., Huber, D.:
Characterization of deep levels by microwave absorption spectroscopy
2nd Conf. on Physics and Technology of GaAs and Other III-V Semiconductors, Budapest, 1986.
Proceedings (Trans-Tech Publications, Switzerland) 1987, p.159

FERENCZI, G.:
The application of a modern deep level spectrometer in the characterisation of semiconductor materials and structures
Mérés és Automatika 35 (1987) p.56, (in Hungarian)

FERENCZI, G.:
The application of deep level spectroscopy in the semiconductor technology
Fizikai Szemle XXXVII, (1987) p.172 (in Hungarian)

FERENCZI, G., Huber, D., Jantsch, W.:
Microwave absorption spectroscopy - a new space charge spectroscopic technique.
Int. Symposium on Defect Recognition and Image Processing in III-V Compounds (DRIP-II) April, 27-29, 1987, Monterey, CA, USA
(to be published by Elsevier)

FERENCZI, G., Londos, C.A., Pavelka, T., Somogyi, M., Mertens, A.:
Correlation of the concentration of the carbon associated radiation damage levels with the total carbon concentration in silicon
(to be published in J.Appl. Phys., 1987)

Jantsch, W., FERENCZI, G., Brunthaler, G., Huber, D.:
Microwave absorption spectroscopy - a novel method for deep level characterization
18.th Int.Conf. on Physics of Semiconductors,
Proceedings, 2 (1987) p.1015

FERENCZI, S.:
Actinic effects of optical radiation
Mérés- és Automatika 35 2 (1987) pp.39-43 (in Hungarian)

GAÁL, I.:
Relations between interfaces and mechanical properties
in: Szilárdtestek felületfizikája (ed. J.Giber)
Müszaki Kiadó, Budapest, 1987, pp.247-196 (in Hungarian)

GAÁL, I., Makarov, P.V., Povarova, K.B.:
Morphological characterization of technically pure tungsten powders
Poroskovaja Metallurgija 6, (1987) pp.4-11 (in Russian)

GAÁL, I., Horacsek, O.:
Chemically driven pore growth,
in: Sintering'85 (Eds.: C.G.Kuczynski, D.P. Uskokovic, H.Palmour, M.M. Ristic)
Plenum Press London, New York, 1987. pp.325-336

GAÁL, I., Horacsek, O.:
Microstructural evolution in molybdenum during the final stage of sintering
Proc. of the VII. Int.Conf. on PM Pardubice (Ed.: M.Slezár)
1987, Vol.3. pp.29-36

Ungar, T.,Stanzl, S., GAÁL, I., Broma, I., Kovács, I.:
The correlation between the cyclic saturation stress and the dislocation structure in single slip oriented Cu crystals at low fatigue amplitudes.
in: Constitutive Relations and their Physical Basis
(Proc. of the VIII.Int. RisØ Symp. on Metallurgy and Materials Sciences
(Eds.: S.I. Andersen et al) 1987, pp.523-528

GERGELY, G., Bodó, Z., Croce, P.:
Determination of the optical constants of metals and semiconductors by combining ellipsometry with electron spectroscopy, microscopy and x-ray specular reflection analysis.
11th Internat. Seminar on Surface Physics, Piechowice May 1987.
Seminar Proc. Ed.: Surface Sci. (in preparation)

GERGELY, G.:
Angular corrections for determining the electron inelastic mean free path (IMFP) by elastic peak electron spectroscopy
Vacuum 37 (1987) p.149

Jablonski, A., GERGELY, G.:
On the standardization of the procedure determining the inelastic mean free path of electrons
Poverhnosztyi, No.10, (1987) p.74 (in Russian)

Seyfried, É., GESZTI, O., Gosztola, L.:
Columnar structure and liquid crystal orientation properties of obliquely evaporated SiO_x thin films
Proc. Symp. Electronics Technology, 1987, pp.324-329

GESZTI, O., Gosztola, L., Seyfried, É.:
Dependence of the columnar structure of obliquely evaporated SiO_x thin films on the angle of deposition and the rate of condensation
J.Non Crystalline Solids 90, (1987) pp.315-318

GOMBOS, G., Mostafa, M.M., Al-Sharaby, H.:
Resistivity measurements in silicon inversion layers
Acta Phys. Hung. 62 1 (1987) p.15.

Zsolt, G., Kovács, G., Porjesz, T., Kármán, T., GOMBOS, G.:
Avalanche current relaxation in p-Si MOSFETs
Acta Phys. Hung. 62 1 (1987) p.19

GÖRÖG, T., Lendvay, E., Rakovics, V.:
GaAs/GaAlAs multilayer structures grown by LPE methods
4th Hung. Conf. on Crystal Growth
Acta Phys. Hungariae 61, (1987) p.149

GYURÓ, I., Dobos, L., Horváth, Zs.J., Pál,E.K., Fineberg, V.I., Kanakova, R.V., Tkhorik, Yu.A.:
SEM investigations of macroscopic crystal defects in GaAs VPE layers
Acta Physica Hungariae 61 2 (1987) pp.263-266

GYURÓ, I., Somogyi, K., Mészáros, I.:
Technological possibilities of the growth of GaAs layer structures from the vapour phase
Finommechanika-Mikrotechnika, 26 6-7, (1987) pp.169-173 (in Hungarian)

GYURÓ, I., Mészáros, I., Somogyi, K.:
The growth of GaAs VPE layers in the kinetically controlled region
Proc. of Symposium on Electronics Technology, 15-18 September 1987, Budapest, pp.110-115

GYURÓ I., Horváth, Zs.J.:
GaAs VPE layers for microwave Schottky tuning varactors
Acta Phys. Hung. 61 (1987) pp.165-168

Mészáros, I., GYURÓ, I., Somogyi, K.:
Computer aided modelling of VPE growth process of GaAs
4th Hung. Conf. on Crystal Growth, July 22-25, 1986., Budapest
Acta Phys. Hungariae, 61 (1987) pp.161-164

HABERMAYER, I.:
An analysis of nonlinear light-current characteristics and anomalous pulse responses of semiconductor layers
2nd Conf. on Physics and Technology of GaAs and other III-V Semiconductors, Budapest, 1986.
Proceedings (Trans-Tech Publications, Switzerland) 1987.

HORVÁTH, Zs.J., Tüttő, P., Németh-Sallay, M., Stubnya, G., Németh, T., Gyuró, I., Fineberg, V.I.:
Breakdown investigations in MIS and MS structures
Acta Phys. Polonica A71 (1987) pp.485-489

HORVÁTH, Zs.J., Pécz, B., Tüttő, P., Jároli, E., Németh-Sallay, M., Gyuró, I.:
I-V pecularities in GaAs-CrAu Schottky and GaAs-Au ion mixed contacts
Cryst. Properties and Preparation 12 (1987) pp.273-276

HUBER, D., Ferenczi, G., Jantsch, W., Mirk, Z., Tichy-Rács, A.:
Application of microwave absorption spectroscopy to the Au center in N-type silicon.
Int. Summer Institute on New Developments in Semiconductor Physics (NDSP-2) 1987, Szeged, Hungary, Abstracts, p.53

IVANOV, P., Tóbiás, F., Borody, H.:
Crack testing of bars and tubes
Mérés és Automatika, 35 2 (1987) pp.60-67 (in Hungarian)

KAZI, K., Tichy-Rács, Á., Mirk, Z., Tajti, L., Mojzes, I., Jászberényi, I., Oláh, A.:
Data transmission in microwave links having fast changing transmission characteristics
Finommechanika-Mikrotechnika 26 6-7, (1987) pp.192-194

KAZI, K., Pődör, B., Horváth, Zs., Tajti, L.:
Varactor tuned voltage controlled microwave oscillator for the X-ban
Proceedings of the Symposium on Electronics Technology, Budapest, 1987, Vol. 1. p.163

Horváth, V., KERTÉSZ, J., Vicsek, T.:
Viscous fingering in a smectic liquied crystal
Europhys.Lett. 4 XX (1987)

Wolf, E.D., KERTÉSZ, J.:
Noise reduction in Eden models I.
J.Physics A-20 (1987) p.L257

KERTÉSZ, J.:
Fluctuations, anisotropy and scaling in growth processes
Phil.Mag. B55 xxx (1987)

Cserti, J., KERTÉSZ, J.:
Asymptotic number of needles in Laplacian growth
J.Phys. A-20 (1987) p.4561

Wolf, E.D., KERTÉSZ, J.:
Surface width exponents for three- and four-dimensional Eden growth
Europhys.Lett. 4, (1987) p.651

KERTÉSZ, J., Wolf, D.E.:
Noise reduction in Eden models II: Surface structure and intrinsic width
J.Phys. A-20 xxx (1987)

Amitrano, C., dr Arcangelis, L., Coniglio, A., KERTÉSZ, J.:
Regular versus irregular Laplacian growth: Multifractal spectroscopy
J.Phys. A-20 xxx (1987)

KERTÉSZ, J.:
Cellular automata: Computer games, teaching tools and research topics
in Proceedings of the IUPAP Conference on Teaching of Nonlinear
Phenomena, ed. G. Marx (in press)

Meakin, P., KERTÉSZ, J., Vicsek, T.:
Noise-reduced diffusion-limited deposition .
Preprint (1987)

Stanley, H.E., Stauffer, D., KERTÉSZ, J., Herrmann, H.J.:
Dynamics of spreading phenomena in two-dimensional Ising system
Preprint (1987)

KERTÉSZ, J., Vicsek, T.:
Pattern formation and effective anizotropy
Fizikai szemle, 2, 49 (1987) 5. T. (in Hungarian)

KOVÁCS, B., Biró, S., Mojzes, I., Szentpáli, B., Németh-Sallay, M.,
Gottwald, P.:
Test patterns for optimization and process control of GaAs MESFET
technology
Proc. Symp. on Electronics Technology, 1987., Budapest, Hungary
Vol.1. pp.190-195

KOVÁCS, B., Biró, S., Mojzes, I., Németh-Sallay, M., Szentpáli, B.:
The influence of ohmic metal composition on the device parameters
Poster in ISDPME, May, 1987. Varna, Bulgaria

KOZMA, L., Henig, E-Th., Warren, R.:
Metal activated recrystallization and creep of tungsten fibres
in: Sintering'85 (Eds.: G.C. Koczynski, D.P.Uskokovic, H.Parlmour,
M.M. Ristic) Plenum Press New York, London, 1987, pp.155-163

LÁBÁR, J.L.:
Effect of relative L-line intensity ratios on the accuracy of standardless
X-ray microanalysis
X-ray Spectrometry, Vol.16 (1987) pp.33-36

LENDVAY, E.:
Galliumantimonide and related semiconductor compounds
Thesis for Doctor of Sciences, Budapest, 1987 (in Hungarian)

LENDVAY, E.:
Review of the search for new semiconducting materials
Fizikai Szemle, XXXVII, (1987) p.161 (in Hungarian)

LENDVAY, E.:
New semiconductors: GaAs and related materials
Akadémiai Kiadó, Budapest, 1987. (in Hungarian)

Fürderer, K., Döring, K-P., Gladisch, M., Haas, N., Herlach, D., MAJOR, J., Mundinger, H-J., Rosenkranz, J., Schafer, W., Schimmele, L., Schmolz, M., Schwarz, W., Seeger, A.:
Vacancy formation in thermal equilibrium in ferromagnetic iron and cobalt studied by the spin rotation of positive muons
Mat.Sci. Forum 15-18 (1987) pp.125-130

Maier, K., Bauer, W., Briggmann, J., Carstanjen, H-D., Decker, W., Diehl, J., Heinemann, V.,MAJOR,J., Schaefer, H.E., Seeger, A., Stoll, H., Wesolowski, P., Widmann, E., Bosch, F., Koenig, W.:
Experimental limits for narrow lines in the excitation function of positron--electron scattering around E^x = 620 keV and E^x = 810 keV
Z.Physik A, 326 (1987) pp.527-529

Arnold, K-P., Baines, C., Döring, K-P., Fürderer, K., Gladisch, M., Herlach, D., Krenke, M., Majer, G., MAJOR, J. , Mundinger, H-J., Rosenkranz , J., Schafer, W., Schimmele, L., Schmolz, M., Seeger, A.:
4T tunneling state and coherent hopping of positive muons in iron at very low temperatures
SIN Newsletter 19 (1987) pp.91-94

MOJZES, I., Kazi, K., Tichy-Rács, Á., Gyuró, I., Horváth, Zs.J.:
Development of a microwave transmitter-receiver unit for microwave distance meter - an example of the application of microwave techniques.
Finommechanika-Mikrotechnika 26 6-7 (1987) pp.161-168 (in Hungarian)

MOJZES, I., Kovács, B.:
GaAs Device Technology - A challange in late 80's
Proc. of 5th International School on Microwave Physics and Engineering 28, Sept. - 3. Oct. 1987., Varna, Bulgaria
Published by World Scientific Inc., 1987.

MOJZES, I., Csányi, F.:
Vacuum termostat for the measurement of Gunn diodes in a coaxial cavity
Finommechanika-Mikrotechnika 26 6-7 (1987) pp.195-197

Malina, V., Sroubek, Z., MOJZES, I., Veresegyházy, R., Pécz, B.:
Interaction of thin gold films with GaP during heat treatment in vacuum
Semicond. Sci.Technol., 2 (1987) pp.428-436

Betko, J., Mersinksky, K., NEMCSICS, Á., Sviszt, P.:
On the electrical properties of semi-insulating GaAs
(Proc. of the 2nd. Conf on Phys. and Technology of GaAs, Budapest,1986)
Crystal Properties and Preparation, Vol.12 (1987) pp.143-146

PAVELKA, T., Ferenczi, G.:
Interpretation of the electric field dependent thermal emission data of deep traps
International Summer Institute on New Developments in Semiconductor Physics (NDSP-2) Szeged, Hungary, 1987. Abstracts p.69

PETRÁS, L., Gyuró, I., Lendvay, E.:
The effect of microgravity on the growth of GaSb
Acta Cryst. A 43 Suppl. (1987) p.C116

PÉCZ, B., Jároli, E., Veresegyházy, R., Mojzes, I., Petrás, L.:
On the interaction of Au with GaP
Proc. of the 2nd Conf. on Phys. and Technol. of GaAS and other Semiconductors, Sept. 8-11 (1986) Budapest
Crystal Properties and Preparation 12 (1987)

Jároli, E., PÉCZ, B., Gyulai, J., Fried, M., Petrás, L., Zsoldos, E., Lohner, T., Mojzes, I.:
Effect of ion beam treatment on thermal annealing of GaAs-Au layer structures
Nuclear Instruments and Methods in Physics Research B19/20 (1987) pp.767-772

Jároli, E., PÉCZ, B., Veresegyházy, R., Pászti, F., Lohner, T., Fried, M., Mojzes, I., Gyulai, J.:
Effect of ion beam mixing on evolution of arsenic from Au-GaAs system
2nd Conf. on Energy Pulse and Particle Beam Modification of Materials, 7-11 Sept., 1987, Dreseden, GDR

PFEIFER, J., Koltai, F.:
Enhanced diffusion of Zn along the SiO_2 Mask/GaAs interface
2nd Conf. on Physics and Technology of GaAs and other III-V Semiconductors, 1986, Budapest,
Proceedings (Trans-Tech Publications, Switzerland) 1987, p.331

POZSGAI, I.:
High lateral resolution X-ray fluorescence analysis in the scanning electron microscopy
Scanning 9 (1987) pp.36-40

POZSGAI, I., Orcsik, É.:
On the study of cleaning and protecting the limestone facing of the Hungarian Parliament Building
Optik, Supplement 2 Vol.76, (1987) p.26.

PŐDÖR, B.:
On the concentration dependence of the thermal ionization energies of impurities in InP
Semiconductor Science and Technology 2 (1987) p.177

PŐDÖR, B., Horváth, Zs., Tajti, L.:
Analysis of varactor tuned Gunn oscillators
Finommechanika-Mikrotechnika 26 (1987) p.186 (in Hungarian)

PŐDÖR, B.:
On the temperature dependence of the 1/f noise in semiconductor devices
Finommechanika-Mikrotechnika 26 (1987) p.216 (in Hungarian)

PŐDÖR, B., Gyuró, I.:
Photoluminescence characterization of residual acceptors in vapour phase GaAs
Proceedings of the Symposium on Electronics Technology, Budapest, 1987. Vol.1., p.267

PŐDÖR, B.:
On electromagnetic wave propagation in general anisotropic media
Proceedings of the 32. Internationales Wissenschaftliches
Kolloquium, TH Ilmenau, GDR, Oct. 26-30, 1987, Vol.2. p.193

PŐDÖR, B.:
Low temperature photoluminescence of vapour phase epitaxial GaAs
Digest of the International Conference on Low Temperature Physics,
Budapest, Nov.17-20, 1987, p.63

RADNÓCZI, G., Vicsek, T., Sander, L.M., Grier, D.:
Growth of fractal crystals in amorphous GeSe films
Physical Review A, Vol.35 9, (1987) p.4012

RÁCZ, M., - Schanda, J.:
Luminance measurement hardware considerations
"Oszvetlenie'87" Conference, Várna, Bulgaria, 1987.
(poster)

RÁCZ, M., Dobovics, M.:
Determination of the modulation transfer function of CCD linear arrays
with slit translation method
Mérés és Automatika, 35 (1987) pp.50-55

RAKOVICS, V., Fornari, R., Paorici, C., Zanotti, L., Mucchino, C.:
Indium-silicon CO doping effects in LEC-grown gallium arsenide crystals
4th Hung. Conf. on Crystal Growth,
Acta Phys. Hung. 61 (1987) p.255

RAKOVICS, V., Görög, T., Lendvay, E.:
Growth of InGaAsP/InP heterostructures for optoelectronic applications
2nd Conf. on Physics and Technology of GaAs and other III-V Semi-
conductors, Budapest, 1986.
Proceedings (Trans-Tech Publications, Switzerland) 1987, p.81.

SOMOGYI, K.:
The mobility of electrons in GaAs epitaxial layers
Finommechanika-Mikrotechnika 26 6-7 (1987) pp.204-210 (in Hungarian)

SOMOGYI, K.:
Hall mobility lowering in GaAs epitaxial layers
Acta Phys.Hung. 61 2 (1987) pp.169-172

SOMOGYI, K.:
On the integrated Hall mobility in VPE GaAs layer
Proc. Symp. Electronics Technology, 1987, Budapest,
Vol.1. pp.336-341

SOMOGYI, M.:
Impedance of GaAs-GaAsP-GaP/Electrolyte interfaces in the 10 kHz-100
kHz frequency range
Crystal Properties and Preparation 12 (1987) p.347

Papp, A., SZENTPÁLI, B.:
The Schottky diode as a microwave detector
Finommechanika-Mikrotechnika 26 6-7 (1987) pp.180-186 (in Hungarian)

SZŐKEFALVI-NAGY, Á., Huang, X.Y., Kirchheim, R.:
Electrical resistivity changes due to hydrogen in palladium
J.Phys. F.: Metal Phys. 17. (1987) pp.427-431

TICHY-RÁCS, Á.:
The meteorological correction factor to microwave distance measurements
Finommechanika-Mikrotechnika, 26 (1987) pp.190-192 (in Hungarian)

TÓTH, L.:
A model of substrate surface roughness effect on the electrical properties of thin films
Vacuum TAIP 37, 1-2, (1987) pp.102-106

URAY, L.:
Temperature dependence of the excess resistivity and thermopower in dilute alloys of tungsten I: Experimental results.
J.Phys. F.Met.Phys. 17, (1987) pp.1013-1020

URAY, L.:
Temperature dependence of the excess resistivity and thermopower in dilute alloys of tungsten II: Two-band model
J.Phys.F.Met.Phys. 17 (1987) pp.1021-1028

VICSEK, T., Kertész, J.:
Laplacian pattern formation
Europhs. News (in press)

Meakin, P., VICSEK, T.:
Diffusion-limited aggregation with radial bias
J.Phys. A20 (1987) p.171

Meakin, P., Family, F., VICSEK, T.:
Viscous fingering simulated by off lattice aggregation
J.Interface and Colloid Sci., 117, (1987) p.394

Family, F., Platt, D., VICSEK, T.:
Deterministic growth model of dendritic pattern formation
J.Phys. A20 xx (1987)

VICSEK, T.:
Formation of interfacial patterns in aggregation and viscous flows
Physica Scr. 36, xx (1987)

Horváth, V., VICSEK, T., Kertész, J.:
Viscous fingering with uniaxial anisotropy
Phys. Rev. A35, (1987) p.2353

Tél, T., VICSEK, T.:
Geometrical multifractality of growing structures
J.Phys. A20 (1987) p.L835

VICSEK, T.:
Comments to fractal growth
Tudomány, 3, (1987) p.61 (in Hungarian)

VICSEK, T.:
Patterns of nature
Delta, 5 (1987) p.8. (in Hungarian)

VERESEGYHÁZY, R., Pécz, B., Gombos, G., Mojzes I.:
Metal compound semiconductor interfaces: Reactivity and the evaporation of volatile component
International Summer Institute on New Developments in Semiconductor Physics, Szeged, Hungary, 1987., NDSP-2 Abstracts, p.95

VERESEGYHÁZY, R., Mojzes, I., Miles, R.E., O'Keefe, M.:
Alloyed AuGeNi ohmic contacts on GaAs
Proc. Symp. on Electronics Technology, Budapest, Hungary, 1987.
Vol.1., pp.411-415

VERESEGYHÁZY, R., Pécz, B., Mojzes I.:
Evolved gas analysis for the investigation of metal-compound semiconductor interaction
5th Intern. School on Phys. Problems in Microelectronics, Varna, Bulgaria, 1987.

VERESEGYHÁZY, R., Pécz, B., Gombos, G., Mojzes, I.:
Metal-compound semiconductor interfaces: reactivity and the evaporation of volatile component
Intern. Summer Inst. on New Developments in Semiconductor Physics
NDSP-2 - Szeged, Hungary, 1987,

VERESEGYHÁZY, R., Mojzes, I., Miles, R.E., O'Keefe, M.:
Alloyed AuGeNi ohmic contacts on GaAs
Finommechanika-Mikrotechnika 26 (1987) pp.159-260

ZSOLDOS, L., Pető, G., Zsoldos, É., Brogren, G., Kanski, J.:
Annealing induced strain in $^{31}P^{+}$ implanted Si (111) and Si(100)
Appl. Phys.Lett 51 (1987) pp.749-751

Hungarian patents

VICSEK, T.:
Comments to fractal growth
Tudomány, 3, (1987) p.67 (in Hungarian)

VICSEK, T.:
Patterns of nature
Delta, 5 (1987) p.8. (in Hungarian)

VERESEGYHÁZY, R., Pécz, B., Compos, G., Mojzes I.:
Metal compound semiconductor interfaces: Reactivity and the evaporation of volatile component
International Summer Institute on New Developments in Semiconductor Physics, Szeged, Hungary, 1987., NDSP-2 Abstracts, p.96

VERESEGYHÁZY, R., Mojzes, I., Miles, R.E., O'Keefe, M.:
Alloyed Au(GeNi ohmic contacts on GaAs
Proc. Symp. on Electronics Technology, Budapest, Hungary, 1987.
Vol.1., pp.411-415

VERESEGYHÁZY, R., Pécz, B., Compos, G., Mojzes, I.:
Evolved gas analysis of the decomposition of metal compound semiconductor interaction
5th Intern. School on Phys. Problems in Microelectronics, Varna, Bulgaria, 1987.

VERESEGYHÁZY, R., Pécz, B., Compos, G., Mojzes, I.:
Metal compound semiconductor interfaces: reactivity and the evaporation of volatile component
Hungarn. Summer Inst. on New Developments in Semiconductor Physics, NDSP-2 - Szeged, Hungary, 1987.

VERESEGYHÁZY, R., Mojzes, I., Miles, R.E., O'Keefe, M.:
Alloyed Au(GeNi ohmic contacts on GaAs
Feingerätechnika-Mikrotechnik 36 (1987) pp.159-160

PÉCZ, B., Pető, G., Zsoldos, E., Dobrev, G., Kanski, I.:
Annealing induced strain in $^{31}P^+$ implanted Si (111) and Si(100)
Appl. Phys Lett 51 (1987) pp.759-761

Applications

No.883/86 (04.03.1986)
Attachment for X-ray fluorescence analysis
Pozsgai, I., Barna, A.

No.1096/86 (17.03.1986)
Method for the examination of electrically active impurities of semiconductor materials or structures and measuring arrangement for carrying out the method.
Ferenczi, G., Jantsch, W.

No.2883/86 (11.07.1986)
Method and tool for deformation by drawing through a hole.
Prohászka J., Varga, L., Hidasi, B., Bartha, L., Vargha, J.

No.5117/86 (09.12.1986)
Procedure for preparation of low-noise Schottky barriers on n-GaAs crystal, preferably applying for microwave diodes.
Szentpáli, B., Németh, T.(Mrs).

No.5118/86 (09.12.1986)
Procedure and circuit schematic for compensated high dinamic range light-measurement.
Makai, J., Makai, J., Urhegyi, K. (Mrs).

No.1164/87 (18.03.1987)
Machining tool and procedure for its production
Horacsek, O.(Mrs), Boncok, J., Varga, L., Bartha, L., Jándy, J., Venk, J., Putz, V., Kreuz, L., Máthé, A.

No.1989/87 (04.05.1987)
Method and apparatus for determining the layer thickness of semiconductor multilayers
Ferenczi, G., Erdélyi, K., Somogyi, M., Boda, J., Füle, G., Aszódi, G.

No.2269/86 (22.05.1987)
Arrangement for stabilisation of semiconductor laser diode optical output power
Andor, L., Tüttő, P.

No.2699/87 (15.06.1987)
Electronic circuit for multi-channel synchron analog/digital signal converter preferably applied in light measuring instruments.
Dobovics, M., Ferenczi, S., Lánc, J., Réti, J., Schanda, J., Urhegyi, K. (Mrs).

No.3710/87 (19.08.1987)
Mounting of two-terminal microwave active devices
Jászberényi, I., Kazi,K., Mojzes, I., Oláh, A., Reisinger, G., Szentpáli, B., Tichy-Rács, Á., Bodolai, P., Csabán, P., Ivanics, L., Kurucz, J.

Patents issued

No. 182 777 (18.02.1986)
Method for determining charged energy status of semiconductors
Ferenczi G., Boda, J., Tóth,F., Horváth,P.

No. - (24.02.1986) Appl. No.: 1989/83
Equipment for contactless temperature measurement of wires and filament
Rakovics, V., Görög, T., Bartha, L., Varga, L., Tóth, A., Ludányi, L.
Tóth,A., Szatmári, A., Monus, A.:

No. 190 855 (13.04.1986)
Device for electron beam processing of solid samples and an ion source to it.
Barna, A., Reisinger, G., Zsoldos, L.

No. 190 811 (13.04.1986)
Method for decomposing and dissolving hard metal scraps by means of anodic oxydation.
Vadasdi, K., Bartha, L., Szilassy, I., Mikéta, G., Tekula, E.(Mrs.)

No. 190 892 (16.05.1986)
Reflection measuring equipment for plan surfaces; glossmeter
Kántor, K., Schanda, J., Makai, J.

No. 191 152 (13.06.1986)
Method for preparation of contacts to $A^{III}B^{V}$ compound semiconductor wafers
Kovács, B., Mojzes, I., Németh, S.M.(Mrs), Vasziljev, S.V., Gerasimenko, N.N.

No. - (23.06.1986) Appl.No.: 4083/84
Barcode indexing determination equipment
Serényi, M., Benesoczki, D.

No. - (23.06.1986) Appl.No. 3365/84
Procedure for the enhancement of the sensitivity of a light measuring apparatus with photodetector
Eppeldauer, G.

No. 191 850 (02.07.1986)
Method and equipment for annealing and hydrodynamic lubrication of refractory metal wires.
Bartha, L., Varga, L., Gaál, I., Elek, K., Csákó, J., Juhász, G., Varga, J., Gróh, R.

No. - (04.08.1986) Appl.No. 1012/83
Method for preparation of high purity tungstic salts from alkaline tungstic solutions
Vadasdi, K., Jeszenszky, A., Oláh, R., Bartha, L., Szilassy, I., Tekula, E. (Mrs), Hornyák, I.

No. - (03.12.1986) Appl.No.: 2886/83
Method for dissolving metals
Vadasdi, K., Gerey, G., Bartha, L., Szilassy, I., Tekula, E. (Mrs).

No. - (27.08.1987) Appl.No. 601/85
Preparation method for ohmic contacts, preferably for compound semiconductors.
Kovács, B., Mojzes, I., Németh, S.M. (Mrs), Voldemarovics, V.Sz., Veresegyházi, R.

No. - (23.09.87) Appl.No. 4849/85
High voltage source providing continuously regulated output voltage, preferably for supplying low-power ion and electron beam machining and evaporating apparatus.